UNIVERSITAT POLITÈCNICA DE CATALUNYA BARCELONATECH

Next generation optical access networks and coexistence with legacy PONs

Juan Camilo Velásquez Micolta

UNIVERSITAT POLITÈCNICA
DE CATALUNYA
BARCELONATECH

PhD thesis

Next Generation Optical Access Networks and Coexistence with Legacy PONs

Author:
Juan Camilo Velásquez Micolta

Advisors:
Josep Joan Prat Gomà
Iván Nicolás Cano Valadéz

Thesis presented in fulfilment for the degree of:
Doctor of Philosophy in Signal Theory and Communications

At the:
Optical Communications Group (GCO)
Department of Signal Theory and Communications (TSC)
Universitat Politècnica de Catalunya (UPC)

Barcelona, July 2019

The work described in this thesis was performed in the Optical Communications Group (GCO) at the Signal Theory and Communications (TSC) department of the Universitat Politecnica de Catalunya (UPC). It was supported by the AGAUR (Agència de Gestió d'Ajuts Universitaris i de Recerca) under grant 2016FI_B 00758, and developed in the framework of the European FP7 COCONUT project and the Spanish Ministry of Science and Innovation FLIPER project TEC2015-70835.

Juan Camilo Velásquez Micolta

"Next Generation Optical Access Networks and Coexistence with Legacy PONs"

Subject Headings: Optical communications, fiber optics, PONs.

Printed in Barcelona, Spain.
ISBN:
Reg:

To my beloved wife Diana

To my parents Marlene and Jorge Iván

"Y Jesús les habló otra vez, diciendo:
Yo soy la luz del mundo; el que me sigue, no andará en
tinieblas, sino que tendrá la luz de la vida."
Jn 8:12

Abstract

Nowadays, Fiber-to-the-Home is one of the most promising solutions to provide broadband services in access networks. However, the fiber is inefficiently used as most of the deployed systems are still based on Time Division Multiplexing Passive Optical Networks (TDM-PONs) providing shared transmission capacities up to 2.5 Gb/s down and 1.25 Gb/s up, among multiple users. Research on high-speed electronics and Wavelength Division Multiplexing (WDM) has allowed the emergence of what is known as the second generation PON (NG-PON2), which specify aggregated capacities up to 40 Gb/s, stacking four channels at symmetric data rates of 10 Gb/s each, for residential scenarios. Nevertheless, the capacity per channel is still shared between multiple users due to the use of TDM. Moreover, the optical spectrum efficiency is low because channels are widely spaced (50 to 100 GHz). In addition, the sensitivity, reach and number of users is limited as consequence of using direct detection (DD) systems. In consequence, and due to the increase in bandwidth demands of new multimedia applications, it is necessary to propose solutions that cope with this tendency and, even more important, that can coexist with legacy systems, being one of the major requirements of network operators to guarantee a smooth and non-disruptive technology migration.

In this thesis, a breakthrough technology such as Ultra-Dense WDM (UDWDM) that allows to allocate a large number of channels spaced only by a few GHz is used. This approach consent to envision the concept of Wavelength-to-the-User, where each costumer can be served with dedicated bandwidth links. The key technologies are based on coherent systems, with inherent wavelength selectivity and improved sensitivity compared to DD systems, thanks to the booster action of a tunable local oscillator (LO) laser.

Because of cost is the main constraint in access networks, especially at the customer premises equipment (Optical Network Unit - ONU), in this thesis, a new class of coherent transceivers, based on low-cost direct modulated lasers and simplified receiver schemes, are proposed and experimentally tested. Moreover, the issue of coexistence is investigated through theoretical studies and real-time implementations, demonstrating full compatibility with legacy systems.

Between the proposed solutions, a simple technique to adjust digitally the direct phase modulation of a distributed feedback (DFB) laser is presented to support flexible transmission rates. Next, several multilevel phase modulation formats for achieving higher transmission rates and better spectral efficiency are experimentally compared. Subsequently, the topic of photonic integration is addressed, demonstrating for the first time an 8-ary hybrid amplitude and phase modulated transmitter (Tx), by using a low-cost, small-footprint and energy efficient dual electro-absorption modulated laser (DEML). Finally, two novel proposals, to reduce the complexity of heterodyne and intradyne detection, are provided to face the typical issue of complexity and high-cost of coherent systems. The former explores the possibility of using only one DFB laser as LO and Tx at the ONU. The later demonstrates for the first time, a novel phase time diversity technique alternating phase modulation at each complex component (in-phase - I and quadrature - Q) achieving a 10 Gb/s/λ transmission with polarization independence.

Acknowledgments

First of all, I want to thank God for being the spiritual guide in each and every tasks I carry out in my life.

Thanks to all my family, especially to my beloved wife Diana, for her unconditional love and encouragement day after day. Thanks to my parents, Marlene and Jorge Iván, to my aunt Myriam and my grandmother Mariela, for their total support and their endurance during these long years outside my lovely country Colombia. Each sacrifice, each prayer and each advice has helped me to achieve the proposed goal.

I want to express my gratitude to my advisor Prof. Josep Prat to give me opportunity to join the GCO group, and develop my PhD thesis in the framework of high relevance research projects, both national and international. Their guidance and experience have positively influenced the development of this work. Furthermore, I am also in debt with my co-advisor Iván Cano, because his support and technical knowledge have helped me to develop most of the work described in this thesis and presented in relevant conferences and peer-reviewed journals.

Thanks to the tribunal of this thesis, integrated by Dr. Antonio Teixeira (IT-Universidade de Aveiro), Dr. Antonio Napoli (Infinera) and Dra. Maria Concepción Santos (UPC), for giving relevance and prestige to this work.

This research work has been possible thanks to the valuable contributions of my colleagues in the GCO. Special thanks to Victor Polo, for his laboratory assistance, for sharing his practical experience and for the nice talks before starting the workday. Moreover, I was very fortunate to be able to work alongside my best friend, Jeison Tabares. We worked side by side, and I feel that each conversation and each of their contributions has enriched me, both personally and professionally. In the same line, I would like to thank the rest of GCO group, Vicent Sales, Josep Segarra, Saeed Ghasemi, and to some colleagues that left the group some time ago, between them Guangyong Chu and Marc Domingo, for the good atmosphere they provided during many working hours. Finally, thanks to Rafael, Rubén and Samael for sharing the daily lunches and for their friendship.

Last but not least, I want to thank AGAUR for its financial support through the grant 2016FI_B_00758, and to the personal of the UPC for their collaboration with the different administrative affairs.

Thanks to all…

Table of Contents

Abstract v

Acknowledgments vii

List of Figures xiii

List of Tables xix

Abbreviations & Acronyms xxi

Symbols xxiii

Chapter 1. Introduction 1

1.1 Passive Optical Networks (PONs) 1
1.1.1 PON architectures 3
1.1.1.1 Time Division Multiplexing PON (TDM-PON) 3
1.1.1.2 Wavelength Division Multiplexing PON (WDM-PON) 4
1.1.1.3 Hybrid WDM ring/TDM tree PON and TWDM-PON 5
1.1.1.4 Ultra-dense wavelength division multiplexing PON (UDWDM-PON) 6
1.1.2 PON roadmap and standardization 7

1.2 Intensity modulated/Direct detection (IM/DD) systems 11
1.2.1 Optical IM transmitter 12
1.2.2 Optical DD receiver 12

1.3 Coherent optical systems 13
1.3.1 Ideal coherent system performance 14
1.3.2 Basic modulation formats 15
1.3.2.1. Amplitude shift keying (ASK) 15
1.3.2.2. Phase shift keying (PSK) 16
1.3.2.3. Differential PSK (DPSK) 16
1.3.3 Asynchronous coherent receivers 17
1.3.3.1. Heterodyne balanced detector for ASK and DPSK signals. 18
1.3.3.2. Phase diversity Rx using intradyne coherent detection. 20

1.4 Thesis motivation and objectives 23

1.5 Thesis outline 24

1.6 Author publications 25
1.6.1. Published works 25
1.6.2. Submitted works 28

Bibliography Chapter 1 29

Chapter 2. Coexistence between UDWDM-PON, NG-PON2, and legacy PONs 33

2.1 Coexistence between NG-PON2 and legacy PONs 34

2.2 COCONUT project: A proposal for NG-PON3 systems 38
2.2.1 COCONUT baseline network architecture 39
2.2.2 COCONUT vs NG-PON2 40
2.2.3 OLT and ONU architectures for UDWDM-PON 41
2.2.3.1. ONU designs and sizing 41
2.2.3.2. OLT designs and sizing 42
2.2.4 Wavelength plan for COCONUT network and coexistence scenarios with legacy PONs 46
2.2.4.1. Coexistence deployment scenarios 46
2.2.4.2. COCONUT coexistence scenarios 47
2.2.5 Inter-channel crosstalk analysis between COCONUT-PON and legacy PONs 51

2.3 Real-time UDWDM-PON implementation 51
2.3.1 CE characterization 52
2.3.1.1. CE characterization using a tunable ECL 52
2.3.1.2. CE isolation according to specific coexistence scenarios 54
2.3.2 Analog heterodyne DPSK system 55
2.3.3 Bidirectional Real-Time DSP-less Heterodyne UDWDM-PON 57
2.3.4 Field-Trial of COCONUT UDWDM-PON with Real-Time Processing, λ-Monitoring and EPON Coexistence. 61
2.3.4.1. Setup and wavelength allocation plan using during the COCONUT demo 61
2.3.4.2. Heterodyne PSK System performance and real-time video-streaming setup 63
2.3.4.3. Coexistence with Legacy EPON system 66

2.4 Chapter summary 68

Bibliography Chapter 2 70

Chapter 3. Direct phase modulated DFB lasers 73

3.1 Direct phase modulation with digital beat signals 74
3.1.1 Digital equalization 76
3.1.2 Experimental validation 77

3.2 Nyquist shaped Tx based on direct phase modulated DFB 83
3.2.1 Numerical simulations 83
3.2.2 Experimental validation 87
3.2.3 UDWDM-PON dimensioning 91

3.3 Chapter Summary 92

Bibliography Chapter 3 93

Chapter 4. Multilevel direct phase modulation of DFB lasers 95

4.1 M-ary DPSK modulation 96
4.1.1 DQPSK signal generation 97
4.1.2 8-DPSK signal generation 98

4.2 Duobinary modulation (DB) 98
4.2.1 Electrical duobinary (EDB) 99
4.2.2 Optical duobinary (ODB) for direct phase modulation 100

4.3 Experimental validation in 6.25 GHz Spaced Coherent UDWDM-PONs 101
4.3.1 Comparison between DPSK, DQPSK and ODB formats 103
4.3.2 7.5 Gb/s Direct DFB Phase Modulation with 8-DPSK 106

4.4 Chapter summary 108

Bibliography Chapter 4 110

Chapter 5. Low-cost transmitters using hybrid amplitude and phase modulation formats. 113

5.1 Time-domain hybrid modulation format (TDHF) 114
5.1.1 Time Interleaved DPSK/ASK Transmitter 115
5.1.2 Experimental validation of time-interleaved DPSK/ASK modulation 117

5.2 Heterodyne DPSK-ASK based on Dual-EML transmitter 121
5.2.1 Assembly and characterization of the dual electro-absorption modulated laser (DEML) 121
5.2.2 DPSK/ASK signal generation 123
5.2.3 Experimental validation of heterodyne DPSK/ASK 123

5.3 Differential 8-APSK DEML Transmitter with intradyne coherent reception 127
5.3.1 8-APSK signal generation 128
5.3.2 Experimental validation of differential 8-APSK transmitter with intradyne coherent detection 129

5.4 Digital pre-emphasis equalization for 10 Gb/s 8-APSK Tx 137
5.4.1 Theory approach 137
5.4.2 Experimental validation and results 138

5.5 Chapter summary 140

Bibliography Chapter 5 142

Chapter 6 . Simplified ONU/OLT architectures for coherent UDWDM-PONs 145

6.1 Conventional coherent TRx 146

6.2 Bidirectional coherent PON with ONU based reused direct modulated LO 147
6.2.1 Experimental setup 147

6.2.2 Results and discussion 148

6.3 Phase time diversity directly modulated DFB with single-PD intradyne receiver .. 150
6.3.1 Phase-time diversity Tx and signal generation 150
6.3.2 Experimental setup with simplified intradyne Rx 151
6.3.3 Results and discussion 152

6.4 Chapter summary 154

Bibliography Chapter 6 156

Chapter 7 . Conclusions and open research lines 159

7.1 General conclusions 159

7.2 Open research lines 161
7.2.1 Techno-economic and energy consumption studies of coherent transceivers and UDWDM architectures 162
7.2.2 Real-time implementation of hybrid modulation formats using photonic integrated devices 162
7.2.3 Metro-access network convergence integrating FTTH, enterprises for 5G services 163

Appendixes 165

A. NG-PON2 upstream inter-channel crosstalk analysis 165

B. Example of nominal central frequencies of ITU-T DWDM grid plus the COCONUT proposed 6.25 GHz grid 169

C. COCONUT coherent heterodyne onu transceiver datasheet for ng-pon3 170

Bibliography Appendixes 172

List of Figures

Figure 1.1. Telecommunication infrastructure 2
Figure 1.2. PON topology 3
Figure 1.3. Basic PON architectures: **(a)** TDM-PON, **(b)** WDM-PON 4
Figure 1.4. Hybrid TWDM-PON architecture 6
Figure 1.5. UDWDM-PON architecture 6
Figure 1.6. PON roadmap 8
Figure 1.7. Wavelength bands allocation of PON standards 10
Figure 1.8. IM/DD system. EML: External modulated laser, DML: External modulated laser 11
Figure 1.9. Ideal coherent receiver 14
Figure 1.10. Schemes of**: (a)** differential pre-coder, **(b)** differential demodulation 17
Figure 1.11. Electrical spectrum of asynchronous coherent systems 17
Figure 1.12. Heterodyne asynchronous Rx for ASK and DPSK signals 18
Figure 1.13. Phase diversity Rx using intradyne coherent detection for DPSK signals 21

Figure 2.1. Reference architecture and points for NG-PON2 system coexisting with legacy systems 34
Figure 2.2. Scheme of a CE with G-PON, XG-PON and NG-PON2 (shared spectrum) coexistence 35
Figure 2.3. Power penalty (Pc) against inter-channel crosstalk (XT) for different ER values of interferer systems at BER = 10^{-4} 37
Figure 2.4. Baseline of the COCONUT architecture 39
Figure 2.5. Number of allocated ONUs as a function of the total bandwidth, in terms of number of optical slots using a dedicated WTTU approach. 42
Figure 2.6. (a) OLT architecture realized with splitters covering full optical bands, **(b)** OLT block diagram based on splitters and two thermal AWGs with complementary frequency response providing 100% spectral efficiency. 43
Figure 2.7. AWG characterization setup: single and tuning AWG scenarios. 44
Figure 2.8. (a) Athermal Gaussian 100 GHz AWG response, **(b)** Thermal flat-top 100 GHz AWG response. 44
Figure 2.9. Interleaving AWG channels by thermal tuning: **(a)** Gaussian, **(b)** flat-top. 45
Figure 2.10. Coexistence scenario between COCONUT and legacy PONs. 47
Figure 2.11. COCONUT coexistence alternatives in PONs using a CE.. 48
Figure 2.12. Setup for CE characterization using a TL 52
Figure 2.13. CE characterization using an ECL: **(a)** CE1, **(b)** CE2 and **(c)** CE3. 54
Figure 2.14. Heterodyne PSK COCONUT TRx prototypes for **(a)** OLT and **(b)** ONU 56
Figure 2.15. Experimental setup schematics(The inset shows the optical spectrum in DS). 58
Figure 2.16. BER against received power for: **(a)** independent DS and US transmissions, **(b)** bidirectional transmission (the inset shows the optical spectra of DS and US separated by 2.5 GHz. 58
Figure 2.17. (a) BER against frequency drift of the LO in the OLT, **(b)** BER against received optical power of UDWDM system coexisting with EPON signals. 59

Figure 2.18. Log10(BER) for different interference powers and CS. The inset in the right show the electrical spectra of two users at CS of 6.25 GHz (upper) and 18.75 GHz (lower) ... 60
Figure 2.19. Field-trial setup schematics. The insets show the optical spectrum of EPON DS and all COCONUT channels in C-band (upper), and the map with the deployed fiber across city of Pisa. 62
Figure 2.20. Optical spectrum distribution during the field-trial: **(a)** DS wavelengths, **(b)** US wavelengths. 63
Figure 2.21. (a) BER against Rx power for 1.25 Gb/s heterodyne DPSK system. The insets show the eye diagrams of the detected signal at BER=10^{-4} (upper) and BER=10^{-9} (lower), **(b)** Electrical spectrum of the Rx signal when just the heterodyne DPSK was in the ODN (upper), and when all systems were active in the ODN (lower). 64
Figure 2.22. Setup implemented for video transmission using Heterodyne PSK prototype 65
Figure 2.23. Video interface box; external design (left) and internal distribution (right) 65
Figure 2.24. (a) Successfully transmitted HD videos during the field-trial demo, **(b)** Complete heterodyne DPSK ONUs bench. 66
Figure 2.25. (a) CE3 at OLTs during the DEMO, **(b)** CE2 at ONUs side during the DEMO ... 66
Figure 2.26. Wavelength allocation used during the COCONUT field-trial ensuring full coexistence. 67
Figure 2.27. (a) EPON OLT transmitted real-time data, **(b)** EPON ONU receiving successfully the video during COCONUT field-trial 67

Figure 3.1. PM responses of the commercial NLK5C5E2KA DFB laser ... 76
Figure 3.2. Pre-equalizer versions for PM response compensation: **(a)** analog and **(b)** digital ... 77
Figure 3.3. (a) Tx scheme for digital beat equalized laser, **(b)** beat signal generation. 78
Figure 3.4. (a) Experimental schematics setup. The insets show the transmitted spectrum for two users Tx_1 and Tx_2 spectrally spaced 6.25 GHz. **(b)** Photo of the laboratory implementation. ... 79
Figure 3.5. Experimental phase shift obtained when changing the signal amplitude and duty cycle at **(a)** R_b = 1.25 Gb/s and **(b)** R_b = 2.5 Gb/s. The level lines indicate the phase shift as proportion to π radians, i.e. 1 represents π radians. The insets shows the I & Q and Eye diagrams for a phase shift of π/2 (top) and π (bottom) radians. The constellations show ± phase shifts and for that reason the complex conjugate also appears. ... 80
Figure 3.6. Sensitivity penalty at BER of 10^{-4} against phase shift from π rad. The x-axis is normalized to π radians, i.e. 1 represents π radians. The insets show the I & Q diagrams of π/2 rad, π rad and 11π/9 rad. The constellations show ± phase shifts and then the complex conjugate also appears. ... 81
Figure 3.7. Rx power against duty cycle for beat phase modulated signals. The insets show the signal spectrum at 50 % and 100% duty cycle at a relative intermediate frequencies (IF) of 5 GHz for R_b = 1.25 Gb/s and at IF = 10 GHz for R_b of 2.5 Gb/s and 5 Gb/s. The red dotted diamonds indicate the performance when amplitude is left constant at the different bit rates. ... 82
Figure 3.8. BER against Rx power for direct phase modulated Tx with duty cycle of 50%, and at R_b of 1.25 Gb/s, 2.5 Gb/s and 5 Gb/s. The insets show the eye diagrams for BER = 10^{-5}. ... 82
Figure 3.9. Simulation Setup for pulse shaping evaluation. ... 84

Figure 3.10. **(a)** Magnitude spectra of the Raised-cosine filter for several roll-off values. **(b)** Sensitivity penalty @BER=10^{-3} vs normalized filter BW for the three pulse-shaping schemes. 85
Figure 3.11. Electrical spectra of 1.25 Gb/s PRBS data and eye diagrams for each case: **(a)** NRZ, **(b)** Gaussian**, (c)** Raised-cosine pulse shaping at the Tx. 85
Figure 3.12. Optical spectra for two users separated by 6.25 GHz for three different pulse-shaping schemes: **(a)** NRZ, **(b)** Gaussian, **(c)** Raised-cosine. 86
Figure 3.13. **(a)** BER against Channel Spacing for Tx1 using three different pulse-shaping filters, **(b)** Rx sensitivity penalty @BER = 10^{-3} for the three pulse-shaping schemes. 86
Figure 3.14. Nyquist shaped Tx for UDWDM-PON validation 87
Figure 3.15. **(a)** Electrical beat square signal and Nyquist shaped signal with α = 0.25 (upper) and α = 1 (bottom) and RF spectrum of the Tx signal without and with Nyquist shaping at R_b = 1.25 Gb/s (**(b)**, **(d)**) and R_b = 2.5Gb/s (**(c)**, **(e)**) for α= 0.25 and α= 1 88
Figure 3.16. **(a)** BER against Rx optical power for Tx_1. Eye diagrams at BER = 3 x 10^{-6} without and with Nyquist shaping at 1.25 Gb/s **(b, c)** and 2.5 Gb/s **(d, e)** respectively. 89
Figure 3.17. BER against channel spacing with and without Nyquist shaping for Tx_1 at R_b = 1.25 Gb/s and R_b = 2.5 Gb/s for (a) DLL = 0 dB and (b) DLL = 15 dB. 90
Figure 3.18. **(a)** BER vs CS for Tx_1 at several differential link-losses (DLL) at R_b = 2.5 Gb/s. The insets show the electrical spectrum of two users spaced 6.25 GHz with DLL of 0 dB and 15 dB, **(b)** CS vs DLL for 1 dB of sensitivity penalty at BER = 10^{-4}. The dotted lines indicate penalties <1dB. 91

Figure 4.1. **(a)** Bipolar pulses for DQPSK signal generation, **(b)** DQPSK constellation 98
Figure 4.2. 8-DPSK constellation 98
Figure 4.3. **(a)** Proposed Tx for duobinary modulation. The insets show the 2-level and 3-level eye diagrams, and the corresponding electrical spectra for i) NRZ data and ii) Duobinary encoded signal before optical modulation, **(b)** Duobinary encoder. 100
Figure 4.4. UDWDM-PON architecture. 101
Figure 4.5. Experimental setup: **(a)** schematics (the insets show the eye diagram of the transmitted electrical signal and the constellation of the received signal; from left to right, DPSK, ODB, DQPSK and 8-DPSK, **(b)** implementation at GCO laboratory. 102
Figure 4.6. **(a)** BER against Rx optical power for a DPSK signal at several bit rates. The eye-diagrams in the right correspond to: **(b)** 1.25 Gb/s, **(c)** 2.5 Gb/s, **(d)** 3.125 Gb/s, and **(e)** 5 Gb/s. 103
Figure 4.7. **(a)** BER against Rx optical power for DQPSK signal (the insets show the eye diagram of the I component and the constellation recovered in the Rx, **(b)** BER against CS for DPSK and DQPSK signals. The insets show the transmitted optical spectrum at CS of 6.25 GHz(left) and 3.75 GHz(right). 104
Figure 4.8. BER against Rx optical power for optical duobinary modulation format (the insets show the eye-diagram for bitrates of 3.125 Gb/s and 6.25 Gb/s). 105
Figure 4.9. BER against Rx optical power for multilevel signals at 1.25 Gbaud; the insets on the right show the spectrum and constellations for DPSK (up), DQPSK (middle) and 8-DPSK (down). 107
Figure 4.10. **(a)** BER against Rx power for multilevel phase modulated signals at 2.5 Gbaud; **(b)** BER against channel separation for 8-DPSK signal at 7.5 Gb/s. 107

Figure 5.1. Electrical modulation signals and phase changes produced on the DFB laser for: **(a)** DPSK modulation, **(b)** ASK modulation, and **(c)** Time-interleaved DPSK/ASK modulation 116

Figure 5.2. Time-interleaved DPSK/ASK implementation, **(a)** setup scheme, **(b)** photo of the implementation at GCO laboratory. 118
Figure 5.3. BER against Rx optical power for ASK Tx after 25 km of SMF. The insets show the eye diagrams at BER of 10^{-5} and 10^{-3} 119
Figure 5.4. (a) BER against amplifier gain for independent ASK and DPSK modulations, **(b)** BER against Rx optical power for ASK, DPSK and DPSK/ASK signals when interleaved data is transmitted. The insets show the eye diagrams of the received ASK and DPSK data at BER of 10^{-5} and 10^{-3}. 120
Figure 5.5. (a) Sectional view of the DEML, **(b)** Assembled DEML chip and lensed fiber faced with the EAM output. 122
Figure 5.6. Characterization of the DEML-1. **(a)** Static characteristics of DFB (V_{EAM} = 0V) and EAM ($I_{bias\ DFB}$ = 80 mA), **(b)** AM and PM responses of the DFB. 122
Figure 5.7. (a) Bipolar-RZ & NRZ signals for DPSK & ASK modulation, **(b)** 2-DPSK/2-ASK constellation. 123
Figure 5.8. Experimental setup and photos of the heterodyne 2-DPSK/2-ASK laboratory implementation. 124
Figure 5.9. BER against received optical power for: **(a)** ASK and DPSK alone signals (R_b = 2.5 Gb/s), **(b)** ASK+DPSK transmission at R_b=5 Gb/s. The insets show the eye diagrams at BER of 10^{-3} and 10^{-5}. 126
Figure 5.10. BER vs LO frequency drift when the EAM is unmodulated (DPSK) and modulated (DPSK/ASK). The eye diagrams correspond to the received data at BER=10^{-3} and 10^{-4} 127
Figure 5.11. (a) Bipolar-RZ & NRZ signals for DQPSK & ASK modulation, **(b)** 8-APSK constellation 128
Figure 5.12. 8-APSK Tx scheme. The insets show the I-Q diagram for the DQPSK, ASK and 8-APSK transmitted optical signals. 129
Figure 5.13. (a) Static characteristics of the DFB (V_{EAM}=0 V) and the EAM (I_{bias} DFB=60 mA), **(b)** Electro-optic responses of the DEML-2 considering RF constraints, **(c)** Measured and Lorentzian fitted linewidth of the DFB 131
Figure 5.14. Intradyne Rx for differential 8-APSK. The insets show the constellation diagrams at each stage: i) recovered complex signal, ii) DQPSK symbols after differential demodulation and frequency estimation, iii) ASK constellation and eye diagram, and iv) recovered 8-APSK symbols 132
Figure 5.15. Implementation of 8-APSK at GCO laboratory. 133
Figure 5.16. BER against Rx power for DQPSK modulation at 1.25 Gbaud (R_b = 2.5 Gb/s) and 2.5 Gbaud (R_b = 5Gb/s). The insets show the I-Q diagram of the recovered symbols at BER = 10^{-5} & 10^{-3}. 133
Figure 5.17. BER against Rx power for ASK modulation at: **(a)** 1.25 Gbaud (R_b=1.25 Gb/s) and **(b)** 2.5 Gbaud (R_b=2.5 Gb/s). The insets show the eye diagram at BER=10^{-5} & BER=10^{-3} for ER=3.8 dB. 134
Figure 5.18. Measurements of α_H parameter for the DFB (V_{EAM}= 0 V) and the EAM ($I_{bias\ DFB}$ = 60 mA) 135
Figure 5.19. BER against Rx power for differential 8-APSK at 1.25 Gbaud/s (R_b = 3.75 Gb/s) and 2.5 Gbaud/s (R_b = 7.5Gb/s). The I-Q diagrams show the recovered symbols at BER=10^{-3} and BER=10^{-5} 136
Figure 5.20. (a) BER vs. received power for the D-EML at 3.125 GBd symbol rate. **(b)** RF photodetected spectrum for 8-APSK at 3.125 GBd, centred at 12.5 GHz intermediate frequency. The insets show the three modulation formats generated by the DEML: (i) ASK, (ii) DQPSK, (iii) 8-APSK. 138

Figure 5.21. With 3.125 Gbaud symbol rate: **(a)** constellation diagrams with/without DPE for DQPSK and 8-APSK, **(b)** power penalty at BER = 10^{-4} vs. number of DPE filter taps.. 139

Figure 6.1. Conventional coherent TRx: **(a)** Tx, **(b)** Rx.....146
Figure 6.2. Experimental setup. The inset show the spectral separation between US and DS signals. 148
Figure 6.3. (a) DS performance CM-LO vs DM-LO, electrical spectra **(b)** CW-LO, (c) DPSK DM-LO. 148
Figure 6.4. (a) System performance in **(a)** btb DS, in the inset eye-diagram for RCSR = 5 dB at -42 dBm, **(b)** btb US, in the inset eye-diagram for RCSR = 5 dB at -46 dBm, **(c)** 50 km transmission performance at optimized RCSR, i.e. 5 dB, **(d)** and **(e)** electrical spectra DPSK DM-LO with RCSR = 0 dB and RCSR = 5 dB, respectively. 149
Figure 6.5. (a) Phase-time diversity Tx, **(b)** electrical sequences: i) bipolar RZ (I), ii) unipolar RZ (Q), and iii) phase-scrambled sequence (I-Q). 151
Figure 6.6. Experimental setup schematics; the inset shows photos of the Tx_1, Tx_2 and the PD 152
Figure 6.7. (a) BER against Rx optical power Tx_1 at several bit rates and eye diagrams at BER=10^{-5} for 5Gb/s and 8 Gb/s, and BER=10^{-3} at 10 Gb/s. **(b)** Sensitivity comparison at 10 Gb/ for Tx_1 (DM), and Tx_2 (EM) with the proposed 2-PD Rx and with a 120º hybrid.....153
Figure 6.8. BER against channel spacing for λ_1. The insets show the optical spectra for a frequency separation of 20 GHz and 50 GHz. 154

Figure A.1. Reference architecture for inter-channel crosstalk calculation in NG-PON2. Source: [2].....166
Figure A.2. Power penalty at BER = 10^{-4} vs upstream inter-channel crosstalk for NG-PON2 167
Figure A.3. Left: XT due to different combinations of I_A and I_{NA} for **(a)** N = 4, **(b)** N = 8, **(c)** N = 16; right: P_c at BER = 10^{-4} due to different combinations of I_A and I_{NA} for **(d)** N = 4, **(e)** N = 8, **(f)** N = 16. 168

List of Tables

Table 1.1. Characteristics of PON standards and NG-PON3 proposal.....9
Table 1.2. PON standards and NG-PON3 proposal characteristics.....10

Table 2.1. CE sample parameters for G-PON, XG-PON, and NG-PON2 (shared spectrum) coexistence.....35
Table 2.2. Key features of COCONUT vs NG-PON2.....40
Table 2.3. Alternatives for COCONUT allocation in a Brownfield scenario.....49
Table 2.4. CEs properties: IL (without connectors) and isolation per port.....53
Table 2.5. Theoretical and measured values for CE1 and CE2 in G-PON (target) - COCONUT (interferer) coexistence scenario.....55
Table 2.6. Rx sensitivity for unidirectional and bidirectional transmission UDWDM PON with analog heterodyne DPSK subsystem.....60
Table 2.7. Wavelength allocation plan for COCONUT field-trial demonstration.....63

Table 3.1. Minimum channel spacing with and without Nyquist shaping.....90

Table 4.1. 8-DPSK symbols with their corresponding phases.....98
Table 4.2. Rx sensitivity at BER = 10^{-3} for multilevel phase modulation formats.....105
Table 4.3. PON dimensioning summary.....108

Table 5.1. Experimental results of time-interleaved DPSK/ASK for supplying different services.....120
Table 5.2. Experimental results of heterodyne DPSK/ASK using an integrated DEML as Tx 127
Table 5.3. Rx sensitivity for ASK modulation at BER = $4x10^{-3}$.....134
Table 5.4 Spectral efficiency for ASK, DPSK, and 8-APSK modulation formats in 6.25 GHz channel grid, and Rx sensitivity for BER = $4x10^{-3}$ after 25 km at 2.5 Gbaud.....136
Table 5.5 10G PON dimensioning and comparison.....140

Table 6.1. Rx sensitivity at BER = 10^{-3} after 50 km at 1.25 Gb/s with reused LO and IF = 5 GHz.....150

Table A.1. Maximum tolerable upstream XT in NG-PON2 for different power penalties at BER = 10^{-4}.....167
Table A.2. Typical values of I_A and I_{NA}, and corresponding XT and Pc at BER = 10^{-4}.....168

Abbreviations & Acronyms

4G	–	Fourth generation
5G	–	Fifth generation
10G-EPON	–	10 Gbit/s Ethernet Passive Optical Network
ADC	–	Analogue to digital converter
AM	–	Amplitude Modulation
ASE	–	Amplifier Spontaneous Emission
APON	–	ATM Passive Optical Network
APSK	–	Amplitude and Phase Shift Keying
ASK	–	Amplitude Shift Keying
ATM	–	Asynchronous Transfer Mode
AWG	–	Arrayed Waveguide Grating
AWGen	–	Arbitrary Wavelength Generator
BBU	–	Base-band Unit
BER	–	Bit Error Rate
BPON	–	Broadband Passive Optical Network
C-band	–	Conventional wavelength band
CE	–	Coexistence Element
CD	–	Chromatic dispersion
CO	–	Central Office
CPRI	–	Common Public Radio Interface
CW	–	Continuous Wave
DAC	–	Digital to Analogue Converter
DD	–	Direct Detection
DEML	–	Dual Electro-absorption Modulated Laser
DFB	–	Distributed Feedback
DML	–	Direct Modulated Laser
DPSK	–	Differential PSK
DS	–	Downstream
DWDM	–	Dense Wavelength Division Multiplexing
EAM	–	Electro-Absorption Modulator
EML	–	External Modulated Laser
EDFA	–	Erbium Doped Fiber Amplifier
EPON	–	Ethernet Passive Optical Network
ER	–	Extinction Ratio
FSAN	–	Full Service Access Network
FTTA	–	Fiber-to-the-Antenna
FTTH	–	Fiber-to-the-Home
FWHM	–	Full Width at Half Maximum
GbE	–	Gigabit Ethernet
GPON	–	Gigabit Passive Optical Network
G-EPON	–	1 Gbit/s Ethernet Passive Optical Network
HD	–	High Definition
IEEE	–	Institute of Electrical and Electronics Engineers
IF	–	Intermediate Frequency
IM	–	Intensity Modulation
IP	–	Internet Protocol

ISI	–	Intersymbol Interference
ITU	–	International Telecommunication Union
L-band	–	Long wavelength band
LO	–	Local Oscillator
MAC	–	Media Access Control
MZM	–	Mach Zehnder Modulator
NG-PON2	–	Second Generation Passive Optical Network
NRZ	–	Non-Return-to-Zero
OBSAI	–	Open Base Station Architecture Initiative
ODN	–	Optical Distribution Network
OLT	–	Optical Line Terminal
ONU	–	Optical Network Unit
OOK	–	On-Off Keying
OSA	–	Optical Spectrum Analyzer
PM	–	Phase Modulation
PMD	–	Physical Media Dependent
PON	–	Passive Optical Network
PRBS	–	Pseudo-random Binary Sequence
PSK	–	Phase Shift Keying
PtMP	–	Point-to-multipoint
PtP	–	Point-to-point
QoS	–	Quality of Service
RAN	–	Radio Access Network
RF	–	Radio Frequency
RMS	–	Root-Mean-Squared
RN	–	Remote Node
RRH	–	Remote Radio Head
RSOA	–	Reflective SOA
RTO	–	Real-time Oscilloscope
Rx	–	Receiver
RZ	–	Return-to-Zero
SMF	–	Single Mode Fiber
SNR	–	Signal to Noise Ratio
SOA	–	Semiconductor Optical Amplifier
TDM	–	Time Division Multiplexing
TDHF	–	Time Domain Hybrid Format
TL	–	Tunable Laser
TRx	–	Transceiver
TTx	–	Tunable Transmitter
Tx	–	Transmitter
TWDM	–	Time & Wavelength Division Multiplexing
UDWDM	–	Ultra-Dense Wavelength Division Multiplexing
US	–	Upstream
VoIP	–	Voice over Internet Protocol
VPI	–	Virtual Photonics Incorporated
WDM	–	Wavelength Division Multiplexing
WTTU	–	Wavelength-to-the-User
XG-PON	–	10-Gigabit Passive Optical Network
XG(S)-PON	–	10-Gigabit (Symmetric) Passive Optical Network
XT	–	Inter-channel crosstalk

Symbols

T	–	Absolute temperature
κ	–	Adiabatic chirp coefficient
ω	–	Angular frequency
T_b	–	Bit time
R_b	–	Bit rate
K	–	Boltzmann constant
c	–	Complex signal
q	–	Electron charge
F_n	–	Electronic receiver noise factor
Δv	–	Frequency chirp
ϕ	–	Instantaneous phase
I	–	In-phase component
α_H	–	Linewidth enhancement factor or Henry's parameter
R_L	–	Load resistor
f_m	–	Modulation frequency
M	–	Number of symbols
P_{LO}	–	Optical power from local oscillator
Ps	–	Optical received power from transmitter
$\Delta\phi$	–	Phase difference
R	–	Photodiode responsivity
B	–	Post-detection electrical bandwidth
Q	–	Quadrature component
t_r	–	Rise-time
α	–	Roll-off factor
BW	–	Signal bandwidth
η	–	Spectral bandwidth efficiency
σ_{sn}	–	Shot noise standard deviation
T_s	–	Symbol period
R_s	–	Symbol rate
σ_{th}	–	Thermal noise standard deviation

Chapter 1. Introduction

Since Sir Charles K. Kao and George A. Hockham demonstrated the possibility of using optical fibers as a new form of communication medium [1], optical networks have revamped to make possible a modern information society and the evolution of Internet as we known nowadays. These advances and a worldwide deployment of optical fibers, have contributed to the increase in transmission capacity, especially in core networks. However, the continued growth in high-speed services such as voice over IP (VoIP), high definition (HD) video streaming, on-line gaming, among other multimedia services, has focused the attention to the last mile or access network [2]. To sustain the increase in customer bandwidth (BW) demands, and to avoid the last-mile bottleneck, the evolution of optical access networks, particularly of Passive Optical Networks (PONs), has been vital [3].

This chapter introduces the concepts of PONs and Fiber-to-the-Home (FTTH) as the most promising technology to provide broadband services in access networks. Moreover, different PON architectures are discussed and the PON roadmap standardization is reviewed. Afterwards, the main concepts of intensity modulation and direct detection (IM/DD), as well as phase modulation (PM) and coherent detection are explained and compared, due to their key role in the implementation of currently deployed and next generation PONs, respectively. Finally, the motivation and objectives of this PhD thesis are revealed, the organization of the rest of the document is presented, and the publications derived from this thesis are listed.

1.1 Passive Optical Networks (PONs)

The structure of a telecommunication network consists of three main portions: core/backbone network, metro/regional network, and access/last-mile network as shown in Figure 1.1.

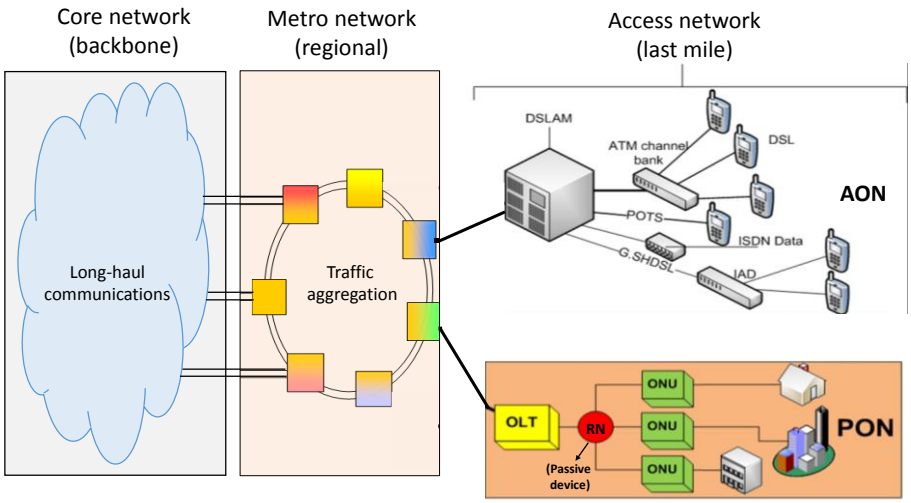

Figure 1.1. Telecommunication infrastructure

Backbone networks are used for long-distance transport and metro/regional networks for grooming and multiplexing functions managing higher aggregated traffic. An optical access network connects the final users to their immediate service provider. At this segment, Fiber-to-the-x (FTTx) technologies, where the "x" typically can stand for Node, Cabinet, Building, or Home, depending on how deep in the field fiber is deployed or how close it is to the costumer, are one of the most deployed alternatives to provide broadband services [4]. Recently, due to the emergence of new standards for CPRI (Common Public Radio Interface) or OBSAI (Open Base Station Architecture Initiative), and with the exponential rise in mobile data consumption, that has led to the deployment of the fourth-generation (4G) radio access networks (RANs) and the envisioning of fifth-generation (5G) mobile networks, the term fiber-to-the-Antenna (FFTA) has been coined, to describe the connection between the Remote Radio Heads (RRH), positioned near to the antennas at the top of the tower, and the Base-band units (BBUs) at the operator premises [5], [6].

With the goal of reducing costs as much as possible, for economically installing optical fiber to bring broadband services to homes, developers invented PONs around 1980's [7]. Nowadays, this approach seems to be a feasible solution for the deployment of next generation wire and mobile networks.

A PON is a type of FTTH deployment, which implements a point-to-multi-point (PtMP) topology, and where much of the equipment located at service premises or Central Office (CO), as well as part of the fiber infrastructure, is shared between multiple user premises.

Compared to an Active Optical Network (AON), where electrical powered switching or routing equipment is used to distribute and collect information to and from users, in a PON an unpowered equipment is used at the distribution network. These characteristics have several advantages in terms of cost, ease of maintenance and upgrading.

A basic PON, as it is depicted in Figure 1.2, establishes connection between the service provider equipment, best-known as Optical Line Terminal (OLT), and the customer premises, where an Optical Network Unit (ONU) is placed. Between them, one or sometimes two feeder optical fibers, a passive Remote Node (RN), and dedicated short drop fibers make up the Optical Distribution Network (ODN).

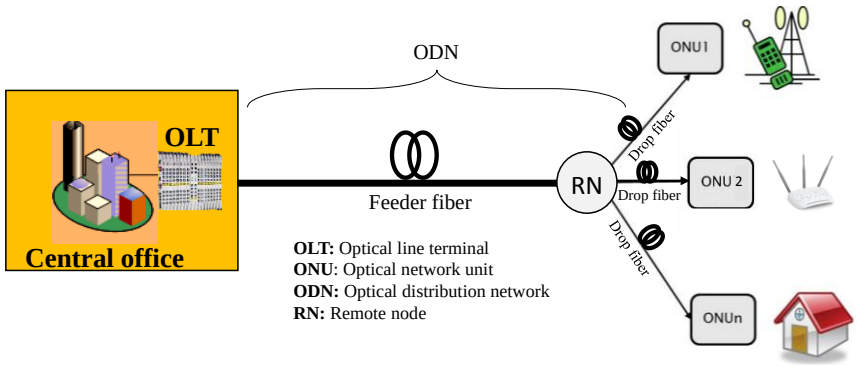

Figure 1.2. PON topology

1.1.1 PON architectures

Over the past years PON architectures have been exploited by many research groups, mainly inspired by time division multiplexing (TDM) and wavelength division multiplexing (WDM) [2], [7], [8]. Next, the main concepts of these architectures are discussed and classified according to the RN that is employed to serve a specific number of customers.

1.1.1.1 Time Division Multiplexing PON (TDM-PON)

A TDM-PON uses a passive power splitter as RN to distribute and combine the traffic to and from the customer premises. In downstream (DS), the signal from the OLT is multiplexed in different time slots and broadcasted to all the ONUs (weak security), where each one recognizes the data through the address labels embedded in the signal. The upstream (US) traffic is transmitted by each ONU in burst mode and in time slots allocated by the OLT,

which must provide additional mechanisms to avoid collisions. To provide bidirectional transmission, one or two fibers transmitting one or two different wavelengths are used [8].

Typically, in a standard commercial TDM-PON structure, the OLT is connected to the ONUs through a 1:32 splitter and the maximum distance covered is usually 20 km. However, in the scientific literature much higher split values, up to 1:4000, have been reported [9]. The splitter losses ($10log_{10}N$ + *Excess losses*) increase with the split ratio (1: N) according to the number of ONUs (N).

Some advantages of TDM are that wavelength agnostic ONUs can be placed without requiring a complex wavelength management control or a large stock. However, the main drawbacks are the reduction of data rate per user and the increase on splitter losses which can be relieved by using reach extenders [10]. PON standards such as EPON, G-PON/E-PON and XG(S)-PON/10G-EPON, use this architecture, which is shown in Figure 1.3(a).

1.1.1.2 Wavelength Division Multiplexing PON (WDM-PON)

A WDM-PON uses a passive WDM filter or Arrayed Wavelength Grating (AWG) as RN [8], with lower losses compared to splitter-based topologies. Signals for different ONUs are carried on independent wavelengths and multiplexed on a shared fiber infrastructure. Each ONU could only receive its own wavelength in case of pre-selected wavelength filters or used tunable components to adapt to a specific DS wavelength, as is shown in Figure 1.3(b). In US, each ONU is also equipped with a laser (tunable or not), creating a logical point-to-point (PtP) connection where each ONU can transmit at its own bit rate (R_b) and dedicated bandwidth.

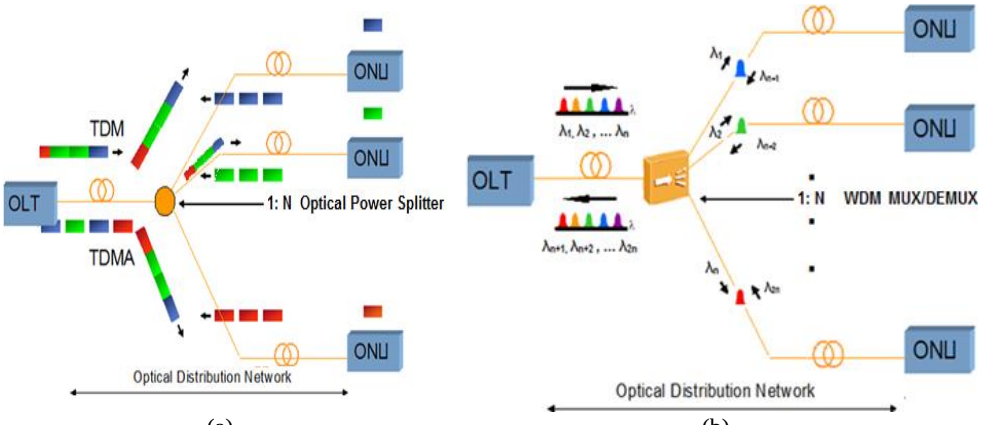

(a) (b)

Figure 1.3. Basic PON architectures: (a) TDM-PON, (b) WDM-PON

WDM has better security than TDM, allowing simple fault localization. In addition, WDM presents better scalability resulting in higher bandwidth capacities and longer reaches. WDM-PON increases the spectral efficiency of the access networks by taking advantage of the high optical bandwidth of optical fibers [11], [12] . However, WDM devices are significantly more expensive and they are limited by the number of wavelengths.

1.1.1.3 Hybrid WDM ring/TDM tree PON and TWDM-PON

To overcome the problems of WDM PONs, different solutions have been developed in the field of hybrid WDM/TDM in the last years. The idea is to mix both concepts to obtain the best of both technologies, accepting more users and increasing the spectrum efficiency. Different proposals such as using 100 ns-λ selective-burst mode transceivers for 40 km reach symmetric 40Gbit/s WDM/TDM-PON [13] or C-band burst-mode transmission for high power budget (64-split with 40km distance) [14], are examples of these hybrid architectures. Other example is SARDANA project developed in the GCO group, where a set of wavelengths is thereby fed together via a common long trunk or ring segment and demultiplexed in remote nodes by WDM demultiplexers, which spreads the data channels towards a bunch of TDM trees. Each tree contains a feeder fiber, a power splitter and short drop fibers, where a same wavelength is shared among multiple ONUs. In this way, a high number of users can be served, requiring low-cost fixed wavelength transceivers at the ONU. This architecture improves the power budget but reduces the overall flexibility of the PON network [15]. Recently another type of hybrid PON called Time and Wavelength Division Multiplexing (TWDM)-PON was proposed by the FSAN and standardized by the ITU as the basic technology of second generation PONs (NG-PON2). In a TWDM-PON, the set of wavelengths that travels through the WDM feeder fiber are broadcasted to all the users using a power splitter as RN and leaving the schedule of the time slots to the media access control (MAC) layer. In this case the ONU should be colorless (wavelength agnostic) and tunable. This could be achieved by using optical filters tuned at specific wavelengths and implementing thermally tuned lasers for transmitting in US. In WDM/TDM, the wavelengths are filtered at the ODN and each of them is routed to a specific TDM tree. Otherwise, an advantage of TWDM is that the ODN does not require a complex configuration and maintenance, using e.g., a power splitter instead of an AWG, keeping compatibility with current Gigabit-capable PON (GPON). Moreover, a colorless ONU reduces the need of stock and then the network costs. A TWDM-PON architecture is shown in Figure 1.4.

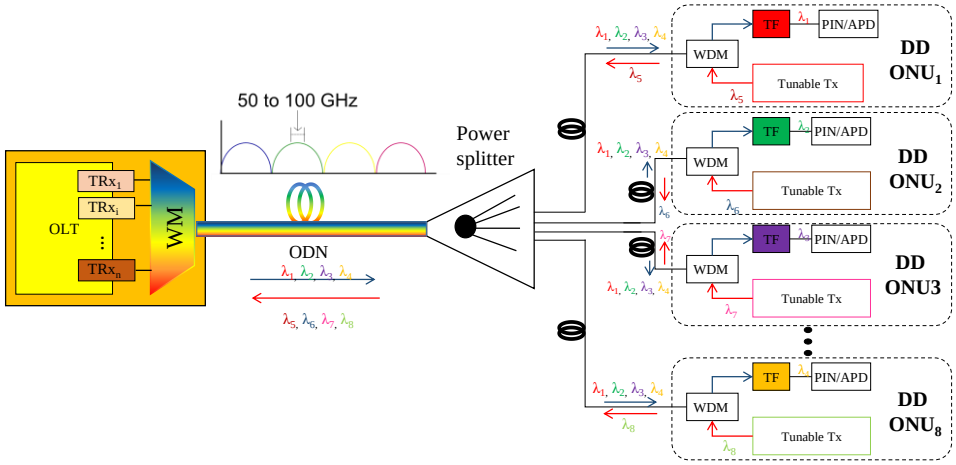

Figure 1.4. Hybrid TWDM-PON architecture

1.1.1.4 Ultra-dense wavelength division multiplexing PON (UDWDM-PON)

A UDWDM-PON is an emergent type of access network that allows to allocate a large number of channels spaced only by a few GHz. To do this possible, and to avoid WDM filters that restrict the channel spacing to higher values in the order of 50GHz or 100GHz, the use of coherent detection is mandatory. In coherent systems, the received signal is mixed with a local oscillator (LO) laser by means of an optical hybrid or coupler. The outputs are proportional to the product of incoming signal and LO optical fields, increasing the wavelength selectivity and the optical power budget above 45dB, and therefore allowing longer reaches of up to 100 km, without optical amplification [16] . Moreover, these characteristics permit to use typical splitter-based topologies and accommodate a larger number of users compared to typical TDM or WDM architectures. In addition, this technology enables the use of advance modulation formats such as QPSK [17] or optical duobinary [18] . A typical UDWDM topology is shown in Figure 1.5.

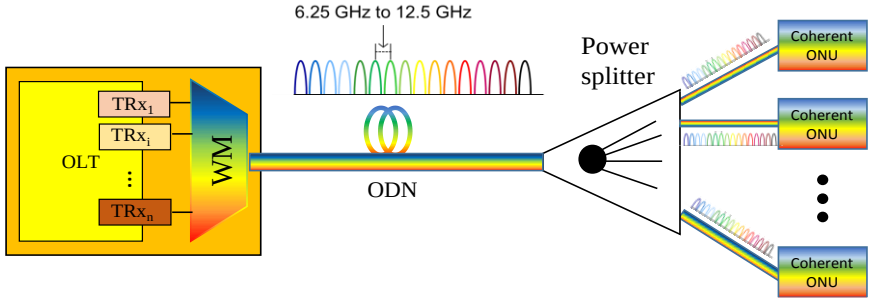

Figure 1.5. UDWDM-PON architecture

1.1.2 PON roadmap and standardization

PONs are the driver for FTTH deployments around the world with approximately 200 million homes passed, and in continuous growth [19]. This makes PON technology and its evolution very important, especially for operators for which the investments in fiber infrastructures represents the largest capital outlay, and with an estimated revenue around $5B in 2015 [7]. Thus, a clear roadmap is not only useful for operators but also for the research community, to know in a time scale, the available technologies and standards that define the potential solutions, and requirements of the access network ecosystem.

First PON standards, before the year 2004, used ATM-based PON (APON and BPON), with aggregate bandwidths in the order of 155 Mbit/s up to 622 Mbit/s. Later, with the use of time division multiplexing (TDM) and Ethernet protocols, aggregated capacities around 2.5 Gbit/s and 1.25 Gbit/s (DS/US respectively) were reached according with the GPON/EPON standards. Nowadays, these are the deployed FTTH solutions [7], [19]. Nevertheless, PON standardization bodies have pushed effort towards higher FTTH capacity systems, causing the arise of Next Generation PONs (NG-PON). By the year 2010, advanced high-speed TDM based optical access systems up to 10 Gbit/s were standardized by ITU (XG-PON) and IEEE (10G-EPON), with asymmetric capacities (DS: 10G & US: 1G) and some field trials were reported [20]. Recently, in recommendation ITU-T G.9807, a 10Gb/s symmetric traffic (XG(S)-PON) solution was standardised [21]. In these systems, the typical guaranteed R_b per user is between 50-300Mb/s, with a shared rate among 32 users and fiber reach about 20km.

To counteract these problems, WDM arose as a solution, allowing transport information through several channels in the same fiber. However, the implementation of pure WDM technology had several hurdles such as the wavelength stability, the need of colorless ONUs and high cost. Several WDM/TDM hybrid architectures were proposed around the year 2010 [22], [23], and research projects such as SARDANA were developed [15], providing service to 1024 users, at 2.5Gbit/s or 10Gbit/s, at distances over 60-100km in a ring+tree topology with remote pumping and access reach up to 20 km. Nevertheless, these capabilities of hybrid architectures have just been recently standardized by the ITU in the new Recommendation ITU-T G.989 [8], where the aggregated bandwidth has been increased significantly until achieving 40-80 Gbit/s, stacking 4 to 8 XG-PON wavelengths and using TDM techniques to provide connectivity to more users and with higher splitting ratios. This new term generation of PONs has been called NG-PON2 and uses the concept of TWDM-PON in which each

wavelength is shared between multiple Optical ONUs by employing TDM. The main challenges of this technology have been the availability of tunable transceivers at ONU, the US burst mode transmission and the need to keep coexistence with legacy PONs [24]. Physical requirements of the standard have been evaluated and the tolerances and performances of different commercial devices compared, particularly for DS transmission [25]. Similarly, a large number of solutions have been recently proposed and tested in bidirectional scenarios [26]–[28].

Until now, all these proposals are based on IM/DD systems limited by higher ODN losses and lower sensitivity performances, and additionally with low optical spectrum efficiencies due to the transmission of single or few wavelengths widely spaced in the fiber. With this in mind, and with the necessity to fulfill the bandwidth demands for higher number of users, some research proposals have been developed. For instance, Cost-effective Coherent Ultra-dense WDM-PON for lambda to the user (COCONUT) project was developed between 2012 and 2016, towards the realization of ultra-dense WDM (UDWDM) PONs, where a considerable number of channels (≥ 256) could be spaced in a 6.25 or 12.5 GHz grid and through dedicated wavelengths, increasing the data rate per user at minimum 1 Gbit/s [29], [30]. The main enabling technologies are coherent systems, with fine wavelength selectivity (without optical filters) and improved sensitivity compared to IM/DD systems. The main objective of COCONUT project was not replacing NG-PON2 technologies, but enhancing NG-PON2 capabilities by increasing the sensitivity and bandwidth efficiency. In this way, it lays the basis towards a future and still undefined PON technology, which could be named the third generation of passive optical networks (NG-PON3). A roadmap summarizing standards, technologies and enablers for PON evolution is shown in Figure 1.6.

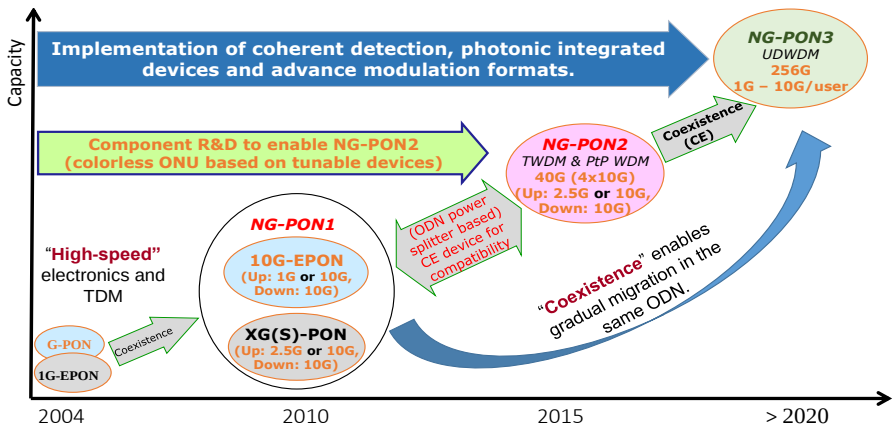

Figure 1.6. PON roadmap

The recommendations published by standardizing bodies like the ITU and the IEEE are described in different documents. These give the guidelines to operators and researchers to look for the appropriate technologies that fulfil and, why not, surpass the minimum requirements in their implementation. Table 1.1 summarizes the PON standards and their main characteristics. An extra-column (NG-PON3) is added not as a standard but for comparison, and as a proposal for a future recommendation.

Table 1.1. Characteristics of PON standards and NG-PON3 proposal.

Standard	**GPON [31]**	**EPON [32]**	**XG(S)-PON[1] [21], [33]**	**10G-EPON [34]**	**NG-PON2 [35]**	**NG-PON3[2]**
Recommen-dation	ITU-T G.984	IEEE 802.3ah	ITU-T G.987 ITU-T G.9807	IEEE 802.3av	ITU-T G.989	-
Year of 1st publication	2003	2004	2010 2018	2009	2014	-
Max. Aggregated capacity (Gb/s) DS/US	2.5 /1.25	1 /1	10/2.5 10/10	10/10	80/20[3] 80/80[4]	256
Multiplexing technology	TDM	TDM	TDM	TDM	TWDM PtP WDM	UDWDM
# wavelengths US/DS	1/1	1/1	1/1	1/1	4-8/4-8	256/256[5]
Channel spacing (GHz)	-	-	-	-	50 - 100	6.25 – 12.5
Split ratio	1:32	1:32	1:64	1:64	1:256	1:256
Min. fiber reach (km)	20	20	20	20	40	100
User data rate	20 – 200 Mb/s	20 – 200 Mb/s	50 – 500 Mb/s	50 – 500 Mb/s	200 – 500 Mb/s	1 Gb/s

These standards occupy different wavelength bands along the optical spectrum. Their distribution is shown in Figure 1.7. Note that due to the inclusion of RF video overlay, the spectral allocation is very restricted, and then new PON solutions must occupy small spectrum

[1] The (S) refers to "Symmetric", a new flavor of XG-PON for symmetric US/DS transmission at 10 Gb/s
[2] Proposal based on results of COCONUT project
[3] Stacking 8 channels asymmetric option
[4] Stacking 8 channels symmetric option
[5] The number of channels will depend on the tunability range of the Tx and LO lasers

portions, with lower guard bands. Then, the proposed UDWDM architecture with coherent technologies and mainly based on Phase Shift Keying (PSK) systems, seems to be a proper solution. However, the coexistence with legacy systems should be a must, to guarantee a smooth and non-restrictive PON evolution. The summary of wavelength bands with the corresponding guard bands is presented in Table 1.2

Table 1.2. PON standards and NG-PON3 proposal characteristics

Standard	Wvalength band (nm)	Guard bands (nm)	
		Lower	Upper
XG(S)-PON/ 10G-EPON	1260 – 1280	-	20
GPON US (Reduced)	1290 – 1330	10	150
GPON US (Narrow)	1300 – 1320	20	160
GPON/EPON DS	1480 – 1500	150-160	24
NG-PON2 TWDM US (wide)	1524 – 1544	24	6
NG-PON2 TWDM US (reduced)	1528 – 1540	28	10
NG-PON2 TWDM US (narrow)	1532 – 1540	32	10
RF-Video	1550 – 1560	6-10	15
XG/10GE-PON DS (indoor)	1575 – 1580	15	16
XG/10GE-PON DS (outdoor)	1575 – 1581	15	15
NG-PON2 TWDM DS	1596 – 1603	15-16	0
NG-PON2 PtP WDM (Expanded)	1524 – 1625	24	-
NG-PON2 PtP WDM (Shared)	1603 – 1625	0	-

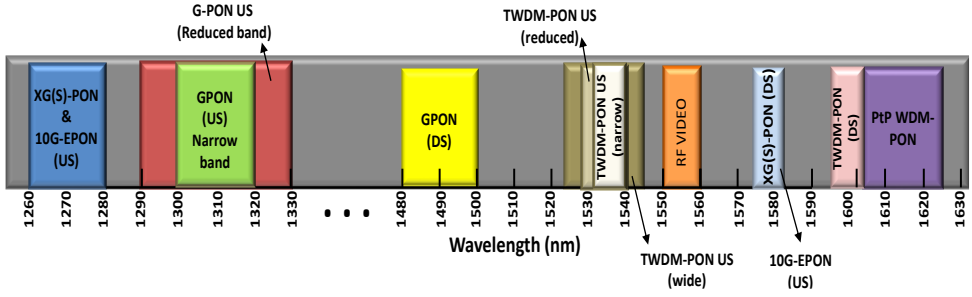

Figure 1.7. Wavelength bands allocation of PON standards

1.2 Intensity modulated/Direct detection (IM/DD) systems

Currently deployed optical fiber communication systems use IM/DD. These systems consist of a laser that is directly (DML) or externally modulated (EML) according to the amplitude of an RF electrical data signal, which switches between a logical "0" representing an "off" state, and a logical "1" representing an "on" state. In direct modulation, the driving current to a semiconductor laser is varied according to the data to be transmitted. In the external modulation, the laser is subjected to a constant bias current emitting a continuous wave (CW), while an external modulator switches the optical power on or off according to the data stream. Direct modulation is simpler but it induces spectrum broadening of the emitted lightwave, known as frequency chirp, that in combination with fiber dispersion, affects the pulse shape degrading the system performance [36]. At higher bit rates, the broadening caused by the chirp limits the reach of the transmission, and then an external amplitude modulator with zero or reduced chirp is typically used.

Once modulated, the optical signal is sent through the fiber, characterized by parameters such as attenuation and dispersion, and arriving to an optical receiver (Rx), composed basically by a photodetector, which converts the incoming optical signal to an electrical one. As consequence of transmission impairments, the signal level is diminished and distorted, so the signal should be amplified and equalized (typically by a low pass filter) prior to data decision. At this point, the level of the detected signal is compared with a suitable threshold for measuring the performance, and to recover the information originally transmitted. Figure 1.8 shows a complete scheme of an IM/DD system, using both, EML and DML.

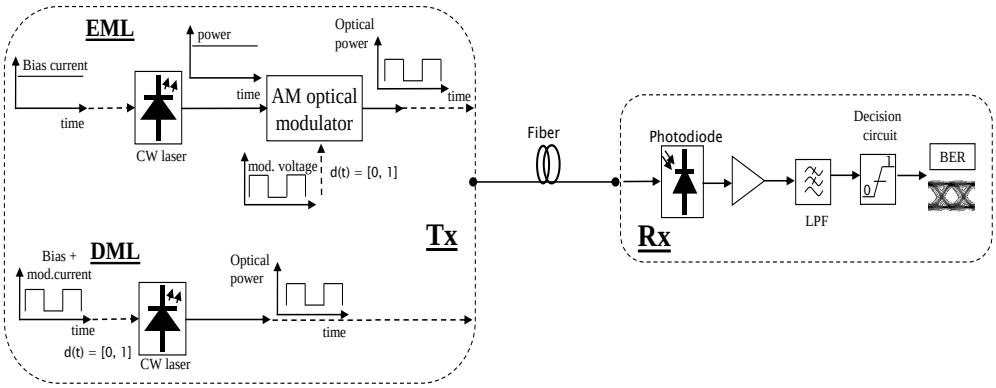

Figure 1.8. IM/DD system. EML: External modulated laser, DML: External modulated laser.

1.2.1 Optical IM transmitter

The output optical signal from the laser can be described by the equation:

$$E_s(t) = A_S(t)e^{j[\omega_s t+\phi_s(t)]} = A_S(t)[cos(\omega_s t + \phi_s(t)) + jsen(\omega_s t + \phi_s(t))] \quad 1.1$$

where $A_s(t)$ is the amplitude, ω_s the frequency and $\phi_s(t)$ the phase of the optical signal. In IM format the information is carried in the amplitude of the signal, while the frequency and the phase are assumed constant. The intensity of the transmitted signal will be represented by:

$$P_s(t) = |A_s(t)|^2 \quad 1.2$$

In IM, also called on-off keying (OOK), a very important parameter to be considered is the extinction ratio (ER), which is the ratio of the two optical power levels of a digital signal generated by the light source. The ER may be expressed as a fraction, in dB, by:

$$ER(dB) = 10\,log\frac{P_1}{P_0} \quad 1.3$$

where P_1 and P_0 are the maximum and minimum optical powers for bits 0 and 1, respectively.

1.2.2 Optical DD receiver

In DD schemes the optical signal is detected by a photodiode (PD) where the photocurrent (I_p) is directly related with the incident optical power ($P_s(t)$) and is given by:

$$I_p(t) = RP_s(t) \quad 1.4$$

where R is the Responsivity of the PD expressed in amperes/watts (A/W).

Afterwards, the signal is normally amplified to maximize the signal to noise ratio (SNR), and low-pass filtered to minimize the effect of intersymbol interference (ISI) and the noise generated in the photodetection and electrical amplification processes, before data decision.

There are mainly two types of noise: shot noise (σ_{sn}), which is always present because of the quantum-nature of light, and thermal noise (σ_{th}), caused by the electronic section of the Rx. Both are white random processes whose variances are determined by [37]:

$$\overline{\sigma^2{}_{sn}} = 2qI_PB \quad 1.5$$

$$\overline{\sigma^2{}_{th}} = \frac{4KTBF_n}{R_L} \quad 1.6$$

where q is the electron charge equal to 1.6×10−19 joules, R_L is the load resistor, K is the Boltzmann constant, F_n is the electronic Rx noise factor of the trans-impedance amplifier, T is the absolute temperature and B is the post-detection electrical bandwidth of the system.

This noise factor, as well as the transmission and fiber impairments, degrades the SNR and in consequence the bit error ratio (BER). The SNR is the ratio between the received power and the noise power generated through the link, plus the noise generated as consequence of photodetection process. For the PIN PD receiver, the SNR may be obtained as [37]:

$$SNR = \frac{(RP_S)^2}{2qB(RP_S) + \frac{4KTBF_n}{R_L}} \quad 1.7$$

In PIN PDs, thermal noise dominates the Rx performance, and then shot noise contribution can be neglected obtaining the thermal noise limit case:

$$SNR_{t\square emal\ noise\ limit} = \frac{R_L R^2 Ps^2}{4KTBF_n} \quad 1.8$$

Finally the corresponding BER considering a Gaussian process can be calculated as [37] :

$$BER = \frac{1}{2} erfc\left(\frac{(SNR)^{\frac{1}{2}}}{2\sqrt{2}}\right) \quad 1.9$$

1.3 Coherent optical systems

Coherent systems provide some advantages over IM/DD systems such as:

- Better sensitivity, due to the use of a LO, generating high power budges and allowing large splitting ratios.
- Increased wavelength selectivity, due to filtering is performed by sharp electrical filters instead of optical filters.
- Use of advanced modulation formats allowing the use of phase, frequency and polarization components of the optical signal, for transmitting more information and for improving the optical spectral efficiency.

Nevertheless, there are some drawbacks that are worth to mention:

- Coherent systems are sensitive to polarization fluctuations in the fiber, then a polarization controller is usually needed.

- Because of the use of a LO, optical hybrids and large number of PDs, coherent Rx are more complex than DD receivers.
- To process higher multilevel formats, coherent systems need high-resolution and high-speed analog to digital converts (ADCs) and digital to analog converters (DACs) which are typically expensive.

Below, the first insight to coherent detection is addressed, and then the basic modulation formats and coherent Rx architectures are discussed.

1.3.1 Ideal coherent system performance

In order to understand the main advantage of coherent systems, it is possible to derive the mathematical description from the Rx scheme shown in Figure 1.9. The LO (typically a laser diode) is a second light source placed at the Rx acting in CW mode and that can be described by:

$$E_{LO}(t) = A_{LO} e^{j(\omega_{LO} t + \phi_{LO}(t))} \quad 1.10$$

where A_{LO} is the amplitude, ω_{LO} the frequency and ϕ_{LO} the phase of the LO signal. As a first approach all these parameters are assumed constant, but in practical scenarios, mainly the phase, can randomly change.

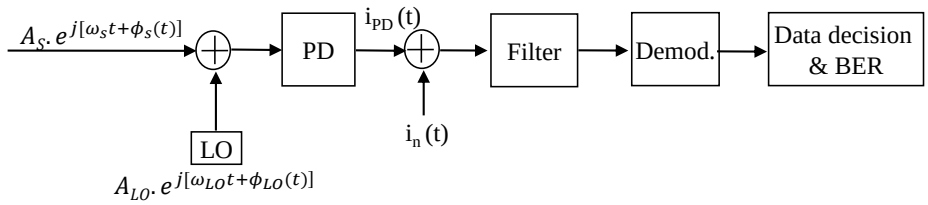

Figure 1.9. Ideal coherent receiver

In practical coherent systems the received signal is mixed with the LO signal by means of an optical hybrid (a term derived from microwave systems). However, at this point, an ideal sum of both signals as well as a frequency and phase matching ($\omega_s = \omega_{LO}$) between both signals are considered.

After mixing, and considering Eq. (1.2) for the incident optical power, following photodetection, from Eq. (1.4) it is possible to assume that the output current is:

$$I_{PD}(t) = R|E_s(t)E_{LO}|^2 = R\left(Ps(t) + P_{LO} + 2\sqrt{Ps(t)P_{LO}}\right) \quad 1.11$$

where again *R* is the Responsivity of the PD expressed in amperes/watts (A/W), and *Ps(t)* and P_{LO} are the optical powers of the received and LO signals, respectively.

Afterwards, $I_{PD}(t)$ is low-pass filtered to limit the noise (shot and thermal) before decision. At the filter output, the SNR, considering a PIN PD, can be calculated as:

$$SNR = \frac{4R^2 P_S P_{LO}}{2qB(RP_{LO}) + \frac{4KTBF_n}{R_L}} \quad 1.12$$

Finally, since usually $P_{LO} >> Ps$, the SNR will be given by [36] :

$$SNR_{shot\ limit} = \frac{2RPs}{qB} \quad 1.13$$

From Eq (1.13), the advantage of coherent detection over DD can be understood. By controlling the LO power, the shot limit case can be achieved even for receivers whose performance is generally dominated by the thermal noise.

The BER depends on the modulation format (ASK, PSK, DPSK, etc), and the coherent scheme used (homodyne, heterodyne or intradyne) as discussed below.

1.3.2 Basic modulation formats

Along this PhD thesis several modulation formats, from binary to multilevel techniques, are used. In this chapter the basic binary formats (ASK and PSK) are commented, while along the other chapters the multilevel schemes will be explained in detail. It is also known, that ASK and PSK can be detected with or without phase tracking. In the first case, coherent optical systems are called synchronous, while in the second case they are known as asynchronous optical systems [38]. In this thesis, asynchronous optical systems are used.

1.3.2.1. Amplitude shift keying (ASK)

The binary amplitude shift keying (ASK) is similar as OOK modulation, and the information is transmitted in the amplitude of the optical signal. Then, in Eq. (1.1), *As(t)* is a variable that takes two possible values 0 and 1, while the frequency and the phase are assumed constant.

Multilevel amplitude modulations formats such as 4-level pulse amplitude modulation (PAM-4) or electrical duobinary (EDB) [39]–[41] have gained interest in TDM-PONs to achieve higher bit rates (≥ 10 G) due to advances in DSP systems, DACs and ADCs technologies.

1.3.2.2. Phase shift keying (PSK)

The binary phase shift keying (BPSK) or simply PSK modulation transmits the information in the instantaneous phase $\phi_s(t)$ of the optical signal with two possible values 0 and π. The amplitude and frequency are constant and then Eq. (1.1) can be expressed by:

$$E_s(t) = A_S e^{j[\omega_s t + \phi_s(t)]} \quad 1.14$$

PSK modulation is very attractive strategy because the increased SNR performance compared with ASK [38], and because it is less affected by fiber nonlinearities due to constant envelope of the signal. The main drawback is concerning the phase detection. The phase can be detected using an optical phase-lock loop (OPLL) system where the LO is synchronized to the incoming carrier [42]. However, this is a complex solution and it demands narrow laser linewidths. An alternative technique is based on simple differential demodulation (multiply and delay operation) where only a two-bit interval is needed, to identify the transmitted data, and where information is carried in the phase difference of two consecutive bits [37] and not in a single instantaneous phase.

1.3.2.3. Differential PSK (DPSK)

As commented before, the optical differential PSK carries data in the phase difference between two consecutive symbols, eluding the need of phase synchronization between Tx and LO lasers [38]. To avoid error propagation at the Rx the transmitted data must be first differentially encoded by using the scheme depicted in Figure 1.10(a). It implements an XNOR operation between the data and a delay version by one-bit period (T_b) of itself. The Rx employs a simple delay and multiply circuit, after photodetection, to find the differential phase as shown in Figure 1.10(b). This Tx and Rx schemes are used in most experiments described along this PhD thesis. The mathematical description of differential demodulation is explained below according to the used Rx scheme.

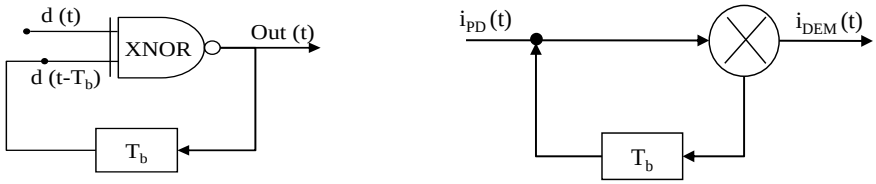

Figure 1.10. Schemes of: (a) differential pre-coder, (b) differential demodulation

1.3.3 Asynchronous coherent receivers

The detection in asynchronous systems is based on the comparison of the power or envelope of the signal, without phase tracking. After optical beating (mix of the received and LO signal) and photodetection, coherent systems can be classified in homodyne, heterodyne or intradyne depending on the use of an intermediate frequency (IF) stage. In a homodyne system, the incoming optical signal is down-converted directly to base-band in the photodetection stage (IF = 0), whereas in heterodyne detection it is down-converted into an IF > BW, where BW is the signal bandwidth. An intradyne system can be considered either a "near-zero" IF heterodyne system, or a homodyne system without phase locking, where IF < BW. An electrical spectral diagram comparing coherent systems is provided in Figure 1.11.

In heterodyne Rx the IF is usually three to five times the base-band signal BW [36], imposing challenges in the BW of the Rx components. Some demonstrations in UDWDM-PONs have shown IF values of only two times base-band signal BW [43], [44], but they continue being larger than for homodyne and intradyne schemes. However, they are easier to implement and then commonly used for detecting both ASK and DPSK modulated data.

System	IF Spectrum	IF
Homodyne		IF = 0 Optical PLL
Intradyne	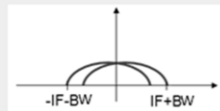	IF < BW
Heterodyne	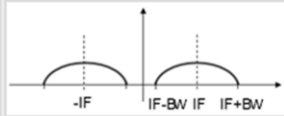	IF > BW

Figure 1.11. Electrical spectrum of asynchronous coherent systems

Below, the mathematical analysis of the three main schemes used along this thesis are explained. They diverge according to the type of optical hybrid used to combine the incoming optical signal containing data information with a LO. In addition, balanced detection schemes are considered instead of single-ended, so that the direct detection (DD) terms can be cancelled and the sensitivity improved.

1.3.3.1. Heterodyne balanced detector for ASK and DPSK signals

Figure 1.12 depicts the Rx heterodyne balanced detector for ASK and DPSK signals. In heterodyne systems, a 3-dB optical coupler is used to combine the incoming and LO signals. This device is also called an 180º optical hybrid because there is a phase difference of 180º between the optical outputs. The Rx scheme depicted below is used in chapter 4 to detect a time interleaved DPSK/ASK signal, where each demodulation stage is performed separately. After data decision, the BER for ASK and DPSK signals could be obtained independently or combined as in section 4.1.

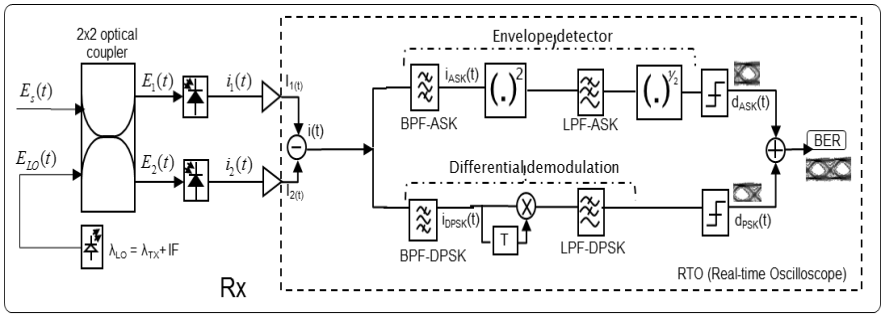

Figure 1.12. Heterodyne asynchronous Rx for ASK and DPSK signals

Assuming identical state of polarization, and for simplicity negligible additive noise, the optical fields of the received and LO signals correspond to the expressions in Eq. (1.14) and Eq. (1.10), respectively. The optical field (E(t)) after coherent mixing, using a 3-dB optical coupler is [38]:

$$E(t) = \begin{bmatrix} E_1(t) \\ E_2(t) \end{bmatrix} = \frac{1}{\sqrt{2}} \begin{bmatrix} 1 & j \\ j & 1 \end{bmatrix} \begin{bmatrix} E_S(t) \\ E_{LO}(t) \end{bmatrix}^{6} \qquad 1.15$$

[6] The matrix $\begin{bmatrix} 1 & j \\ j & 1 \end{bmatrix}$ corresponds to a π-hybrid bidirectional optical coupler and will be used for convenience.

In the photodetection process, the output current is proportional to the incident optical power. According to Eq. (1.11) and Eq. (1.2), with $\omega_{IF} = \omega_S - \omega_{LO}$ and without considering bandwidth limitations, it is possible to arrive to:

$$i_1(t) = \frac{R}{2}\left[P_S(t) + P_{LO} + 2\sqrt{Ps(t)P_{LO}}\, sin(\omega_{IF}t + \phi_s(t) - \phi_{LO}(t))\right] \quad 1.16$$

$$i_2(t) = \frac{R}{2}\left[P_S(t) + P_{LO} - 2\sqrt{P_S(t)P_{LO}}\, sin(\omega_{IF}t + \phi_s(t) - \phi_{LO}(t))\right] \quad 1.17$$

To eliminate the DD terms, both photocurrents $i_1(t)$ and $i_2(t)$ are subtracted as follows:

$$i(t) = i_1(t) - i_2(t) = 2R\sqrt{P_S(t)P_{LO}}\, sin(\omega_{IF}t + \phi_s(t) - \phi_{LO}(t)) \quad 1.18$$

Remember that in Eq (1.14), the additive noise is not considered, but in an experimental case the photodetected current should be band-pass filtered (BPF) around the IF with an equivalent bandwidth *B* to limit the noise before demodulation.

Moreover, in experimental scenarios, the phase of the transmitted signal ($\phi_s(t)$) depends on the phase of the modulating data ($\phi_d(t)$), as well as on the random phase of the optical carrier ($\phi_{ns}(t)$). On the other hand, the LO is an unmodulated laser with a random variable phase ($\phi_{LO}(t) = \phi_{nLO}(t)$). Then, the balanced photodetected current ($i(t)$) is defined by:

$$i(t) = i_1(t) - i_2(t) = 2R\sqrt{P_S(t)P_{LO}}\, sin(\omega_{IF}t + \phi_d(t) + \phi_{ns}(t) - \phi_{nLO}(t)) \quad 1.19$$

At this point and following the proposed Rx scheme of Figure 1.12, the ASK data can be recovered by applying an envelope detector (square, low pass filter and square-root operations), and the DPSK data recovered implementing a differential demodulation scheme.

Envelope detector for ASK signal

For ASK and after squaring the balanced photodetected signal, Eq. (1.19) results in:

$$i_{ASK}(t) = \big(i(t)\big)^2 = 4R^2P_S(t)P_{LO}[sin^2(\omega_{IF}t + \phi_d(t) + \phi_{ns}(t) - \phi_{nLO}(t))] \quad 1.20$$

Applying the following trigonometric identity: $sen^2\theta = \frac{1-cos\,2\theta}{2}$, and after applying a low-pass filter (LPF) around *B*, Eq. (1.20) results in:

$$i_{ASK}(t) = 2R^2P_S(t)P_{LO} \quad 1.21$$

Considering the square-root the final ASK data expression is:

$$i_{ASK}(t) = R\sqrt{2P_{LO}P_S(t)} \quad 1.22$$

Differential demodulation for DPSK signal

To recover the DPSK data, we apply differential demodulation by multiplying the incoming signal by a copy of itself but delayed one-bit period (*T*), equivalent to a bit time ($T = T_b$):

$$d_{DPSK(t)} = i_{DPSK}(t) \cdot i_{DPSK}(t - T_b) \quad 1.23$$

After applying a low-pass filter (LPF) around *B*, the frequencies higher than the data rate can be eliminated, obtaining:

$$d_{DPSK(t)} = 2R^2 P_{LO}\sqrt{P_s(t)P_s(t-T_b)}\,cos(\omega_{IF}T_b + \Delta\phi_d(t) + \Delta\phi_{ns}(t) - \Delta\phi_{nLO}(t)) \quad 1.24$$

Where $\Delta\phi_d(t) - \phi_d(t - T_b)$ represents the phase variations between consecutive symbols, and $\Delta\phi_{ns}(t) = \phi_{ns}(t) - \phi_{ns}(t - T_b)$ and $\Delta\phi_{LO}(t) = \phi_{LO}(t) - \phi_{LO}(t - T_b)$ represent the residual phase noises of the received and LO signals, respectively. Ideally, this residual phase noise between consecutive symbols is negligible [36], thus $\phi_{ns}(t) \cong \phi_{ns}(t - T_b)$ and $\phi_{nLO}(t) \cong \phi_{nLO}(t - T_b)$, obtaining:

$$d_{DPSK(t)} = 2R^2 P_{LO}\sqrt{P_s(t)P_s(t-T_b)}\,cos\big(\omega_{IF}t + \Delta\phi_d(t)\big) \quad 1.25$$

To maximize the decision variable, with binary data and for heterodyne detection, $\omega_{IF}T_b$ must be an integer multiple of 2π, this is, IF should be at least two-times R_b ($2R_b$) to avoid spectral overlapping. Finally, as $cos(\alpha) = cos(2n\pi + \alpha)$, the recovered DPSK data is:

$$d_{DPSK(t)} = 2R^2 P_{LO}\sqrt{P_s(t)P_s(t-T_b)}\,cos\big(\Delta\phi_d(t)\big) \quad 1.26$$

1.3.3.2. Phase diversity Rx using intradyne coherent detection.

Conventional coherent receivers use phase and polarization diversity schemes based on a 90º hybrid optical coupler, in order to recover the in-phase (I) and quadrature (Q) components of the transmitted signal, and to align the polarization of received and LO signals in order to compensate the polarization fluctuations in the fiber [45], [46]. This is especially relevant in order to implement multilevel modulation, where the information symbols are distributed around all the complex plane [47], [48]. However, a 90º optical hybrid is a complex and expensive device that adds cost to the coherent Rx. With the aim of reducing the complexity and the cost of the coherent Rx (i.e., by decreasing the number and the cost of the components), a variation of the aforementioned Rx by replacing the 90° hybrid with a 120º hybrid, also known as 3x3 optical coupler, was proposed by J. Pietzsch [49]. Although the use of such a coupler introduces inherently a small power penalty (about 1.8 dB), this coupler

is more appropriate for mass-scale development and is ideal for low-cost ONU to be installed in access networks. In addition, although the 3x3 Rx is based on single-ended detection, it is possible to perform a linear combination of the electrical currents so that the DD terms can be canceled [50]. Below, a mathematical description of an intradyne detection is presented as fundamental device of most of the tests performed in this PhD thesis.

In this chapter, only DPSK detection is considered as modulation format, however along other chapters multilevel modulation formats like DQPSK, 8-DPSK or hybrid 8-APSK are treated, with minimum changes at demodulation and demmaping stages, which will be explained in due course. In addition, only phase diversity is considered. Some experiments have reported simplified polarization diversity schemes based on 2x2 optical couplers and Alamouti-coding [51], but with heterodyne detection. The topic of polarization diversity is not a scope of this thesis and it is left for further investigation.

Consider the Rx scheme (Figure 1.13), whose front-end is based on a 3x3 optical coupler and 3 PD followed by corresponding trans-impedance electrical amplifiers.

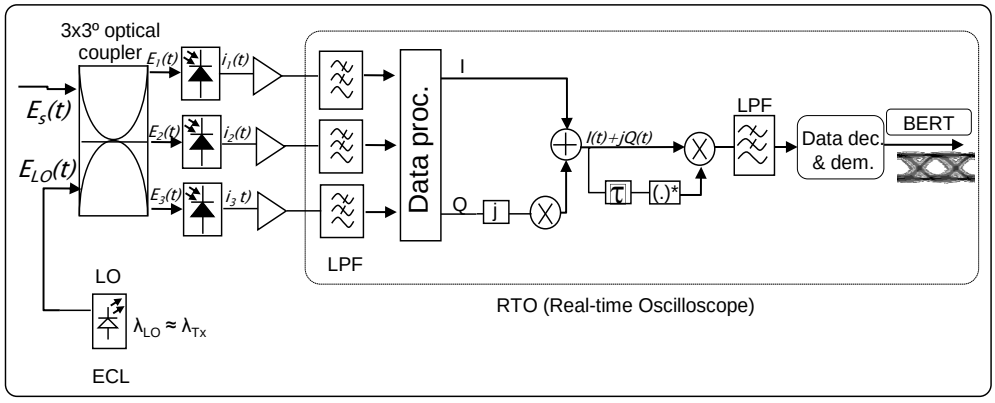

Figure 1.13. Phase diversity Rx using intradyne coherent detection for DPSK signals

Again, and for simplicity, identical state of polarization between received and LO signals, and negligible additive noise are assumed. Considering the optical fields of the received and LO signals described in Eq. (1.14) and Eq. (1.10) respectively, the optical signal after coherent mixing using a 3x3 optical coupler is described by [50]:

$$\begin{bmatrix} E_1(t) \\ E_2(t) \\ E_3(t) \end{bmatrix} = \frac{1}{3}\begin{bmatrix} \alpha & \beta & \beta \\ \beta & \alpha & \beta \\ \beta & \beta & \alpha \end{bmatrix}\begin{bmatrix} E_S(t) \\ 0 \\ E_{LO}(t) \end{bmatrix} \qquad 1.27$$

where the coefficients α and β, of an ideal symmetric 3x3 optical coupler matrix are:

$$\alpha = e^{\frac{-j4\pi}{9}} - e^{\frac{j2\pi}{9}}, \quad \beta = e^{\frac{-j4\pi}{9}} + 2e^{\frac{j2\pi}{9}}$$

After photodetection and without bandwidth limitations the output photocurrents are:

$$\begin{bmatrix} i_1(t) \\ i_2(t) \\ i_3(t) \end{bmatrix} = \frac{R}{3}\begin{bmatrix} |E_S(t)|^2 + |E_{LO}(t)|^2 \\ |E_S(t)|^2 + |E_{LO}(t)|^2 \\ |E_S(t)|^2 + |E_{LO}(t)|^2 \end{bmatrix} + \frac{2R}{3}\begin{bmatrix} |E_S(t)||E_{LO}(t)|\cos\left(\omega_{IF}t + \Delta\phi(t) + \frac{2\pi}{3}\right) \\ |E_S(t)||E_{LO}(t)|\cos\left(\omega_{IF}t + \Delta\phi(t)\right) \\ |E_S(t)||E_{LO}(t)|\cos\left(\omega_{IF}t + \Delta\phi(t) - \frac{2\pi}{3}\right) \end{bmatrix} \quad 1.28$$

Moreover, for intradyne detection $\omega_{IF} \approx 0$, and with $P_s(t) = {A_s}^2(t)$ and $P_{LO} = {A_{LO}}^2$:

$$\begin{bmatrix} i_1(t) \\ i_2(t) \\ i_3(t) \end{bmatrix} = \frac{R}{3}\begin{bmatrix} P_S(t) + P_{LO}(t) \\ P_S(t) + P_{LO}(t) \\ P_S(t) + P_{LO}(t) \end{bmatrix} + \frac{2R}{3}\begin{bmatrix} \sqrt{P_S(t)P_{LO}(t)}\cos\left(\Delta\phi(t) + \frac{2\pi}{3}\right) \\ \sqrt{P_S(t)P_{LO}(t)}\cos\left(\Delta\phi(t)\right) \\ \sqrt{P_S(t)P_{LO}(t)}\cos\left(\Delta\phi(t) - \frac{2\pi}{3}\right) \end{bmatrix} \quad 1.29$$

The first term of Eq. (1.29) represents the direct detection terms and the second the beat components, with a relative phase difference of $2\pi/3$ radians or approximately 120º, between the three photodetected components.

A drawback of this architecture is that it uses single-ended detection compared with the 90º hybrid-based Rx with balanced photodetection. Then, if there are many WDM channels in the network, the direct detection terms become relatively large and must be cancelled to reduce the power noise by interferer channels. Then, to obtain the I and Q components cancelling the DD terms, the following linear operations must be performed [50]:

$$\begin{cases} i_I(t) = i_2(t) - 0.5\left(i_3(t) + i_3(t)\right) = R\sqrt{P_s(t)P_{LO}}\cos(\Delta\phi(t)) \\ i_Q(t) = \frac{\sqrt{3}}{2}(i_3(t) - i_1(t)) = R\sqrt{P_s(t)P_{LO}}\sin(\Delta\phi(t)) \end{cases} \quad 1.30$$

Finally, to recover the transmitted data, the complex samples must be multiplied by the complex conjugate of the previous symbol (differential demodulation) obtaining:

$$d_{DPSK(t)} = [I(t) + jQ(t)][I(t - T_b) - jQ(t - T_b)] \quad 1.31$$

After operating and applying some trigonometric identities it is possible to obtain:

$$d_{DPSK(t)} = R^2 P_{LO}\sqrt{P_s(t)P_s(t - T_b)}\left[\underbrace{\cos\left(\Delta\phi(t) - \Delta\phi(t - T_b)\right)}_{I} + \underbrace{j\sin\left((\Delta\phi(t) - \Delta\phi(t - T_b)\right)}_{Q}\right] \quad 1.32$$

where $\Delta\phi(t) = \phi_s - \phi_{LO}$. Again, in Eq (1.27), additive noise is not considered, however in experimental scenarios the photodetected current should be low-pass filtered around an equivalent bandwidth *B* to reduce the additive noise and crosstalk components. In addition, and considering that the phase noise caused by the random phase variation of the optical carrier and LO have minimum variations between consecutive symbols (ideally negligible) [36], the recovered data can be obtained from:

$$d_{DPSK(t)} = R^2 P_{LO} \sqrt{P_s(t) P_s(t-T_b)} \left[\underbrace{cos\left(\phi_d(t) - \phi_d(t-T_b)\right)}_{I} + \underbrace{j\, sin\left(\phi_d(t) - \phi_d(t-T_b)\right)}_{Q} \right] \quad 1.33$$

1.4 Thesis motivation and objectives

Legacy PON systems, based on IM/DD technologies, provide limited transmission capabilities. The reduced bandwidths may not cope with the demands of new multimedia applications such as online gaming, VoIP, or HD video streaming. Moreover, they run over optical power splitting ODNs, and therefore it is a requirement that new PON systems can re-use the deployed telecom infrastructure splitters. As consequence, this PhD thesis had two major challenges: first, to develop low-cost coherent solutions that improve the sensitivity and bandwidth capacities, and second to guarantee their coexistence with Legacy PONs. Taking these two goals into account and having reviewed the state of the art of optical access networks, a series of specific objectives were proposed:

1. To study different coexistence scenarios between UDWDM-PON, NG-PON2 and legacy PON systems, through theoretical calculations and experimental implementations.
2. To optimize the technique of direct phase modulation of a DFB laser and extend it with Nyquist shaped transmitters, to face the problem of crosstalk between adjacent channels in UDWDM-PONs.
3. To implement multilevel phase modulation formats in UDWM-PONs to achieve higher transmission speeds and better optical spectral efficiencies.
4. To propose simple and flexible transmitters able to provide diverse and reconfigurable services to different class of costumers, implementing hybrid amplitude and phase modulation formats, by using an ordinary DFB laser and a low-cost photonic integrated device such as the DEML.

5. To investigate novel coherent detection schemes aiming at reducing the complexity and cost of conventional coherent receivers.

1.5 Thesis outline

All the pointed objectives are addressed along the next 6 chapters of this document, which has been organized as follows:

Chapter 2 comprises one of the main objectives of this PhD thesis, the study of different coexistence scenarios between different PON systems. First, a theoretical study of the coexistence element (CE) requirements, standardized in the new ITU-T G.989 recommendation is presented. Then, the concept of Wavelength-to-the-User is demonstrated with the presentation of the main results of the European COCONUT project, especially those where the author contributed.

In Chapter 3, a simple digital equalization technique is proposed to perform direct phase modulation of a commercial DFB laser. Moreover, the concern of crosstalk between adjacent channels emitting at different optical powers in UDWDM-PON is studied. To overcome this problem, the use of Nyquist pulse shaping at the Tx is proposed and evaluated through numerical simulations and experimental tests.

Chapter 4 describes the extension of the optimized DPSK modulation to multilevel formats, for achieving higher bit rates as well as better spectral efficiencies. Three well know schemes, DQPSK, Optical duobinary and 8-DPSK are studied and compared in terms of Rx sensitivity and channel bandwidth utilization.

Chapter 5 puts forward two versatile implementations of hybrid modulation formats. First, a time-domain hybrid format (TDHF), which combine ASK and DPSK signals in the same bit period is demonstrated, and the transmitted signal detected with a balanced heterodyne coherent Rx. Afterwards, a novel application of a photonic integrated DEML is experimentally demonstrated, transmitting a multilevel amplitude and direct phase modulated optical signal to achieve a low-cost 10 Gb/s transmitter.

Chapter 6 deals with the complexity and cost of conventional coherent receivers. First, the use of only one DFB laser as DPSK optical transmitter and at the same time as LO, is proposed at the ONU. Secondly, and for the first time, a novel phase time diversity technique alternating phase modulated signals in both I and Q components, is designed and experimentally

demonstrated, reducing the ONU components of an intradyne coherent Rx to only 1 PD per polarization, and additionally with polarization independence.

Finally, in chapter 7, the conclusions of this doctoral research are summarized and some proposals for further studies are stated to implement versatile and cost-effective optical metro-access networks.

1.6 Author publications

1.6.1. Published works

1. J. Camilo Velásquez, J. Tabares, J. Prat, "*Differential 8-APSK monolithically integrated Dual-EML transmitter for flexible coherent PONs*", OSA Optic Letters, vol. 44, no. 11, pp. 2760 – 2763. June. 1, 2019.
   DOI: 10.1364/OL.44.002760

2. J. Camilo Velásquez, M. Domingo, V. Polo, and J. Prat, "*Time Interleaved DPSK/ASK Transmitter with Directly Beat Modulated DFB for Coherent WDM-PON*", in Proc. 44th European Conference on Optical Communication (ECOC-2018), p. We2.69, Rome, Italy. Sep. 23 – 27, 2018.
   DOI: 10.1109/ECOC.2018.8535143

3. J. Camilo Velásquez, I. Cano, J. Tabares, V. Polo and J. Prat, "*Direct Phase Modulation for UDWDM ONU with Beat Signals*", in 20th International Conference on Transparent Optical Networks (ICTON-2018), p. Th.B1.2, Bucharest, Romania. Jul. 1 – 5, 2018.
   DOI: 10.1109/ICTON.2018.8473615

4. J. Camilo Velásquez, J. Tabares, Iván. N. Cano & J. Prat, "*1.25 - 2.5 Gb/s Simple Nyquist Transmitters for Coherent UDWDM-PON with Enhanced Spectral Efficiency*", Integrated and Fiber Optics (FIOP), vol. 64, no. 4, pp. 219 – 228. Apr. 19, 2018.
   DOI: 10.1080/01468030.2018.1461281

5. J. Camilo Velásquez, M. Domingo, V. Polo and J. Prat, "*Simultaneous DPSK-ASK Modulated Dual-EML Transmitter for Coherent UDWDM-PON*", in Proc. Optical Fiber Communication Conference and Exhibition (OFC-2018), p. M3B.4, San Diego (CA), USA Mar. 11 – 15, 2018.
   DOI: 10.1364/OFC.2018.M3B.4

6. J. Camilo Velásquez, Iván. N. Cano, V. Polo, M. Domingo, J. Prat, "*15 dB Differential Link-Loss UDWDM-PON with Direct Beat Phase Modulated DFB*", IEEE Photonics Technology Letters (PTL), vol. 30, no. 2, pp. 137 – 140. Jan. 15, 2018.
DOI: 10.1109/LPT.2017.2776738

7. M. Presi, M. Artiglia, F. Bottoni, M.Ranello, I. N. Cano, J. Tabares, J. C. Velásquez, S. Ghasemi, V. Polo, G. Y. Chu, , J. Prat, G.Azcárate, R. Pous, C. Vilà, H. Debrégeas, A. Rafel, E. Ciaramella,, "*Field-Trial of a High-Budget, Filterless, λ-to-the-User, UDWDM-PON Enabled by an Innovative Class of Low-Cost Coherent Transceivers*", IEEE/OSA, Journal of Lightwave Technology (JLT), vol. 35, no. 23, pp. 5250 – 5259. Dec. 1, 2017.
DOI: 10.1109/JLT.2017.2748597

8. J. Camilo Velásquez, J. Tabares, Iván. N. Cano, V. Polo and J. Prat, "*Coherent Nyquist UDWDM-PON with 2.5 Gb/s/user and 15 dB Differential Link-Loss*", in 2017 International Workshop on Fiber Optics in Access Network (FOAN-2017), Munich, Germany. Nov. 6 – 8, 2017.
DOI: 10.1109/FOAN.2017.8215249

9. M.Ranello, I. N. Cano, J. Tabares, J. C. Velásquez, S. Ghasemi, V. Polo, G. Y. Chu, , J. Prat, R. Pous, G.Azcárate, C. Vilà, H. Debrégeas, A. Rafel, F. Bottoni, M. Presi, E. Ciaramella,, "*Field-trial of a λ-to-the-user high-budget PON using a novel class of low-cost coherent transceivers and compatible with EPON system operation*", in 19th International Conference on Transparent Optical Networks (ICTON-2017), p. Tu.B1.3, Girona, Spain. Jul. 2 – 6, 2017.
DOI: 10.1109/ICTON.2017.8025154

10. I. Cano, J. Camilo Velásquez, V. Polo and J. Prat, "*Bidirectional Real-Time DSP-less Heterodyne UDWDM-PON*", in 19th International Conference on Transparent Optical Networks (ICTON-2017), p. Tu.B2.5, Girona, Spain. Jul. 2 – 6, 2017.
DOI: 10.1109/ICTON.2017.8024856

11. J. Camilo Velásquez, Iván. N. Cano, V. Polo and J. Prat, "*Direct Beat Phase Modulated DFB for flexible 1.25-5 Gb/s Coherent UDWDM-PONs*", in Proc. Optical Fiber Communication Conference and Exhibition (OFC-2017), p. Th2A.32, Los Angeles (CA), USA.Mar. 19 – 23, 2017.
DOI: 10.1364/OFC.2017.Th2A.32

12. Iván. N. Cano, J. Camilo Velásquez, V. Polo and J. Prat, "*10 Gbit/s Phase Time Diversity Directly Modulated DFB with Single-PD Intradyne Receiver for Coherent WDM-PON*", in 43th European Conference on Optical Communication (ECOC-2016), p. W.4.P1.SC1.3, Düsseldorf, Germany. Sep. 18 – 22, 2016.

13. I. N. Cano, J. Prat, J. Tabares, J. C. Velásquez, S. Ghasemi, V. Polo, G. Y. Chu, M. Presi, E. Ciaramella, M.Ranello, F. Bottoni, M. Artiglia, G. Cossu, R. Pous, G.Azcárate, C. Vilà, H. Debrégeas, G. Vall-lossera, A. Rafel, "*Field-Trial of Low-Cost Coherent UDWDM-PON with Real-Time Processing, λ-Monitoring and EPON Coexistence*", in 43th European Conference on Optical Communication (ECOC-2016), p. M.1.E.5, Düsseldorf, Germany. Sep. 18 – 22, 2016.

14. V. Sales, J. Segarra, V. Polo, J. Camilo Velásquez and J. Prat, "An UDWDM-PON using low-cost coherent transceivers with limited tunability and heuristic DWA", IEEE/OSA Journal of Optical Communications and Networking (JOCN), vol. 8, no. 8, pp. 582 – 599. Jul. 26, 2016.
DOI: 10.1364/JOCN.8.000582

15. I. Cano, J. Camilo Velásquez, V. Polo and J. Prat, "*Multilevel Direct DFB Phase Modulation in 6.25GHz Spectrally Spaced UDWMD PONs*", in 18th International Conference on Transparent Optical Networks (ICTON-2017), p. Mo.B2.1, Trento, Italy. Jul. 10 – 14, 2016.
DOI: 10.1109/ICTON.2016.7550260

16. J. Prat, I. N. Cano, M. Presi, J. Tabares, M.Ranello, J. C. Velásquez, F. Bottoni, S. Ghasemi, V. Polo, G. Y. Chu, M. Artiglia, R. Pous, G.Azcárate, C. Vilà, H. Debrégeas, E. Ciaramella, "*Ultra-dense WDM Access Network Field Trial*", in 2016 21st European Conference on Networks and Optical Communications (NOC-2016), Lisbon, Portugal. Jun. 1 – 3, 2016.
DOI: 10.1109/NOC.2016.7506996

17. Iván N. Cano, F. Bottoni, J.Camilo Velásquez, Marco Presi, E. Ciaramella, J.Prat, "*Bidirectional Coherent PON with ONU Based on Reused Direct-Modulated LO*", in Proc. Optical Fiber Communication Conference and Exhibition (OFC-2016), p. M3C.7, Anaheim (CA), USA. Mar. 20 – 24, 2016.
DOI: 10.1364/OFC.2016.M3C.7

18. Iván N. Cano, J.Camilo Velásquez, J. Prat, "*7.5 Gb/s Direct DFB Phase Modulation with 8-DPSK for 6.25GHz Spaced Coherent UDWDM PONs*", in Proc. Optical Fiber Communication Conference and Exhibition (OFC-2016), p. M3C.4, Anaheim (CA), USA. Mar. 20 – 24, 2016.
    DOI: 10.1364/OFC.2016.M3C.4

1.6.2. Submitted works

1. J. Prat, J. Camilo Velásquez, and J. Tabares, "*Direct PSK-ASK Modulation for Coherent udWDM*", to 21th International Conference on Transparent Optical Networks (ICTON-2019), [Invited], Angers, France. Jul. 9 – 13, 2019.
2. J. Tabares, J. Camilo Velásquez, A. Napoli, and J. Prat, "Direct Amplitude-Phase Modulated Dual EML 10 Gb/s Optical Transmitter", to 45th European Conference on Optical Communication (ECOC-2019), Dublin, Ireland. Sep 22 – 26, 2019.

Bibliography Chapter 1

[1] C. K. Kao and G. A. Hockham, "Dielectric-fibre surface waveguides for optical frequencies," *Proc. Inst. Electr. Eng.*, vol. 113, no. 7, pp. 1151–1158, Jul. 1966.

[2] L. G. Kazovsky, W.-T. Shaw, D. Gutierrez, N. Cheng, and S.-W. Wong, "Next-Generation Optical Access Networks," *J. Light. Technol.*, vol. 25, no. 11, pp. 3428–3442, Nov. 2007.

[3] J. Prat, Ed., *Next-generation FTTH passive optical networks: research towards unlimited bandwidth access*. Dordrecht: Springer, 2008.

[4] C. F. Lam, *Passive Optical Networks: Principles and Practice*. Boston: Elsevier Inc, 2007.

[5] VIAVI Solutions, "Fiber to the Antenna (FTTA). State of the art FTTA testing solutions from VIAVI," 07-May-2019. [Online]. Available: https://www.viavisolutions.com/en-us/fiber-antenna-ftta. [Accessed: 07-May-2019].

[6] J. Segarra, V. Sales, and Prat, Josep, "Versatile metro-access network integrating FTTH, enterprises, IoT and 5G services [Invited]," in *Proc. 21st Int. Conf. on Transp. Opt. Netw. (ICTON)*, Angers, France, 2019.

[7] D. Nesset, "PON Roadmap [Invited]," *J. Opt. Commun. Netw.*, vol. 9, no. 1, pp. A71–A76, Jan. 2017.

[8] E. Wong, "Next-Generation Broadband Access Networks and Technologies," *J. Light. Technol.*, vol. 30, no. 4, pp. 597–608, Feb. 2012.

[9] I. Van de Voorde, C. M. Martin, I. Vandewege, and X. Z. Oiu, "The superPON demonstrator: an exploration of possible evolution paths for optical access networks," *IEEE Commun. Mag.*, vol. 38, no. 2, pp. 74–82, Feb. 2000.

[10] R. Kjaer, I. Monroy, L. Oxenlowe, P. Jeppesen, and B. Palsdottir, "Bi-directional 120 km Long-reach PON Link Based on Distributed Raman Amplification," in *2006 IEEE LEOS Annual Meeting Conference Proceedings*, Montreal, QC, Canada, 2006.

[11] N. Cheng and F. Effenberger, "WDM PON: systems and technologies," in *Proc. 36th Eur. Conf. on Opt. Commu. (ECOC)*, Torino, Italy, 2010.

[12] K. Grobe and J.-P. Elbers, "PON in adolescence: from TDMA to WDM-PON," *IEEE Commun. Mag.*, vol. 46, no. 1, pp. 26–34, Jan. 2008.

[13] K. Taguchi, H. Nakamura, K. Asaka, S. Nakano, S. Kimura, and N. Yoshimoto, "100-ns λ-selective burst-mode transceiver for 40-km reach symmetric 40-Gbit/s WDM/TDM-PON," in *Proc. 36th Eur. Conf. on Opt. Commu. (ECOC)*, London, UK, 2013.

[14] S. Ihara *et al.*, "Experimental demonstration of C-band burst-mode transmission for high power budget (64-split with 40km distance) TWDM-PON systems," in *Proc. 39th Eur. Conf. on Opt. Commu. (ECOC)*, London, UK, 2013.

[15] J. Prat *et al.*, "Results from EU project SARDANA on 10G extended reach WDM PONs," in *Proc. Opt. Fiber Commu. Conf. (OFC)*, San Diego, CA, USA, 2010.

[16] H. Rohde, S. Smolorz, E. Gottwald, and K. Kloppe, "Next generation optical access: 1 Gbit/s for everyone," in *Proc. 35th Eur. Conf. on Opt. Commu. (ECOC)*, Viena, Austria, 2009.

[17] I. N. Cano, A. Lerin, and J. Prat, "DQPSK Directly Phase Modulated DFB for Flexible Coherent UDWDM-PONs," *IEEE Photonics Technol. Lett.*, vol. 28, no. 1, pp. 35–38, Jan. 2016.

[18] I. N. Cano, A. Lerin, M. Presi, V. Polo, E. Ciaramella, and J. Prat, "6.25Gb/s differential duobinary transmission in 2GHz BW limited direct phase modulated DFB for udWDM-PONs," in *Proc. 40th Eur. Conf. on Opt. Commu. (ECOC)*, Cannes, France, 2014.

[19] F. J. Effenberger, "Industrial Trends and Roadmap of Access," *J. Light. Technol.*, vol. 35, no. 5, pp. 1142–1146, Mar. 2017.
[20] S. Jain *et al.*, "World's First XG-PON Field Trial," in *Proc. Opt. Fiber Commu. Conf. (OFC)*, San Diego, California, 2010.
[21] International Telecommunication Union, "ITU-T G.9807.1 Recommendation: 10-Gigabit-capable symmetric passive optical network (XGS-PON)." 06/16.
[22] J. Prat *et al.*, "Hybrid ring-tree WDM/TDM-PON optical distribution network," in *Proc. 11st Int. Conf. on Transp. Opt. Netw. (ICTON)*, Ponta Delgada, Portugal, 2009.
[23] G. Das, B. Lannoo, D. Colle, M. Pickavet, and P. Demeester, "A hybrid WDM/TDM PON architecture using wavelength selective switches," in *2010 IEEE 4th International Symposium on Advanced Networks and Telecommunication Systems*, Mumbai, India, 2010.
[24] H. Roberts, N. Proite, P. Lee, and C. Smith, "Lessons Learned from NG-PON2 Systems Developments and Deployment," in *Proc. Opt. Fiber Commu. Conf. (OFC)*, San Diego, CA, USA, 2019.
[25] J. Camilo Velásquez, "Analysis of performances and tolerances of the second generation passive optical networks (NG-PON2) for FTTH systems," Master thesis, Universitat Politecnica de Catalunya, Castelldefels, Spain, 2014.
[26] Y. Guo, S. Zhu, G. Kuang, Y. Yin, D. Zhang, and X. Liu, "Demonstration of a Symmetric 40 Gbit/s TWDM-PON Over 40 km Passive Reach Using 10 G Burst-Mode DML and EDC for Upstream Transmission [Invited]," *J. Opt. Commun. Netw.*, vol. 7, no. 3, p. A363, Mar. 2015.
[27] Zhengxuan Li *et al.*, "Symmetric 40-Gb/s, 100-km Passive Reach TWDM-PON with 53-dB Loss Budget," *J. Light. Technol.*, vol. 32, no. 21, pp. 3991–3998, Nov. 2014.
[28] L. Yi, Z. Li, M. Bi, W. Wei, and W. Hu, "Symmetric 40-Gb/s TWDM-PON With 39-dB Power Budget," *IEEE Photonics Technol. Lett.*, vol. 25, no. 7, pp. 644–647, Apr. 2013.
[29] "COst-effective COhereNt Ultra-dense-WDM-PON for lamda-To-the-user access." [Online]. Available: http://www.ict-coconut.eu.
[30] M. Presi *et al.*, "Field-Trial of a High-Budget, Filterless, λ -to-the-User, UDWDM-PON Enabled by an Innovative Class of Low-Cost Coherent Transceivers," *J. Light. Technol.*, vol. 35, no. 23, pp. 5250–5259, Dec. 2017.
[31] International Telecommunication Union, "ITU-T G.984.1 Recommendation: Gigabit-capable passive optical networks (GPON): General characteristics." Mar-2008.
[32] The Institute of Electrical and Electronics Engineers, Inc, "IEEE 802.3ah Standard for Local and metropolitan area networks. Ethernet in the First Mile (EFM): 1G-EPON." 2004.
[33] International Telecommunication Union, "ITU-T G.987 Recommendation: 10-Gigabit-capable passive optical network (XG-PON) systems: Definitions, abbreviations and acronyms." 2012.
[34] The Institute of Electrical and Electronics Engineers, Inc, "IEEE 802.3av-2009 - IEEE Standard for Information technology-- Local and metropolitan area networks-- Specific requirements-- Part 3: CSMA/CD Access Method and Physical Layer Specifications." 2009.
[35] International Telecommunication Union, "ITU-T G.989.2 Recommendation, 40-Gigabit-capable passive optical networks (NG-PON2): Physical Media Dependent Layer Specification." 2018-2014.
[36] L. Kazovsky, A. E. Willner, and S. Benedetto, *Optical Fiber Communication Systems*. Boston: Artech House Publishers, 1996.
[37] J. Senior, *Optical Fiber Communications: Principles and Practice*, Edición: Revised. Harlow, England ; New York: Prentice Hall, 2008.

[38] K.-P. Ho, *Phase-modulated optical communication systems*. New York: Springer, 2005.
[39] Y. Fu, K. Zhang, M. Bi, and W. Hu, "Multi-Dimensional Coded PAM4 Modulation for TDM-PON based on 10G Optical Devices," in *Proc. Asia Comm. and Phot. Conf.*, Wuhan, China, 2016.
[40] C. Sun, S. H. Bae, and H. Kim, "Transmission of 28-Gb/s Duobinary and PAM-4 Signals Using DML for Optical Access Network," *IEEE Photonics Technol. Lett.*, vol. 29, no. 1, pp. 130–133, Jan. 2017.
[41] D. T. van Veen and V. E. Houtsma, "Proposals for Cost-Effectively Upgrading Passive Optical Networks to a 25G Line Rate," *J. Light. Technol.*, vol. 35, no. 6, pp. 1180–1187, Mar. 2017.
[42] J. G. Proakis, *Digital Communications*, 4th ed. Boston, MA: McGrawHill, 2001.
[43] I. N. Cano, A. Lerín, V. Polo, and J. Prat, "Simplified Polarization Diversity Heterodyne Receiver for 1.25Gb/s Cost-Effective udWDM-PON," in *Proc. Opt. Fiber Commun. Conf. (OFC)*, San Francisco, CA, USA, 2014.
[44] I. N. Cano, J. C. Velasquez, V. Polo, and J. Prat, "Bidirectional real-time DSP-less heterodyne UDWDM-PON," in *Proc. 19th Int. Conf. on Transp. Opt. Netw. (ICTON)*, Girona, Spain, 2017.
[45] S. J. Savory, "Digital Coherent Optical Receivers: Algorithms and Subsystems," *IEEE J. Sel. Top. Quantum Electron.*, vol. 16, no. 5, pp. 1164–1179, Sep. 2010.
[46] D. Lavery, R. Maher, D. S. Millar, B. C. Thomsen, P. Bayvel, and S. J. Savory, "Digital Coherent Receivers for Long-Reach Optical Access Networks," *J. Light. Technol.*, vol. 31, no. 4, pp. 609–620, Feb. 2013.
[47] P. J. Winzer and R.-J. Essiambre, "Advanced Optical Modulation Formats," *Proc. IEEE*, vol. 94, no. 5, pp. 952–985, May 2006.
[48] S. Tsukamoto, K. Katoh, and K. Kikuchi, "Coherent demodulation of optical multilevel phase-shift-keying signals using homodyne detection and digital signal processing," *IEEE Photonics Technol. Lett.*, vol. 18, no. 10, pp. 1131–1133, May 2006.
[49] J. Pietzsch, "Scattering matrix analysis of 3*3 fiber couplers," *J. Light. Technol.*, vol. 7, no. 2, pp. 303–307, Feb. 1989.
[50] C. Xie *et al.*, "Colorless coherent receiver using 3x3 coupler hybrids and single-ended detection," *Opt. Express*, vol. 20, no. 2, pp. 1164–1171, Jan. 2012.
[51] M. S. Erkilinc *et al.*, "Comparison of Low Complexity Coherent Receivers for UDWDM-PONs (λ-to-the-user)," *J. Light. Technol.*, vol. 36, no. 16, pp. 3453–3464, Aug. 2018.

Chapter 2. Coexistence between UDWDM-PON, NG-PON2, and legacy PONs

One of the most important network operator requirements for the deployment of next generation optical access networks is the coexistence with legacy systems [1], [2]. Coexistence refers to the ability for two or more system generations to operate simultaneously on a common fiber section [1]. To achieve this goal, the system should be scalable to increase the capacity when service demands grow and to support some degree of flexibility that maximizes the use of free spectrum. Furthermore, the system should serve different types of costumers (e.g, business or residential) depending on the addressed market [2]. This flexibility enable different coexistence scenarios on the same ODN, aiming at reducing the infrastructure cost, and easing a smooth and non-disruptive migration towards new PON systems.

In this chapter, an analysis of the coexistence between the recently standardized NG-PON2 solution and legacy systems as GPON is evaluated in section 2.1. The availability of wavelength spectrum bands is analyzed as well as the use of the Coexistence Element (CE), a key component to guarantee compatibility between the different PON systems. Afterwards, section 2.2 introduces the concept of Wavelength to the User (WTTU) in the framework of COCONUT project [3], [4]. As well, cost-efficient ONU/OLT architectures are discussed and a wavelength plan is presented to guarantee coexistence with NG-PON2 and other legacy systems. Finally, in section 2.3, two real-time experiments are described, including the field-trial of the COCONUT project, demonstrating an innovate class of transceivers which could support 1 Gb/s per user in a UDWDM-PON with channels spaced only 6.25 GHz [5]–[7]. With these results, the proposed solution could be applied either to enhance certain features of the NG-PON2 solution [8] or in a future NG-PON3 system [1], [9].

2.1 Coexistence between NG-PON2 and legacy PONs

To achieve coexistence between different systems, the availability of wavelength spectrum bands must be considered, as well as, the use of proper isolating devices, at both OLT and ONU premises. In ITU-T PON standards, and particularly in NG-PON2, the use of appropriate wavelength blocking filters (WBF) at the ONU, and a wavelength band filter, named as CE, are essential to properly isolate all the systems operating in the same ODN.

CE (also named WDM1r or CEM, according to PONs coexistence scenario) is defined in ITU-T G.989 Recommendation (Rec.) [10] as a bidirectional functional element used to provide inter-PON connectivity for multiple PON systems in the same ODN. Technical parameters are contained in ITU-T Rec. G.984.5 [11] and its amendment [12]. Figure 2.1 depicts the functional optical access network architecture and reference points for NG-PON2 system coexisting with legacy systems. The ODN consists of the power splitter and the CE. Optionally, reach extenders defined in ITU-T Rec. G.984.6 [13], could be included, however they are not taken into account here for the coexistence analysis.

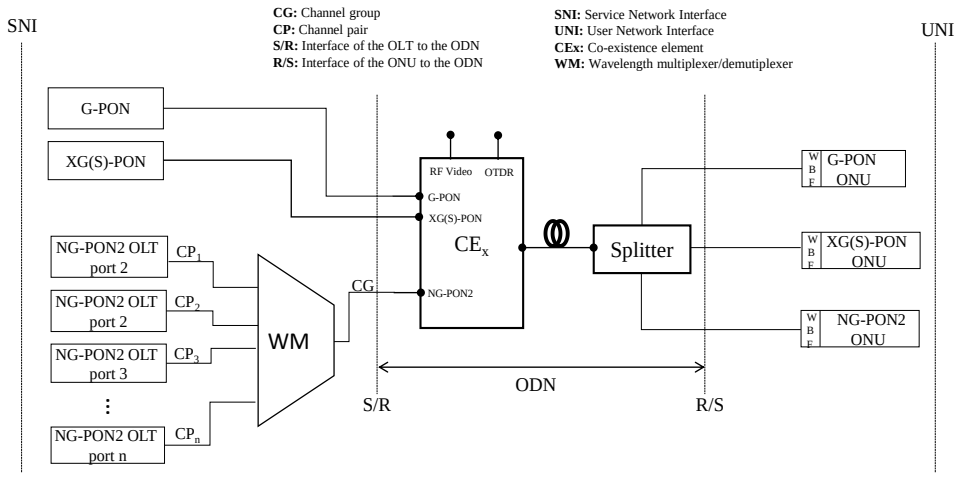

Figure 2.1. Reference architecture and points for NG-PON2 system coexisting with legacy systems

Because of the optical technologies specified for NG-PON2 shall be compatible with legacy power splitting ODNs and, at the same time, they should be flexible in terms of capacity when needed (pay as you grow) [1], [14], a non-wavelength-selective ODN was preferred by some operators [2], and finally adopted in NG-PON2 coexistence scenario with legacy PON systems. Nevertheless, the advantages of low splitting losses and physical security in

wavelength-selective ODNs should be considered in greenfield scenarios (also supported by NG-PON2), which may implement wavelength filters only, or a combination of both wavelength and power splitters [15].

Then, diverse coexistence scenarios can be implemented according to operator needs, and the CE requirements, in terms of insertion losses (ILs) and per port isolation. The values depend on the legacy PON systems (GPON, XG(S)-PON and NG-PON-2) coexisting, and the wavelength bands defined per each of them. As an example, the scenario where GPON, XG-PON and NG-PON2 (TWDM and PtP WDM PON) need to coexist is analyzed, as depicted in Figure 2.2.

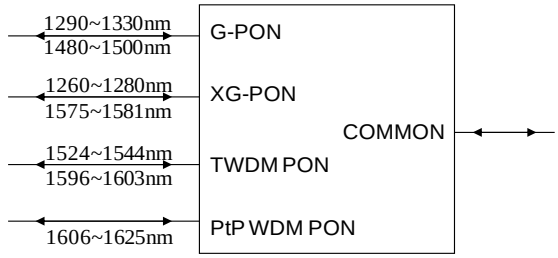

Figure 2.2. Scheme of a CE with G-PON, XG-PON and NG-PON2 (shared spectrum) coexistence

The maximum IL per port ranges from 0.8 dB to 1.3 dB between the filter common port and the port defined NG-PON2 and each legacy system. Table 2.1 summarizes these values standardized in ITU-T Rec. G-984.5 [11].

Table 2.1. CE sample parameters for G-PON, XG-PON, and NG-PON2 (shared spectrum) coexistence

Specification	Value
Loss without connectors for G-PON bands	≤0.8 dB (1290-1330 nm and 1480-1500 nm)
Loss without connectors for XG-PON1 bands	≤1.1 dB (1260-1280 nm and 1575-1581 nm)
Loss without connectors for TWDM PON bands	≤1.2 dB (1524-1544 nm and 1596-1603 nm)
Loss without connectors for PtP WDM PON band	≤1.3 dB (1606-1625 nm)
Max optical power	+23 dBm
Return Loss	> 50 dB
Directivity	> 50 dB

A simple formula allows to derive indicative isolation values for CE. For simplicity, only the coexistence of two PON systems will be considered, in this case, NG-PON2 and GPON. The CE per port isolation values in a multi-coexistence scenario is treated in detail in [12]. The expression used for multichannel scenarios such as NG-PON2 is [11]:

$$I_{WDM} = \Delta_{ODN} - XT - \Delta P - I_{BiDi} - B_{comp} + 10\log_{10} N \quad (2.1)$$

where:

- I_{WDM} = CE port isolation at the interferer wavelength for the WDM device enabling coexistence in dB.
- Δ_{ODN} = ODN loss difference in dB for the target signal (minimum) and the interfering signal (maximum).
- XT = allowed inter-channel crosstalk power ratio in dB.
- ΔP = ONU launched power ratio in dB between the target signal (minimum) and the interfering signal (maximum).
- I_{BiDi} = isolation in the receive path (external to the WDM used for coexistence) at the interferer wavelength, e.g. from the internal transceiver diplexer (BiDi).
- N = Number of WDM channels.
- B_{comp} = relative bandwidth compensation factor to account for signal bandwidth difference between the target signal and the interfering signal, given by [11]:

$$B_{comp} = 10\, log_{10}(R_{int}/R_{target}) \quad (2.2)$$

where R_{int} and R_{target} are the bit rates of the interferer and target signals, respectively.

The inter-channel crosstalk (XT) is a key parameter to calculate the isolation requirements of the CE, and it is defined in ITU-T Rec. G.698.1 as the ratio of total power in the disturbing channels (P_{int}) to that in the wanted channel (P_{target}) [16]:

$$XT(dB) = 10\, log_{10}\left(\frac{P_{int}}{P_{target}}\right) \quad (2.3)$$

Several authors [17]–[20] have analyzed different crosstalk cases in systems with large number of WDM channels as in NG-PON2 using TWDM-PON, in order to calculate the proper isolation requirements of wavelength multiplexers (WM) at OLT side. A deep study of XT case in US for NG-PON2 is presented in Appendix A.

With this in mind, to calculate the allowed XT from a specific tolerable inter-channel crosstalk penalty *(Pc)*, in a scenario where a single interfering PON system is considered, the following equation should be used [12]:

$$P_C(dB) = 10\,log_{10}\left(1 - 10^{\frac{XT}{10}}\frac{ER+1}{ER-1}\right) \quad 2.4$$

where *ER* is the linear extinction ratio.

Using this formula, the maximum allowed crosstalk can be obtained for three different values of extinction ratio 10 dB, 8.2 dB and 6 dB which corresponds with the minimum values established in US for each standard, G-PON (1.25G), XG-PON/NG-PON2 (2.5G) and NG-PON2 (10G), respectively. From Figure 2.3, it can be deduced that if the tolerable *Pc* is 0.5 dB at BER = 10^{-4}, the maximum allowed XT values are -12 dB, -11 dB and -10.5 dB respectively. If the implementer wants to design a scenario with greater allowed penalties, XT values could be higher.

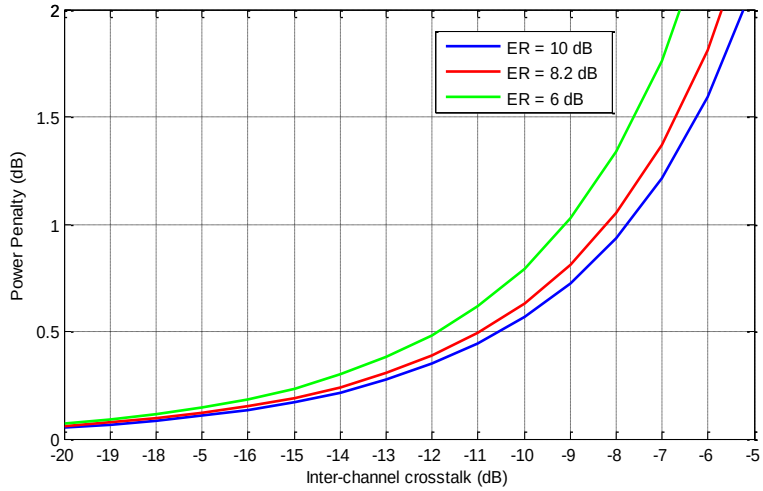

Figure 2.3. Power penalty (Pc) against inter-channel crosstalk (XT) for different ER values of interferer systems at BER = 10^{-4}

For example, to calculate CE isolation (I_{WDM}), a NG-PON2 system transmitting in US at 2.5 Gb/s and being interfered by a GPON system is analyzed. For NGPON2 tolerating 0.5 dB penalty, in a GPON and NG-PON2 coexistence scenario, the allowed XT is approximately -11 dB. For B+/N1 ODN classes, the minimum transmitted power for a NG-PON2 ONU is 4 dBm [21] and the maximum transmitted power for a GPON ONU is 5dBm [22]. Therefore,

the ΔP = -1 dB. For NG-PON2 an unamplified OLT has been assumed, and Δ_{ODN} = 15 dB (value chosen as the worst case). The post WDM isolation (I_{BiDi}) is assumed to be 1dB (typical circulator IL) [22]. The bit rate compensation factor, taking into account a G-PON ONU transmitting at 1.25Gbit/s and a NG-PON2 ONU transmitting at 2.5Gbit/s is -3dB. So, the required WDM isolation (I_{WDM}) at the NG-PON2 port of the CE, being interfered by a G-PON wavelength at 1.25 Gbit/s, could be calculated taken into account that N = 1 (G-PON interfering channels). Then, from Eq. (2.1), I_{WDM} = 29 dB.

In the opposite case, G-PON system is interfered by a four-channel NG-PON2 system (N = 4) each one operating at 2.5 Gbit/s and for B+/N1 ODN classes, where the minimum transmitted power for a GPON ONU is 0.5 dBm [22], and the maximum transmitted power for a NG-PON2 ONU is 9 dBm [21]. Therefore, ΔP = -8.5 dB, and the calculated isolation would be I_{WDM} = 36 dB.

2.2 COCONUT project: A proposal for NG-PON3 systems

The first part of this PhD thesis was developed between 2014 and 2016, in the framework of the European COCONUT project. The COCONUT proposal aimed at the definition, study and realization of a new fully scalable optical access network, significantly extending the network dimensions in terms of bandwidth utilization, reach and number of accommodated users. The proposed access network evolves from the almost-commercial WDM-PON architecture to the realization of the UDWDM solutions, envisioning the “wavelength-to-the-user concept [3], [4].

The key enabling technologies are cost-effective coherent transceivers, based on Direct Modulated Lasers and simplified coherent receivers which provide higher sensitivity and inherent wavelength selectivity compared with direct detection schemes, and thus suitable for serving lot of users. In addition, COCONUT drove the realization of flexible and bandwidth-efficient next-generation networks, compatible with the existing PON infrastructures. In the following sub-sections, the COCONUT approach is described in detail, from its baseline architecture, through some proposed ONU and OLT subsystems design and dimensioning, the wavelength plan and a conscious analysis of different coexistence scenarios with legacy systems. Part of this work is covered in the deliverables 2.1 and 2.3 of the COCONUT project and was published in [23], [24].

2.2.1 COCONUT baseline network architecture

The highest level of requirements that drive a PON technology come from the network operators and are determined by the services it is planning to offer to their customers in terms of location and capability. Moreover, compatibility with existing deployed infrastructure, capability of reusing legacy ODNs and coexistence with legacy PON systems are key points to guarantee a smooth and non-disruptive network upgrade. The COCONUT architecture fulfills these coexistence requirements proposing a splitter-based PON, thus avoiding optical filters at the ODN that could limit the bandwidth extension or require changes in the external infrastructure. Moreover, it allows to serve a higher number of users (e.g 265 users over 60 km reach), each one operating at 1.25 Gb/s or 10 Gb/s, thanks to the UDWDM spacing (6.25, 12.5 or 25 GHz), and the higher power budget (>45 dB). These properties result of the enhanced receiver sensitivity, enabled by the use of coherent technologies with flexible wavelength allocation. The COCONUT architecture is useful for supporting, over the same fiber infrastructure of current PONs, different applications such as mobile back-haul, micro and macro cells, as well as fixed-line users (either residential or business), as depicted in Figure 2.4. The main difference among these scenarios is the functionality of the ONU: i) it feeds a Wi-Fi spot or ii) wired devices such as a PC or TV, or iii) the ONU feeds a 3GPP cell. According to traffic demand forecasts, a connection of 1.25 Gbit/s per user (1 G Ethernet to the user) fulfills scenarios i) and ii), while 10 Gbit/s can be required for macro cells in iii). In addition, the wavelengths can be dedicated to each ONU or shared between several users by applying a TDMA protocol at the MAC layer and using burst mode transceivers [24], [25].

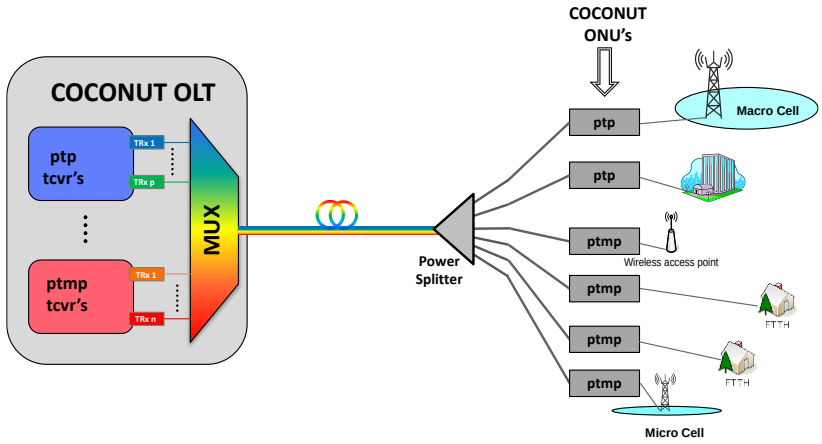

Figure 2.4. Baseline of the COCONUT architecture. Source: [24]

2.2.2 COCONUT vs NG-PON2

Although NG-PON2 was recently standardized by the ITU aiming at evolving on next generation PONs, it is not yet decided what will be the next step to follow by network operators on future deployments. COCONUT reported results [4]–[7] represent a promising competitive technology which emerge as an alternative for enabling advanced features in NG-PON2 or for a future NG-PON3.

In contrast to NG-PON2, COCONUT uses coherent detection and UDWDM at the physical layer. These two characteristics help on a reduction in channel spacing and an increase of number of channels. As well, COCONUT offers some benefits when benchmarked against NG-PON2 because COCONUT ONUs Rx do not need optical filters or broad guard bands. Moreover, COCONUT provide high Rx sensitivity, thus requiring a lower transmitted power, and enabling to multiplex more channels (being the limit the eye-safety power of 21.3 dBm [24]) and minimizing the fiber non-linearity effects. Table 2.2 summarizes the main differences between NG-PON2 and the COCONUT approach.

Table 2.2. Key features of COCONUT vs NG-PON2

	COCONUT [24]	**NG-PON2 [21]**
Wavelength channels	64 – 128 – 256	4 – 8 (TWDM) and/or 16 (PtP WDM)
Channel spacing	6.25 – 12.5 – 25 GHz	50 – 100 GHz
Channel bit rates	1.25, 2.5 and 10 Gb/s (DS and US)	2.5 and 10 Gb/s (DS and US)
Max. aggreg. capacity	256 Gb/s (at 1G) 2.5 Tb/s (at 10 G)	40 G – 80 G (wirh TWDM) 160 Gb/s (with PtP WDM)
Rx sensitivity	-48 @ 1.25G, BER 10^{-3} -38 @ 10G, BER 10^{-3} (US and DS)	-30 @ 2.5G, BER 10^{-4} (US) -28 @ 10G, BER 10^{-3} (DS)

For example, an NG-PON2 channel slot, can be, in theory, divided into 16 sub-wavelengths with 6.25 GHz spacing, allowing a capacity of 20 Gbit/s (with a 1.25 Gbit/s per ONU) per each 100 GHz channel, thus doubling the capacity/per channel if using the COCONUT approach. Nevertheless, the practical scenario depends on the technologies used in the design of the OLT and ONU architectures, as will be discussed in next sub-section.

2.2.3 OLT and ONU architectures for UDWDM-PON

The proposed architectures for the network elements were based on coherent transceivers. At the ONU side, the most important goal was to have a low-cost realization in order to provide an affordable deployment. This goal is achieved by using tunable lasers (TLs) based on cheap distributed feedback (DFB) lasers. At the central office (CO), the OLT implementation reproduces the same ONU design for each user, integrating all counterparts in full unique OLT equipment covering all the deployed ONUs of the PON. Next analysis and the derived results are obtained from COCONUT studies and have been published in [23].

2.2.3.1. ONU designs and sizing

ONU architectures were designed based on coherent homodyne or heterodyne detection, using a tunable laser (TL) as the LO and other TL as the Tx, based on direct modulation, and employing two different wavelengths for US and DS transmission to avoid Rayleigh Backscattering (RB). The TLs were non-preselected low-cost DFB laser, with limited tunability (2 nm with +/-10ºC) adjusted by heating and with a constant linear variation of 0.1 nm/°C [26], [27]. This temperature range can be easily reached with a Peltier. With different bands or with the same band for US and DS, a coupler (2x2 optical hybrid, WDM filter or circulator) separates both directions. As well, other option for using only one TL in the ONU, by introducing data to a cost-effective reflective semiconductor optical amplifier (RSOA), was also studied and demonstrated [28].

Considering the limited tuning range limitation of DFB lasers, a simple general dimensioning of the number of ONUs can be performed. Figure 2.5 depicts the number of allocated ONUs as a function of the total bandwidth, in terms of number of optical wavelength channels, using a dedicated WTTU approach. If the TLs were fully tunable lasers, the number of allocated ONUs would correspond linearly with the number wavelength channels until reaching the power limit of 256 ONUs (considering a transmitted power of -3 dBm for respecting eye-safety regulations of 21.3 dBm). This point is at 12.8 nm bandwidth, for 6.25 GHz channel spacing. On the other hand, considering the limited tuning range of low-cost DFB lasers, combined with the condition that the ONUs transmitting wavelength cannot be pre-selected, disables an ONU to operate at most of the spectrum band and this can lead to interference with nearby active ONUs. This essential issue was analyzed and solved with the proposed statistical multiplexing strategies discussed in [23], [26].

For example, as a specific result, using the Maximum Admittance algorithm [23] at 0.1% blocking probability, the total optical bandwidth reserved for COCONUT should be increased to 14.1 nm at the same channel spacing. These values are represented by the dark blue line in Figure 2.5, where it can be observed that the tendency follows a quasi linear function, with a slope slightly lower than for full tunability, up to the 256 ONUs at 282 channels, hence losing less than 10% (12.8/14.1 = 90%) in channel spectral efficiency. Under harsh environmental temperature variations, the required slots can increase up to 315 channels, however detailed analyses are out of the scope of this PhD thesis, and can be found in [23].

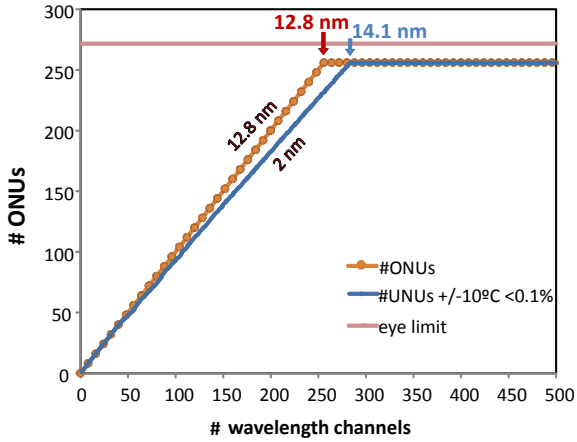

Figure 2.5. Number of allocated ONUs as a function of the total bandwidth, in terms of number of optical slots using a dedicated WTTU approach.

2.2.3.2. OLT designs and sizing

The OLT implementation is likewise based on coherent transceivers, serving all the deployed ONUs in the PON. A very simple architecture can be realized with power splitters, covering the whole deployed working optical bands without any filtering, whenever one is using different or the same band for US and DS as is depicted in Figure 2.6(a). Although, this architecture has advantages in terms of wavelength band availabilities, an optical amplifier (OA), which can be an erbium-doped fiber amplifier (EDFA) or a semiconductor optical amplifier (SOA), should be introduced to satisfy the power budget.

In contrast, another OLT architecture based on a 1 × M ports arrayed waveguide grating (AWG) as the WM, and combined with splitters to serve a high number of users (see Figure 2.6(b)) is proposed, thus providing lower IL and a better power budget, and even avoiding amplification for moderate distance reaches because of the high coherent detection sensitivity.

However, this architecture has some drawbacks regarding to the AWG spectral efficiency, which is the ratio between the 3-dB response and the channel spacing. This efficiency is only of 75% for a 3-dB flat-top bandwidth, and hereafter, some channels will suffer high attenuation because of the low response of the AWG in the transition bands.

In order to have full spectral 100% efficiency, the use of an athermal AWG combined with a thermal AWG or two thermal AWGs was proposed in [23]. By tuning the spectral response, the output channels can be interleaved through a temperature control in such a way that when a maximum is achieved in one AWG port, in the other neighboring AWG port, there is a minimum and vice versa. In this way, both AWGs have complementary frequency responses and, therefore, a 100% spectral efficiency was achieved (see inset of Figure 2.6(b)). If the US and DS transmissions are done in different bands, half of the M ports of each AWG can be devoted to the DS band and the other half to the US band. If the US and DS transmissions share the same band, each port will serve both directions. If there are not enough ports in an AWG to cover both the DS/US bands, the same architecture can be duplicated: one branch with two AWGs can be used for DS and the other branch with two more AWGs for US, with a circulator separating the US and DS branches.

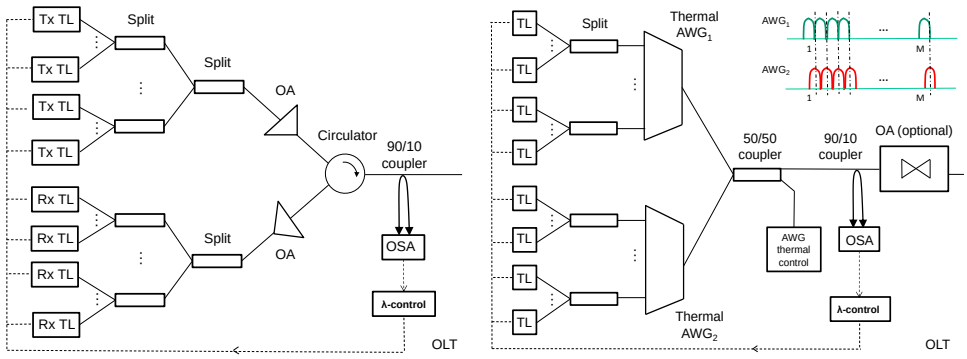

Figure 2.6. (a) OLT architecture realized with splitters covering full optical bands, (b) OLT block diagram based on splitters and two thermal AWGs with complementary frequency response providing 100% spectral efficiency.

To prove this proposal, several athermal and thermal AWGs were measured, characterizing their IL, spectral response, and tuning range in order to evaluate their use in the OLT design.

Two sorts of AWGs were available: Gaussian passband and flat-top passband, presenting a Gaussian or a flat-top passband channel shape, respectively.

In a first scenario (Figure 2.7), a single 100 GHz channel spaced athermal Gaussian 41-port AWG1 was tested to evaluate its spectral response. An EDFA was used as a broadband light source and was directly connected to one input of a 2x2 optical coupler, whose output ports were connected to two AWGs. Two output port of the AWG1 were connected to an optical spectrum analyzer (OSA), through a 3x3 coupler and two ON/OFF optical switches, which select the output port to be measured. The amplified spontaneous emission (ASE) response of the EDFA was compensated to provide an exact AWG spectral response.

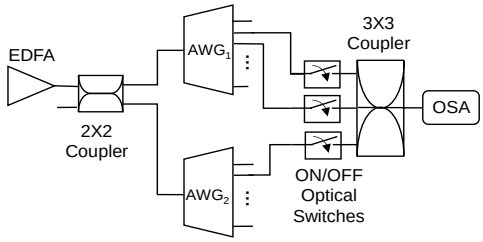

Figure 2.7. AWG characterization setup: single and tuning AWG scenarios.

The ITU channels 32 (1551.72 nm) and 33 (1550.92 nm), spaced 100 GHz apart, were filtered through the AWG, and the full width at half-maximum (FWHM) or 3 dB bandwidth obtained was 60 GHz, providing a 60% spectral efficiency. The IL was in the order of 3.0 dB, and the cross point (CP) between these consecutive channels was around 11 dB below the IL, showing a maximum IL (MIL) of 14 dB (Figure 2.8(a)).

In the same scenario, a 100 GHz thermal flat-top 40-port AWG without temperature control was also tested for ITU channels 29 (1554.13 nm) and 30 (1553.33 nm), providing an IL in the order of 7.5 dB and showing a 77.5 GHz FWHM, so around 75% spectral efficiency (Figure 2.8(b)). The CP was around 6.4 dB below the IL; thus, the MIL was 14 dB.

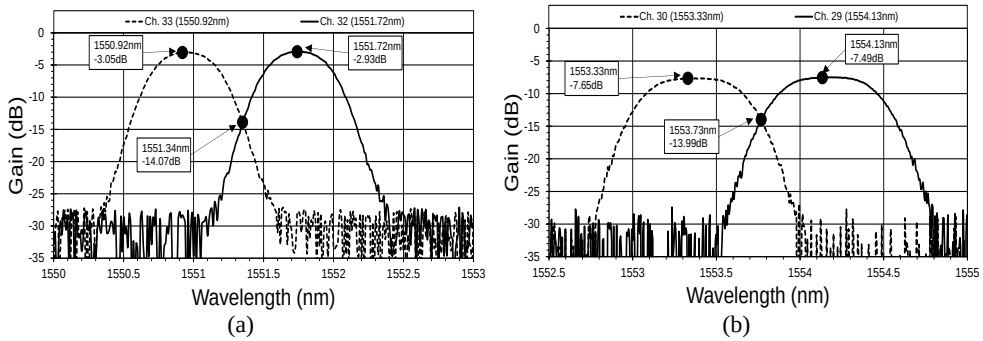

Figure 2.8. (a) Athermal Gaussian 100 GHz AWG response, (b) Thermal flat-top 100 GHz AWG response.

Afterwards, in a second tuning setup scenario (Figure 2.7), two AWGs were measured simultaneously to test the thermal performance (Figure 2.9(a)). A third optical switch connects the signal from the thermal AWG_2, which is controlled by the temperature, to the OSA, tuning the AWG_2 channel 50 GHz from the nominal frequency in order to allocate its peak at the CP of the other two channels of AWG_1, with all optical switches ON. Once the peak was centered, the channels were measured separately.

The peak of channel 33 in the thermal Gaussian AWG_2 was tuned to be allocated at the CP of channels 32 and 33 of AWG_1, which were kept without temperature variation. Once the temperature in AWG_2 is increased up to 60°C, which was the maximum operative rating, the peak reached the CP. Figure 2.9(a) and Figure 2.9(b) show the interleaving of the AWG channels for the Gaussian and flat-top responses, respectively.

With two flat-top AWGs, by tuning to interleave channels so that one AWG peaks at the CP of the other AWG, a ripple of only 0.7 dB is obtained and a MIL of 8.2 dB is reached. But using Gaussian AWGs, the ripple is 1.9 dB and the MIL is just 4.9 dB, giving the best result.

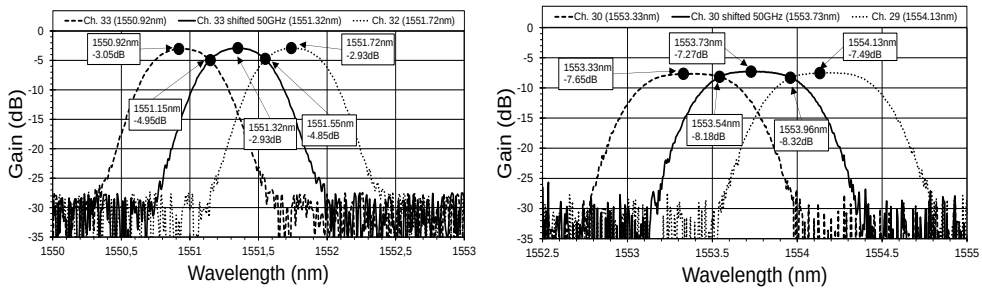

Figure 2.9. Interleaving AWG channels by thermal tuning: (a) Gaussian, (b) flat-top

For this OLT architecture (Figure 2.6(b)), combining two thermal AWGs with splitters at the AWG ports, and defining the AWG channel port spacing as W GHz, the number of AWG required ports (M_r) per band would be:

$$M_r = [B_0/W] \tag{2.5}$$

where B_0 is the total bandwidth needed to allocate all operative channels.

For 256 users with two TLs in different US/DS bands in the out/indoor case, a 100 GHz AWG port spacing and an operation band of 310 channels, a total of 20 ports are needed. Then, employing a 41-port AWG, 20 ports can be devoted for DS and the other 20 ports for US. Other details of the architectures, and the calculations are explained in detail in [23].

2.2.4 Wavelength plan for COCONUT network and coexistence scenarios with legacy PONs

In order to guarantee a smooth migration in PON roadmap, the CE at the CO, and a WBF in front of the ONU transceiver are needed, as it was explained in section 2.1 for NG-PON2. At the same time, the wavelength bands of the new PON systems has to be fully compatible with previous ones. Therefore, a wavelength plan was a key point for the COCONUT network. Next section analyses the possible network deployment scenarios and the available wavelength spectrum to allocate the COCONUT system. Also, the XT analysis is applied between NG-PON2 and the COCONUT system.

2.2.4.1. Coexistence deployment scenarios

COCONUT PON could be deployed over two network scenarios: Greenfield and Brownfield. A Greenfield scenario is where no previous installed fiber infrastructure is considered and the wavelength channels could be allocated in the entire spectrum grid with wider channel spacing. Thus, is less challenging from the technical point of view, with no restriction for legacy with other PON systems. Splitter and/or AWG based ODN could be implemented increasing the overall power budget. On the other hand, in the Brownfield scenario a PON system is implemented over an existing ODN infrastructure [2], [14]. The latter presents two options: first, when a complete coexistence with legacy PON systems must be guaranteed, and second, when no coexistence is assumed, resembling the case of a Greenfield scenario, in terms of the available operating bandwidth and providing freedom in spectral allocation, but with design limitations in terms of power budget due to the legacy splitter-based ODN.

Currently, legacy GPON/EPON and XG(S)/10GE-PON systems are the scenario for coexistence with the COCONUT proposal. The recent NG-PON2 TWDM standard and its optional PtP WDM architecture are also to be regarded. When the COCONUT deployment has concurrence with any other system, it must be non-intrusive and must avoid any interference with the standardized systems. The coexistence scenario between COCONUT and the diverse legacy systems is shown in Figure 2.10. The CE is a part of the ODN as well as the splitters and feeder optical fiber, bounded by the S/R and R/S points, while the WBF is a part of the ONU.

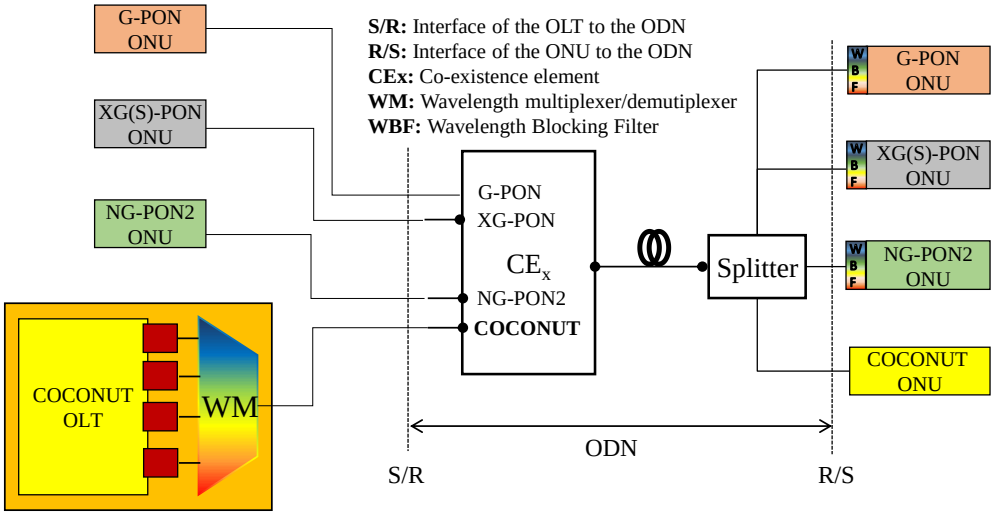

Figure 2.10. Coexistence scenario between COCONUT and legacy PONs.

2.2.4.2. COCONUT coexistence scenarios

Considering the wavelength bands defined for each PON system (Fig 1.7 in chapter 1), it is clear that the COCONUT system needs to re-use the spectrum defined for one or more of the legacy systems, due to the lack of available optical spectrum, and because guard bands between each PON generation, have to be considered to allow coexistence in the same system. One possibility is to avoid coexistence with NGPON2, because if COCONUT is deployed, better services are offered and there is no need to install another new system. Moreover, COCONUT systems could re-use NG-PON2/PtP WDM concept of Spectrum Flexibility [21]. This means that the wavelength channels can be located anywhere in the full C and L bands subject to spectrum availability depending on a coexistence scenario in US and/or DS direction.

Establishing then coexistence scenarios that support the different existing PON generations; GPON, XG(S)-PON, RF-VIDEO, NG-PON2, and the COCONUT system, a CE can be used as is illustrated in Figure 2.11, where the numbers 1 to 6 show the possible interconnection alternatives between the CE ports, and the legacy and COCONUT OLTs. It is important to mention that CE ports are bidirectional, to support DS and US.

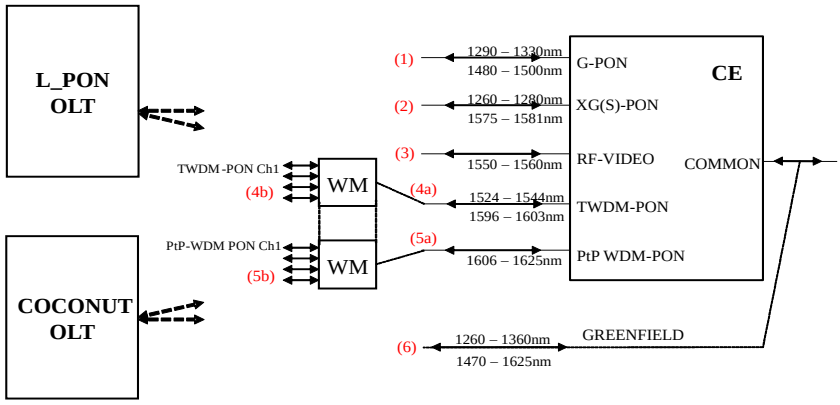

Figure 2.11. COCONUT coexistence alternatives in PONs using a CE.

Table 2.3 summarizes the wavelength bands specified for each PON system, as possible alternatives identified for the spectral allocation of the COCONUT wavelength channels. Some considerations are:

- The values of the number of channels calculated in Table 2.3 for each case, have been determined considering the full wavelength bands and the channel spacing (CS) defined for each standard. The CS depend on the filter characteristics of the band pass filters of each channel. These characteristics should be analyzed and considered for further studies (FFS) taking into account that COCONUT channels do not need optical filters due to the use of coherent detection, with optical bandwidths of less than 4GHz (homodyne schemes) transmitting at 1.25Gbit/s, allowing that more channels can be allocated.
- The guard bands between legacy PONs depend on the isolation characteristics of the band pass filters of each port in the CE. These characteristics could be obtained from Eq. (2.1) in a system where only two PON systems coexist. However, when more than two systems coexists (e.g GPON, XG-PON1, RF-VIDEO, TWDM-PON and COCONUT), as is shown Figure 1.7 in chapter 1, the analysis is more complex and the details are specified in [12].
- Third, considering COCONUT systems and thanks to the use of coherent detection and the narrow spectral characteristics of COCONUT channels:
  - The interference caused by other channels will not affect the COCONUT system until they overlap.
  - In the opposite case, the interference caused by COCONUT over other PON systems can be strongly reduced. This may lead to narrowing down the guard bands from 10

or 15nm to a fraction nm, allowing to place more UDWDM channels. This is considering that:

- COCONUT can use FSK and PSK modulations, where the instantaneous transmitted power is constant, so the interference over IMDD can be lower.
- The transmitted power per COCONUT channels is lower compared with IM/DD systems such as NG-PON2, because of the better Rx sensitivity.

Table 2.3. Alternatives for COCONUT allocation in a Brownfield scenario[1]

#	Option	BW DS (nm)	CS[2] (GHz)	COCONUT channels at 6.25GHz and aggregated bit rate with 1.25 Gbit/s	COCONUT channels at 12.5GHz and aggregated bit rate at 10 Gbit/s
1	G-PON narrow	20	100	400 (500 Gbit/s)	200 (2 Tbit/s)
2	XG-PON1	6	100	120 (250 Gbit/s)	60 (600 Gbit/s)
3	RF-VIDEO	10	6.25	200 (250 Gbit/s)	100 (1 Tbit/s)
4a	TWDM-PON wide	7	100	140 (175 Gbit/s)	70 (700 Gbit/s)
4b	TWDM-PON wide (Sharing WM with COCONUT)	100G x N (N=1,…,3)	100	#ch = (16) x N (N = 1…3) #ch/6.25*1.25 = x Gb/s	#ch = (10) x N (N:1…3) #ch/12.5*10 = x Gb/s
5a	PtP WDM PON (different WM with TWDM)	19	6.25	380 (475 Gbit/s)	190 (1.9 Tbit/s)
5b	PtP WDM PON (Shared WM with COCONUT)	50G x N (N=1,..3)	6.25	#ch = (8) x N (N:1…3) #ch/6.25*1.25 = x Gb/s	#ch =(5) x N (N:1…3) #ch/6.25*1.25 = x Gb/s
4b+ 5b	One shared WM between TWDM, PtP - WDM and COCONUT)	50G x N (N=1,..8)	6.25	#ch = (8) x N (N:1…7) #ch/6.25*1.25 = x Gb/s	#ch =(5) x N (N:1…7) #ch/6.25*1.25 = x Gb/s
6	Greenfield	255	6.25	5100[3] (6.375 Tb/s)	2550 (25.5 Tbit/s)

[1] The values are theoretical and do not consider isolation requirements and limited thermal laser's tunability.
[2] These values correspond to the channels spacing between wavelengths of legacy or COCONUT system.
[3] The power per channel should be reduced to -16 dBm to comply with eye-safety regulations.

The options 4a and 5a refer to the cases when COCONUT would be allocated along all the wavelength band of TWDM or PtP WDM options, and different WM are used between COCONUT and TWDM or PtP WDM.

The options 4b and 5b refer to the cases when COCONUT would share the wavelength band with TWDM or PtP WDM, replacing 1, 2 or 3 channels of these systems by COCONUT channels, and sharing the WM with only one of them.

The option 4b+5b refers to the case when only one WM would be used for NG-PON2 (TWDM & PtP WDM) and COCONUT. In this case the wavelength band used for DS would be 1596 – 1625nm and for US two wavelength range could be considered (1524 – 1544nm) or (1603 – 1625nm). The available bandwidth as well as the number of channels, and the aggregated bit rate, will depend of the NG-PON2 channels used by COCONUT (1…8), and according to the spectral characteristics and the guard bands used. This is FFS.

Considering case 5a, where COCONUT system would replace the PtP WDM option of NG-PON2, the wavelength band would be 1606 – 1625nm and could be used with spectral flexibility for US and DS transmission. In this case considering the CS defined for COCONUT (6.25 GHz and 12.5GHz), an example of wavelength grid aligned with ITU-T DWDM fixed grid [29] is presented in Appendix B. To obtain the frequency grid the initial 100GHz grid, can be sub-divided by successive factors of two. It is important to clarify that this process could be applied in other wavelength bands, depending on the coexistence scenario to be considered.

In option 6 (Greenfield), it would be possible to allocate a maximum of 5100 number UDWDM channels in a 250 nm spectrum band. Here, the transmitted power per channel should be reduced to -16 dBm, to be below the eye safety limit; for the huge splitting, low loss wavelength multiplexers and optical amplifiers should be used.

It is important to mention that all the calculations in Table 2.3 are theoretical, and only consider full wavelength band laser tunability. However, for the out/indoor real conditions, the limited thermal tunability of low-cost commercial lasers such as DFB lasers (2 nm ± 10ºC) must be considered, to choose one or two wavelength bands for US and DS. Details of these calculations are not presented in this PhD thesis, but can be found in [23].

2.2.5 Inter-channel crosstalk analysis between COCONUT-PON and legacy PONs

The inter-channel crosstalk analysis explained in section 2.1 is presented in a coexistence scenario where COCONUT system has to coexist with NG PON2. Consider the case 5a of Table 2.3, where 64 COCONUT channels replace 4 PtP WDM channels in 1603 – 1625 nm band, and an allowed penalty (*Pc*) of 0.5 dB for XT= -11 dB. For a B+/N1 ODN class, the minimum transmitted power of NG-PON2 ONU is 4 dBm [21] and the maximum transmitted power for a COCONUT ONU is fixed to -3 dBm. Moreover, an unamplified OLT has been selected for NG-PON2. Therefore, the calculated parameters to be replaced in Eq. (2.1) are:

- $\Delta P = 7$ dB.
- $\Delta_{ODN} = 15$ dB. This value could vary depending on ONU locations
- I_{BiDi} is assumed to be 0 dB.
- N = Number of WDM channels
- $B_{comp} = 10\log_{10}(1.25/2.5) = -3$dB.

So, the required WDM isolation (I_{WDM}) at the NG-PON2 port of the CE being interfered by a COCONUT system at 1.25 Gbit/s will be $I_{WDM} = 40$ dB

2.3 Real-time UDWDM-PON implementation

The key enabling technologies for implementing the proposed UDWDM architecture are the development of low-cost coherent transceiver (TRx) based on directly modulated lasers and simplified coherent Rx, and at the same time able to coexist with current deployed PONs. In this section, the characteristics of one of the analog prototypes based on DPKS modulation are explained, and its packaging in a compact metal box is shown. As well, the characterization of some wavelength band filters used as CE is discussed in detail as the key element to guarantee full coexistence with legacy systems. Finally the real-time implementation of an UDWDM-PON is commented, first in a laboratory test-bed [30] only with DPSK based prototypes, and second in a field-trial demonstration with multiple DPSK and ASK coherent prototypes, realized over 10 km of dark fiber link installed around the city of Pisa, Italy [5]–[7]. In both cases successful coexistence with a real EPON system was achieved.

2.3.1 CE characterization

The CE characterization was performed over three different wavelength band filters (CE1, CE2 and CE3) provided by British Telecom (BT), partner of the COCONUT project consortium. In that characterization, the IL and isolation values per each CE port were measured for all the spectrum bands of each legacy PON system, and to verify if they comply with the minimum requirements in different coexistence scenarios. The characterization was done using two different light sources, a broadband light source, and a tunable External Cavity Laser (ECL). The first emitted visible light coupled onto the end of a multimode optical fiber (MMF). As a coupling between MMF and single mode fiber (SMF) was needed, the emitted power was relatively very low (around -67 dBm) and the dynamic range was approximately between 30 to 32 dB, considering the average OSA noise floor. On the other hand, the ECL provided high optical power (around -5 dBm) and then a dynamic range of 50 to 55 dB, but with a limited tunability between 1485 nm and 1625 nm. Nevertheless, the wavelength plan for COCONUT was designed to work around 1550 nm, then the characterization below 1485 nm was not relevant, and it is not presented in this thesis.

2.3.1.1. CE characterization using a tunable ECL

An Agilent 8164B ECL was used to perform the characterization of the three CE units. To perform this characterization the ECL was adjusted in steps of 0.1nm or 12.5 GHz. The setup used is depicted in Figure 2.12. The CEs provided by BT were 1x2 WDM filters with a common port, one G/EPON port and a NG-PON port, where the proposed COCONUT system was connected to coexist with legacy GPON/EPON.

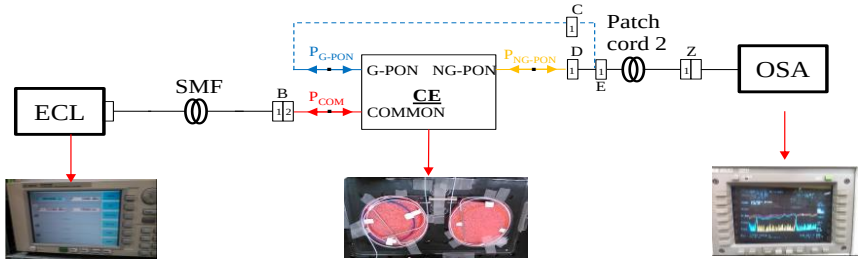

Figure 2.12. Setup for CE characterization using a TL

The results of the characterization of CE1, CE2 and CE3 are presented in Figure 2.13 and summarized in Table 2.4. The IL measured for CE1 showed that this filter did not comply with the minimum specifications for NG-PON bands provided by BT in [31]. Regarding the

GPON DS band, the minimum IL measured (1.1dB) was close to the specification and it could comply considering that a matting of each pair of connectors can generate an uncertainty of ±0.3dB (considering a maximum ±0.6dB in the ECL setup) [32], and additionally, End-of-Life (EoL) loss of 0.5 dB should be considered. Regarding the IL, CE2 and CE3, complied with the standard specification for all NG-PON bands, but CE1 did not. At the same, it could be concluded that CE2 and CE3 did not comply with the minimum IL specified for GPON DS band due to the IL > 0.8dB, however considering the factors explained before this value was acceptable. Table 2.4. shows the maximum and minimum resulting values of the CEs IL and isolation in dBs for all the defined PON bands along the tuning range (1485 -1625nm) of the ECL, including a COCONUT proposed band (1544 – 1575nm) highlighted in bold.

Regarding the measured isolation values, it was found that all CEs comply with the minimum specification, in a scenario where for example an NG-PON system (operating at minimum of 2.5 Gb/s and with only one channel) and a GPON system are coexisting. Nevertheless, the XT analysis explained before should be applied at each scenario, depending of the systems that would coexist and their number of channels.

Table 2.4. CEs properties: IL (without connectors) and isolation per port

Parameter	CE port	PON Recomm.	Wavelength band (nm)	BT specification [4]	Measured values		
					CE1	CE2	CE3
IL (dB)	GPON	G-PON DS	1584 – 1500	< 0.8 (+0.5)	1.67	1.36	1.04
	NG-PON	TWDM US	1524 – 1544	< 1 (+0.5)	5.13	0.61	0.91
		COCONUT	**1544 – 1575**		**6.18**	**0.58**	**0.59**
		XG-PON DS	1575 – 1581		6.14	0.61	0.59
		TWDM DS	1596 – 1603		9.14	0.48	0.62
Isolation (dB)	COM - GPON	TWDM - US	1524 – 1544	> 25	32.9	35.4	31.3
		XG-PON DS	1575 – 1581		32.3	36.3	33.5
		TWDM - DS	1596 – 1603		34.4	40.7	37
	COM – NG-PON	G-PON DS	1485 – 1500	> 30	45	43	46

[4] Provided by BT in the document RC 9354 for G-PON Passive Optical WDM Filter for Co-existence with a NG-PON system operating at 2.5 Gb/s. The ports are labeled according to BT Specification.

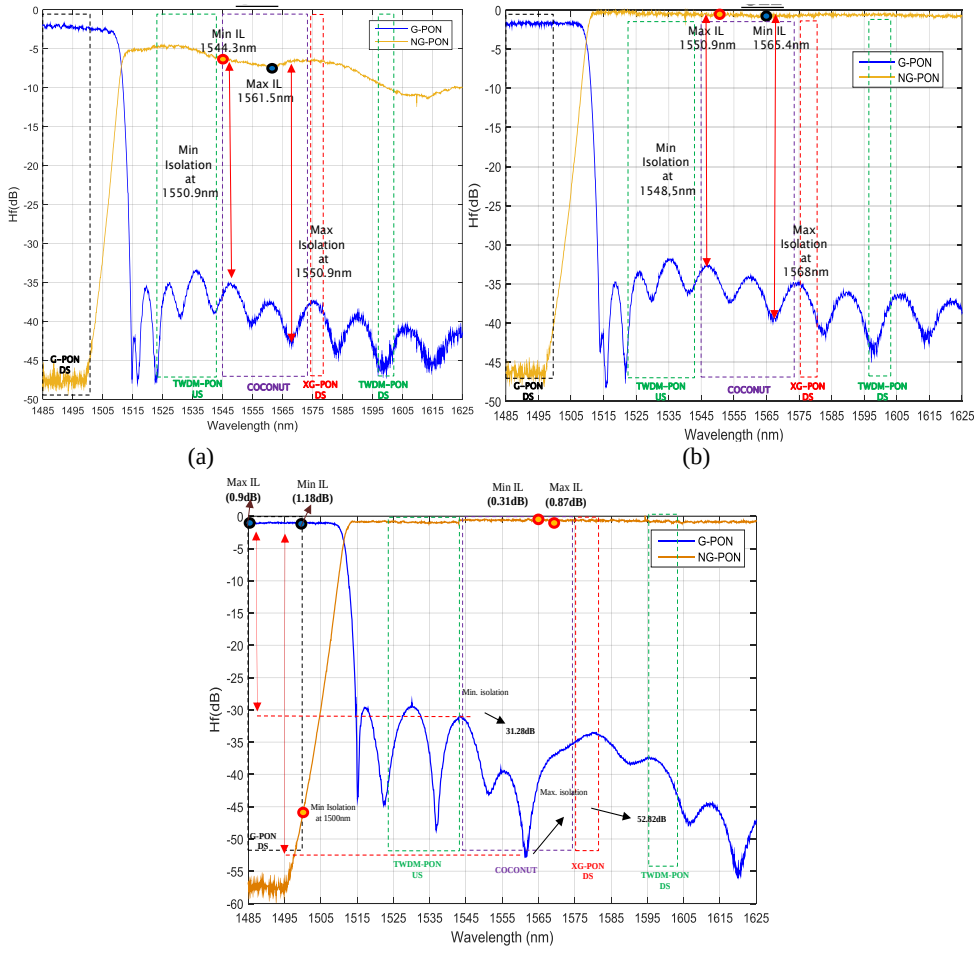

Figure 2.13. CE characterization using an ECL: (a) CE1, (b) CE2 and (c) CE3.

2.3.1.2. CE isolation according to specific coexistence scenarios

The required network isolation values can change depending on the coexistence scenario and the conditions such as ONU optical transmission powers, the minimum tolerable penalty due to crosstalk, the number of crosstalk sources and the OLT receiver sensitivity. An analysis can be done following the procedure described in previous sections for verifying the minimum isolation values (I_{WDM}) of the CE, for different scenarios where legacy GPON should coexist with a multi-channel system like COCONUT, operating at bit rate of 1.25 Gb/s. Table 2.5 compares the theoretical I_{WDM} needed at different scenarios, when GPON is the target system, with P_c = 0.5 dB ($XT = 10.5\ dB$), and Δ_{ODN} varying from 5 to 15 dB (worst case), with the

measured isolation for CE2 and CE3, the two CE with lower IL at the proposed COCONUT wavelength band (1544 nm – 1575 nm).

Comparing the theoretical CEs isolation, and with the values measured in the characterization, it can be affirmed that both filters (CE2 and CE3) would be useful when I_{WDM} < 33 and 31 dB (scenarios highlighted in bold), respectively. As can be deduced, a COCONUT interferer system with up to 64 channels could be allowed, with Δ_{ODN} = 5dB. In case of Δ_{ODN} = 15dB (worst case) the maximum number of COCONUT channels would be 4. An intermediate case with Δ_{ODN} = 10 dB would admit a COCONUT system of 8 channels using CE3 and 16 channels using CE2. Nevertheless, if a COCONUT system with a maximum of 256 channels need to be allocated in a coexistence scenario with G-PON a new CE should be placed with a minimum isolation of 39 dB, in the less restrictive case, and up to 49 dB in the worst case.

Table 2.5. Theoretical and measured values for CE1 and CE2 in G-PON (target) - COCONUT (interferer) coexistence scenario

Theoretical				**Measured values (1544 – 1575 nm band)**	
Scenario	**Δ_{ODN} (dB)**	**N**	**Min I_{WDM} (dB)**	**CE2**	**CE3**
1	5	2	**18**	33	31
	15		**28**		
2	5	4	**21**		
	15		**31**		
3	5	8	**24**		
	15		34		
4	5	16	**27**		
	15		37		
5	5	32	**30**		
	15		40		
6	5	64	**33**		
	15		43		
7	5	128	36		
	15		46		
8	5	256	39		
	15		49		

2.3.2 Analog heterodyne DPSK system

One of the COCONUT subsystems was based on a DPSK Tx (performed direct phase modulation of a DFB laser) [33], and an heterodyne Rx, where only one DFB was employed as LO and as CW light source externally modulated by an RSOA, which acted as phase modulator. The Rx on the OLT implemented also heterodyne detection but using a separately DFB as LO. The packaging of the analog prototypes on compact metal boxes developed for

the COCONUT field-trial was done by the author, including the design and fixation of all the elements. Some photos of the OLT and ONU prototypes are shown in Figure 2.14. The datasheet of the heterodyne ONU prototype is described in Appendix C of this thesis and could be a reference for a future NG-PON3 ONU.

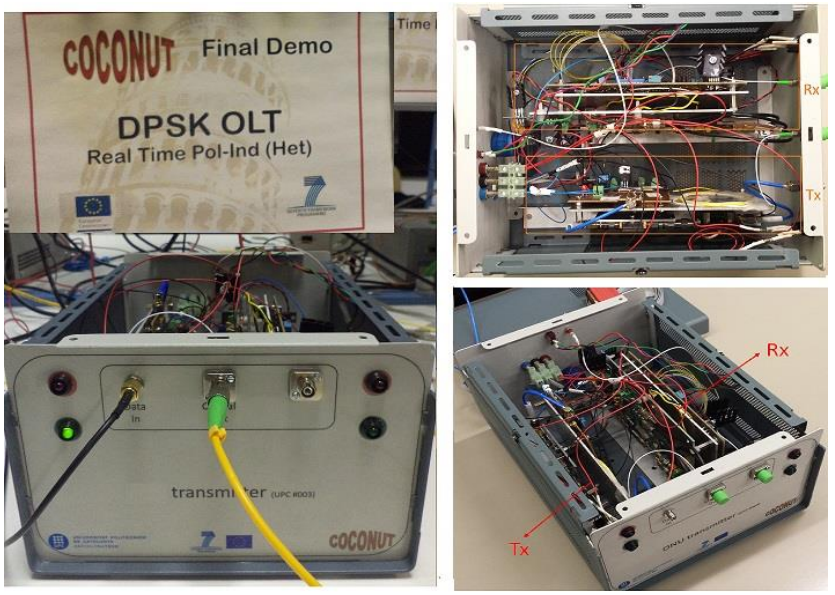

(a)

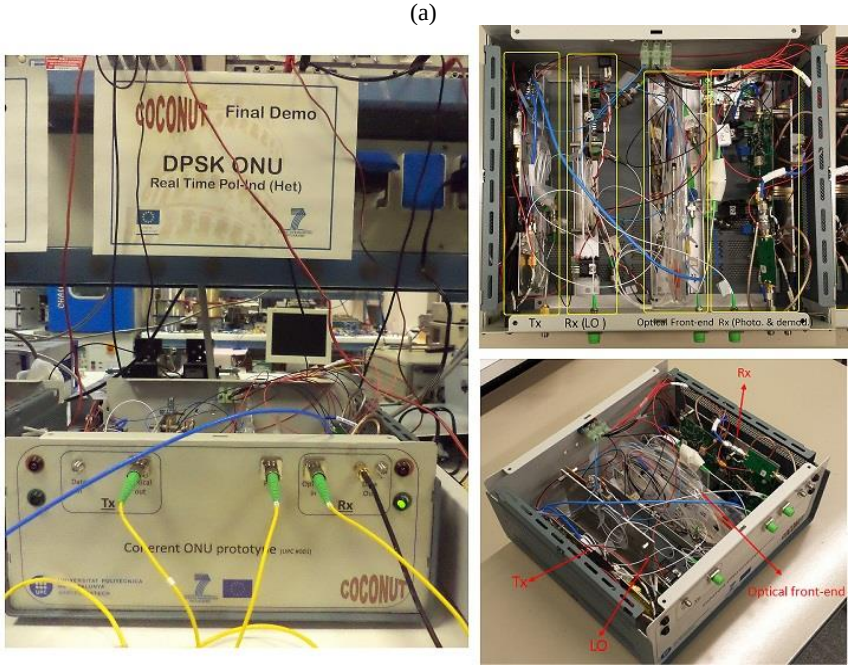

(b)

Figure 2.14. Heterodyne PSK COCONUT TRx prototypes for(a) OLT and (b) ONU

2.3.3 Bidirectional Real-Time DSP-less Heterodyne UDWDM-PON

Before presenting the field-trial results of the COCONUT project, it is interesting to comment a bidirectional real-time test developed in GCO laboratory with the COCONUT prototypes, whose results were published in [30]. In this work, a bidirectional phase shift keying (PSK) real-time UDWPON based on stand-alone simplified transceivers (TRx) without digital signal processing (DSP) and polarization insensitive heterodyne detection was tested. A diagram of the experimental setup is depicted in Figure 2.15.

At the OLT side, the Tx consisted of a pre-equalized directly modulated DFB that produced a DPSK optical signal. The modulating data was a 1.25 Gbit/s 2^{31}-1 Pseudo Random Binary Sequence (PRBS). The DFB was controlled in temperature and emitted at DS wavelength around 1549.34 nm and with 2 dBm of optical power. The generated signal passed through a circulator for separating DS and US, and was coupled to the ODN.

At the ONU, the Rx was based on a polarization insensitive heterodyne scheme using a single photodiode (PD) per polarization [34]. An optical circulator first separated DS/US and a 3-dB optical coupler mixed the DS with a LO signals. The latter was produced by a DFB laser controlled in temperature. The LO emission frequency was shifted by 2.5 GHz from the DS and its optical power was limited to -3 dBm. A polarization beam splitter (PBS) divided the output from the coupler and each polarization component was detected by a single 7 GHz BW PD. The electrical signals were independently high-pass filtered at cut-off frequency of 1.2 GHz and electrically amplified. Then, an analogue delay and multiply circuit differentially decoded the signal and afterwards the data streams were added, low-pass filtered at 1 GHz and amplified. Finally, the BER was measured with a BER tester (BERT).

The ONU Tx exploited the same DFB acting as LO. The LO output was equally divided through a 3-dB optical coupler and seeded an RSOA. A 1.25 Gb/s 2^{23}-1 PRBS was modulated by the RSOA in phase. The US optical signal then passed through the optical circulator and was sent to the ODN with a power level of -3 dBm. The US signal was detected at the OLT by an identical polarization diversity heterodyne Rx as the one in the ONU.

The ODN consisted of 20 km of SMF and a 1:4 power splitter. A second 5 km spool was added for the UDWDM as drop fiber. One of the CE characterized in last section, specifically CE2, multiplexed/demultiplexed the UDWDM and EPON signals. A variable optical attenuator (VOA) emulated further splitting and limited the optical power after the fiber link.

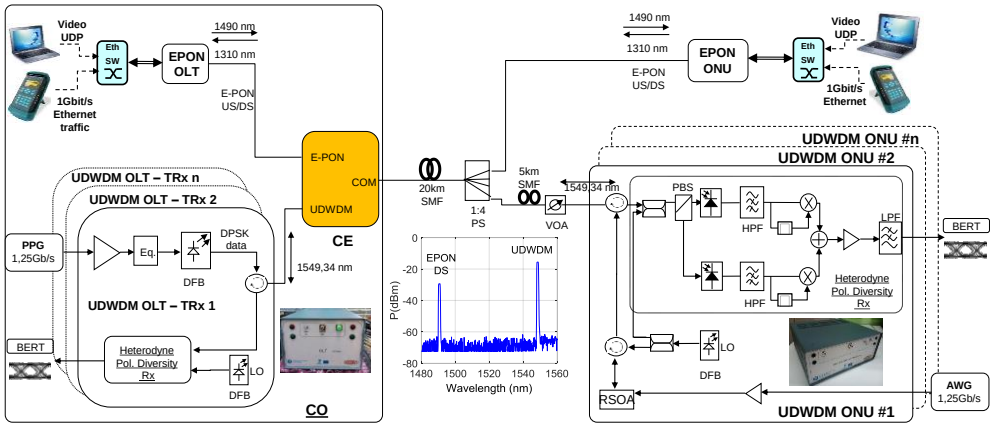

Figure 2.15. Experimental setup schematics (The inset shows the optical spectrum in DS).

First, the performance of the DS and US independent transmissions was measured. The results are plotted in Figure 2.16(a). In DS, an Rx sensitivity of –39 dBm was obtained at a forward error correction (FEC) level BER of 10^{-3}, and –33 dBm at BER=10^{-9}. In US, the Rx sensitivity was -40 dBm at BER=10^{-3} and -34 dBm at BER=10^{-9}. The difference between DS and US was around 1 dB, because the RSOA produces a clearer phase modulated signal than the direct modulated DFB.

Then, the bidirectional setup was tested. As described before, there was a spectral separation of 2.5 GHz between DS and US. Rx sensitivities were –37.5 dBm and –38.5 dBm at BER= 10^{-3} for DS and US transmission respectively, and of -31.5 dBm and -32.5 dBm at BER=10^{-9} as is shown in Figure 2.16(b). A penalty of about 1.5 dB is observed with respect to independent transmission due to a residual spectral overlap between the signals side-lobes and the Rayleigh Backscattering effect.

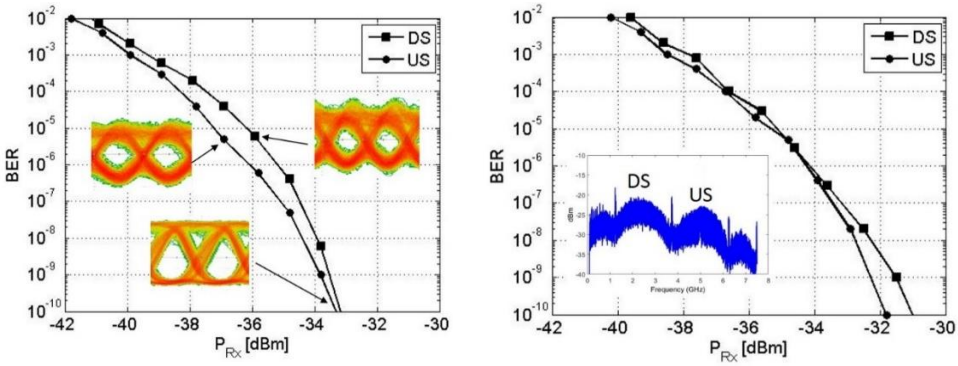

Figure 2.16. BER against received power for: (a) independent DS and US transmissions, (b) bidirectional transmission (the inset shows the optical spectra of DS and US separated by 2.5 GHz.

Another possible cause of penalty in the bidirectional case was the laser frequency drifts between ONU and OLT. This effect was evaluated by setting the received optical power in the OLT at -32.5 dBm (corresponding to BER=10^{-9}) and tuning the LO emission frequency in steps of 12.5 MHz. The BER against frequency drift of the LO, is plotted in Figure 2.17(a). As the LO moved away, the BER was degraded. A drift of ±80 MHz was tolerated for a 1 dB penalty, this was considered when passing from BER=10^{-9} to 5x10^{-8} (see Figure 2.16(b)).

Along this chapter, it has been seen that one of the major requirements for future access networks is to coexist with legacy deployed systems, as is stayed in NG-PON2 standard [21]. Then, a CE was added as optical mux/demux at the OLT output, and DS and US transmission were tested while simultaneously a commercial EPON system (λ_{US}=1310nm, λ_{DS}=1490nm) operated in the same ODN. Ethernet traffic at 1 Gb/s, including video streaming, was sent over the EPON system, in both US and DS. The effect on the UDWDM system was minor and the results are plotted in Figure 2.17(b). The main effect on the UDWDM was a residual baseband noise, caused by the direct detection of the EPON signal as can be seen in the electrical spectrum (inset of Figure 2.17(b)). However, the heterodyne DPSK Rx can filter most of these components and the penalty in the performance was limited below 1 dB in both DS and US. In addition, the EPON system was detected with negligible penalty; hence no effect was observed on the video transmitted.

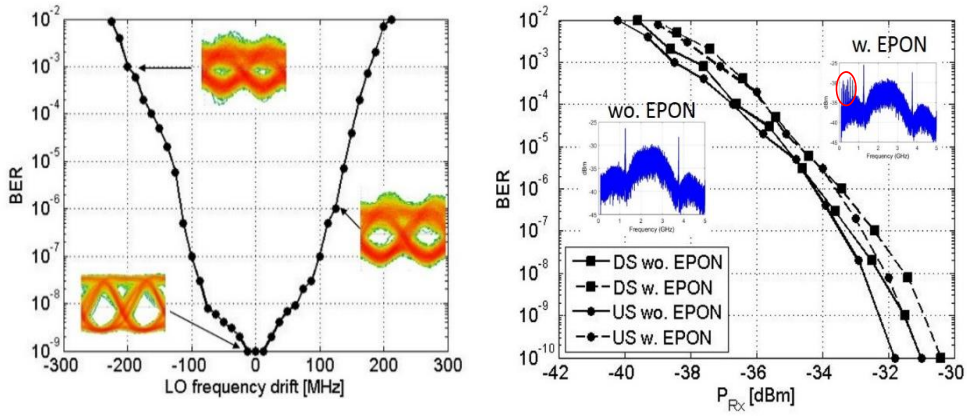

(a) (b)

Figure 2.17. (a) BER against frequency drift of the LO in the OLT, (b) BER against received optical power of UDWDM system coexisting with EPON signals.

Finally, the minimum CS and the effect of power difference between users in the UDWDM-PON was evaluated. For this, a second ONU was added to the setup and coupled to the ODN. The first user was left at a constant Tx power and wavelength and arrived with -35 dBm to

the OLT Rx for a BER=3x10^{-5}. Conversely, the Tx power of the second user and its wavelength were varied. Figure 2.18 plots BER level curves for different CS and interference power (P_{int} = P_{user2} – P_{user1}) among users. From Figure 2.18, it can be deduced that the minimum CS to keep a 1 dB penalty (from level of BER=10^{-5} to BER=10^{-4}) was 12.5 GHz, with a tolerable power difference of 18 dB between the target system and the interferer system, which corresponds to approximately 64 users emitting at 0 dBm each.

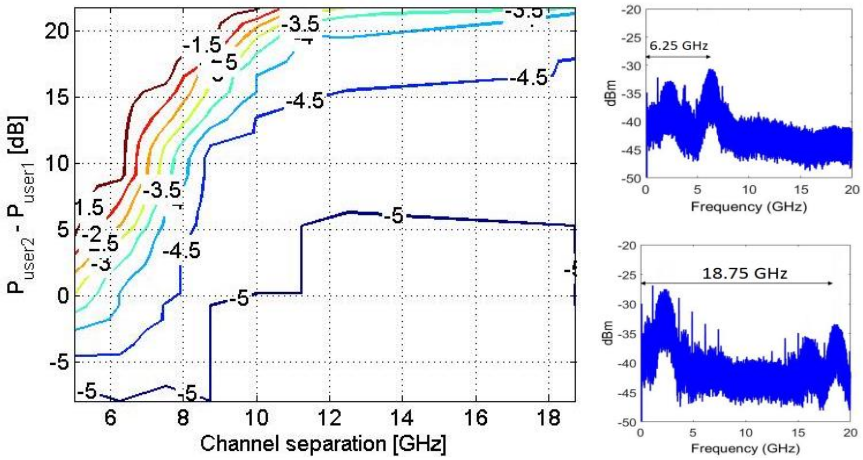

Figure 2.18. Log10(BER) for different interference powers and CS. The insets in the right show the electrical spectra of two users at CS of 6.25 GHz (upper) and 18.75 GHz (lower)

Table 2.6 summarizes the obtained results of this bidirectional Real-Time DSP-less Heterodyne UDWDM-PON.

Table 2.6. Rx sensitivity for unidirectional and bidirectional transmission UDWDM PON with analog heterodyne DPSK subsystem

	Unidirectional		**Bidirectional without EPON coexistence**		**Bidirectional with EPON coexistence**	
BER	DS	US	DS	US	DS	US
10^{-3}	-39 dBm	-40 dBm	-37.5 dBm	-38.5 dBm	-37 dBm	-37.5 dBm
10^{-9}	-33 dBm	-34 dBm	-31.5 dBm	-32.5 dBm	-31dBm	-31.5 dBm

2.3.4 Field-Trial of COCONUT UDWDM-PON with Real-Time Processing, λ-Monitoring and EPON Coexistence.

On February 2016th the COCONUT project field-trial was carried out in a public demonstration, where the most relevant concepts (network capacity upgrade by reusing legacy infrastructure, co-existence with legacy PONs and statistical wavelength allocation) and the functionalities enabled by the two main-stream COCONUT transceivers were demonstrated. The system testbed allowed the successful transmission of multiple PON signals and real time service distribution over an optical fiber network deployed in the city center of Pisa, which was made available at Scuola Superiore Sant'Anna (SSA) premises.

UPC was one of the main partners of the project developing the tasks related to the heterodyne and homodyne analog DPSK prototypes, as well as the experiments to guarantee full coexistence with the legacy EPON system. The author contributions were focused in demonstrate the real-time broadcasting of multiple HD videos using the heterodyne DPSK prototype, and simultaneously, the design and test of the coexistence scenario during the field-trial.

Below, the field-trial testbed and the wavelength plan are presented, and in addition, two experiments are described, the first one related to the heterodyne DPSK prototype performance, and the second to the coexistence of multiple COCONUT channels with an EPON system.

2.3.4.1. Setup and wavelength allocation plan using during the COCONUT demo

A scheme of the network is depicted in Figure 2.19. It comprises two OLTs (COCONUT and a legacy EPON). The COCONUT OLT down-streamed 14 WDM signals having different format and line rate: 2x1.25 Gb/s (DPSK), an 8x1.25 Gb/s on a 6.25 GHz grid (ASK), and 4x10 Gb/s (ASK) with 100 GHz separation. In addition, 3 US WDM signals (2x1.25 Gb/s DPSK and 1x1.25 Gb/s ASK) where placed in the ODN which comprised 10 km of deployed dark SMF in a loop between SSA labs the Pisa city center. Although it was quite short, the loop was composed of many different splits and cable trunks optically joined by means of SC optical connectors in various distribution points, with a total insertion loss of about 10 dB. After this external trunk, the optical distribution network continued in the lab and was composed of power splitters and additional strands of drop fibers of various lengths to connect the 5 ONUs so that different use cases (short and long reaches) could be tested. With this

configuration, the ODN loss between the OLT and the ONUs ranged between 18 and 40 dB and the fiber reach ranged from 10 to 35 km.

The DS signals were connected to a 100 GHz AWG which multiplexed and demultiplexed the DS and US channels. Each ONU selected its own DS channel by proper tuning its LO without any optical filtering. An HR-OSA connected to the common port of the AWG monitored both DS and US by tapping 1 dB power. Then, a CE was placed to insert an EPON signal, and to guarantee full coexistence between COCONUT and the legacy EPON system. The inset in Figure 2.19 shows the optical spectrum of all channels in the same ODN.

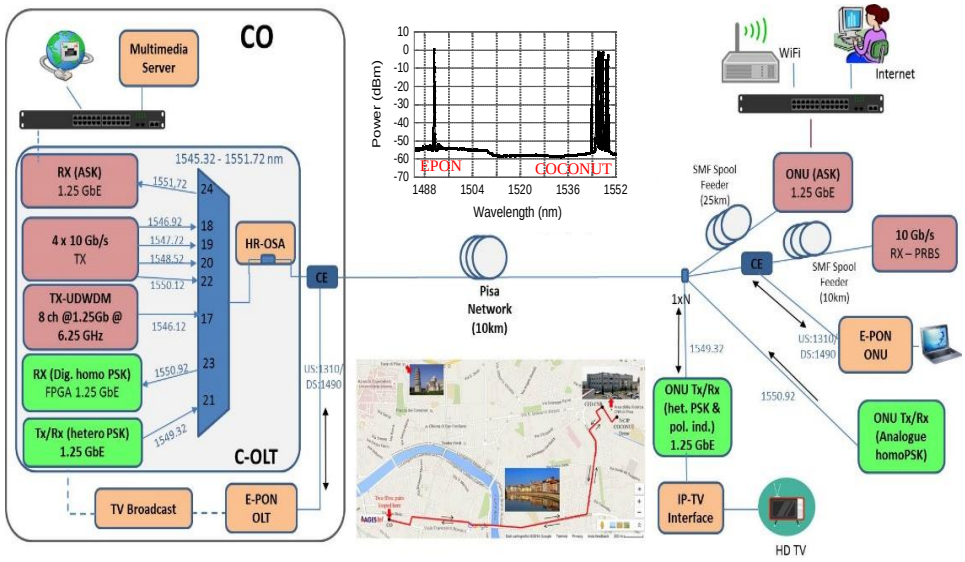

Figure 2.19. Field-trial setup schematics. The insets show the optical spectrum of EPON DS and all COCONUT channels in C-band (upper), and the map with the deployed fiber across city of Pisa.

The use of different transceivers aimed at demonstrating not only the feasibility and co-existence of the two main COCONUT flavors (ASK and DPSK), but also the realization of different functionalities and use cases. Each OLT transceiver was connected to a corresponding ONU which was equipped with the corresponding technology. Notably, the optical distribution network did not contain any optical filter, although it is shared by the many COCONUT channels and a legacy PON system.

The COCONUT transceivers were operated at wavelengths in the C-band between 1546.12 nm and 1551.72 nm in the operating range of the HR-OSA. For each system, a corresponding AWG channel was assigned based on the ITU 100 GHz grid standard [29]. The exact wavelengths used in the testbed are shown in Figure 2.20(a) and Figure 2.20(b) and detailed

in Table 2.7. It is worth to note that the US signal spectrum recorded at the OLT input, shows not equalized power levels; indeed, this reflects the different ODN losses experienced by the three ONUs, placed at different distances and at different power splitting points of the testbed.

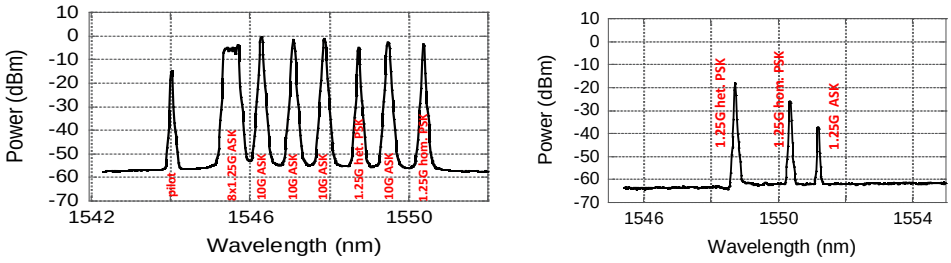

(a) (b)

Figure 2.20. Optical spectrum distribution during the field-trial: (a) DS wavelengths, (b) US wavelengths.

Table 2.7. Wavelength allocation plan for COCONUT field-trial demonstration

Setup	Link	Wavelength (nm)	Central Frequency (THz)	ITU channel
8 x 1.25 G ASK	DS	1546.12	193.900	39
	US	1551.72	193.200	32
4 X 10 G ASK	DS	1546.92	193.800	38
		1547.72	193.700	37
		1548.51	193.600	36
		1550.12	193.400	34
1.25 G heterodyne DPSK	DS	1549.32	193.900	35
	US	1549.32 + 0.02	193.902	
1.25 G homodyne DPSK	DS	1549.52[5]	193.300	33
	US	1549.52	193.300	

2.3.4.2. Heterodyne PSK System performance and real-time video-streaming setup

One of the main experiments carried out during the COCONUT public demo was a fully operative analog heterodyne DPSK prototype at 1.25 Gb/s. The OLT and ONU DPSK prototypes, whose technical characteristics were described in sub-section 2.3.3, were placed in separate benches and connected through the described fiber link. The ONU Rx sensitivity

[5] This wavelength was used as dummy channel (in CW mode) corresponding to the analog homodyne prototype whose performance was not tested.

at FEC level was around -38 dBm as is plotted in Figure 2.21 (a). There was a penalty of <1 dB between optical back-to-back (btb) and ODN transmissions, basically due to -25 dB reflectance of the ODN. Even with the spectral separation of 2.5 GHz between US and DS, that limited the interference caused by the added baseband noise (Figure 2.21 (b)), when all the channels were coexisting, and in presence of some RB, the performance was degraded by 1.5 dB, mainly due to the 10 Gb/s channels which added as noise in the whole receiver spectrum. The US was also active in these results.

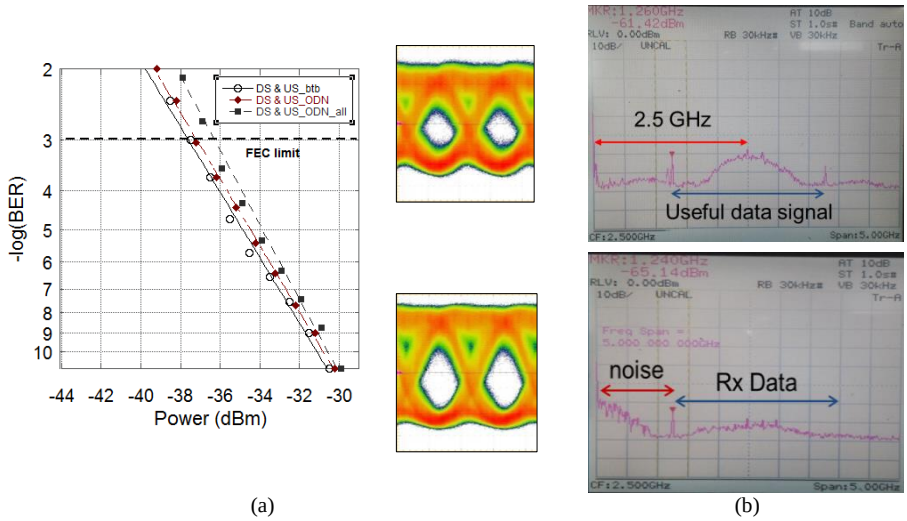

Figure 2.21. (a) BER against Rx power for 1.25 Gb/s heterodyne DPSK system. The insets show the eye diagrams of the detected signal at BER=10^{-4} (upper) and BER=10^{-9} (lower), (b) Electrical spectrum of the Rx signal when just the heterodyne DPSK was in the ODN (upper), and when all systems were active in the ODN (lower).

In order to test the transmission of services through the heterodyne system, a video-streaming setup was implemented as depicted in Figure 2.22. An HD video was broadcasted by using a PROMAX HD Video player module provided by PROMAX Electronica. Three more videos were sent simultaneously using PROMAX module 324 for a total traffic of 110 Mb/s approximately. PROMAX module 421 converted asynchronous serial interface (ASI) signals to internet protocol (IP) and added an XOR forward error correction (FEC) column. The videos were transmitted by using the real-time transport protocol (RTP). Additionally, a PRBS 2^{31}-1 was encapsulated in a Gigabit Ethernet frame and transmitted through a Trend GbEth Unipro traffic generator. All the Ethernet signals were combined by means of an Ethernet switch (SW) which also provided connectivity to the E-PON OLT. Both COCONUT heterodyne ONU and E-PON ONU detected the broadcasted HD videos.

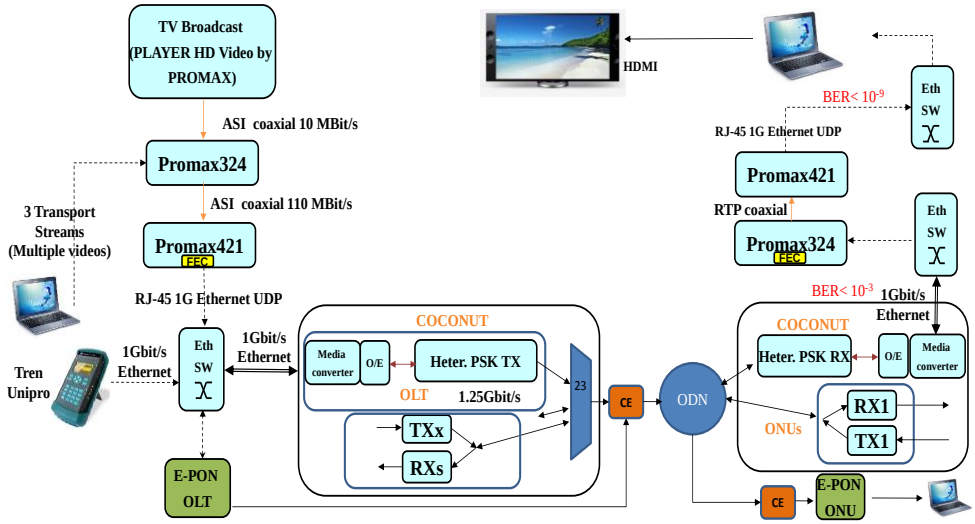

Figure 2.22. Setup implemented for video transmission using Heterodyne PSK prototype

In order to modulate the DPSK transceivers, the Ethernet signal was transformed through Media Converters (MC), one placed at the OLT and one placed at the ONU. The box containing the MCs is shown in Figure 2.23.

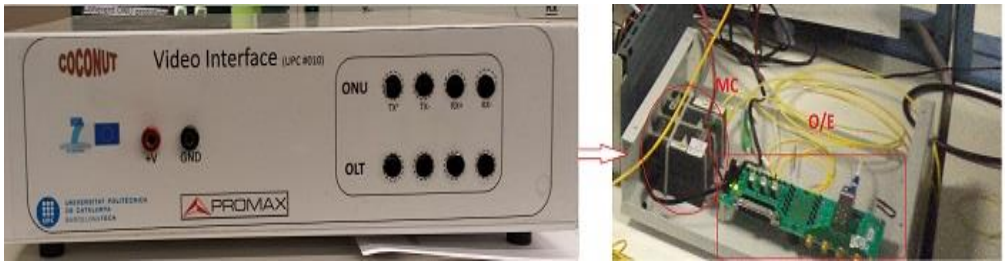

Figure 2.23. Video interface box; external design (left) and internal distribution (right)

Once the optical signals were detected at the COCONUT ONU, the bits were transformed back to Ethernet frames by a second MC. The MC was connected to an Ethernet SW as well as to a PROMAX 324 module, which removed the FEC. The PROMAX 324 was connected to PROMAX 421 device to provide a signal to a PC. The PC was connected to an external screen through an HDMI interface to display the videos as observed in Figure 2.24(a). The complete ONUs bench is shown in Figure 2.24(b), which the heterodyne PSK ONU prototype, the video interface and the PROMAX modules for video broadcasting can be seen.

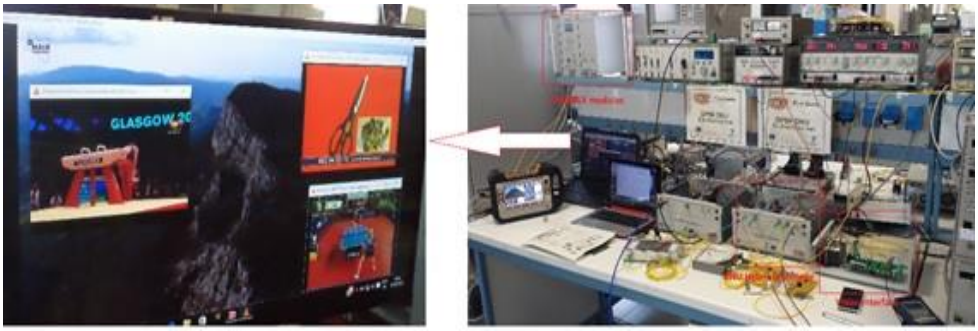

Figure 2.24. (a) Successfully transmitted HD videos during the field-trial demo, (b) Complete heterodyne DPSK ONUs bench.

2.3.4.3. Coexistence with Legacy EPON system

COCONUT and E-PON signals were transmitted simultaneously taking advantage of the CEs provided by BT, which were described and characterized in sub-section 2.3.1. CE3 was placed at CO at the output of the AWG in order to combine and separate the E-PON and the COCONUT channels (Figure 2.25(a)). CE2 was placed at costumer premises in order to act as WBF for the E-PON ONU and to provide connectivity to the 4 x 10G setup as is depicted in Figure 2.25(b).

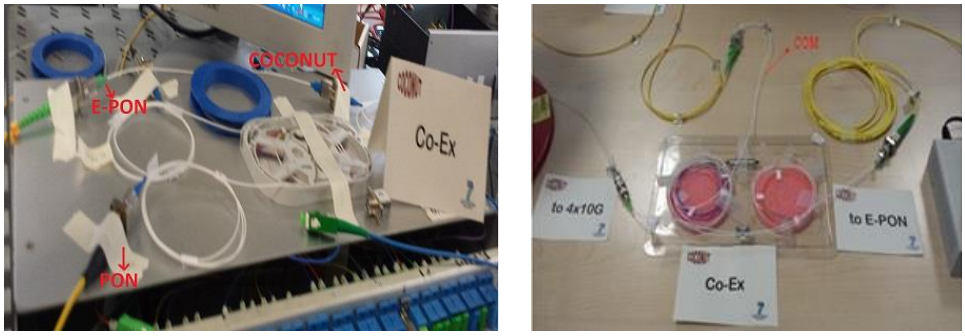

(a) (b)

Figure 2.25. (a) CE3 at OLTs during the DEMO, (b) CE2 at ONUs side during the DEMO

In addition, the wavelength plan specified for COCONUT system gives the possibility to coexist with legacy PON systems without interference between systems. Considering the practical possibility of ignoring the RF-video band, because it has low usage, for example if the video is transmitted as IP-TV, the wavelengths used by COCONUT in the demonstration, would not overlap with GPON/E-PON, XG-PON and NG-PON2 wavelengths as is shown in Figure 2.26.

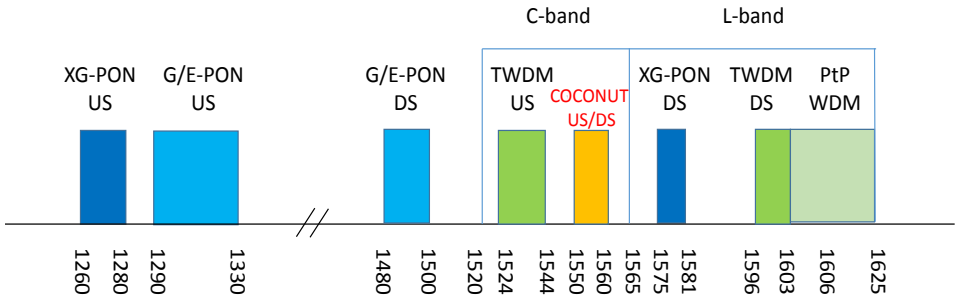

Figure 2.26. Wavelength allocation used during the COCONUT field-trial ensuring full coexistence.

Finally, Figure 2.27(a) and Figure 2.27(b) show the E-PON OLT and ONU respectively, operating and transmitting successfully the video in coexistence with COCONUT signals. When adding the EPON to the COCONUT network, the performance of the COCONUT systems was not affected. Previous paragraphs explain that the major effect was because of the other COCONUT channels. Furthermore, the EPON system did not suffered interference due to overlaying the COCONUT signals on the same ODN and continued transmitting the video without any interruption.

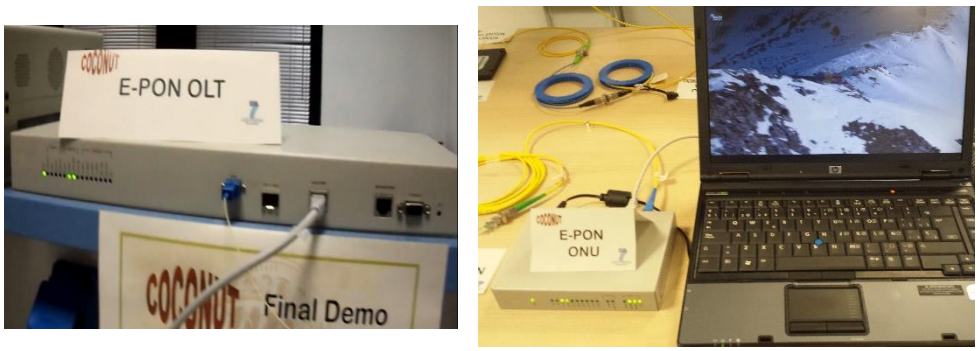

(a) (b)

Figure 2.27. (a) EPON OLT transmitted real-time data, (b) EPON ONU receiving successfully the video during COCONUT field-trial

In this chapter, technical characteristics of the transceivers developed for the COCONUT prototypes has been specified. Moreover, next chapters of this PhD thesis cover different novel proposals which enhance the features of the developed COCONUT ONUs keeping their low-cost and simplicity.

2.4 Chapter summary

This chapter comprises one of the main objectives of this PhD thesis as is the study of different of coexistence between the future NG-PON networks and the current deployed systems as E-PON.

First, a theoretical study of the coexistence requirements standardized in the new ITU-T G.989 recommendation of 40G capable NG-PON2 was presented, highlighting the need of two important elements, a CE at the CO, and a WBF at customer premises. The former acts as wavelength filter multiplexing and demultiplexing the US and DS signals of both the legacy and the NG-PON systems. The latter allows to reject the interferer channels acting as an optical filter at each ONU. The minimum isolation requirements at each port of the CE were calculated in and NG-PON2 – G-PON coexistence scenario to minimize the effect of inter-channel crosstalk in US transmission. In the worst case (maximum differential ODN loss difference in dB for the target signal and the interfering signal) the required isolations (I_{WDM}) were 29 dB and 36 dB at NG-PON2 and G-PON port respectively.

Second, the concept of "Wavelength-to-the-User" was introduced with the presentation of the work developed in the European COCONUT project, which demonstrated a new paradigm of low-cost coherent transceivers enabling the implementation of an UDWDM-PON. Among the studies done by the author, the design and dimensioning of some ONU and OLT architectures were discussed considering the limited thermal tunability of commercial DFB lasers (2nm with ±10ºC). Regarding the ONU architecture, and in order to serve 256 ONUs operating at 1.25 Gb/s, at least 282 channels spaced 6.25 GHz are needed losing less than 10% (12.8/14.1 = 90%) in channel spectral efficiency. In addition, an alternative OLT architecture by using an athermal AWG combined with a thermal AWG or two thermal AWGs was proposed by tuning the spectral response, interleaving the output channels in such a way that AWGs have complementary frequency responses in order to have full spectral efficiency.

Afterwards, a wavelength plan for the COCONUT network was proposed, analyzing several network scenarios and the available wavelength spectrum. Also, the analysis of US inter-channel crosstalk applied between NG-PON2 and G-PON was repeated between NG-PON and the COCONUT system depending on the number of channels to be used. The required I_{WDM} at the NG-PON2 port of the CE being interfered by a COCONUT system at 1.25 Gbit/s

is I_{WDM} = 40 dB. The opposite case was not analyzed, and it is left FFS, where the large BW difference between the COCONUT and the interferer signals (I_{BIDI} = 9) should be considered.

Finally, the characterization of several CEs were presented and two real-time experiments were explained including some results of the COCONUT field-trial. Both experiments demonstrated full coexistence with a commercial E-PON system thanks to the use of the CE. The author contribution in the field trial was focused mainly in two experiments. First, the design and demonstration of a real-time HD video-streaming using the analog heterodyne DPSK prototype. Second, the transmission of standard definition video using the commercial EPON system with full coexistence with the COCONUT deployed network. Both experiments were tested across a 10 km dark fiber link between SSA laboratories and Pisa city center added to 10 km of extra SMF placed into the SSA labs, demonstrating that there was not mutual interference between the systems. The results of this experiments have been widely published in [5]–[7].

These studies and experiments formed the basis for the investigation on novel proposals to be presented in following chapters. In chapter 3, a fully digital reconfigurable TRx based on direct phase modulation of a DFB laser will be explained, able to support higher data rates, by employing multilevel formats (see chapter 4) or hybrid modulation formats (see chapter 5), and simplified coherent Rx, reusing the LO laser, or implementing phase scrambling techniques (chapter 6).

Bibliography Chapter 2

[1] D. Nesset, "PON Roadmap [Invited]," *J. Opt. Commun. Netw.*, vol. 9, no. 1, pp. A71–A76, Jan. 2017.

[2] P. Chanclou, A. Cui, F. Geilhardt, H. Nakamura, and D. Nesset, "Network operator requirements for the next generation of optical access networks," *IEEE Netw.*, vol. 26, no. 2, pp. 8–14, Mar. 2012.

[3] J. Prat *et al.*, "Towards ultra-dense wavelength-to-the-user: The approach of the COCONUT project," in *Proc. 15th Int. Conf. on Transp. Opt. Netw. (ICTON)*, Cartagena, Spain, 2013.

[4] "COst-effective COhereNt Ultra-dense-WDM-PON for lamda-To-the-user access." [Online]. Available: http://www.ict-coconut.eu.

[5] I. N. Cano *et al.*, "Field-Trial of Low-Cost Coherent UDWDM-PON with Real-Time Processing, λ-Monitoring and EPON Coexistence," in *Proc. 42nd Eur. Conf. on Opt. Commu. (ECOC)*, Düsseldorf, Germany, 2016.

[6] M. Presi *et al.*, "Field-Trial of a High-Budget, Filterless, λ -to-the-User, UDWDM-PON Enabled by an Innovative Class of Low-Cost Coherent Transceivers," *J. Light. Technol.*, vol. 35, no. 23, pp. 5250–5259, Dec. 2017.

[7] J. Prat *et al.*, "Ultra-dense WDM access network field trial," in *Proc. 21st Eur. Conf. on Netw. and Opt. Commu. (NOC)*, Lisbon, Portugal, 2016.

[8] International Telecommunication Union, "ITU-T G.984.1 Recommendation: Gigabit-capable passive optical networks (GPON): General characteristics." Mar-2008.

[9] G. Vall-llosera *et al.*, "COCONUT cost, power consumption and migration analysis: A route towards NG-PON3," in *Proc. 17th Int. Conf. on Transp. Opt. Netw. (ICTON)*, Budapest, Hungary, 2015.

[10] International Telecommunication Union, "ITU-T G.989 Recommendation, 40-Gigabit-capable passive optical networks (NG-PON2): Definitions, abbreviations and acronyms." Oct-2015.

[11] International Telecommunication Union, "ITU-T G.984.5 Recommendation, Gigabit-capable passive optical networks (G-PON): Enhancement band." May-2018.

[12] International Telecommunication Union, "ITU-T G.984.5 Recommendation, Gigabit-capable passive optical networks (G-PON): Enhancement band. Amendment 1." May-2018.

[13] International Telecommunication Union, "ITU-T G.984.6 Recommendation: Gigabit-capable passive optical network (G-PON): Reach Extension." Mar-2008.

[14] D. Nesset, "NG-PON2 Technology and Standards," *J. Light. Technol.*, vol. 33, no. 5, pp. 1136–1143, Mar. 2015.

[15] International Telecommunication Union, "ITU-T G.989.1 Recommendation, 40-Gigabit-capable passive optical networks (NG-PON2): General requirements." Mar-2013.

[16] International Telecommunication Union, "ITU-T G.698.1 Recommendation: Multichannel DWDM applications with single-channel optical interfaces." Nov-2009.

[17] W. Poehlmann, R. Bonk, H. Schmuck, and Th. Pfeiffer, "Cross-talk analysis & mitigation for TWDM-PON upstream path," in *Proc. 40th Eur. Conf. on Opt. Commu. (ECOC)*, Cannes, France, 2014.

[18] R. Bonk, W. Poehlmann, H. Schmuck, and Th. Pfeiffer, "Cross-talk in TWDM-PON beyond NG-PON2," in *Proc. Opt. Fiber Commu. Conf. (OFC)*, Los Angeles, CA, USA, 2015.

[19] Hee Yeal Rhy, Gwang Yong Yi, Han Hyub Lee, and Sang Soo Lee, "Inter-channel Crosstalk Impairment of Time and Wavelength Division Multiplexing Passive Optical Network," in *Proc. 39th Eur. Conf. on Opt. Commu. (ECOC)*, London, UK, 2013.

[20] H. H. Lee, H. Y. Rhy, G. Y. Yi, J. H. Lee, and S. Lee, "Investigation on Burst-mode Inter-channel Crosstalk in XG-PON and TWDM-PON," in *Proc. Opt. Fiber Commu. Conf. (OFC)*, San Francisco, CA, USA, 2014.

[21] International Telecommunication Union, "ITU-T G.989.2 Recommendation, 40-Gigabit-capable passive optical networks (NG-PON2): Physical Media Dependent Layer Specification." May-2014.

[22] THORLABS, "Single Mode Fiber Optic Circulators." [Online]. Available: http://www.thorlabs.de/newgrouppage9.cfm?objectgroup_id=373.

[23] V. Sales, J. Segarra, V. Polo, J. C. Velásquez, and J. Prat, "UDWDM-PON Using Low-Cost Coherent Transceivers With Limited Tunability and Heuristic DWA," *J. Opt. Commun. Netw.*, vol. 8, no. 8, p. 582, Aug. 2016.

[24] J. Prat *et al.*, "Technologies for Cost-Effective udWDM-PONs," *J. Light. Technol.*, vol. 34, no. 2, pp. 783–791, Jan. 2016.

[25] G. Vall-llosera, A. Rafel, E. Ciaramella, and J. Prat, "COCONUT requirements for residential, business and outdoor scenarios," in *Proc. 15th Int. Conf. on Transp. Opt. Netw. (ICTON)*, Cartagena, Spain, 2013.

[26] V. Sales, J. Segarra, V. Polo, and J. Prat, "Statistical UDWDM-PONs Operating With ONU Lasers Under Limited Tunability," *IEEE Photonics Technol. Lett.*, vol. 27, no. 3, pp. 257–260, Feb. 2015.

[27] V. Polo, P. Borotau, A. Lerin, and J. Prat, "DFB laser reallocation by thermal wavelength control for statistical udWDM in PONs," in *Proc. 40th Eur. Conf. on Opt. Commu. (ECOC)*, Cannes, France, 2014.

[28] G. Y. Chu, A. Lerín, I. N. Cano, V. Polo, J. A. Tabares, and J. Prat, "Exploiting RSOA for Uplink Transmission with Coherent Detection for Low Cost UDWDM-PON," in *Asia Communications and Photonics Conference 2014*, Shanghai, 2014, p. AF2B.1.

[29] International Telecommunication Union, "ITU-T G.694.1 Recommendation, Spectral grids for WDM applications: DWDM frequency grid." Feb-2012.

[30] I. N. Cano, J. C. Velasquez, V. Polo, and J. Prat, "Bidirectional real-time DSP-less heterodyne UDWDM-PON," in *Proc. 19th Int. Conf. on Transp. Opt. Netw. (ICTON)*, Girona, Spain, 2017.

[31] British Telecommunications plc, "Specification RC 9354 for GPON passive optical filter for co-existence with a NG-PON." 2010.

[32] Dennis Derickson, *Fiber Optic Test and Measurement*. New Jersey,USA: Hewlett-Packard. Prentice Hall, 1998.

[33] I. N. Cano, A. Lerin, V. Polo, and J. Prat, "Direct Phase Modulation DFBs for Cost-Effective ONU Transmitter in udWDM PONs," *IEEE Photonics Technol. Lett.*, vol. 26, no. 10, pp. 973–975, May 2014.

[34] I. N. Cano, A. Lerín, V. Polo, and J. Prat, "Simplified Polarization Diversity Heterodyne Receiver for 1.25Gb/s Cost-Effective udWDM-PON," in *Proc. Opt. Fiber Commu. Conf. (OFC)*, San Francisco, CA, USA, 2014.

Chapter 3. Direct phase modulated DFB lasers

As explained in chapter 2, current deployed FTTH PONs are based on TDM using only one or two shared wavelengths ($\lambda_{DS}/\lambda_{US}$) widely spaced around 50 or 100 GHz [1]. However, with the expected growth in fixed broadband subscriptions and mobile traffic, these systems may not cope with the expected BW demands [2], [3]. As a feasible solution, we have proposed the UDWDM approach, implementing the WTTU concept, and reducing the channel spacing (CS) to 6.25 or 12.5 GHz grid, increasing the optical spectrum efficiency (SE) [4].

The enabling technologies are the coherent TRx that provide higher sensitivity and inherent wavelength selectivity compared to DD systems [5], Nevertheless, the complexity of conventional coherent TRx has limited their attractiveness in access networks. To overcome this constraint, we recently proposed a cost-effective coherent TRx based on a Direct Modulated Laser (DMLs), and a simplified coherent Rx [6]. Recently, we experimentally demonstrated that these transceivers support 1 Gb/s per subscriber in a 6.25 GHz grid UDWDM-PON [7]–[9].

Although traditionally intensity modulation (IM) is used in deployed PONs, either the phase or frequency of the optical carrier can also be modulated to transmit information in a single optical carrier. Phase modulation (PM) and coherent detection are very attractive strategies because of their improvement in Rx sensitivity, and their higher tolerance to fiber nonlinearities compared to IM/DD systems [10]. As well, PM with coherent detection improve SE enabling the use of multilevel modulation as will be presented in chapter 4. This is possible because positive and negative sides of both I and Q components in the complex plane are used [10].

Other aspect, that is a major concern in UDWDM-PONs, is the unwanted spectral side-lobes resulting when modulating the optical carrier. Since the frequency grid is very narrow, these spectral components cause interference to adjacent channels, yielding to BER degradation. To overcome this problem, the use of Nyquist pulse shaping in the Tx has been broadly studied as a solution to reduce the optical spectrum width, and thus minimizing the interference between neighbor channels, and leading to improvement of the optical SE [11]–[14].

In the first section of this chapter, the results of a simply digital equalization technique to perform direct phase modulation of a DFB laser is presented. The proposed method is validated in a 25-km of SMF link with intradyne coherent detection. The results has been published in [15], [16].

In the second part of this chapter, a directly phase modulated Tx with Nyquist pulse shaping is presented, showing the feasibility for a low-cost implementation of an UWDM-PON with 440 users operating at bitrates of 2.5Gb/s, and allocated in a 6.25 GHz optical spectral grid. This technique demonstrated, for the first time to the best of our knowledge, in [17], [18]. The simplicity of the coherent TRx compared to other high cost solutions based on external modulators [11], [12] demonstrates the potential feasibility as a solution in next generation FTTH systems.

3.1 Direct phase modulation with digital beat signals

When directly modulating a laser, both an IM and an intrinsic frequency modulation (FM) are produced [19], [20]. If IM is desired, the amplitude of the modulating current is changed to obtain a variation in the optical output power, whereas the FM is a residual undesirable effect known as frequency chirp ($\Delta\nu$), or simply chirp. This chirp causes a spectral broadening during the transmission through the optical fiber, leading to ISI and degrading the system performance. At the same time, a controlled chirp or frequency deviation, can be used to produce a desired phase change of the optical carrier and then to perform PM, with a quasi-negligible residual IM.

The relationship between the IM and FM in a laser is described by the extensively studied laser rate-equations, which define how the photon and carrier densities change with the time, and their influence in the optical field inside the laser cavity [20], [21]. From these equations it is clear that the optical intensity is proportional to the photon number, which depend of the

carrier density via the photon rate equation. In addition, the FM, and thus the chirp can be related directly to the photon density or output power $P(t)$ by [22], [23]:

$$\Delta\nu(t) = \frac{\alpha_H}{4\pi}\left(\frac{d}{dt} ln\, P\,(t) + \kappa P(t)\right) \tag{3.1}$$

where α_H is the linewidth enhancement factor, also known as Henry parameter, and κ is the adiabatic chirp coefficient due to the non-linear gain.

According to the modulation frequency (f_m), the first or second term of Eq. 3.1 dominates. At mid frequencies (10 MHz < f_m < 5 GHz) the second term, i.e. the adiabatic chirp, prevails. For larger frequencies (f_m > 5 GHz) the first term of Eq. 3.1, i.e. the transient chirp, is dominant and the frequency chirp gets proportional to f_m. In addition, it is important to mention that the thermal effects are not considered in Eq. 3.1 since there are only significant at lower frequencies (f_m < 10 MHz) [20], [24].

The α_H and κ parameters are specific to each laser and can be inferred from the ratio between the IM response (H_{AM}) and the FM response (H_{FM}). H_{AM} can be obtained easily using a Vector Network Analyzer for a large range of frequencies, while H_{FM} can be calculated from H_{AM} using a series of mathematical relations, derived from the use of some optical devices as discriminators (Mach-Zehnder (MZ) Interferometer [24] or optical filter [25]). The latter was used to characterize the DFB lasers employed during the experimental tests presented in this thesis. The most important characteristics to be guaranteed is that the optical filter has a well-defined linear zone, narrow BW and high slope for achieving a proper frequency discrimination [25].

Because one of the most relevant topics in this thesis is to understand how to perform the direct phase modulation, it is very important to remember the relation between the frequency shift, i.e. the chirp, and the change in the instantaneous optical phase $(\phi(t))$. Both are related thru a derivative term expressed by:

$$\Delta\nu(t) = \frac{1}{2\pi}\frac{d\phi(t)}{dt} \Leftrightarrow \phi(t) = 2\pi\int \Delta\nu(t)dt \tag{3.2}$$

In the frequency domain Eq. 3.2 can be expressed by:

$$\Delta\nu(\omega) = \frac{1}{2\pi} j\omega\Delta\phi(\omega) \Leftrightarrow \Delta\phi(\omega) = \frac{2\pi}{j\omega}\Delta\nu(\omega) \tag{3.3}$$

From Eq. 3.3 is possible to relate the PM response (H_{PM}) with H_{PM}, calculating the FM and PM efficiencies. Both can be obtained by the ratio between the phase and frequency changes according to the modulating current as is expressed by:

$$\frac{\Delta\phi}{\Delta I}\left[\frac{Degree}{mA}\right] = \frac{2\pi}{j\omega}\frac{\Delta\nu}{\Delta I}\left[\frac{MHz}{mA}\right] \qquad 3.4$$

3.1.1 Digital equalization

For PM applications, it is important to know the phase response of the laser as function of the modulation frequency. According to Eq. 3.4 the PM response can be inferred if the H_{FM} is obtained. As an example, the commercial DFB laser NLK5C5E2KA of modulation BW > 10 GHz was characterized at Optical Communications Group (GCO) laboratory, applying the optical filter discriminator method proposed by K. Sato et al [25]. Having measured the AM responses at both sides of the optical filter discriminator (H_{AM}^{+} and H_{AM}^{-}) and having calculated the H_{FM}, the H_{PM} was obtained at different modulation frequencies as is shown in Figure 3.1

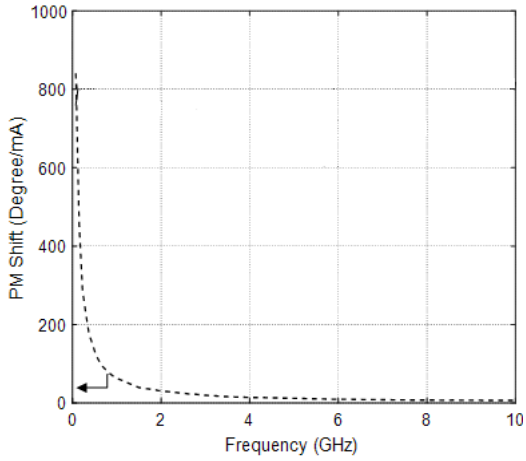

Figure 3.1. PM responses of the commercial NLK5C5E2KA DFB laser

The PM response shows that at low frequencies (< 1 GHz) there was a quick-decreasing dynamic consistent with the theoretical model of a pole $1/j\omega$ at the origin of coordinates as described in Eq. 3.3. Then the idea is to flatten the obtained curve to have a uniform response in all modulated frequencies. This can be performed applying a differentiator with transfer function $j\omega$ and implemented as a first-order high pass filter (HPF) preceding the laser. The

proposed equalization can be realized though an analog R-C network [26], and digitally, by programing a 1 tap finite impulse response (FIR) filter [15], [16]. Both, analog and digital equalizer schemes are depicted in Figure 3.2(a) and Figure 3.2(b), respectively.

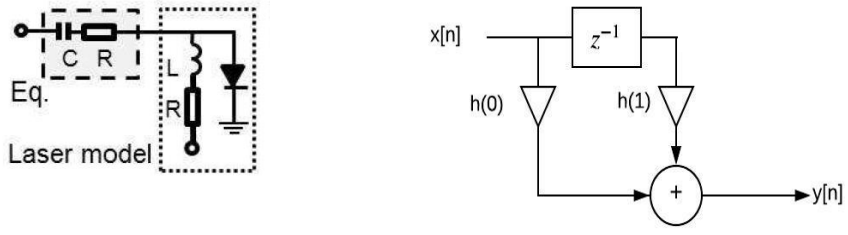

(a) (b)

Figure 3.2. Pre-equalizer versions for PM response compensation: (a) analog and (b) digital

The proposed beat phase modulation uses the digital version of the pre-equalizer. As an example, to obtain a proper binary phase modulated signal, phase shifts of π-radians must be generated. These phase shifts could be obtained considering the relation studied by R. Vodhanel [10]:

$$\Delta v(t) \cdot \Delta t = 0.5 \tag{3.5}$$

where Δt is the pulse width or duty cycle of the produced bipolar modulating signal. According to Eq. 3.2 the $\phi(t)$ is the time integral of the laser chirp, and consisted with Eq. 3.1 where at mid frequencies the adiabatic laser chirp prevails, it can be deduced that:

$$\left(\frac{\alpha}{4\pi}\kappa P(t)\right) \cdot \Delta t = 0.5 \tag{3.6}$$

It is noticed a double dependency from $P(t)$ and Δt, two parameters which can be adjusted by software. As a result, short pulses directly modulating the laser can generate optical phase changes according to signal power and duty cycle as we demonstrated in [15], [16].

3.1.2 Experimental validation

To study the proposed technique a 2^{15}-1 non-return to zero (NRZ) PRBS was differentially encoded and digitally equalized by means of a 1-tap FIR filter. The result was a three level

signal whose amplitude and duty cycle were digitally adjusted. The data signal was uploaded into an arbitrary waveform generator (AWGen) and the output power was varied by means of an 8 GHz electrical amplifier (SHF98P). The electrical waveform directly modulated the previously characterized DFB laser that was biased at 75 mA, in the regime where transient chirp is reduced. Then an optical DPSK signal proportional to the laser adiabatic chirp was generated. Figure 3.3(a) shows the completed Tx scheme, and Figure 3.3(b) shows the data waveform and phase changes during the generation process according with the bipolar return to zero (RZ) signal.

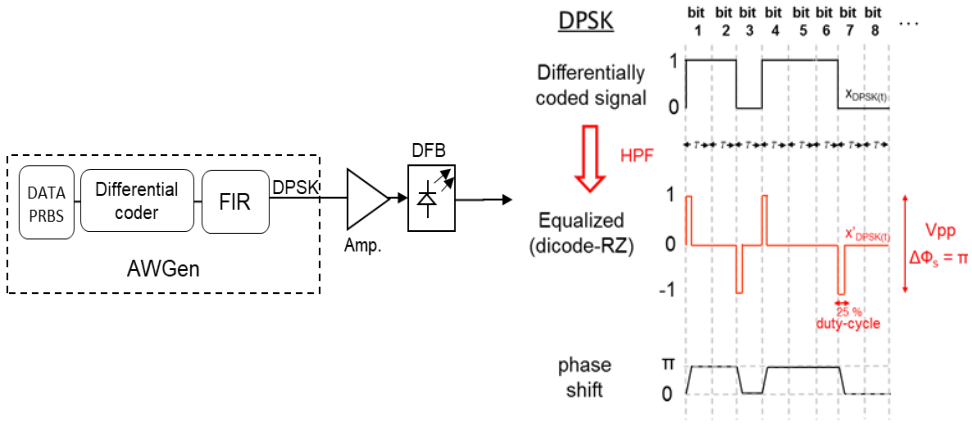

Figure 3.3. (a) Tx scheme for digital beat equalized laser, (b) beat signal generation

The proposed technique was experimentally tested in an UDWDM-PON composed by two identical Tx spectrally spaced 6.25 GHz. The complete setup as well as a real photo of the laboratory implementation are depicted in Figure 3.4(a) and Figure 3.4(b) respectively. Tx_1 was the previously referenced DFB (NLK5C5E2KA) which had 4 MHz linewidth, and emitted at λ_1 = 1544.9 nm. Tx_2 was another DFB (NX8563LB) with 2.5 GHz modulation BW and emitted at λ_2 = 1544.95 nm. Data 2 was also a PRBS 2^{15}-1 with a different seed to keep it uncorrelated with respect to Tx_1 data and with equal launched power of 0 dBm. Both users were combined in an optical 3 dB coupler and sent through 25 km of SMF. Afterwards, a VOA emulated the ODN losses and limited the Rx optical power.

The Rx was based on intradyne detection with a 3x3 optical coupler which mixed the optical signal with a LO. The LO was a 100 kHz linewidth ECL with 0 dBm optical power emitting at $\lambda_{LO} = \lambda_1$ = 1544.9 nm. The three outputs of the optical coupler were detected with 10 GHz p-i-n PDs followed by low-noise electrical amplifiers. The electrical signals were low-pass

filtered at R_b, sampled and processed with a 50 GSa/s real-time oscilloscope (RTO). Then, they were combined to obtain the I and Q components as described in [27]. Each component was differentially demodulated and then added. Afterwards, the samples passed through a 4th order low-pass filter at cutoff frequency of R_b and the BER was computed. The Rx can be implemented in real-time with digital processing as demonstrated in [7].

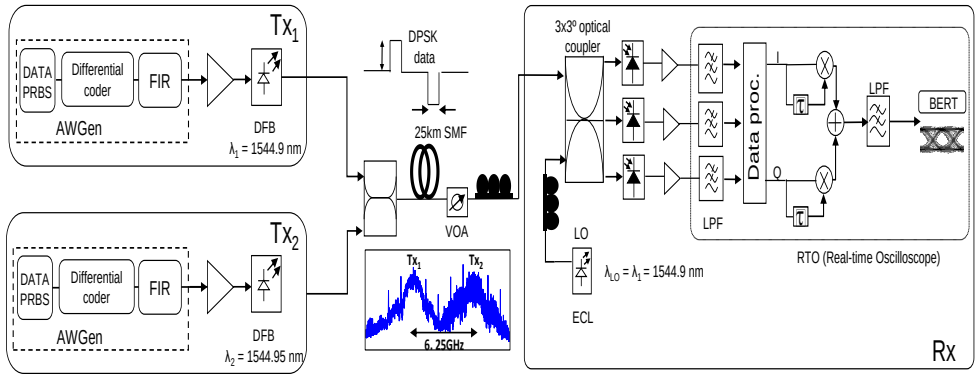

(a)

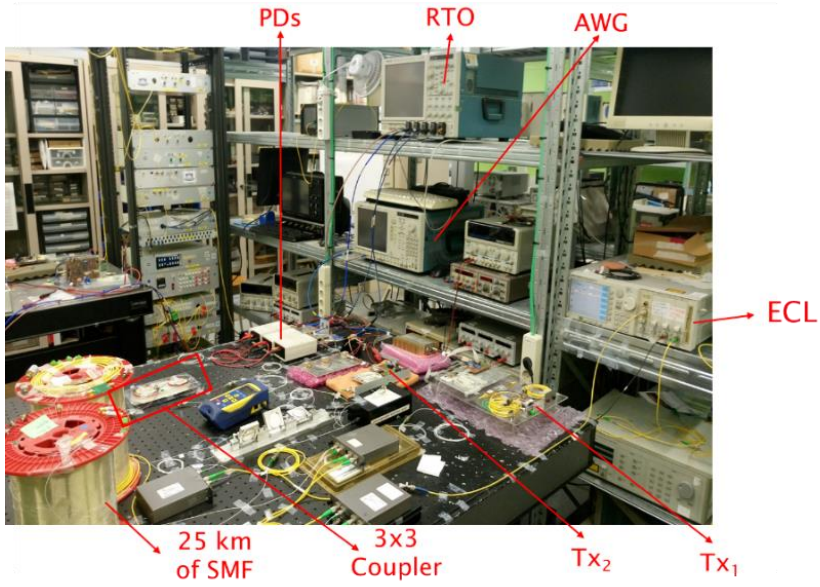

(b)

Figure 3.4. (a) Experimental schematics setup. The insets show the transmitted spectrum for two users Tx_1 and Tx_2 spectrally spaced 6.25 GHz. (b) Photo of the laboratory implementation.

To study the proposed technique, the setup was configured in optical btb, and the amplitude and duty cycle of the modulating signal were varied. The phase shift produced by the directly

modulated DFB was measured from the computed I and Q components of 2^{15} bits. The results are plotted in Figure 3.5(a) and Figure 3.5(b) for R_b = 1.25 Gb/s and 2.5 Gb/s respectively. For Rb = 5 Gb/s similar results were obtained. The colored level lines were normalized to π radians phase. The required amplitude and duty cycle values to get a π-phase shift for binary DPSK modulation are located inside the 0.8π area. When the proper values are set, the eye-diagram is clearly open, and the constellation points can be easily distinguished after differentially demodulated the Rx data (insets of Figure 3.5(a) and Figure 3.5(b)).

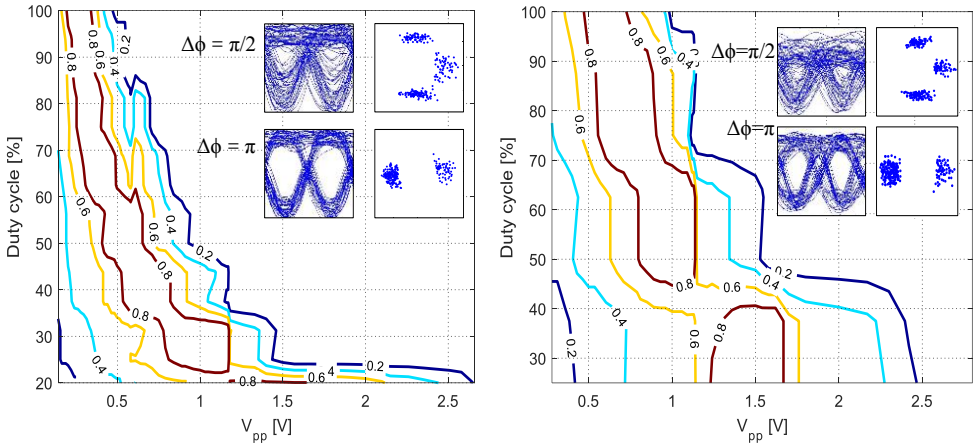

(a) (b)

Figure 3.5. Experimental phase shift obtained when changing the signal amplitude and duty cycle at (a) R_b = 1.25 Gb/s and (b) R_b = 2.5 Gb/s. The level lines indicate the phase shift as proportion to π radians, i.e. 1 represents π radians. The insets shows the I & Q and Eye diagrams for a phase shift of π/2 (top) and π (bottom) radians. The constellations show ± phase shifts and for that reason the complex conjugate also appears.

The reason for using 0.8π rad as boundary was derived from Figure 3.6. The required Rx power to achieve a BER = 10^{-4} was measured for the three considered R_b (1.25 Gb/s, 2.5 Gb/s, and 5 Gb/s). The beat signal had 50% duty cycle, and the power penalty was computed respect the phase difference from π radians. As observed, to keep the penalty <1 dB, the phase shift should be between 0.8π to 1.2π.

Afterwards, the effect of changing the duty cycle of the modulating signal was evaluated. Its amplitude, represented by the peak-to-peak voltage, was set to 0.5 V, 0.9 V and 1.6 V for the R_b of 1.25 Gb/s, 2.5 Gb/s, and 5 Gb/s respectively to get phase variations of π-radians.

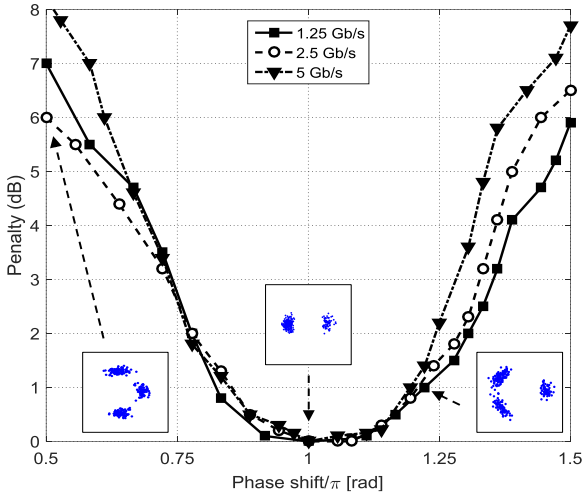

Figure 3.6. Sensitivity penalty at BER of 10^{-4} against phase shift from π rad. The x-axis is normalized to π radians, i.e. 1 represents π radians. The insets show the I & Q diagrams of π/2 rad, π rad and 11π/9 rad. The constellations show ± phase shifts and then the complex conjugate also appears.

Figure 3.7 shows the Rx sensitivity at BER = $4x10^{-3}$ against the duty cycle for R_b = 1.25 Gb/s, 2.5 Gb/s, and 5 Gb/s. For R_b = 1.25 Gb/s the penalty is negligible (<1 dB) for all duty cycles. On the other hand, for R_b = 2.5 Gb/s and 5 Gb/s, the penalty increases to almost 2 dB and 1.5 dB respectively for duty cycles > 50%. The reason for this penalty is mainly because in addition to the PM, there is also an inherent IM that cannot be cancelled because the HPF equalizing the laser PM response also modifies the IM response at lower frequencies. This remaining peaky IM introduces distortion in the detected signal that increased with R_b. The residual IM can be minimized searching the optimum amplitude of the RF modulating signal [26]. As well, it should be noted that the transmitted signal BW was more confined at 100% duty cycle compared with 50%. For 5 Gb/s, it was not possible to measure at 25% duty cycle because of limitation in the AWGen resolution. Another remark from Figure 3.7 is that the amplitude could be fixed to Vpp = 0.9 (indicated by the dotted diamonds), and only the duty cycle must be accordingly adapted in the Tx when changing the R_b, for a simpler and fully-digital reconfiguration of the equalizer preceding the laser. This is of special interest since linear electrical amplifiers are expensive especially at larger BWs.

After demonstrating the feasibility of the beat modulation technique, the sensitivity performance of the UDWM-PON was evaluated. The BER of Tx_1 was measured in optical btb and with the 25 km of SMF for a direct phase modulated Tx whose modulating signal had a duty cycle of 50%.

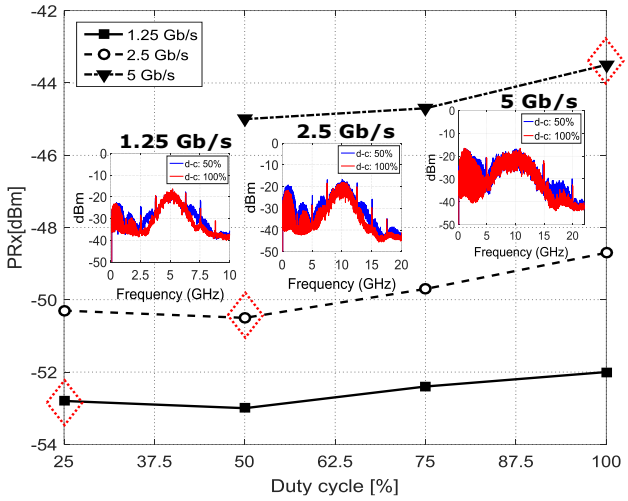

Figure 3.7. Rx power against duty cycle for beat phase modulated signals. The insets show the signal spectrum at 50 % and 100% duty cycle at a relative intermediate frequencies (IF) of 5 GHz for R_b = 1.25 Gb/s and at IF = 10 GHz for R_b of 2.5 Gb/s and 5 Gb/s. The red dotted diamonds indicate the performance when amplitude is left constant at the different bit rates.

The results are plotted in Figure 3.8. In optical btb the Rx sensitivities for BER of 4 x10^{-3} were approximately -53 dBm, -50.5 dBm and -45 dBm at R_b of 1.25 Gb/s, 2.5 Gb/s and 5 Gb/s respectively. Penalties below 0.5 dB were obtained when 25 km of SMF were added. The lower performance of the 5 Gb/s signal is explained by the limited BW of the electrical amplifier and the increase of the residual IM.

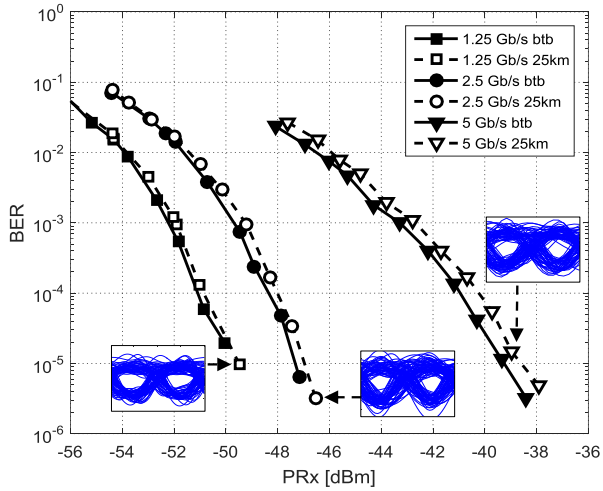

Figure 3.8. BER against Rx power for direct phase modulated Tx with duty cycle of 50%, and at R_b of 1.25 Gb/s, 2.5 Gb/s and 5 Gb/s. The insets show the eye diagrams for BER = 10^{-5}.

3.2 Nyquist shaped Tx based on direct phase modulated DFB

In UDWDM-PON systems with high channel count and narrow CS a very high granularity can be achieved, especially at lower R_b. However, it can be quite challenging to transmit information when the bitrate per channel is increased and the emitted power difference between them is enlarged. This is attributable to the unwanted spectral side-lobes resulting when the optical carrier is modulated. These spectral components cause interference to adjacent channels, yielding to BER degradation. One possible solution relies on Nyquist pulse shaping, a technique to compress the signal bandwidth. This section presents the implementation of Nyquist pulse shaping along with the proposed direct phase modulation of a DFB laser, for keeping the lower complexity and cost of the Tx. First the benefit of using Gaussian or Nyquist shaping filters is evaluated through numerical simulations. Then the experimental validation in an UDWDM-PON with channels separated only by 6.25 GHz and tolerating a differential link-loss of 15 dB is presented. Finally, an UDWDM-PON is dimensioned considering the proposed solutions.

3.2.1 Numerical simulations

Usually, binary sequences representing user data with logical values 0 and 1 are mapped into the electrical domain in NRZ format to provide an electrical swing according to the data sequence. However, additional electrical filtering can be applied to data before optical modulation to modify the dynamics of the electrical pulses yielding to spectral shaping [11].

To evaluate the benefit of applying shaping filters in the TX, several simulations were performed with VPIphotonics™ and MATLAB® using the Monte-Carlo method. The simulation setup was composed of two users with Tx consisting of an ideal phase modulator which generated a 0 - 180º PSK signal.

The modulating data was a 2^{15}-1 PRBS differentially encoded at R_b of 1.25 Gb/s with rise-time $t_r = 0.1T_b$, where T_b is the bit period. Additionally, two types of shaping filters (Gaussian and Raised-cosine) were applied to data before optical modulation, modifying the dynamics of the electrical pulses and its spectrum width. The complete simulation setup was composed by two users combined in a 3-dB optical coupler as presented in Figure 3.9.

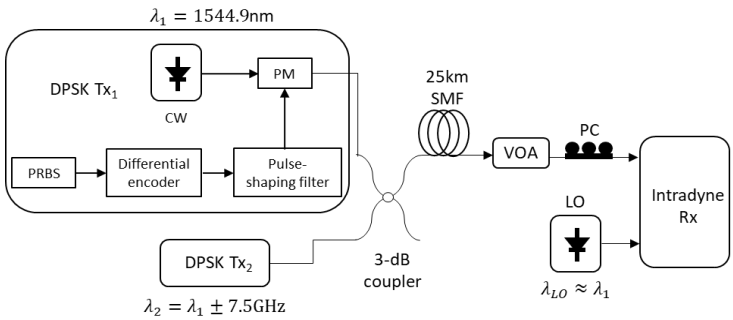

Figure 3.9. Simulation Setup for pulse shaping evaluation.

Two type of pulse shaping filters were tested. First, the sharp symbol transitions were smoothed to Gaussian dynamics (t_r defined by elapsed time between 10% and 90% of the rising edge) depending on the 3-dB filter BW calculated by:

$$BW = 0.35/t_r \tag{3.7}$$

Second, a Raised-cosine filter was used to adjust the spectral shape beyond the Nyquist BW. For the last, the parameter that defines the filter was the roll-off (α) factor which ranged between 0 and 1. For this shaping technique, the lower α, the higher spectral compression (see Figure 3.10(a)) and consequently the lower the total filter BW defined by:

$$BW = (1 + \alpha)\frac{R_b}{2} \tag{3.8}$$

The optical power of each generated DPSK signal was set to 0 dBm and launched through 25 km of SMF. Then VOA emulated further splitting and adjusted the power arriving to the Rx. The signal was detected with a coherent intradyne Rx based on a 3x3 optical coupler [10].

To find the optimal parameters (BW and α) for the shaping filters, the Rx power was set at the value that produced BER = 10^{-3} for NRZ format. Then, the sensitivity penalty due to the insertion losses of the shaping filters was computed. The results are shown in Figure 3.10(b). For the Gaussian filter, a power penalty larger than 1 dB was observed for $BW < 1.2/T_b$. Therefore, its BW was set at $1.2/T_b$ (corresponding to $t_r = 0.29T_b$). For the Raised-cosine filter, the penalty in the case of maximum BW (corresponding to α = 1) was 3.5 dB; lower values of α increase the filter insertion losses. Therefore, the BW of the Raised-cosine filter was limited to $BW = 1/T_b$ to reduce at most the effect of the modulated secondary lobes without producing excessive degradation in the BER, at the Rx.

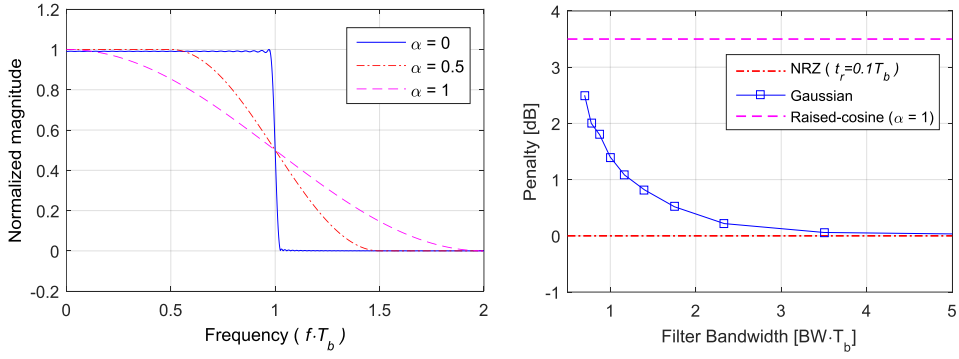

Figure 3.10. (a) Magnitude spectra of the Raised-cosine filter for several roll-off values. (b) Sensitivity penalty @BER=10^{-3} vs normalized filter BW for the three pulse-shaping schemes.

At the Tx, the shaping filter converts the PRBS data into an electrical signal able to drive the laser for optical PSK modulation. Figure 3.11 shows the original NRZ electrical spectrum before and after the shaping filters. The corresponding eye diagrams for each case are plotted as well, to appreciate the dynamics of the electrical data.

For the NRZ signal, it is observed that the sharp transitions between symbols result in high-frequency harmonic components. There was a significant power beyond 1.25 GHz and the main to secondary spectral lobes power suppression (MSPS) was 14dB. With electrical Gaussian filtering, the symbol transitions were smoothed and the MSPS was 18 dB. When using the Raised-cosine filter, the electrical pulses were sinc-shaped with all the power limited to the data bandwidth and the MSPS was > 60 dB.

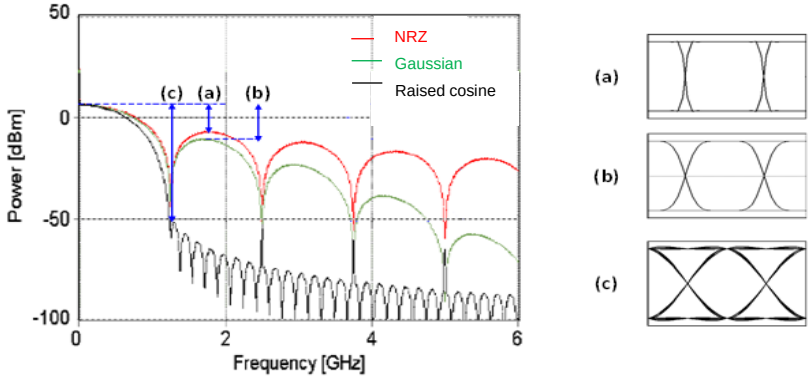

Figure 3.11. Electrical spectra of 1.25 Gb/s PRBS data and eye diagrams for each case: (a) NRZ, (b) Gaussian, (c) Raised-cosine pulse shaping at the Tx.

Afterwards, the second user (Tx_2) was added into the network with identical pulse shaping. Figure 3.12 plots the optical spectra of both channels separated 6.25 GHz. The NRZ, Gaussian shaped and Raised-cosine filtered signals show a MSPS of 12 dB, 13 dB and 19 dB respectively. The latter thus is expected to reduce the CS. It is interesting to note that the optical MSPS values are lower than the electrical due to the non-linear characteristic of the PM that produces strong Bessel harmonic components in the optical domain [28].

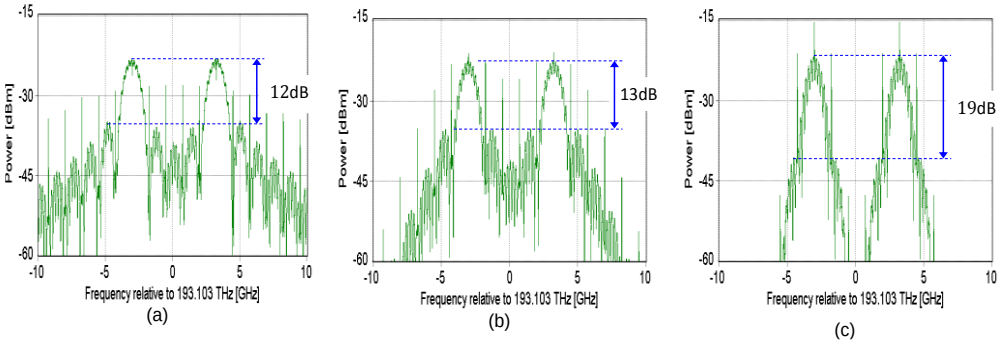

Figure 3.12. Optical spectra for two users separated by 6.25 GHz for three different pulse-shaping schemes: (a) NRZ, (b) Gaussian, (c) Raised-cosine.

Next, the CS was evaluated. For this, Tx_2 optical frequency was shifted from -7.5 GHz to 7.5 GHz with respect to Tx_1 emission frequency. The BER degradation was measured in the fixed user Tx_1 (Figure 3.13(a)). These values were translated into power penalty at a sensitivity of BER=10^{-3} considering the single channel as reference (Figure 3.13(b)). The CS values at 1 dB penalty were 2.8 GHz, 2.2 GHz and 1.8 GHz for NRZ, Gaussian and Raised-cosine pulse-shaping respectively. Notably, there was no penalty at a 6.25 GHz spacing and even less than 2.5 GHz could be achieved when shaping the pulse.

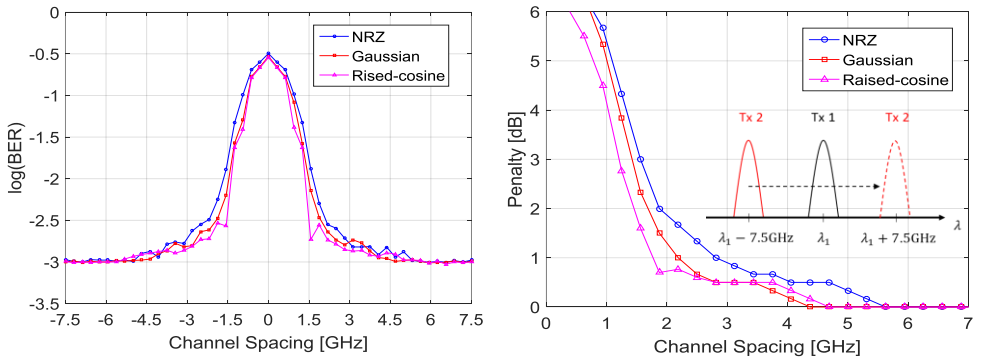

Figure 3.13. (a) BER against Channel Spacing for Tx1 using three different pulse-shaping filters, (b) Rx sensitivity penalty @BER = 10^{-3} for the three pulse-shaping schemes.

3.2.2 Experimental validation

Once the technique was evaluated through simulations, it was applied to two identical transmitters (Tx_1 and Tx_2), each one composed by the two aforementioned DFB lasers of 4 MHz and 3 MHz linewidth, and modulation BWs of 10 GHz and 2.5 GHz, respectively. Both DFB lasers were biased at 75 mA, value at which the adiabatic chirp dominated. Data consisted of two uncorrelated differentially encoded 2^{15}-1 PRBS at R_b of 1.25 Gb/s and 2.5 Gb/s. The data sequences were digitally equalized, to ensure 0-π phase changes, as explained in section 3.1. However, before modulating the DFBs, each digital signal was shaped applying a Raised-cosine FIR filter of 64-taps. The resulting samples were uploaded to a 20 GSa/s AWGen and the electrical output signals were amplified with an 8 GHz BW(SHF98P) and 12 GHz BW (TBI-781) RF amplifiers for directly modulating each DFB. The complete Tx and the generated Nyquist shaped DPSK signal is depicted in Figure 3.14.

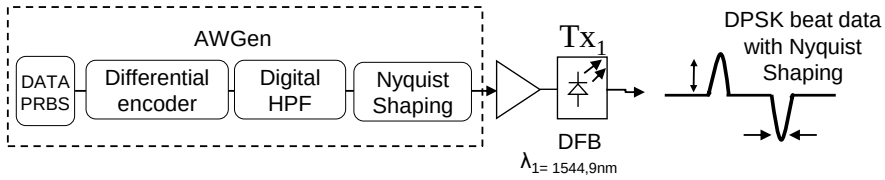

Figure 3.14. Nyquist shaped Tx for UDWDM-PON validation

The complete setup was similar to the UDWDM-PON scenario depicted in Figure 3.4. Both Tx_1 and Tx_2 were launched at PTx = 0 dBm, thermally tuned for emitting at similar wavelengths λ_1 = 1549nm and λ_2 = 1549.1nm ± 6.25 GHz, combined with a 3-dB optical coupler, and sent through 25 km of SMF. A VOA reproduced the splitting losses and limited the power in the intradyne Rx. In this case a 100 kHz ECL, with P_{LO} = 0 dBm, and emitting at $\lambda_{LO} = \lambda_1$ = 1544.9 nm was used. The data recovery after photodetection was done similarly than in the experiment of sub-section 3.1.2.

To test the Nyquist shaped DPSK transmission, two electrical signals, one with and another without Nyquist-shaping, were digitally generated. Figure 3.15(a) shows the electrical data at R_b = 1.25 Gb/s along with the Nyquist shaped waveform for α factor of 0.25 (upper) and 1 (lower). Figure 3.15(b), Figure 3.15(c), Figure 3.15(d), and Figure 3.15(e) present the photo-detected spectra at a relative intermediate frequency (IF) of 10 GHz for signals at R_b of 1.25 Gb/s and 2.5 Gb/s. It was observed that the lateral lobes were eliminated, but the main lobe was not compacted as expected with externally modulated Txs [11]. This is because the direct

phase modulation is a non-linear modulation that leads to harmonics following the Bessel function solutions [28]. Conversely, the BW of the residual IM generated was narrowed, due to it was produced by a linear modulation, being particularly noticed for lower α values.

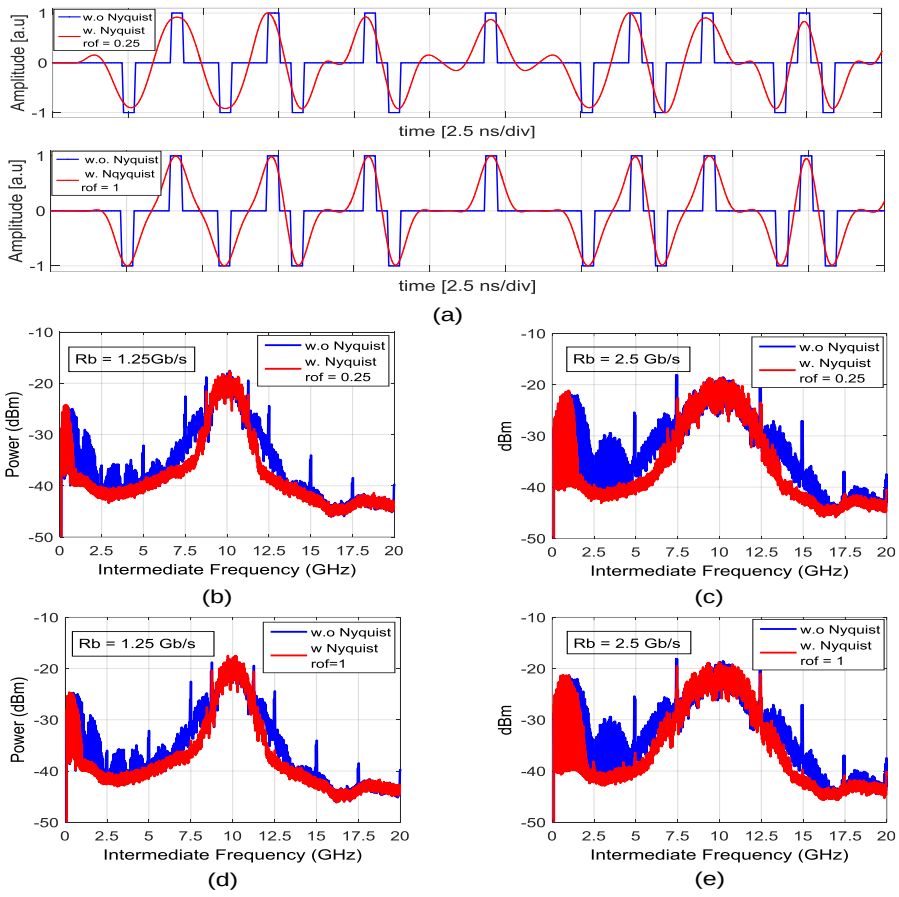

Figure 3.15. (a) Electrical beat square signal and Nyquist shaped signal with α = 0.25 (upper) and α = 1 (bottom) and RF spectrum of the Tx signal without and with Nyquist shaping at R_b = 1.25 Gb/s ((b), (d)) and R_b = 2.5Gb/s ((c), (e)) for α= 0.25 and α= 1.

First, the PtP system with Tx_1 was tested. Since the effect of lower α is barely perceived, a value of α = 1 was used. The amplitude of the electrical waveforms was optimized, and the DFB laser was directly modulated at R_b of 1.25 Gb/s and 2.5 Gb/s. The BER curves are plotted in Figure 3.16(a). The Rx sensitivities measured at a forward error correction (FEC) BER of 10^{-3} were -52 dBm and -49.5 dBm respectively without Nyquist shaping. These values were approximately 3 to 5.5 dB better with respect to the obtained with Nyquist shaping (-49 dBm and -44 dBm for 1.25 Gb/s and 2.5 Gb/s correspondingly). The performance degradation is

because the strong filtering introduces distortion, thus reducing the eye-opening at the Rx. This effect is clearly observed in the eye diagrams of Figure 3.16(c) and Figure 3.16(e) where Nyquist-shaping was applied compared to Figure 3.16(b) and Figure 3.16(d) at R_b of 1.25 Gb/s and 2.5 Gb/s respectively. The use of a matched filter in the Rx would improve the eye-opening and thus the performance [11].

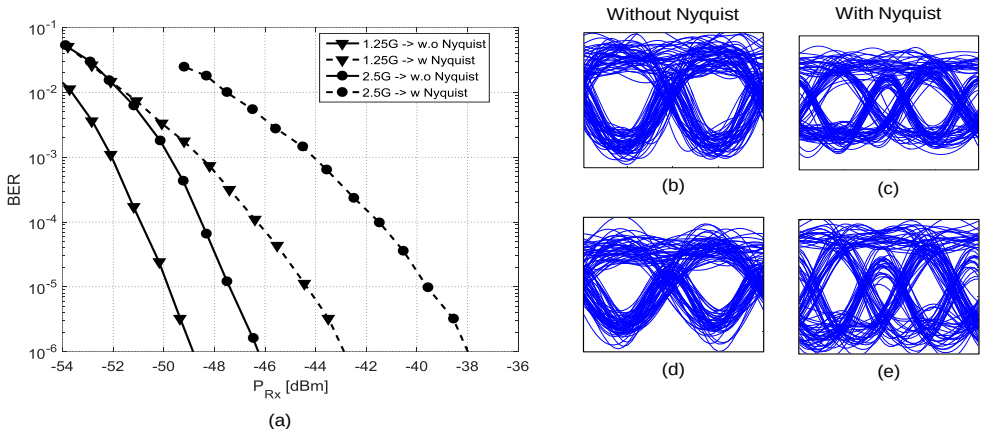

Figure 3.16. (a) BER against Rx optical power for Tx_1. Eye diagrams at BER = 3 x 10^{-6} without and with Nyquist shaping at 1.25 Gb/s (b, c) and 2.5 Gb/s (d, e) respectively.

As the Nyquist shaped signals produced a lower optical BW, the minimum achievable spectral separation between neighbor users was evaluated. Tx_2 was added and modulated identically to Tx_1. Both Tx_1 and Tx_2 had the same launched power (0 dBm). Tx_2 wavelength (λ_2) was tuned in temperature and shifted in steps of 1.25 GHz from/to a spectral separation of +/-12.5 GHz. The Rx optical power was left constant at the value where BER $\approx 2 \cdot 10^{-4}$ for Tx_1. Then, the sensitivity of Tx_1 was evaluated when Tx_2 caused interference at different CS.

Figure 3.17(a) plots the BER against the CS with and without Nyquist shaping. For both cases the minimum CS to keep the penalty <1 dB (according to Figure 3.16(a)) was 3.125 GHz and 4.375 GHz at R_b of 1.25 Gb/s and 2.5 Gb/s, respectively. Thus, there was no improvement in CS when using Nyquist shaping due to the beat signals already produced a confined spectrum.

Then, the effect on CS when the optical signals had different power was studied. Tx_2 launched power was set 15 dB higher than Tx_1 (DLL = 15 dB), for the spectral side-lobes to become relevant, and the CS measurements were then repeated. Figure 3.17(b) show the BER against the CS at R_b = 1.25 Gb/s and R_b = 2.5 Gb/s for Tx_1.

For R_b = 1.25 Gb/s, the CS needed to keep the penalty <1 dB was 5 GHz when no spectral shaping was employed. However, for the Nyquist filtered signal, the CS was just 4.375 GHz. Similarly, when doubling the R_b to 2.5 Gb/s, the required CS were 6.25 GHz and 8.75 GHz, with and without Nyquist shaping respectively. For a DLL = 15 dB, Nyquist shaped pulses gave an advantage and improved the CS by 25%. As a result, the Nyquist shaped Tx at both 1.25 Gb/s and 2.5 Gb/s could work in a 6.25 GHz spaced PON of DLL = 15 dB.

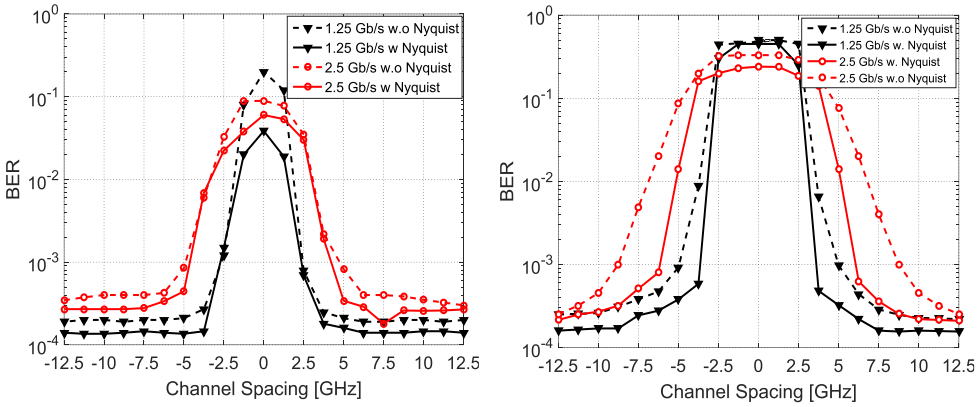

(a) (b)

Figure 3.17. BER against channel spacing with and without Nyquist shaping for Tx_1 at R_b = 1.25 Gb/s and R_b = 2.5 Gb/s for (a) DLL = 0 dB and (b) DLL = 15 dB.

To have more clarity, the results are summarized in

Table 3.1

Table 3.1. Minimum channel spacing with and without Nyquist shaping

Bit rate	**1.25 Gb/s**				**2.5 Gb/s**			
DLL	0 dB		15 dB		0 dB		15 dB	
Nyquist shaping	NO	YES	NO	YES	NO	YES	NO	YES
CS	3.125 GHz		5 GHz	3.75 GHz	4.375 GHz		8.75 GHz	6.25 GHz

Finally, it could be interesting to know at which value should be set the emitting power of a specific channel that needs to be randomly tuned in the UDWDM-PON to limit the penalty incurred using Nyquist pulse shaping. Figure 3.18(a) shows the BER against the CS for Tx_1 at R_b = 2.5 Gb/s and DLL values changing from -15 dB to 15 dB between users (Tx_1 and Tx_2). It was noticed that the minimum CS to keep the penalty ≤1 dB (quantified from Figure 3.16(a)

when passing from BER = 10^{-4} to BER = $7 \cdot 10^{-4}$) is of 4.375 GHz. However, when the optical power of the Tx_2 is 15 dB higher, the minimum CS increases to 6.25 GHz. Additionally, Figure 3.18(b) depicts the required CS to keep penalty ≤ 1 dB, at R_b = 2.5 Gb/s when changing the DLL from -15 dB to 15 dB. It was observed that the emitted optical power of the channel being randomly tuned, should be reduced in 15 dB when its spectrum is passing just over the neighbor channel in order to limit the penalty at the fixed user, as indicate in Figure 3.18(b).

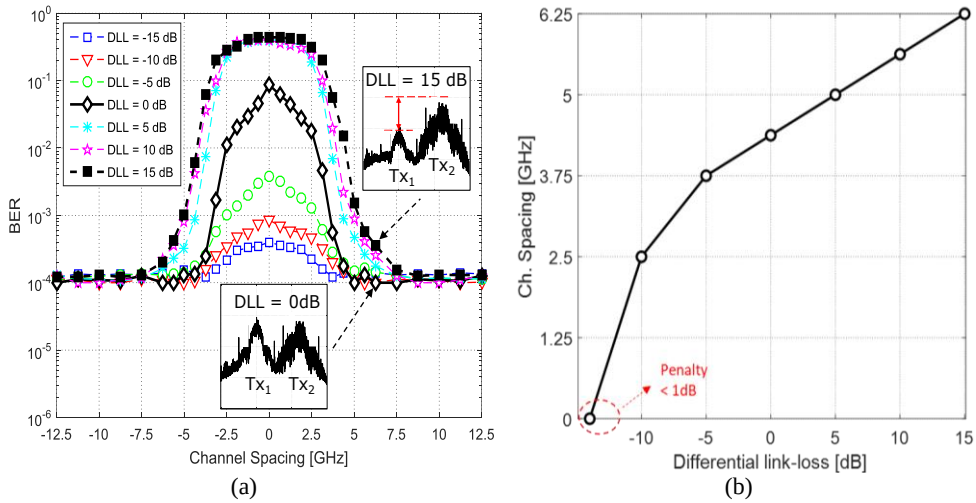

Figure 3.18. (a) BER vs CS for Tx_1 at several differential link-losses (DLL) at R_b = 2.5 Gb/s. The insets show the electrical spectrum of two users spaced 6.25 GHz with DLL of 0 dB and 15 dB. (b) CS vs DLL for 1 dB of sensitivity penalty at BER = 10^{-4}. The dotted lines indicate penalties <1dB.

3.2.3 UDWDM-PON dimensioning

With the results presented, the UDWDM-PON can be dimensioned in a greenfield scenario, with Nyquist shaped channels, and occupying the PtP WDM wavelength band for NGPON2 (1603 nm – 1625 nm) [29]. The total ONUs that could potentially be served at 2.5 Gb/s/user could be derived from:

$$\#\ channels\ =\ \frac{22\ \text{nm}\ \text{x}\left(125\ \text{GHz}/1\ nm\right)}{6.25\ GHz} = 440$$

The aggregated capacity then nearly reaches 1.1 Tb/s (400 x 2.5 Gb/s). However, it is important to consider the eye safety frontier (21.3 dBm [6]). With this value in mind, the emitted power per channel should be limited to only -6 dBm. Thus, the available link budget is 38 dB, which allows splitting losses of 27 dB (for 1:512 optical splitter) and 55 km reach

(fiber attenuation = 0.2 dB/km) with a performance above the FEC threshold. Furthermore, the proposed system would allow a DLL of 15 dB with a maximum penalty of 1 dB.

3.3 Chapter Summary

In this chapter, the use of direct phase modulation was proposed as a very attractive strategy due its low cost compared with external modulation. Additionally, phase modulation increases the Rx sensitivity due to the average power of the signal, and it is less affected by fiber nonlinearities due to constant envelope of the signal compared to IM. To overcome the complexity of phase detection, differential demodulation was employed and then the transmitted signal was differentially pre-coded.

To perform the mentioned PM, a simply digital equalization technique was proposed to obtain the required 0-π phase variations in DPSK modulation. The use of digital equalization provides flexibility to the Tx by adjusting the amplitude and duty cycle of the modulating signal. Rx sensitivities of -53 dBm, -50.5 dBm and -45 dBm were experimentally demonstrated at 1.25 Gb/s, 2.5 Gb/s, and 5 Gb/s in a 25 km SMF link using intradyne coherent detection. These results along with the low complexity of the transceivers potentially makes this technique an attractive option for flexible future optical access networks.

Moreover, the concern of crosstalk between adjacent channels in UDWDM-PON was studied, as well as the 15-dB DLL requirement of ITU standards. The use of Nyquist pulse shaping at the Tx was proposed and evaluated through numerical simulations as well as experimental tests, showing the possibility to allocate neighbor users as low as 6.25 GHz, operating at Rb of 2.5 Gb/s, and fulfilling the DLL requirement of 15 dB. Compared to a Tx without Nyquist shaping there was a 25 % less in CS required between adjacent channels with penalties between 3 and 4.5 dB at Rb at 1.25Gb/s and 2.5 Gb/s respectively. These penalties could be reduced if proper matching filters are placed in the DSP of the Rx and its implementation is encouraged for future work.

Considering these results, the technical feasibility of an UDWDM-PON was demonstrated, showing the potentially for serving 440 users, with aggregated capacity of 1.1 Tb/s, and an available link budget of 38 dB taking into account the eye-safety limit of 21.3 dBm.

Bibliography Chapter 3

[1] International Telecommunication Union, "ITU-T G.694.1 Recommendation, Spectral grids for WDM applications: DWDM frequency grid." Feb-2012.

[2] E. Agrell *et al.*, "Roadmap of optical communications," *J. Opt.*, vol. 18, no. 6, pp. 1–40, Jun. 2016.

[3] D. Nesset, "PON Roadmap [Invited]," *J. Opt. Commun. Netw.*, vol. 9, no. 1, pp. A71–A76, Jan. 2017.

[4] J. Prat *et al.*, "Towards ultra-dense wavelength-to-the-user: The approach of the COCONUT project," in *Proc. 15th Int. Conf. on Transp. Opt. Netw. (ICTON)*, Cartagena, Spain, 2013.

[5] L. G. Kazovsky, S. Benedetto, and A. E. Willner, *Optical fiber communication systems*. Boston: Artech House, 1996.

[6] J. Prat *et al.*, "Technologies for Cost-Effective udWDM-PONs," *J. Light. Technol.*, vol. 34, no. 2, pp. 783–791, Jan. 2016.

[7] I. N. Cano *et al.*, "Field-Trial of Low-Cost Coherent UDWDM-PON with Real-Time Processing, λ-Monitoring and EPON Coexistence," in *Proc. 42nd Eur. Conf. on Opt. Commu. (ECOC)*, Düsseldorf, Germany, 2016.

[8] M. Presi *et al.*, "Field-Trial of a High-Budget, Filterless, λ -to-the-User, UDWDM-PON Enabled by an Innovative Class of Low-Cost Coherent Transceivers," *J. Light. Technol.*, vol. 35, no. 23, pp. 5250–5259, Dec. 2017.

[9] J. Prat *et al.*, "Ultra-dense WDM access network field trial," in *Proc. 21st Eur. Conf. on Netw. and Opt. Commu. (NOC)*, Lisbon, Portugal, 2016.

[10] K.-P. Ho, *Phase-modulated optical communication systems*. New York: Springer, 2005.

[11] R. M. Ferreira *et al.*, "Coherent Nyquist UDWDM-PON With Digital Signal Processing in Real Time," *J. Light. Technol.*, vol. 34, no. 2, pp. 826–833, Jan. 2016.

[12] D. Lavery, M. Paskov, and S. J. Savory, "Spectral Shaping for Mitigating Backreflections in a Bidirectional 10 Gbit/s Coherent WDM-PON," in *Proc. Opt. Fiber Commun. Conf. (OFC)*, Anaheim, CA, 2013.

[13] J. D. Reis, A. Shahpari, R. Ferreira, D. M. Neves, M. Lima, and A. L. Teixeira, "Nyquist Signaling for Spectrally-Efficient Optical Access Networks," in *Proc. Opt. Fiber Commun. Conf. (OFC)*, San Francisco, California, 2014.

[14] G. Bosco, V. Curri, A. Carena, P. Poggiolini, and F. Forghieri, "On the Performance of Nyquist-WDM Terabit Superchannels Based on PM-BPSK, PM-QPSK, PM-8QAM or PM-16QAM Subcarriers," *J. Light. Technol.*, vol. 29, no. 1, pp. 53–61, Jan. 2011.

[15] J. C. Velásquez, I. N. Cano, V. Polo, and J. Prat, "Direct beat phase modulated DFB for flexible 1.25–5 Gb/s coherent UDWDM-PONs," in *Proc. Opt. Fiber Commun. Conf. (OFC)*, Los Angeles, CA, USA, 2017.

[16] J. C. Velasquez, I. N. Cano, V. Polo, M. Domingo, and J. Prat, "15-dB Differential Link-Loss UDWDM-PON With Direct Beat Phase Modulated DFBs," *IEEE Photonics Technol. Lett.*, vol. 30, no. 2, pp. 137–140, Jan. 2018.

[17] J. C. Velasquez, J. Tabares, I. N. Cano, V. Polo, and J. Prat, "Coherent Nyquist UDWDM-PON with 2.5 Gb/s/user and 15 dB differential link-loss," in *International Workshop on Fiber Optics in Access Network (FOAN)*, Munich, 2017.

[18] J. C. Velásquez, J. Tabares, I. N. Cano, and J. Prat, "1.25–2.5 Gb/s Simple Nyquist Transmitters for Coherent UDWDM-PON with Enhanced Spectral Efficiency," *Fiber Integr. Opt.*, vol. 37, no. 4, pp. 219–228, Jul. 2018.

[19] D. Mahgerefteh, Y. Matsui, X. Zheng, and K. McCallion, "Chirp Managed Laser and Applications," *IEEE J. Sel. Top. Quantum Electron.*, vol. 16, no. 5, pp. 1126–1139, Sep. 2010.
[20] K. Petermann, *Laser Diode Modulation and Noise*. Dordrecht, Netherlands: Kluwer Academic Publishers, 1988.
[21] G. P. Agrawal, *Fiber-Optic Communication Systems*, 4 edition. New York: Wiley, 2010.
[22] L. Bjerkan, A. Royset, L. Hafskjaer, and D. Myhre, "Measurement of laser parameters for simulation of high-speed fiberoptic systems," *J. Light. Technol.*, vol. 14, no. 5, pp. 839–850, May 1996.
[23] R. Tucker, "High-speed modulation of semiconductor lasers," *J. Light. Technol.*, vol. 3, no. 6, pp. 1180–1192, 1985.
[24] J.-G. Provost and F. Grillot, "Measuring the Chirp and the Linewidth Enhancement Factor of Optoelectronic Devices with a Mach–Zehnder Interferometer," *IEEE Photonics J.*, vol. 3, no. 3, pp. 476–488, Jun. 2011.
[25] K. Sato, S. Kuwahara, and Y. Miyamoto, "Chirp characteristics of 40-gb/s directly Modulated distributed-feedback laser diodes," *J. Light. Technol.*, vol. 23, no. 11, pp. 3790–3797, Nov. 2005.
[26] I. N. Cano, A. Lerin, V. Polo, and J. Prat, "Direct Phase Modulation DFBs for Cost-Effective ONU Transmitter in udWDM PONs," *IEEE Photonics Technol. Lett.*, vol. 26, no. 10, pp. 973–975, May 2014.
[27] C. Xie *et al.*, "Colorless coherent receiver using 3x3 coupler hybrids and single-ended detection," *Opt. Express*, vol. 20, no. 2, pp. 1164–1171, Jan. 2012.
[28] S. Haykin, *Introduction to analog and digital communications*, 2nd ed. Hoboken, NJ: John Wiley & Sons, 2007.
[29] International Telecommunication Union, "ITU-T G.989.2 Recommendation, 40-Gigabit-capable passive optical networks (NG-PON2): Physical Media Dependent Layer Specification." May-2014.

Chapter 4 . Multilevel direct phase modulation of DFB lasers

In chapter 3, UDWDM-PON based on direct phase modulated lasers and coherent detection were presented as potential solutions for implementing cost-efficient PONs. DPSK is a more robust format than ASK, due to its tolerance to fiber-non linearities. On the hand it was seen that coherent systems present lower sensitivities, and inherent wavelength selectivity than IM/DD systems. In addition, future PONs pursue higher and flexible data rates, better SE and support for heterogeneous services [1], [2]

One of the possible solutions to achieve these goals, is the use of multilevel modulation formats which allows to transmit several bits per symbol for increasing the effective R_b. In other words, at a fixed R_b more symbols are transmitted and then the required BW is reduced. This relieves in some way the need for high-speed electronics and optoelectronics and improves the tolerance to some transmission impairments as chromatic dispersion (CD) [3]. Nevertheless, their use can produce some performance degradation in comparison to binary modulation schemes [4]. As well, the trade-off between data rate and reach needs to be considered [5].

Multilevel modulation for multigigabit transmission can be implemented using amplitude modulation, phase modulation or hybrid multilevel amplitude/phase modulation. Although multilevel amplitude modulation (M-ASK) attracts a wide interest in the research community [6], [7], this approach presents substantial Rx sensitivity penalty compared to binary OOK, due to the unequal amplitude level spacings needed by signal-dependent noise arising from square-law detection [3]. On the contrary, the work developed in this thesis is focused in phase and hybrid multilevel modulation formats.

Typically, the enabling technologies for multilevel modulation are external I-Q modulators based on Mach-Zehnder Modulators (MZM) at the Tx, and sophisticated DSP techniques [8], [9] with advanced FEC mechanisms [10], at the Rx. The associated complexity of these solutions, and the high cost of their implementation, have limited their attractiveness in access networks.

In first section of this chapter, two types of multilevel formats for PM are presented as affordable solutions, depending on how the symbols are assigned in the Tx. First two types (DQPSK and 8-DPSK) are called memory-less formats because the symbols are assigned irrespective of the symbols sent before or after. Afterwards, a correlative or line coding format called duobinary (DB) is discussed. Investigation of hybrid formats is left for chapter 5.

In the second section the results of [11] are presented. In that work, we demonstrated that a 2.5 GHz limited BW DFB laser can be directly modulated in phase using multilevel electrical signals, and without spectral shaping. Single carrier modulation formats such as differential quadrature PSK (DQPSK) or optical duobinary (ODB) were tested and compared. The transmitted signal was detected with an intradyne Rx and simple data processing. Since the hardware of the TRx is not changed when varying the modulation format, it could be selected by software.

Finally, in the third section, an 8-DPSK modulation format implemented through a direct modulated 2.5 GHz bandwidth (BW) laser is presented. With this approach, the R_b is scaled to 7.5 Gb/s keeping the CS as low as 6.25 GHz, in a 50 km UDWDM-PON, thus achieving an optical spectral efficiency of 1.2 bits/s/Hz, without additional spectral shaping. The proposed technique is compared in terms of receiver sensitivity and channel separation to DQPSK and DPSK modulation formats. These results were demonstrated, for the first time, in the 2016 Optical Fiber Communication Conference and Exhibition (OFC) [12]. Having the versatility of changing the modulation format could allow for flexible data rates and adapt to the requirements of different users in the PON.

4.1 M-ary DPSK modulation

When employing multilevel formats, a determinate number of bits are coded on *M* symbols. Each symbol is related to a sole sequence of *k* bits forming and *M*-ary alphabet of size [4]:

$$M = 2^k \;\Leftrightarrow\; k = log_2\, M \qquad 4.1$$

These symbols are transmitted at each symbol duration of $T_s = 1/R_s$, where R_s is the symbol rate, given by:

$$R_s = \frac{R_b}{log_2 M} \ [baud] \tag{4.2}$$

From Eq. 4.2 it is possible to obtain the spectral BW efficiency (η) of a digital system that transmits k bits during T_s seconds, using a BW or CS in Hz, applying:

$$\eta = \frac{R_s log_2 M}{CS} = \frac{1}{CST_b} [b/s/Hz] \tag{4.3}$$

where T_b is the effective bit time. From Eq. 4.3, it can be deduced that η is directly proportional to R_b, which can be maximized using multilevel modulation formats. On the other hand, the standard CS of DWDM has been continuously reduced from 200 GHz to 100 GHz, 50 GHz, 25 GHz and inclusive to 12.5 GHz (0.1 nm) [13].

4.1.1 DQPSK signal generation

As presented in chapter 2, in an optical differential-PSK system the information is encoded in the phase difference ($\Delta\phi$) between consecutive bits, where $\Delta\phi$ can take values of $(0, 2\pi/M, \dots, 2\pi(M-1)/M)$[14]. As previously seen in chapter 3, in the DPSK format the binary data is encoded as either a 0 or π phase shifts. In DQPSK, each symbol is composed by two bits ($M = 4$), and $\Delta\phi$ take values of $0, \pi/2, \pi, 3\pi/2$. Moreover, R_s is equal to half the total R_b and η is doubled.

The transmitted signal may be written in complex notation as:

$$E_s = E_0 e^{j(\omega_0 t + \Delta\phi_i(t))} \tag{4.4}$$

where E_0 is the amplitude and ω_0 is the angular frequency. The combination of two bits using the Gray mapping rule [15], determinates the $\Delta\phi$ of each transmitted symbol. The digital symbols must be mapped onto different peak-to-peak amplitudes and then differentially encoded. In addition, a digital equalization block and/or pulse shaping functions could be added before modulating the laser. Figure 4.1(a) represents the mapped symbols as five-level signal RZ bipolar symmetric signal, used to generate phase changes of $0, \pm\pi/2, \pm\pi$. Figure 4.1(b) represents the corresponding constellation diagram.

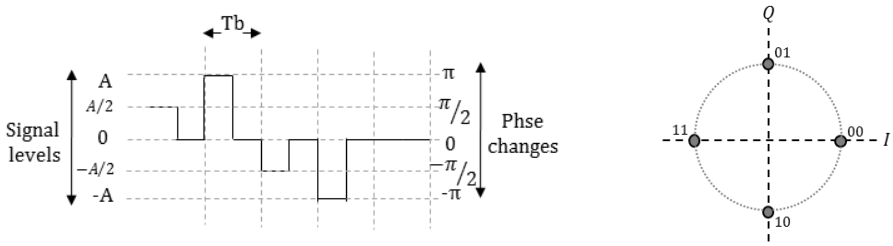

Figure 4.1. (a) Bipolar pulses for DQPSK signal generation, (b) DQPSK constellation.

4.1.2 8-DPSK signal generation

Following the explanation for DQPSK signal generation, the 8-DPSK format uses 8-levels to map the generated symbols which can take up to 8 different phase shifts values [14]. Table 4.1 shows the input bits combination following gray codding, $\Delta\phi$ values and the I-Q components values in the complex plane. Figure 4.2 plots the generated constellation.

Table 4.1. 8-DPSK symbols with their corresponding phases.

Bits (d3 d2 d1)	Δϕ	I	Q
000	0	1	0
001	$\pi/4$	$\sqrt{2}/2$	$\sqrt{2}/2$
011	$\pi/2$	0	1
010	$3\pi/4$	$-\sqrt{2}/2$	$\sqrt{2}/2$
110	π	-1	0
111	$5\pi/4$	$-\sqrt{2}/2$	$-\sqrt{2}/2$
101	$3\pi/2$	0	-1
100	$7\pi/4$	$\sqrt{2}/2$	$-\sqrt{2}/2$

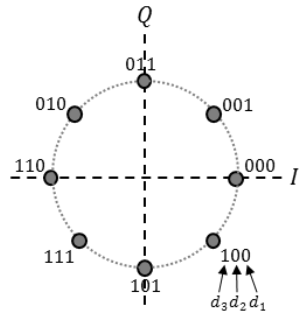

Figure 4.2. 8-DPSK constellation.

As result, in 8-DPSK, each symbol is composed by three bits generating an alphabet of size $M = 8$. Moreover R_s is equal to the third part the total R_b and η is increased in three times.

4.2 Duobinary modulation (DB)

There are other kind of data modulation formats, called correlated or line coding formats, which introduce memory by using a symbol pattern to represent a single bit. The most known format is called duobinary (DB) modulation, and it was first proposed by A. Lerner for transmitting R_b bits/s using BW < $R_b/2$ Hz [16]. This property allows to transmit information

using less BW at a fixed R_b and without reducing the R_s, enlarging the M size. These characteristics improves the tolerance to impairments like CD and increase η [3].

As the information does not follows the Nyquist criterium of R_b /2 Hz the duobinary pulses will have intersymbol interference (ISI). However, this ISI is introduced in a controlled manner in the Tx to allow its cancelation at the Rx [15].

To understand the advantages, let consider the transmitted signal like:

$$\sum_{k=-\infty}^{\infty} d_k q(t - kT_b) \tag{4.5}$$

Where $d_k = 0{,}1$ are the data bits, *q(t)* is the transmitted pulse, and *t = kT (k = 0, ±1, …, n)*are the sampling instances. In order to avoid ISI, *q(t)* must meet the condition [15]:

$$q(kT_b) = \begin{cases} 1, & k = 0 \\ 0, & k \neq 0 \end{cases} \tag{4.6}$$

This condition is known as the Nyquist criterion for zero ISI. This condition is achieved applying a raised-cosine pulse shaping to the NRZ coded signal as seen in chapter 2. Conversely, the duobinary approach follows the condition [15]:

$$q(kT_b) = \begin{cases} 1, & k = 0, 1 \\ 0, & otherwise \end{cases} \tag{4.7}$$

This condition adds a second nonzero value at the sampling instances *kT*, introducing ISI but in a controlled manner. This allows to transmit pulses that are longer in time but with smaller BW, and then more tolerant to dispersion.

The introduction of ISI at the Tx can be unraveled at the Rx by using differential decoding. However to avoid propagation errors the data must be differentially encoded at the Tx [17].

4.2.1 Electrical duobinary (EDB)

The duobinary signal can be digitally generated by using a 2-tap FIR filter and then a low pass filter, or by using a simple analog low pass filter (LPF), typically a 4th order Bessel filter, at 0.25-0.3R_b [17]. The result of applying a LPF to the input binary bits (0,1) is a three-level signal with three possible levels (1, 0, -1). There are some combinations that never occur like (1 0 1) or (-1, 0, -1). As well between a 1 and a -1 there is always a 0. This produces a correlated sequence with smother transitions and spectral compression. This scheme is known as electrical duobinary (EDB) since the three-level electrical signal is typically used to

perform IM by using a MZM biased at quadrature-point. The signal amplitude is swept in the whole range of the linear zone of the MZM transfer function [18], producing a three-level power signal. This scheme has been widely used by the research community specially to face the CD issue [19]–[21]. Nevertheless, when a three-level signal is transmitted two problems appear, first the SNR decreases due to the lower eye-opening, requiring proper equalization, and two different thresholds must be set adding complexity to the Rx.

4.2.2 Optical duobinary (ODB) for direct phase modulation

To overcome this problem, the MZM could be biased at the null-point, with the signal amplitude twice the switching voltage of the MZM, producing a two-level optical signal, which can be easily detected by a simple photodiode needing only one threshold. This scheme is known as optical duobinary (ODB) and it has been demonstrated to improve around 5 dB the Rx sensitivity compared to EDB [18].

However, the referenced proposal is still a high cost solution due to the use of external MZM. As a novelty, a direct phase modulation of a 2.5 GHz BW limited DFB laser with differential duobinary data, and asynchronous intradyne RX was recently demonstrated in [11], [22]. Since phase shifts of $\pm\pi$ correspond to the same signal level, the three-level electrical signal is converted into a binary one, easing the Rx. As is explained in [22], the duobinary encoder is implemented by using a single XNOR with a 2-bit delay feedback, followed by a 4th order low-pass Bessel filter with cutoff BW at $0.3R_b$. The pre-coder differentially codified data twice, first to unravel the intersymbol interference caused by the duobinary encoding, and second, for the signal to carry data in the phase difference between two consecutive symbols avoiding the need of phase locking in the Rx. The duobinary encoder as well as the complete Tx is plotted in Figure 4.3.

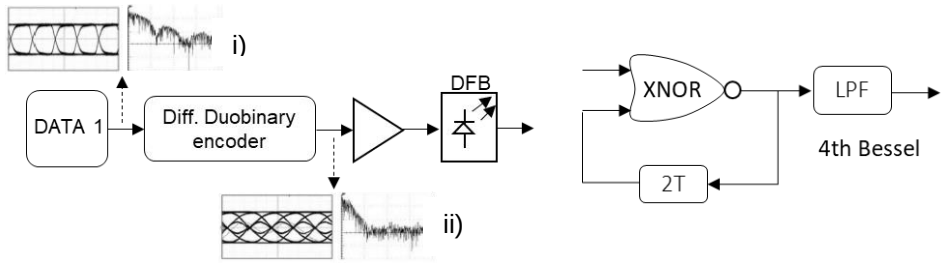

(a) (b)

Figure 4.3. (a) Proposed Tx for duobinary modulation. The insets show the 2-level and 3-level eye diagrams, and the corresponding electrical spectra for i) NRZ data and ii) Duobinary encoded signal before optical modulation, (b) Duobinary encoder.

4.3 Experimental validation in 6.25 GHz Spaced Coherent UDWDM-PONs

The considered architecture was based on a standard splitter-based tree PON with 6.25 GHz ultra-dense channel spacing as illustrated in Figure 4.4. OLT and ONU transceivers had the same technology and complexity. They were equipped with non-pre-selected wavelength DFB lasers tuned in temperature, allowing them to span across several frequency slots in the grid [2]. The ODN was composed by a 50 km SMF, and the power splitter allowed the optical signals to reach each ONU and providing coexistence with legacy PONs. Each ONU used coherent detection with inherent wavelength selectivity to improve the Rx sensitivity.

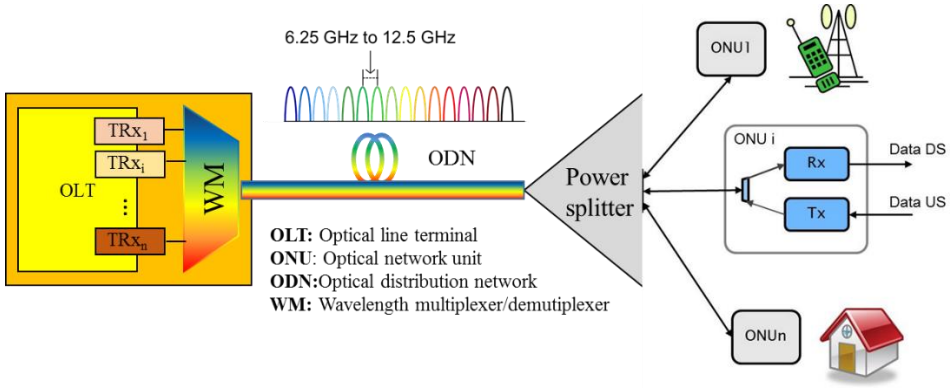

Figure 4.4. UDWDM-PON architecture.

Based on the described architecture, a unidirectional setup was configured as a proof of concept of the previously explained techniques. Although the experimental validation corresponds to two different tests, the setup shown below is similar, then it will be described once to avoid redundancy. The setup and a photo of the implementation in the GCO laboratory are shown in Figure 4.5(a) and Figure 4.5(b) respectively. The details about the DBF lasers used as Tx and LO are given by separately for each test.

Regarding to the data generation, in both tests, a sequence of 2^{18} symbols was generated for each modulation format, differentially coded into DPSK, DQPSK or 8-DPSK, and mapped into 2, 4 and 8 levels, respectively. Each signal level corresponds to an electrical voltage or current value at the output of the waveform generator. For the ODB format, the signal was low-pass filtered and coded as previously explained. The samples were uploaded to an AWGen whose output was electrically amplified for directly modulating the phase of a 2.5

GHz BW DFB laser. A phase modulated signal was obtained by deriving the frequency variations produced by the adiabatic chirp [23]. The optical signal was sent through 50 km of SMF with 0 dBm optical launched power. At the end of the link a VOA adjusted the Rx power and emulated splitting losses in the PON. A polarization control was used to compensate the state of polarization fluctuations in the fiber, however a system based on polarization scrambling [23] can be used to avoid it.

Similarly, in both test the Rx consisted of a 3x3 120º optical coupler which mixed the optical data signal with a LO, emitting at similar wavelength than the Tx.

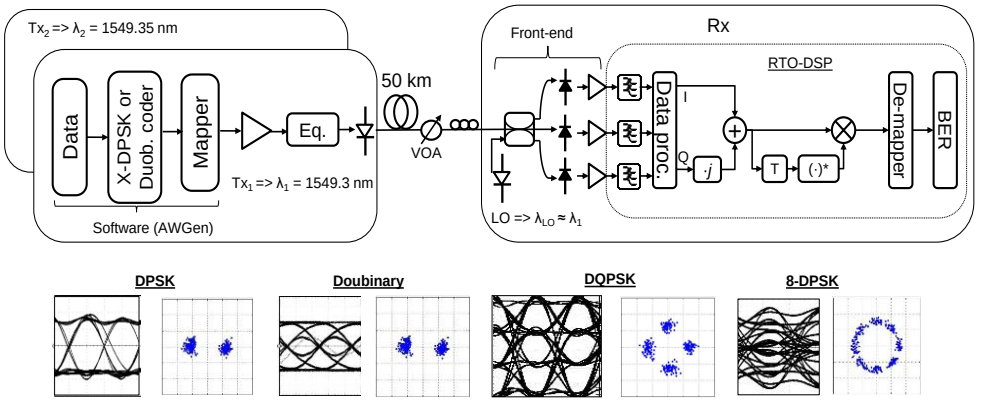

(a)

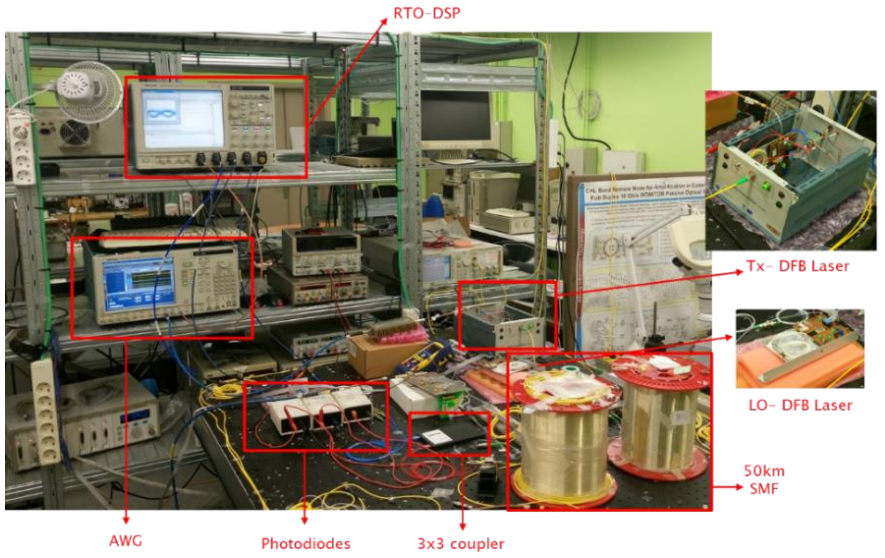

(b)

Figure 4.5. Experimental setup: (a) schematics (the insets show the eye diagram of the transmitted electrical signal and the constellation of the received signal; from left to right, DPSK, ODB, DQPSK and 8-DPSK, (b) implementation at GCO laboratory.

The three outputs of the optical coupler were detected with 10 GHz p-i-n- PDs followed by low-noise electrical amplifiers. The electrical signals were sampled and processed with a 50 GSa/s RTO. The three components were combined to obtain the I and Q parts. The processed complex samples were multiplied with the complex conjugate of the previous symbol for differential demodulation. Afterwards, the samples passed through a 4th order LPF with cut-off frequency of 2.4 GHz. The symbols decision was performed after averaging 10 samples. The symbols were then de-mapped to bits and the BER computed. The same Rx was used for all the modulation formats, i.e., only the de-mapper block was changed.

4.3.1 Comparison between DPSK, DQPSK and ODB formats

The results commented below were published in [11]. For these tests the Tx was composed by a DFB with 4 MHz linewidth and its emission wavelength was 1548 nm. The LO was another DFB with 2 MHz linewidth and 0 dBm output power.

DPSK

The first tests were performed with the simplest modulation format, i.e. DPSK. The performance in terms of the BER against the Rx optical power is plotted in Figure 4.6(a). At FEC level BER of 10^{-3} the Rx sensitivity was around -48 dBm for 1.25 Gb/s. The Rx sensitivity fell to -44 dBm when the bit rate was doubled to 2.5 Gb/s, and further lowered to -43 dBm at 3.125 Gb/s. The penalty observed in these two cases was expected as the bitrate was increased. For these three data rates the eye diagrams of the received signal were wide opened as observed in Figure 4.6(b), 4.6(c), and 4.6(d). When testing with 5 Gb/s, the eye-diagram got closed (Figure 4.6(e)) and the performance did not reach the BER target.

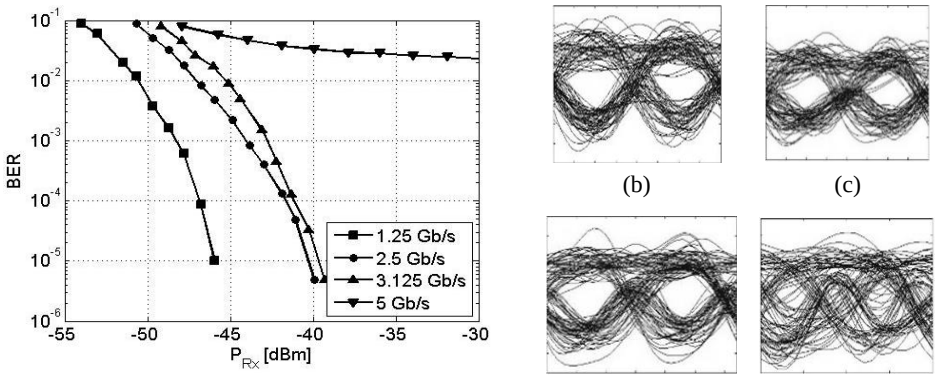

Figure 4.6. (a) BER against Rx optical power for a DPSK signal at several bit rates. The eye-diagrams in the right correspond to: (b) 1.25 Gb/s, (c) 2.5 Gb/s, (d) 3.125 Gb/s, and (e) 5 Gb/s.

As seen in Figure 4.6(a), there was a BER floor above 10^{-2} even for high Rx optical power values. This was expected since the DFB in the Tx had approximately a 2 GHz BW. Higher modulation formats were then studied for increasing the bit rate.

DQPSK

First, data was coded into a DQPSK signal and mapped to four levels for direct modulation of the laser. The bitrate was thus increased while maintaining the total BW. The results are plotted in Figure 4.7(a). At target FEC BER of 10^{-3}, the Rx sensitivity was -43 dBm at 2.5 Gb/s. This value was just 1 dB lower than the obtained for DPSK. When further increasing the bitrate to 5 Gb/s, the measured Rx sensitivity was -40 dBm, hence there was only a 3 dB penalty with respect to 2.5 Gb/s. Remarkably there was no floor appearing in the BER curves and the constellation could be distinguished (inset of Figure 4.7(a)). Hence, the bit rate could be increased four-fold, from 1.25 Gb/s to 5 Gb/s, with a penalty of 8 dB by changing the modulation format from DPSK to DQPSK. There are two possible causes for this high penalty: the residual AM added to the detected signal when performing the direct PM, and the increased phase noise due to the more stringent linewidth requirements for DQPSK [24].

On the other hand, to verify the CS requirements and the improvement in SE, a second DFB laser with linewidth of 1 MHz, emitting at optical power of 0 dBm, and wavelength λ_2, was modulated with an independent symbol sequence and added to the network. Both users (λ_1 and λ_2) operated at R_b = 2.5 Gb/s. The LO in the Rx was adjusted to detect user 1 (λ_1) which was fixed and the effect of neighbor channels (lower and upper) was measured at a constant Rx optical power of -40 dBm. The λ_2 was varied from λ_1-0.08 nm to λ_1+0.08 nm by thermal tuning. The BER against the CS is plotted in Figure 4.7(b) for both modulation formats.

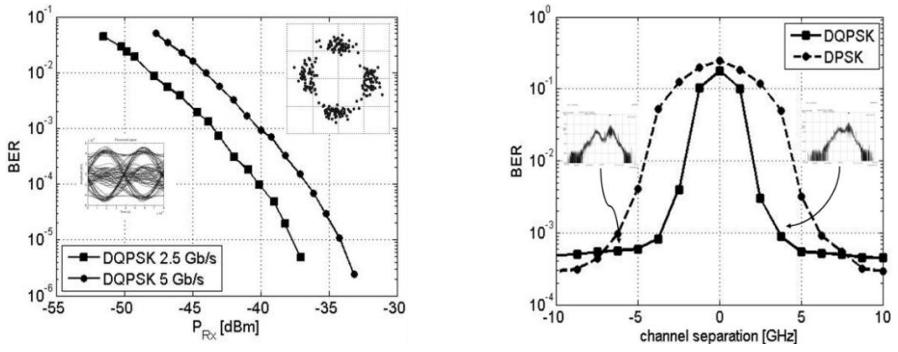

(a) (b)

Figure 4.7. (a) BER against Rx optical power for DQPSK signal (the insets show the eye diagram of the I component and the constellation recovered in the Rx, (b) BER against CS for DPSK and DQPSK signals. The insets show the transmitted optical spectrum at CS of 6.25 GHz(left) and 3.75 GHz(right).

For DQPSK, the minimum CS to keep the penalty <1 dB was as low as 5 GHz. In contrast, for the same R_b, with DPSK modulation a CS of 8.75 GHz was needed.

ODB

Finally, the ODB modulated signal was tested. The results are plotted in Figure 4.8. The measured Rx sensitivities at BER of 10^{-3} were -45 dBm and -40 dBm at 3.125 Gb/s and 5 Gb/s, respectively. Even if the performance was similar to the DQPSK case, it is relevant to comment that the filters at 5 Gb/s were not optimized and it is expected that the results could be slightly better. Nevertheless, the bitrate was increased to 6.25 Gb/s and the signal could still be detected with an Rx sensitivity of -38 dBm at the target BER. The eye diagrams shown in Figure 4.8 are wide opened even for the 6.25 Gb/s case, however higher bit rates would require an equalization block at the Rx. Due to the lack of enough analogue low-pass filters, the CS test were not performed for ODB signals.

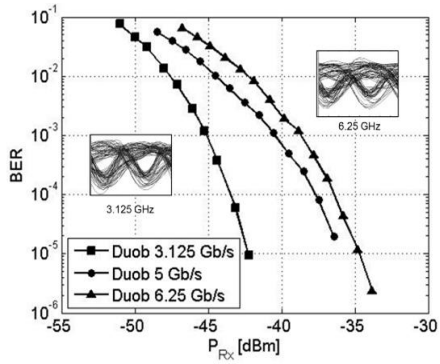

Figure 4.8. BER against Rx optical power for optical duobinary modulation format (the insets show the eye-diagram for bitrates of 3.125 Gb/s and 6.25 Gb/s).

For clarity, Table 4.2 summarizes the archived results in terms of Rx sensitivity. Note that the Tx and the Rx were not completely optimized due to these tests were a concept demonstration. Some cells are left in blank because the signal was only tested at 1.25 Gbaud and 2.5 Gbaud for DPSK and DQPSK formats, and the ODB was only tested from R_b of 3.125 Gb/s.

Table 4.2. Rx sensitivity at BER = 10^{-3} for multilevel phase modulation formats.

R_b	DPSK	DQPSK	ODB
1.25 Gb/s	-48 dBm	-	-
2.5 Gb/s	-44 dBm	-43 dBm	-
3.125 Gb/s	-43 dBm	-	-45 dBm
5 Gb/s	Floor	- 40 dBm	-40 dBm
6.25 Gb/s	-	-	-38 dBm

4.3.2 7.5 Gb/s Direct DFB Phase Modulation with 8-DPSK

The results of the following experiment with 8-DPSK modulation were presented in [12]. With this modulation format the R_b was increased to 7.5 Gb/s. Similarly than in the experiment described before, a sequence of 2^{18} symbols were generated and codified into DPSK, DQPSK or 8-DPSK format and mapped into 2, 4 and 8 levels respectively. The multilevel samples were uploaded to an AWGen producing a signal at 1.25 Gbaud/s or 2.5 Gbaud/s. The high-pass electrical signal was electrically amplified and used to directly modulate an equalized 2.5 GHz BW DFB laser. The Rx was similar as the one described before, consisting of an intradyne scheme based on a 3x3 120º optical coupler. For these experiments the Tx and LO lasers were two DFB lasers with linewidths of 1 MHz, emitting at $\lambda_1 \approx \lambda_{LO} \approx 1549.3$ nm, and with optical powers of 0 dBm. First, the system performance with a DPSK signal at 1.25 Gb/s was measured. The electrical signal was amplified to diminish the residual carrier. The results are shown in Figure 4.9. At BER = 10^{-3}, an Rx sensitivity as low as -51 dBm was obtained. Then the laser was modulated with a DQPSK signal at 2.5 Gb/s and the operation point was optimized. As seen in Figure 4.9, the Rx sensitivity was of -44 dBm approximately. The 7 dB penalty with respect to DPSK was due to the increased residual IM in the signal, together with the higher phase noise. However, no BER floor was observed in the measurement range. When increasing the modulation format to 8-DPSK (3.75 Gb/s), the performance was still below BER=10^{-3} with an Rx sensitivity of around -36 dBm. Such a strong penalty appeared because of the high phase noise in the signal as there was no phase estimation stage in the Rx. This is observed in in the inset of Figure 4.9, where it is difficult to distinguish the 8-DPSK points in the constellation diagram. In addition, the 8-DPSK modulating signal required higher peak-to-peak amplitude than DPSK and DPQSK, causing an increment in the residual IM power. Figure 4.9 also includes the signal spectrum of the Rx signals, which is almost identical for the three cases, and even more important occupying the same spectral BW.

Afterwards, the symbol rate was increased to 2.5 Gbaud. The results are plotted in Figure 4.10(a). The DPSK signal was firstly tested and an Rx sensitivity of -46.5 dBm was measured at BER=10^{-3}. The penalty with respect to 1.25 Gb/s was of 4.5 dB. For the DQPSK case (bitrate of 5 Gb/s), the Rx sensitivity was -40 dBm, which was 4 dB higher than at 2.5 Gb/s. Then, when testing with 8-DPSK at 7.5 Gb/s, the signal was still detected at BER=10^{-3} with an Rx sensitivity of -31.5 dBm. Notably, the three modulation formats presented penalties of 4.5 dB approximately when doubling the bit rate.

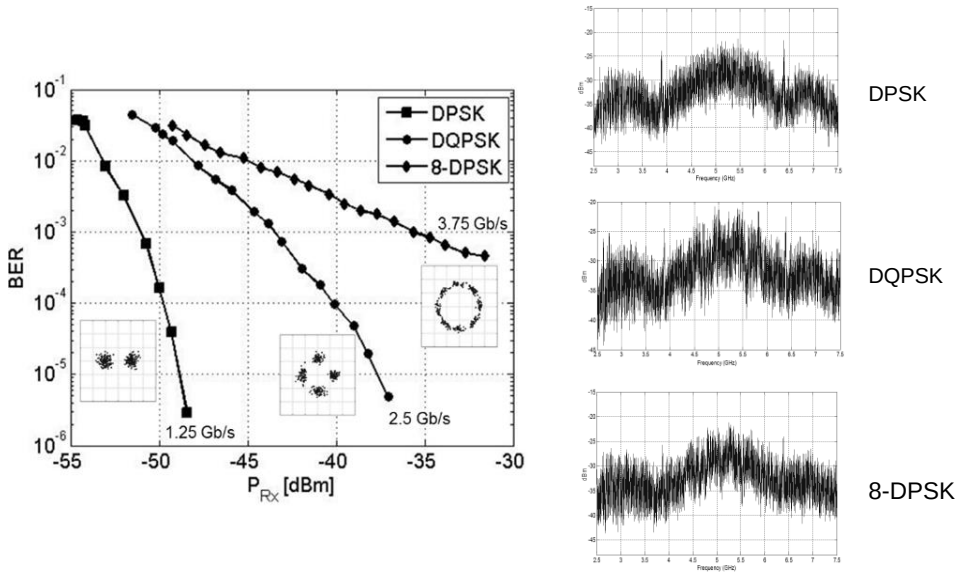

Figure 4.9. BER against Rx optical power for multilevel signals at 1.25 Gbaud; the insets on the right show the spectrum and constellations for DPSK (up), DQPSK (middle) and 8-DPSK (down).

To evaluate the channel spacing, a second DFB emitting at λ_2, with a linewidth of 1 MHz and Tx power of 0 dBm, was modulated with an independent symbol sequence. Then, this new user was tuned in temperature and λ_2 was changed from 1549.2 to 1549.4 nm. The Rx optical power was set at -30.5 dBm and the BER was measured. The results are in Figure 4.10(b). As it can be observed, the channels should be separated by 6.25 GHz to keep a penalty < 1 dB (BER > 10^{-3}). Moreover, the SE for 8-DPSK was 1.2 bit/s/Hz, this is 3 times higher than for DPSK.

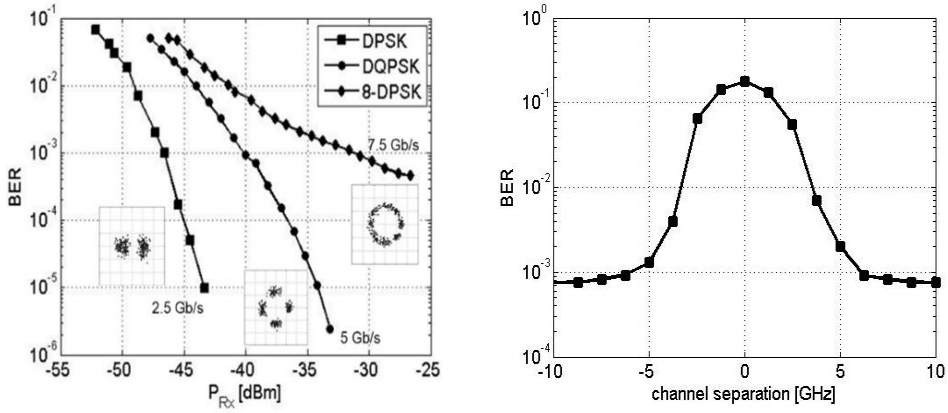

(a) (b)

Figure 4.10. (a) BER against Rx power for multilevel phase modulated signals at 2.5 Gbaud; (b) BER against channel separation for 8-DPSK signal at 7.5 Gb/s.

Finally, considering the worst Rx sensitivity (-31 dBm for 8-DPSK at 7.5 Gb/s), a launched power of 0 dBm per user and the 50 km fiber link, at least 64 users could be served in the PON. Table 4.3 summarizes the highest total capacity in upstream of the PON for each modulation format in a total BW of 400 GHz (64 users). Even though the sensitivity is limited for the 8-DPSK, it can provide 7.5 Gb/s in a 6.25 GHz channel spaced UDWDM. This could potentially allow to adapt the transceivers according to the user needs. For clarity, the achieved results in terms of Rx aggregate capacity, for the three considered multilevel phase modulation formats, and the recently standardized NG-PON2 standard, are posted in Table 4.3.

Table 4.3. PON dimensioning summary

R_b	Modulation format	Total PON capacity
2.5 Gb/s	DPSK	160 Gb/s
5 Gb/s	DQPSK	320 Gb/s
7.5 Gb/s	8-DPSK	480 Gb/s
NG-PON 2	OOK	40 Gb/s

4.4 Chapter summary

In this chapter, the investigation of direct phase modulation of commercial DFB lasers was extended to multilevel formats for achieving higher bit rates as well as better spectral efficiencies.

A direct phase modulated DFB laser with DPSK, DQPSK and ODB modulation phase formats were experimentally tested in a 50 km fiber link with intradyne coherent detection. By using multilevel formats (DQPSK and ODB) an optical signal at R_b of 5 Gb/s was obtained with a limited 2.5 GHz BW laser, achieving a Rx sensitivity of -40 dBm at BER of 10^{-3}. For DPSK a bit rate higher than 3.125 Gb/s were not possible to implement because of the limited BW of the laser. The highest bitrate was of 6.25 Gb/s with ODB format, achieving a Rx sensitivity of -38 dBm, and showing the potential for higher bit rates, but using lower spectral BW.

Furthermore, to scale at R_b = 7.5 Gb/s, a DFB laser was directly modulated with an 8-DPSK signal and experimentally demonstrated in the same 50 km UDWDM-PON. Rx sensitivities of -36 dBm and -31 dBm at BER=10^{-3} were achieved for bit rates of 3.75 Gb/s and 7.5 Gb/s with intradyne coherent detection. With a launched power of 0 dBm, up to 64 users could be

served in the PON. The minimum channel spacing to keep the penalties < 1 dB was 6.25 GHz, giving a spectral efficiency of 1.2 bit/s/Hz; this is 3 times higher than for DPSK.

In both experiments the same Rx was employed to detect DPSK, DQPSK, 8-DPSK, and duobinary data, providing simplicity to the system. The use of these modulation formats can potentially render the PON adaptable to the user bit rate needs. Furthermore, the modulation format could be negotiated at the ONU registration process, and it could be potentially configured by software giving flexibility to the PON without affecting the overall performance. These characteristics make the proposed techniques attractive for a cost-efficient TRx in UDWDM-PONs, with improved spectral efficiency.

Bibliography Chapter 4

[1] A. Shahpari *et al.*, "Coherent ultra dense wavelength division multiplexing passive optical networks," *Opt. Fiber Technol.*, vol. 26, pp. 100–107, Dec. 2015.

[2] J. Prat *et al.*, "Technologies for Cost-Effective udWDM-PONs," *J. Light. Technol.*, vol. 34, no. 2, pp. 783–791, Jan. 2016.

[3] P. J. Winzer and R.-J. Essiambre, "Advanced Optical Modulation Formats," *Proc. IEEE*, vol. 94, no. 5, pp. 952–985, May 2006.

[4] B. Sklar, *Digital communications: fundamentals and applications*, 2nd ed. Upper Saddle River, N.J: Prentice-Hall PTR, 2001.

[5] G. Bosco, "Advanced Modulation Techniques for Flexible Optical Transceivers: The Rate/Reach Tradeoff," *J. Light. Technol.*, vol. 37, no. 1, pp. 36–49, Jan. 2019.

[6] Y. Fu, K. Zhang, M. Bi, and W. Hu, "Multi-Dimensional Coded PAM4 Modulation for TDM-PON based on 10G Optical Devices," in *Proc. Asia Comm. and Phot. Conf.*, Wuhan, China, 2016.

[7] V. Houtsma, D. van Veen, and H. Chow, "Demonstration of Symmetrical 25 Gb/s TDM-PON with Multilevel Interleaving of Users," *J. Light. Technol.*, vol. 34, no. 8, pp. 2005–2010, Apr. 2016.

[8] S. Tsukamoto, K. Katoh, and K. Kikuchi, "Coherent demodulation of optical multilevel phase-shift-keying signals using homodyne detection and digital signal processing," *IEEE Photonics Technol. Lett.*, vol. 18, no. 10, pp. 1131–1133, May 2006.

[9] S. J. Savory, "Digital Coherent Optical Receivers: Algorithms and Subsystems," *IEEE J. Sel. Top. Quantum Electron.*, vol. 16, no. 5, pp. 1164–1179, Sep. 2010.

[10] T. Mizuochi *et al.*, "Next generation FEC for optical transmission systems," in *Proc. Opt. Fiber Commun. Conf. (OFC)*, Atlanta, GA, USA, 2003.

[11] I. N. Cano, J. C. Velásquez, V. Polo, and J. Prat, "Multilevel direct DFB phase modulation in 6.25 GHz spectrally spaced UDWDM PONs," in *Proc. 18th Int. Conf. on Transp. Opt. Netw. (ICTON)*, Trento, Italy, 2016.

[12] I. N. Cano, J. C. Velásquez, and J. Prat, "7.5 Gb/s direct DFB phase modulation with 8-DPSK for 6.25 GHz spaced coherent UDWDM-PONs," in *Proc. Opt. Fiber Commun. Conf. (OFC)*, Anaheim, CA, USA, 2016.

[13] International Telecommunication Union, "ITU-T G.694.1 Recommendation, Spectral grids for WDM applications: DWDM frequency grid." Feb-2012.

[14] I. B. Djordjevic and B. Vasic, "Multilevel coding in M-ary DPSK/differential QAM high-speed optical transmission with direct detection," *J. Light. Technol.*, vol. 24, no. 1, pp. 420–428, Jan. 2006.

[15] J. G. Proakis, *Digital Communications*, 4th ed. Boston, MA: McGrawHill, 2001.

[16] A. Lender, "The duobinary technique for high-speed data transmission," *Trans. Am. Inst. Electr. Eng. Part Commun. Electron.*, vol. 82, no. 2, pp. 214–218, May 1963.

[17] Hari Shankar, "Doubinary Modulation for Optical Systems." Inphi Corporation, 2002.

[18] M. Rannello, M. Presi, and E. Ciaramella, "Optical vs. Electrical Duobinary Coding for 25 Gb/s PONs based on DSP-free Coherent Envelope Detection," in *Proc. Opt. Fiber Commu. Conf. (OFC)*, San Diego, CA, USA, 2018.

[19] D. v. Veen and V. Houtsma, "Cost Effective 25 Gbps Optical Access Technology," in *Proc. 42nd Eur. Conf. on Opt. Commu. (ECOC)*, Düsseldorf, Germany, 2016.

[20] X. Gu *et al.*, "Duobinary technique for dispersion reduction in high capacity optical systems-modelling, experiment and field trial," *IEE Proc. - Optoelectron.*, vol. 143, no. 4, pp. 228–236, Aug. 1996.

[21] C. Sun, S. H. Bae, and H. Kim, "Transmission of 28-Gb/s Duobinary and PAM-4 Signals Using DML for Optical Access Network," *IEEE Photonics Technol. Lett.*, vol. 29, no. 1, pp. 130–133, Jan. 2017.

[22] I. N. Cano, A. Lerin, M. Presi, V. Polo, E. Ciaramella, and J. Prat, "6.25Gb/s differential duobinary transmission in 2GHz BW limited direct phase modulated DFB for udWDM-PONs," in *Proc. 40th Eur. Conf. on Opt. Commu. (ECOC)*, Cannes, France, 2014.

[23] I. N. Cano, A. Lerin, V. Polo, and J. Prat, "Polarization independent single-PD coherent ONU receiver with centralized scrambling in udWDM-PONs," in *Proc. 40th Eur. Conf. on Opt. Commu. (ECOC)*, Cannes, France, 2014.

[24] I. N. Cano, A. Lerin, and J. Prat, "DQPSK Directly Phase Modulated DFB for Flexible Coherent UDWDM-PONs," *IEEE Photonics Technol. Lett.*, vol. 28, no. 1, pp. 35–38, Jan. 2016.

Chapter 5 . Low-cost transmitters using hybrid amplitude and phase modulation formats

With the arise of the 5G era, the data traffic and BW demands of new and versatile mobile and fixed services is expected to keep increasing in access networks. Additionally, stringent requirements in terms of peak data rate (Gb/s), user experienced data rate (Mb/s), SE (bit/s/Hz), latency (ms), and particularly the network energy efficiency compared with 4G are envisaged [1].

From the physical layer perspective, the research on alternative modulation formats will play a critical role to determine the system throughput, complexity and reliability. In 4G networks, orthogonal frequency division multiplexing (OFDM) has been adopted as the leading technique in the RF domain [2], [3], with advantages such as the scalable spectrum partitioning from individual subcarriers to a sub-band and the entire OFDM spectrum, providing high flexibility [3]. However, OFDM is unable to meet many of the new demands of upcoming 5G networks such as the asynchronous transmission of different types of data in narrow bands. This is because OFDM requires different users to be highly synchronized, otherwise there will be large interference among adjacent sub-bands [2]. Even though OFDM has gain interest in optical communications, thanks to the high tolerance to ISI and its ability to adapt the transmitted signal to the frequency characteristics of the channel, OFDM has a number of drawbacks including its high peak-to average power ratio (PAPR), the sensitivity to frequency offset and phase noise, and the implementation cost, meanly of ADCs and DACs, and the DSP required [4]. The latter point is very important in fast DSP implementations which use fixed point, due to DACs and ADCs usually require more bits to represent the wide dynamic range of OFDM signals compared to single carrier formats, for guarantying enough

resolution and to reduce quantization noise [5]. Therefore, single carrier formats such as QPSK or 16-QAM, which only requires two levels (one-bit resolution) or four levels (two-bit resolution), respectively, could be considered good choices for future 5G optical networks. Nevertheless, as is expressed by G. Bosco in [6], the standard QAM formats only offer a coarse granularity in spectral efficiency and, consequently, a coarse granularity in the achievable transmission reach. To overcome this problem, several techniques such as time-domain hybrid formats (TDHF) [7], [8], and hybrid amplitude and phase modulation formats such as Amplitude and Phase Shift Keying (APSK) are being considered for more efficient 5G WDM networks [1].

In this chapter, three novel proposals based on hybrid modulation schemes and coherent transceivers are presented as potential solutions for increasing the BW flexibility and the optical SE in WDM-PONs. First, a THDF scheme where two different formats are mixed in time-domain, and where a DFB laser is directly and simultaneously modulated in amplitude and phase is presented, based on the results demonstrated in [9]. Second, an optical hybrid domain 2-DPSK/2-ASK modulation with heterodyne detection is presented, taking benefit of a small footprint integrated dual electro-absorption modulated laser (DEML), with low power consumption. The results of this implementation are published in [10]. Finally, the same device is used to extend the research to an 8-ary hybrid optical modulation called 8-APSK, with pre-differential codification. In this work we deeply characterized the DEML to understand the chirp behavior of both the DFB and the EAM sections, and to optimize the low-cost direct modulation. The modulated data signal is recovered using an intradyne coherent Rx based on 3x3 optical coupler, to increase the R_b, the SE and the Rx sensitivity. The main results are published in [11] and submitted in [12].

5.1 Time-domain hybrid modulation format (TDHF)

In TDHF, two different modulation formats are mixed in the time domain and used to modulate the same optical carrier performing a hybrid transmission [6]–[8]. Normally this idea has been explored using high cost I-Q modulators at the Tx and complex coherent receivers based on 90º optical hybrids. This high complexity and cost, compared with direct-detection schemes, have limited their attractiveness in access networks. To face with these problems, and to provide some degree of flexibility on the TRx, a novel tX scheme based on

a simultaneous amplitude and direct phase modulation of a DFB laser with a common hardware, and functionalities selected via software commands is proposed.

5.1.1 Time Interleaved DPSK/ASK Transmitter

As explained in chapter 3, a DML behaves as an optical frequency modulator with an intrinsic frequency chirp related with the optical phase variation (see Eq. 3.2). The phase term of the electrical field, defined by Eq. 1.1, depends on the RF current swing (I_{RF}), which is directly related with the peak-to-peak amplitude of the modulating signal, and the frequency modulation depth κ_f, related with the chirp. In the proposed PM, the data sequence for generating the DPSK modulation includes a derivative term (digital HPF), to properly equalize the phase response and to obtain the desired phase changes.

In the proposed TDFH, the modulation technique consists of dividing the bit in two parts. The first half bit period is used for producing a DPSK optical signal, and then the unoccupied part is used to transmit additional information, in this case with ASK modulation. Both signals have the same R_b, and after each fragment is coded and equalized accordingly, both are added. Then, the time interleaved data sequence will have bit rate of $2R_b$.

For DPSK modulation the data is differentially encoded and digitally equalized by means of a first order HPF. The result is a RZ signal whose duty-cycle and amplitude are optimized to obtain π phase changes, controlling the effect of the adiabatic chirp [13]. The ASK data is codified as a bipolar RZ signal and delayed by half the bit period. The amplitude of the ASK data is adjusted to minimize the interference with the DPSK data. The aim is to avoid undesired phase changes over the DPSK signal whose duty cycle was adjusted to $0.25T_b$ for the same reason. The codification and equalization of both signals as well as the evolution of the optical phase is presented in Figure 5.1

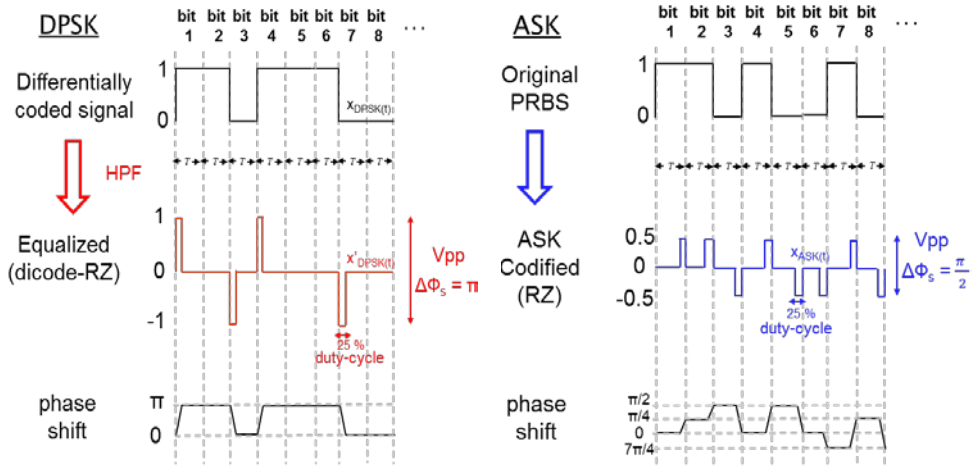

(a) (b)

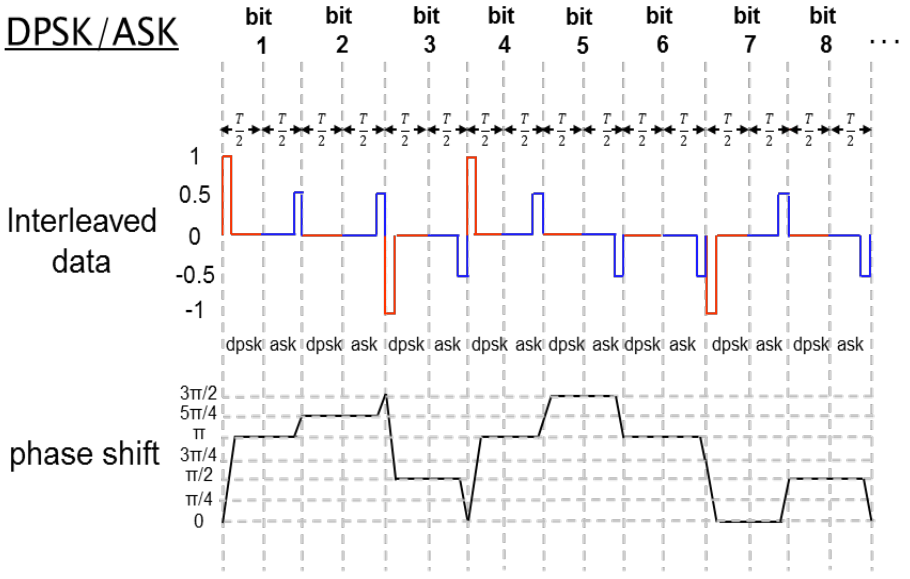

(c)

Figure 5.1. Electrical modulation signals and phase changes produced on the DFB laser for: (a) DPSK modulation, (b) ASK modulation, and (c) Time-interleaved DPSK/ASK modulation.

5.1.2 Experimental validation of time-interleaved DPSK/ASK modulation

Two 2^{15}-1 PRBS data with different seeds were generated at R_b of 1.25 Gb/s, and processed following the procedure explained in the preceding section. The result was an interleaved data sequence at R_b of 2.5 Gb/s. The scrambled data were uploaded to an AWGen. The waveform was amplified by means of an 8 GHz BW linear electrical amplifier (SHF98P) and directly modulated a DFB laser (NLK5C5E2KA). The DFB laser had 4 MHz linewidth and 10 GHz modulation BW. It was biased at 80 mA and emitted at λ_{Tx} = 1544.9 nm with launched power of PTx = 0 dBm. The optical signal had alternated DPSK and ASK modulation and was sent through 25 km of SMF. A VOA was used to reproduce splitting losses and limit the power into the Rx. A polarization controller compensated the fluctuations in the state of polarization caused by the fiber. It could be avoided implementing a polarization diversity scheme [14].

The Rx consisted on a heterodyne balanced scheme. A 3-dB optical coupler mixed the incoming signal with a LO. The LO was a 100 kHz linewidth ECL with 0 dBm optical power tuned at an IF of 5 GHz from λ_{Tx}. The coupler outputs were detected with two 10 GHz p-i-n-PDs followed by low-noise electrical amplifiers. The electrical signals were sampled and processed with a 50 GSa/s RTO. The two components were combined for balanced detection and band-pass filtered. After synchronization, the samples were divided in half bit periods to obtain the ASK and DPSK data independently. For the former we employed a power detector (squared and low-pass filtered) and for the later, the samples were differentially demodulated with a delay and multiply operation and low-pass filtered. Finally, the BER considering both ASK and DPSK data was computed.

The scheme of the setup, as well as a photo of the laboratory implementation are depicted in Figure 5.2. In that picture it is possible to identify the Tx Laser, the Rx PDs, as well as LO (ECL), and the fiber-spools used.

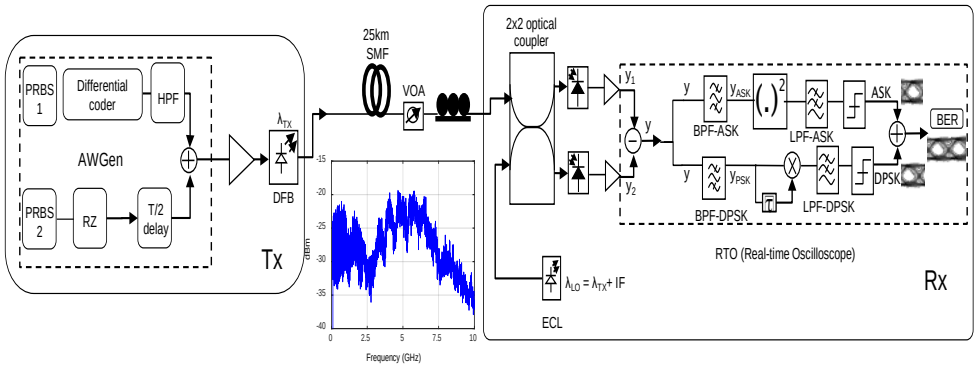

(a)

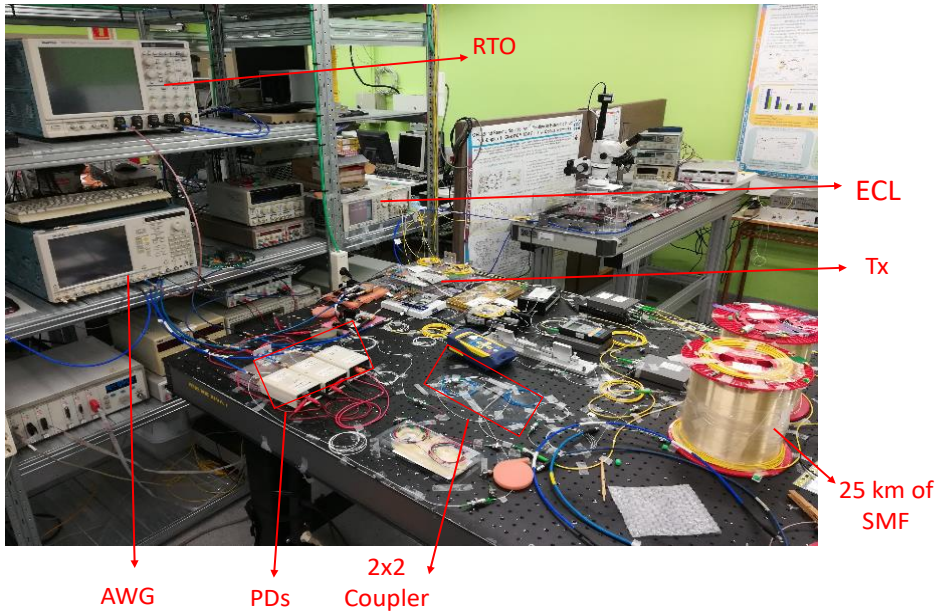

(b)

Figure 5.2. Time-interleaved DPSK/ASK implementation, (a) setup scheme, (b) photo of the implementation at GCO laboratory.

ASK performance

First, the system with pure ASK modulation was tested. After 25 km of SMF the Rx sensitivities measured at FEC limit of BER = $4x10^{-3}$ (second generation FEC limit [15]) were -44.5 dBm and -42 dBm for R_b of 1.25 Gb/s and 2.5 Gb/s respectively. The BER results are plotted in Figure 5.3 for R_b of 1.25 Gb/s and 2.5 Gb/s.

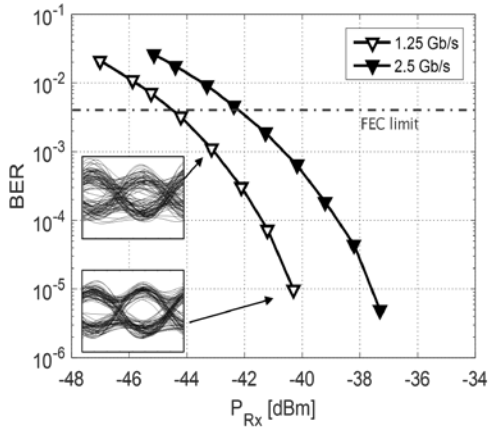

Figure 5.3. BER against Rx optical power for ASK Tx after 25 km of SMF. The insets show the eye diagrams at BER of 10^{-5} and 10^{-3}.

Time-interleaved DPSK/ASK performance

To implement the DPSK/ASK technique, the amplitude of both electrical modulating data was adapted. With a fixed Rx optical power, the gain of the electrical amplifier preceding the Tx laser was tuned. The effect on the individual BER was measured for independent ASK and DPSK modulations. The results are plotted in Figure 5.4(a). The ASK performs better with higher gain because the ER increases. However, for the PM data there is an optimum value which corresponds to a π phase shift [13]. Hence there was a trade-off between both modulations.

An amplifier gain of 13.1 dB (scrambling point in Figure 5.4(a)), corresponding to amplitudes of 0.55 V and 1.0 V peak-to-peak (Vpp), was used for ASK and DPSK modulating data, respectively. After selecting the proper amplitudes, the interleaved DPSK/ASK Tx was tested. The results are plotted in Figure 5.4(b). The Rx sensitivity was -44 dBm at BER = $4x10^{-3}$. Remarkably, this value was 2 dB better than ASK at the same R_b showing a benefit when employing the interleaved signal. The insets in Figure 5.4(b) clearly show the eye diagram of the time interleaved signal. The eye diagram is open in the first and second half-bit for the DPSK and ASK respectively, while it is closed in the other half.

To understand the cross-effect between data formats, the individual BER curves of the ASK and DPSK components are included in Figure 5.4(b). At the same BER = $4x10^{-3}$, the Rx sensitivity for the ASK transmission was -41 dBm. Compared to the performance shown in Figure 5.3, this Rx sensitivity is 3.5 dB worse. The reason for such penalty is that the amplitude of the ASK modulating sequence was reduced approximately by a factor of two, to

avoid phase distortions in the DPSK signal. This limited the ER and lowered the Rx sensitivity by 3.5 dB. For the DPSK, the Rx sensitivity was -47.5 dBm which is 6.5 dB better than the ASK part. The interleaved BER curve lies in average between the DPSK and ASK ones. A finer optimization of the amplitudes of the electrical signals could reduce the difference between the ASK and DPSK.

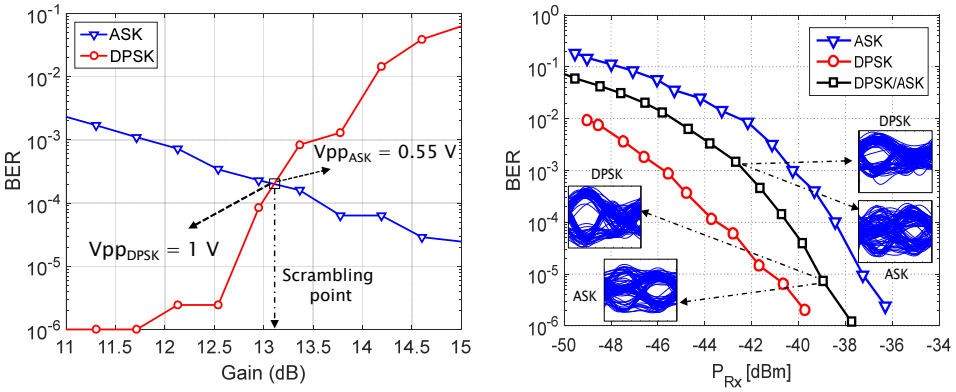

Figure 5.4. (a) BER against amplifier gain for independent ASK and DPSK modulations, (b) BER against Rx optical power for ASK, DPSK and DPSK/ASK signals when interleaved data is transmitted. The insets show the eye diagrams of the received ASK and DPSK data at BER of 10^{-5} and 10^{-3}.

Finally, the performance of the DPSK/ASK solution with the DPSK at the same Rx power of -42 dBm is compared, appreciating that different classes of service could be served. For example, interactive applications, as conversational voice and video, which are error tolerant but with a critical delay (<<1 s) [16] constraint, could be transmitted with DPSK ensuring a first generation FEC (minimum BER = 1.5×10^{-4}) [15], with less redundancy bits. In contrast a text messaging service, with non-critical delay (~10 s) [16] but less error tolerant, could employ ASK with a second generation FEC (minimum BER = $4 \cdot 10^{-3}$) [15]. With this flexibility, the proposed technique is a potential solution for a Tx that could support different End-user multimedia Quality of Service (QoS) categories according with the latency and error limits. For reasons of clarity, the aforementioned results are summarized in Table 5.1.

Table 5.1. Experimental results of time-interleaved DPSK/ASK for supplying different services

Service	Modulation format	Rx Sensitivity at BER = 4×10^{-3} after 25-km SMF link	Required FEC level at PRx= -42 dBm
Voice and video	DPSK	-47.5 dBm	1.5×10^{-4} (1st gen.)
Text messaging	ASK	-41 dBm	4×10^{-3} (2nd gen.)

5.2 Heterodyne DPSK-ASK based on Dual-EML transmitter

In recent years, monolithic integration on InP (Indium Phosphide), a binary semiconductor composed of indium and phosphorus, has been explored in order to produce complex integrated photonic components for WDM-PONs, with small footprint, low power consumption and multiple functions. Recently a BPSK electro-absorption modulator (EML) [17] and a dual-EML (DEML) [18] were proposed as a single integrated Tx for simplifying the ONU. The DEML has been used in several applications such as combining AM and FM formats for dispersion tolerant transmission [19], for minimizing residual AM [20] in a directly phase modulated DFB laser, and as dual-output DEML for Full Duplex DPSK-ASK and DPSK-SSB ONU in an UWDM-PON [21].

In this section a novel application of the DEML is presented, where the laser and the electro-absorption modulator (EAM) are simultaneously modulated in phase (DPSK) and amplitude (ASK), correspondingly. The transmitted 2-DPSK/2-ASK optical signal is tested at R_b = 5 Gb/s and detected with a simple heterodyne coherent Rx. The results are published in [10].

5.2.1 Assembly and characterization of the dual electro-absorption modulated laser (DEML)

The DEML is a monolithically integrated photonic device with two independent modulation inputs, one for the DFB laser and one for the EAM in the same active layer [19]. A schematic representation is shown in Figure 5.5(a). The length of the DFB and EAM sections are around 470 μm and 75 μm respectively and have 50 Ω resistors for impedance matching. The DEML chip was fixed on a ceramic sub-mount mount (size 2 mm x 6 mm x 0.5 mm), and a temperature sensor (R_{NTC}) was placed beside the chip to keep an operating condition (~26ºC) using an external temperature control. An RF circuit board was assembled to provide the RF access to the DFB and EAM. A picture of the assembled DEML sub-mount, and the lensed fiber faced with the EAM output is shown in Figure 5.5(b).

GCO lab has several DEML units provide by III-V lab, France, as result as the partnership during the European COCONUT Project [22]. Here, the characterization of one of them, which will be named as DEML-1 is presented. The other will be described in next section.

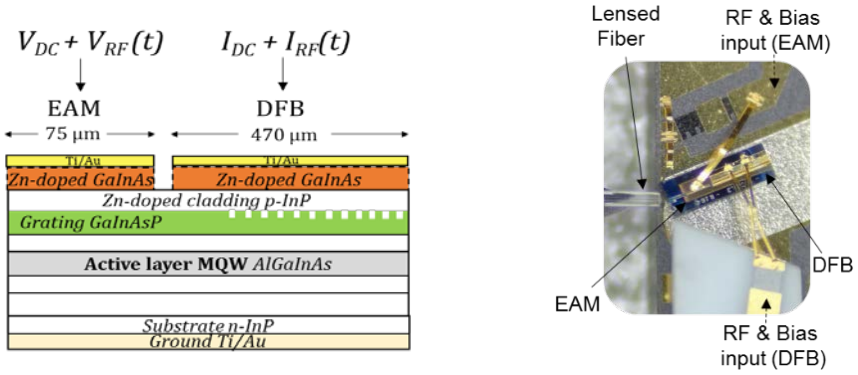

(a) (b)

Figure 5.5. (a) Sectional view of the DEML, (b) Assembled DEML chip and lensed fiber faced with the EAM output.

The DEML-1 output power against the DFB bias current and the EAM bias voltage (V_{EAM}) are plotted in Figure 5.6(a). It is noted that the DFB threshold current is as low as 7 mA and the EAM linear region is between -1.1 and -2.1 V. In addition, the amplitude and phase response of the DFB were measured following the method described in [23]. The results are shown in Figure 5.6(b). The effect of the adiabatic chirp in the lower frequencies (< 2 GHz) of the PM response is clearly observed as an exponential decreasing behavior which had to be compensated, to obtain a flatter curve for PM. This can be done using the technique described in chapter 3, and published in [24], [25].

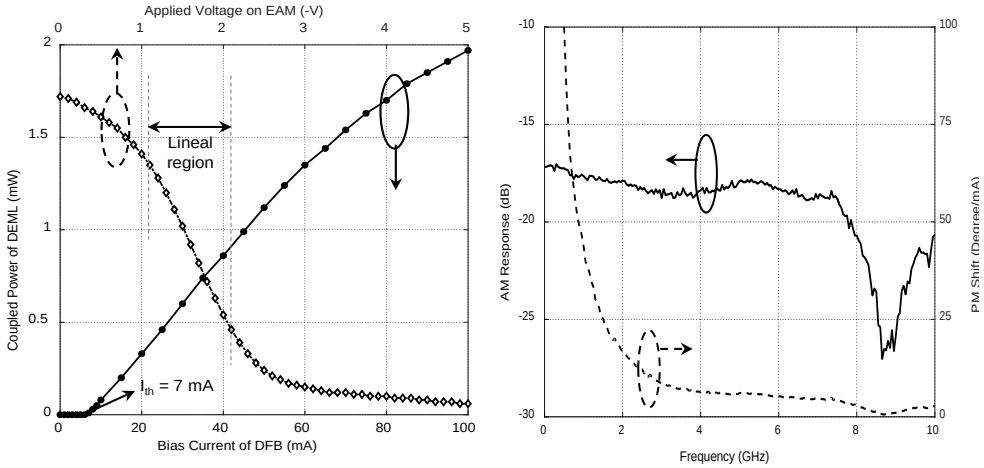

(a) (b)

Figure 5.6. Characterization of the DEML-1. (a) Static characteristics of DFB (V_{EAM} = 0V) and EAM ($I_{bias\ DFB}$ = 80 mA), (b) AM and PM responses of the DFB.

5.2.2 DPSK/ASK signal generation

For the DFB, a binary data were differentially coded, and the symbols mapped as a 2-ary signal with two phase variations (0, π), for direct phase modulation of the laser as explained in chapter 3. For the EAM, a typical NRZ unipolar coded signal was used for ASK modulation of the transmitted signal. Both sequences (Figure 5.7(a)) are uploaded to an AWGen and digitally synchronized. The electrical signals modulating the DEML produced a 4-ary constellation (Figure 5.7(b)) where the symbols were located along the I-axis, with two possible phases variations (0 and π) corresponding to DPSK modulation, and two concentric rings representing the two-level (a_0, a_1) ASK modulation.

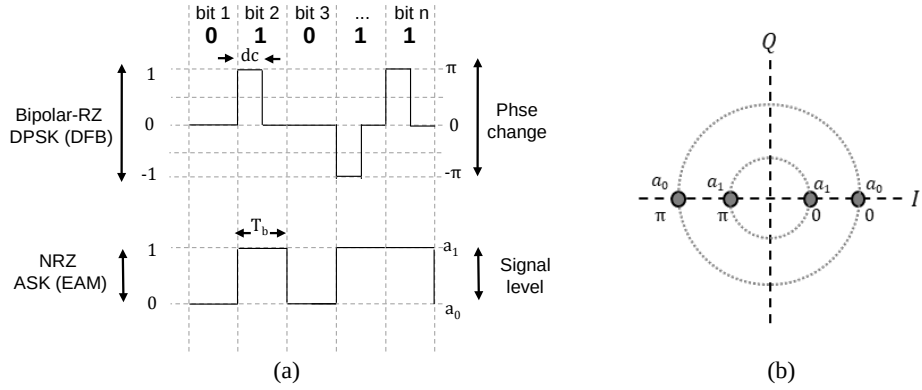

Figure 5.7. (a) Bipolar-RZ & NRZ signals for DPSK & ASK modulation, (b) 2-DPSK/2-ASK constellation.

5.2.3 Experimental validation of heterodyne DPSK/ASK

The complete Tx was based on a DEML whose two sections (DFB and EAM) were independently modulated with different uncorrelated data streams of R_b = 2.5 Gb/s, each. For the DFB, data was a 2^{15}-1 PRBS differentially encoded and digitally equalized by means of a 1-tap FIR filter emulating a high-pass function. The result was a bipolar RZ signal whose duty cycle and amplitude were adjusted to obtain π phase changes [13], [25]. The EAM was modulated with a 2^{15} NRZ PRBS with a different seed to be uncorrelated with the DFB one. The amplitudes of both electrical signals were adjusted with two identical 10 GHz BW electrical amplifiers and injected to the corresponding sections. The DFB was biased at 80 mA to obtain high output power. The DFB produced a DPSK optical signal whose amplitude was modulated with the EAM and passed through an isolator for minimizing optical

reflections. As the signals were synchronized, we could generate a four-level signal doubling the bit rate but keeping the same bandwidth of the single ASK or DPSK signal, as can be appreciated in the optical modulated spectra (see Figure 5.8) for each case. The launched power and wavelength were P_{Tx} = -1 dBm and λ_{Tx} = 1556.16 nm, respectively. The DEML output signal was sent through a 25 km SMF link. Afterwards, a VOA emulated the coupling losses and limited the power into the Rx. A polarization controller compensated the fluctuations in the state of polarization caused by the fiber. A scheme of the setup and some photos of the implementation at GCO laboratory are presented in Figure 5.8, where the assembled sub-mount and the assembled RF circuit board are clearly distinguished.

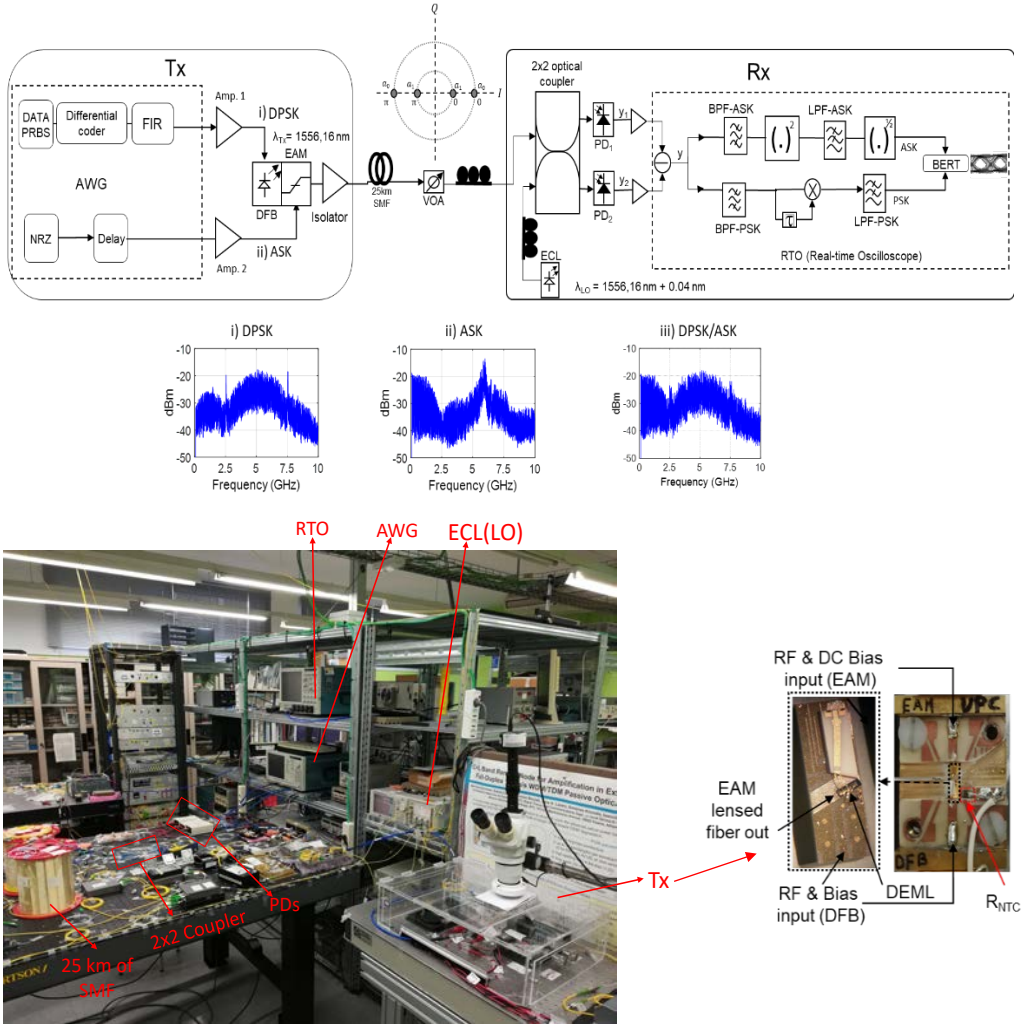

Figure 5.8. Experimental setup and photos of the heterodyne 2-DPSK/2-ASK laboratory implementation.

The Rx was based on a heterodyne balanced scheme. A 3-dB optical coupler mixed the incoming signal with a LO signal. The LO was a 100 kHz linewidth ECL with 0 dBm optical power and tuned at IF of 5 GHz from the Tx carrier. The coupler outputs were detected with two 10 GHz p-i-n- PDs followed by low-noise electrical amplifiers. The electrical signals were sampled and processed with a 50 GSa/s RTO. The two components were combined for balanced detection and processed to obtain independently the ASK and DPSK data. ASK demodulation was done with an envelope detector (the signal was band-pass filtered, squared, low-pass filtered and root-squared), and the simultaneous DPSK data, was differentially demodulated with a delay and multiply operation and then low-pass filtered. Finally, the BER was computed for both data streams.

ASK performance

First, in optical btb, the conventional EML with ASK modulation at R_b = 2.5 Gb/s was tested. The modulating signal had a peak-to-peak voltage (Vpp) of 1.48 V and the EAM was biased at -1.8 V. Figure 5.9(a) shows the BER against the received optical power. At the FEC threshold of BER = 10^{-3} the measured Rx sensitivity was -39.5 dBm.

DPSK performance

Afterwards, the EAM was unbiased and the DFB was modulated in phase (DPSK) with a beat signal having a duty-cycle = 50% and Vpp = 1.85 V to obtain 0-π radians phase swing. The Rx sensitivity was -45.5 dBm at BER = 10^{-3} as is shown in Figure 5.9(a). The better sensitivity is due to the larger distance between the constellation points for DPSK compared to ASK.

DPSK/ASK performance

Finally, the combined DPSK/ASK signal was tested. The DFB was directly modulated in phase and synchronously its amplitude was modulated with the EAM signal described previously. Figure 5.9(b) plots the BER against the ROP with the combined DPSK/ASK modulation. At a combined BER = 10^{-3}, the Rx sensitivity was -37 dBm approximately. Notably, when transmitting through 25 km of SMF, the measured penalty was just 0.5 dB. There was a penalty of around 2.5 dB compared with ASK modulation alone, however, the bit rate was doubled. Then, the LO optical power was increased up to 6 dBm to compensate the losses, and a Rx sensitivity of -40 dBm was achieved at the same combined BER. There are two reasons that explain the limitation in the performance. The first one is that the EAM

reduces the amplitude of the signal and thus the eye aperture of the DPSK signal in half of the bits when the EAM absorbs the light. Second, when the EAM is modulated, the wavelength slightly fluctuates and shows drifts mainly because of temperature variations in the chip. This is attributable to the fast amplitude transitions in the EAM which vary the temperature due to the thermal heating in the resistor matching the EAM to 50Ω.

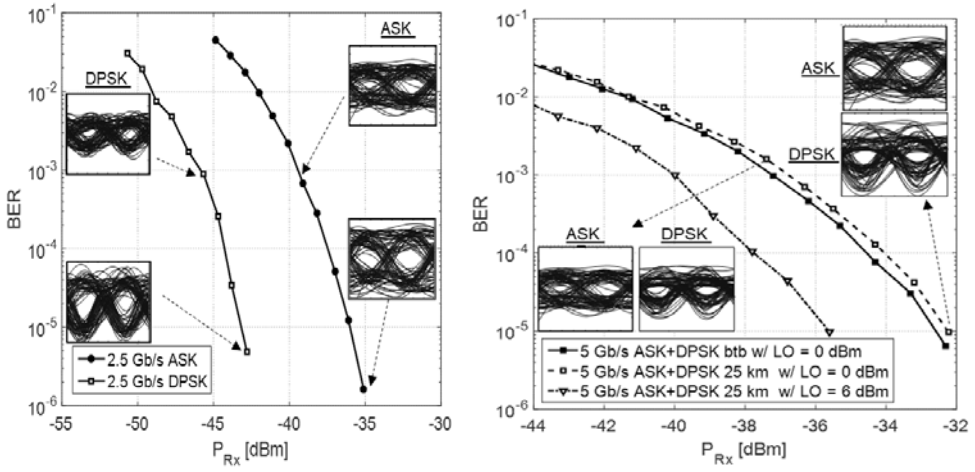

(a) (b)

Figure 5.9. BER against received optical power for: (a) ASK and DPSK alone signals (R_b = 2.5 Gb/s), (b) ASK+DPSK transmission at R_b=5 Gb/s. The insets show the eye diagrams at BER of 10^{-3} and 10^{-5}.

After know the performance, the effect of the frequency drift was evaluated for DPSK alone and for DPSK/ASK signals together. In both cases, the received optical power was fixed to achieve a BER ≈ 10^{-4}. The LO emission frequency was tuned in steps of 25 MHz. The BER against LO frequency is plotted in Figure 5.10. Frequency drift degraded more the ASK+DPSK modulation than the DPSK alone. For ASK+DPSK modulation a drift of ±50 MHz produced 1 dB of penalty (quantified passing from BER=10^{-4} to 3x10^{-4} in Figure 5.9(b)); while for DPSK alone (EAM unmodulated) the penalty was only of 0.5 dB, with a frequency drift tolerance of ±80 MHz, for reaching 1 dB of penalty (quantified passing from BER=10^{-4} to 8x10^{-4} in Figure 5.9(a)). These results clearly support the feasibility for modulating simultaneously the DFB in phase and the EAM in amplitude, indicating that the DEML can potentially produce a QAM signal.

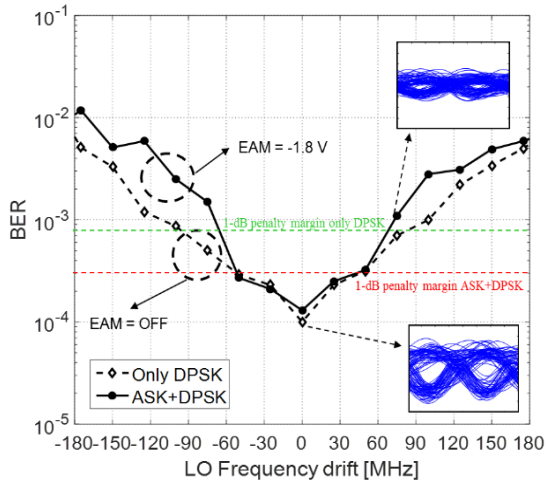

Figure 5.10. BER vs LO frequency drift when the EAM is unmodulated (DPSK) and modulated (DPSK/ASK). The eye diagrams correspond to the received data at BER=10^{-3} and 10^{-4}.

For reasons of clarity, the results are summarized in Table 5.2

Table 5.2. Experimental results of heterodyne DPSK/ASK using an integrated DEML as Tx

Modulation format	**Bit rate**	**Rx Sensitivity at BER = 10^{-3} (Optical btb and P_{LO} = 0 dBm)**	**Rx Sensitivity at BER = 10^{-3} (25-km SMF and P_{LO} = 6 dBm)**	**Frequency drift tolerance for 1 dB of penalty**
DPSK	2.5 Gb/s	-45.5 dBm	-	±50 MHz
ASK	2.5 Gb/s	-39.5 dBm	-	-
DPSK/ASK	5 Gb/s	-37 dBm	-40 dBm	±80 MHz

5.3 Differential 8-APSK DEML Transmitter with intradyne coherent reception

The previous section introduced a novel application of a DEML showing a simultaneous 2-DPSK/2-ASK modulation where the transmitted optical signal was detected with a heterodyne coherent Rx. To take benefit of the complex I-Q plane, and to extend the research, a simultaneous differential quadrature phase shift keying (DQPSK)/ASK or differential 8-APSK modulation was demonstrated through the same DEML. The primary objectives compared with the heterodyne scheme were to maximize the spectral efficiency, increase the

R_b and improve the Rx sensitivity by using an intradyne coherent Rx. The results were published in [11].

5.3.1 8-APSK signal generation

Similar than for the 2-DPSK/2-ASK signal, the transmitted 8-APSK signal was composed by the combination of two synchronous modulations. For the DFB, the quaternary data to generate the DQPSK signal was composed by two uncorrelated bit streams ($d_1(t)$ and $d_2(t)$). The symbols were codified as a 4-ary signal with four different phase variations (0, ±π/2, π), mapped into a multi-level signal and differentially encoded for direct phase modulation of the laser as explained in chapter 4. For the EAM, data were a third PRBS sequence ($d_3(t)$) coded as a unipolar NRZ signal, and uncorrelated with the data used to modulate the DFB. Both sequences (Figure 5.11(a)) were uploaded to an AWGen and digitally synchronized. The electrical signals modulating the DEML produced an 8-ary constellation (Figure 5.11(b)) where the symbols are located along the I and Q axes with four possible phases variations representing the DPSK modulation, and two concentric rings representing the two-level (a_0, a_1) ASK modulation.

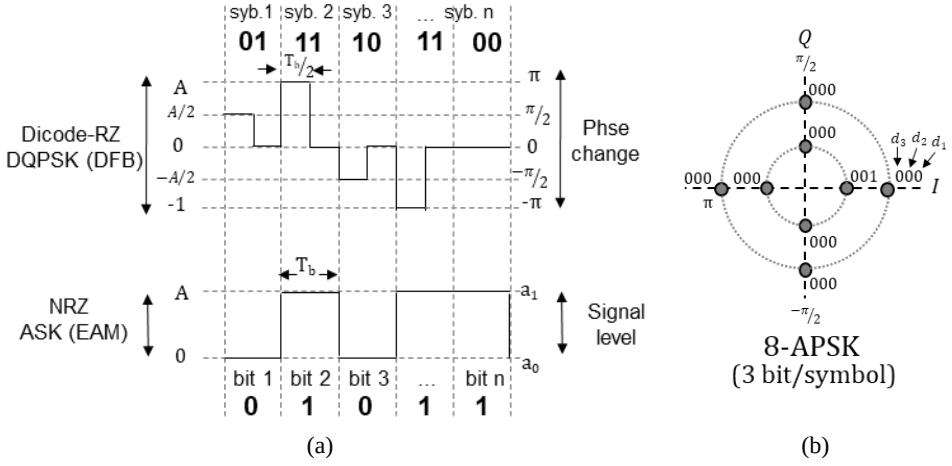

Figure 5.11. (a) Bipolar-RZ & NRZ signals for DQPSK & ASK modulation, (b) 8-APSK constellation

It is important to remember that in practical scenarios, the transmitted phase ($\phi_s(t)$) is a combination of the instantaneous phase of the data (ϕ_d) with four possible values (0, ±π/2, π), and the phase noise ($\phi_{ns}(t)$). The latter is a consequence of the random variable phase of the optical carrier.

5.3.2 Experimental validation of differential 8-APSK transmitter with intradyne coherent detection

The complete transmitter was based on the chip labeled DEML-2, with the same dimensions (DFB of 470 μm and EAM of 50 μm) that the DEML-1 used in the heterodyne 2-DPSK/2-ASK experiment, and both sections were independently modulated. For the DFB, a quaternary data was mapped into a four-level signal and differentially encoded for direct phase modulation of the laser. The symbol sequence was digitally equalized by means of a 1-tap FIR filter with high-pass response as described in chapter 3, generating a five-level bipolar-RZ signal. The equalized electrical waveform generated a phase modulated signal by differentiating the frequency variations of the directly modulated laser produced by the adiabatic chirp. This frequency deviation was proportional to the modulating current. Therefore, the phase changes of the optical signal were controlled adjusting the duty cycle and amplitude of the bipolar RZ shaped modulating waveform, as is explained in [13], [25]. The EAM was modulated with a unipolar NRZ coded binary signal as described before. Both symbol sequences were uploaded to an AWGen and digitally synchronized. The AWGen produced two electrical signals at 2.5 Gbaud, one for the DFB (Rb = 5 Gb/s) and other for the EAM (Rb = 2.5 Gb/s). The amplitude of both electrical signals was tuned with two identical 10 GHz BW electrical amplifiers and injected to the corresponding sections of the DEML. The result was an optical 8-APSK signal with four orthogonal phases (φ0(t), φ1(t), φ2(t), φ3(t)) and two possible amplitudes (a0(t), a1(t)) at R_b = 7.5 Gb/s. The setup and constellation diagram of the 8-APSK signal are shown in Figure 5.12.

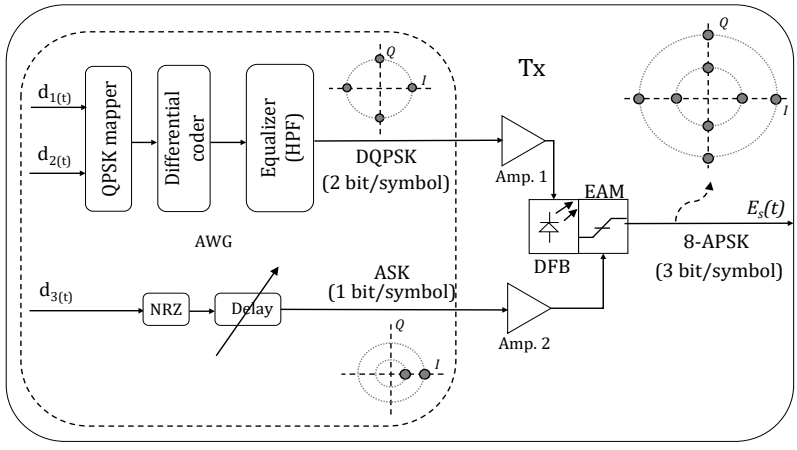

Figure 5.12. 8-APSK Tx scheme. The insets show the I-Q diagram for the DQPSK, ASK and 8-APSK transmitted optical signals.

A similar DEML as the one used in section 5.2 was used with a similar DFB wavelength was λ_{Tx} = 1556.16 nm. An external temperature control was used to keep an operative condition in the chip of 26°C. As well as for the DEML-1 unit the static characteristics of the DFB and the EAM of DEML-2 were measured. The results are plotted in Figure 5.13(a). The DFB threshold current is as low as 7 mA. The DFB was operated at bias current of 60 mA (a balance between wavelength stability, bandwidth (BW) and output power). The optical output power is limited by the modulator effective insertion loss, which results from the choice of the EAM bias point. When a static bias of -2 V was applied to the EAM section, the output power of the DEML was 0 dBm. The dynamic characteristics of the DFB and the EAM were also measured following the method described by K. Sato, et al [23]. The modulation BW of the EAM was larger than 10 GHz, however, in the current setup and due to constraints of the RF circuitry (i.e. cable lengths, bondings, and parasitic packaging effects), the effective modulation BW of the DFB was limited to 1.7 GHz as can be appreciated in Figure 5.13(b). In addition, the measured DFB linewidth was 300 KHz as can be appreciated after applying a Lorentzian fit function (see Figure 5.13(c)).

A lensed fiber was faced and properly aligned with the EAM output of the DEML. An optical isolator was fused to the lensed fiber for minimizing optical reflections. The optical output signal was sent through a 25 km single mode fiber (SMF) link. Afterwards, a variable optical attenuator (VOA) emulated the splitting losses of the passive optical network (PON) and limited the power into the Rx. A polarization controller compensated the fluctuations in the state of polarization caused by the fiber.

The Rx was based on a coherent intradyne scheme. A 3x3 optical coupler mixed the incoming signal with a local oscillator (LO). The LO was a 100 kHz linewidth external cavity laser (ECL) with 3 dBm optical power and tuned to similar Tx wavelength $\lambda_{Tx} \approx \lambda_{LO}$. The optical signals at the coupler outputs were detected with three 10 GHz p-i-n PDs followed by low-noise trans-impedance amplifiers and then low-pass filtered. The three photo-detected currents were sampled and processed by a real-time oscilloscope. Next, *I* and *Q* components of the complex signal (*c(t)*) were obtained as described in chapter 1.

Considering the intradyne scheme, and knowing that after optical mixing the angular frequency and phase differences between the received and the LO signals are defined by $\omega_{\mathrm{IF}} = \omega_{\mathrm{s}} - \omega_{\mathrm{LO}}$ and $\Delta\phi(t) = \phi_{\mathrm{s}}(t) - \phi_{\mathrm{LO}}(t)$, the complex signal results in:

$$c(t) = I(t) + jQ(t) = A_s(t)A_{LO}e^{j(\omega_{IF}t+\Delta\phi t)} = A_s(t)A_{LO}e^{j\left(\omega_{IF}t+\phi_{\mathrm{d}}(t)+\phi_{\mathrm{e}}(t)\right)} \qquad 5.1$$

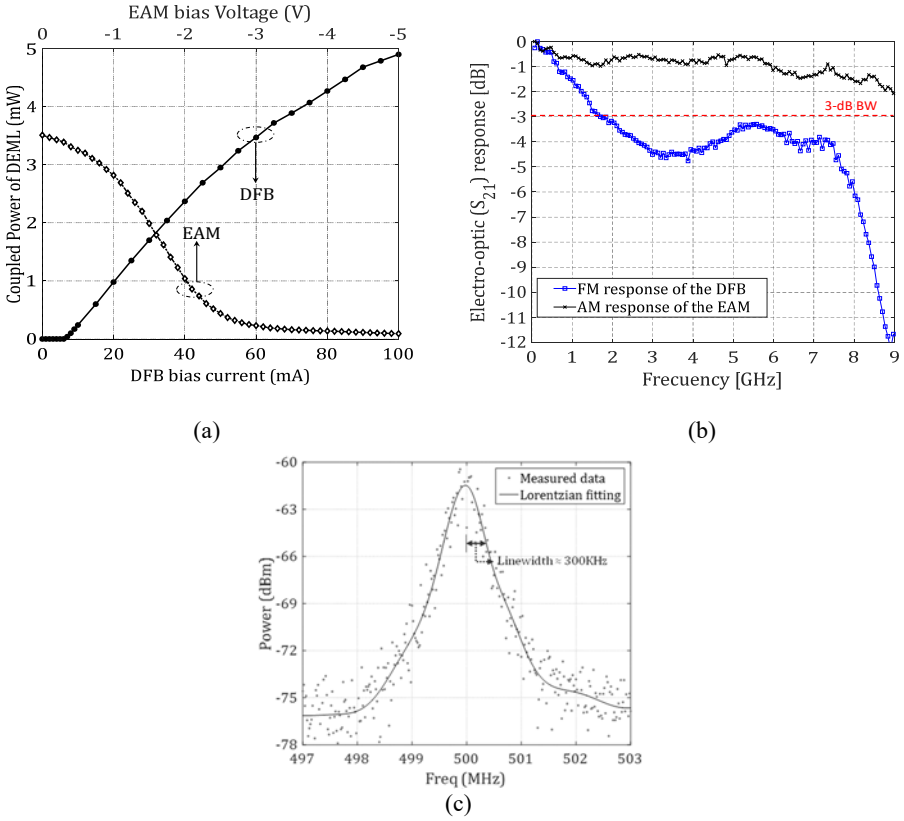

Figure 5.13. (a) Static characteristics of the DFB (V_{EAM}=0 V) and the EAM (I_{bias} DFB=60 mA), (b) Electro-optic responses of the DEML-2 considering RF constraints, (c) Measured and Lorentzian fitted linewidth of the DFB.

where $\phi_{\mathrm{e}}(t) = \phi_{\mathrm{ns}}(t) - \phi_{\mathrm{nLO}}(t)$ is the combined phase noise and $A(t) = A_s(t)A_{LO}$ the amplitude after the optical mixing.

The DQPSK and ASK signals were simultaneously demodulated. ASK demodulation was done with an envelope detector (square-root of the complex modulus) as follows:

$$A(t) = |c(t)| = \sqrt{c(t)c^*(t)} \tag{5.2}$$

The DQPSK signal was differentially demodulated by multiplying with the complex conjugate of a symbol period (T_b) delayed signal as follows:

$$P(t) = c(t)c^*(t - T_b) \tag{5.3}$$

$$P(t) = \left[A(t)e^{j(\omega_{IF}t+\phi_{\mathrm{d}}(t)+\phi_{\mathrm{e}}(t))}\right]\left[A(t-T_b)e^{-j(\omega_{IF}t-\omega_{IF}T_b+\phi_{\mathrm{d}}(t-T_b)+\phi_{\mathrm{e}}(t-T_b))}\right]$$

$$P(t) = \left[A(t)A(t-T_b)e^{j(\omega_{IF}T_b+\Delta\phi_{\mathrm{d}}(t)+\Delta\phi_{\mathrm{e}}(t))}\right] \tag{5.4}$$

with $\Delta\phi_d(t) = 0, \pm\pi/2, \pi$ are the four possible phase difference between consecutive symbols, and $\Delta\phi_e(t) = \phi_e(t) - \phi_e(t - T_b)$ is the remainder phase noise.

To cancel the amplitude component from the DQPSK signal (*P(t)*) the obtained ASK signal (*A(t)*) was multiplied by a symbol-period delay version of itself ($A(t\text{-}T_b)$), then inverted, and multiplied by the obtained DQPSK signal. Finally, the DQPSK and the ASK data were recovered by applying a low-pass filter before data decision to remove the high-frequency terms from the products. For the DQPSK data, it was necessary to apply a frequency estimation stage, since the phase modulation is highly affected for the frequency detuning [26], [27], which in this particular experiment was caused by the temperature instabilities in the chip. Frequency estimation was done by applying a differential m[th] power algorithm at the Rx [28]. The algorithm allowed to compensate the frequency detuning and eliminated the residual phase noise by averaging over an estimation block of 300 symbols.

After being recovered, the symbols were demapped and the BER computed over the three bit streams. The Rx scheme and a photo of the complete setup are depicted in Figure 5.14 and Figure 5.15, respectively

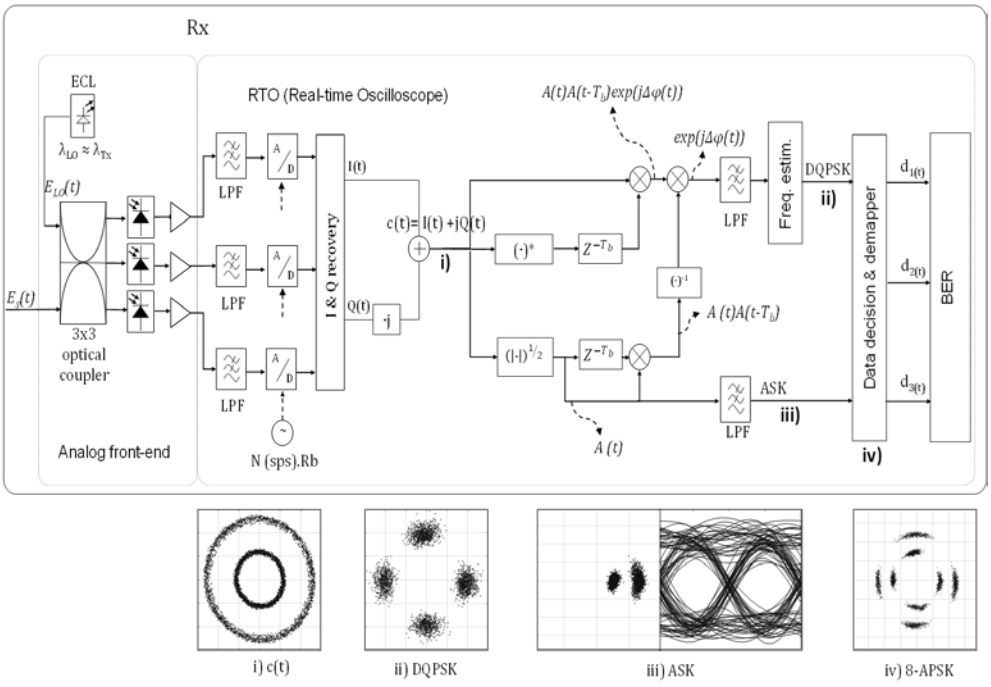

Figure 5.14. Intradyne Rx for differential 8-APSK. The insets show the constellation diagrams at each stage: i) recovered complex signal, ii) DQPSK symbols after differential demodulation and frequency estimation, iii) ASK constellation and eye diagram, and iv) recovered 8-APSK symbols

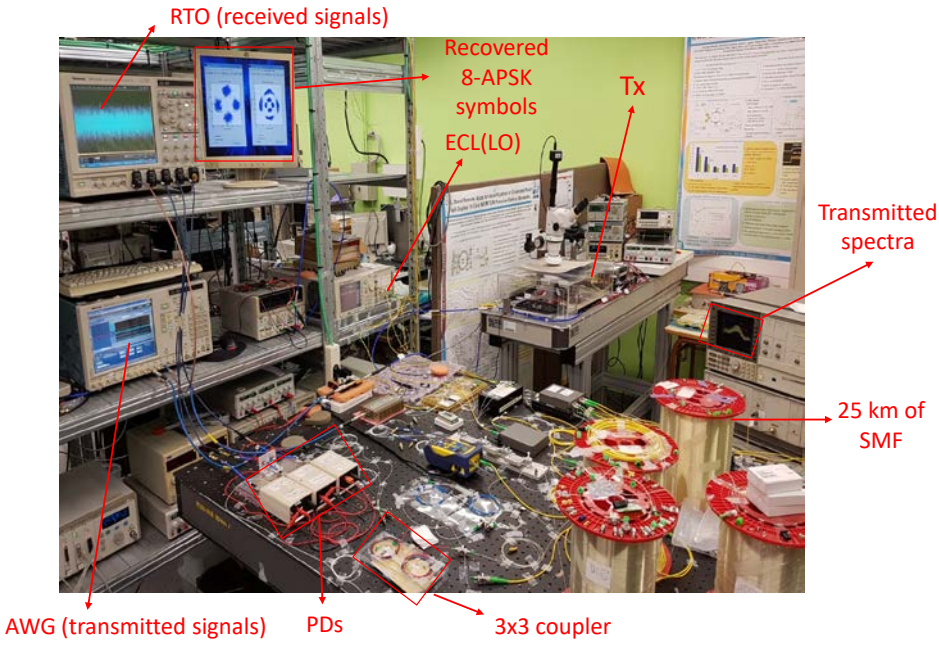

Figure 5.15. Implementation of 8-APSK at GCO laboratory.

DQPSK performance

First, the direct DQPSK modulation was tested at 1.25 Gbaud and 2.5 Gbaud. The EAM was unbiased and the DFB was phase modulated with a proper digital signal of duty-cycle = 50% and peak to peak voltages of Vpp = 0.64 V and Vpp = 1.48 V respectively. In optical back to back (btb), Rx sensitivities of -49 dBm and -46.5 dBm were achieved at second generation FEC limit of BER = $4x10^{-3}$ [13]. The results are as plotted in Figure 5.16.

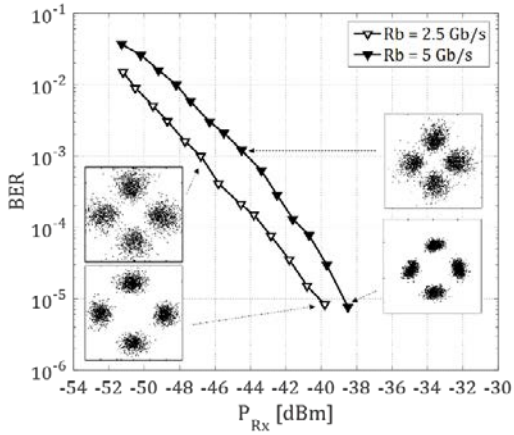

Figure 5.16. BER against Rx power for DQPSK modulation at 1.25 Gbaud (R_b = 2.5 Gb/s) and 2.5 Gbaud (R_b = 5Gb/s). The insets show the I-Q diagram of the recovered symbols at BER = 10^{-5} & 10^{-3}.

ASK performance

Afterwards, the ASK modulation was tested at the same baud rates. The EAM was biased at -2.2 V and we tested the performance for three different extinction ratio (ER) values of 2, 3.8 and 5.1 dB. The measured BER against the Rx optical power (ROP) at 1.25 Gbaud and 2.5 Gbaud are presented in the curves of Figure 5.17(a) and Figure 5.17(b) respectively. The achieved Rx sensitivities at the same FEC limit of BER=4x10^{-3} are presented in Table 5.3

Table 5.3. Rx sensitivity for ASK modulation at BER = 4x10^{-3}

	ER(dB)		
***R$_b$* (Gb/s)**	2	3.8	5.1
1.25	-46.5 dBm	-49 dBm	-51 dBm
2.5	-43 dBm	-46.5 dBm	-48.5 dBm

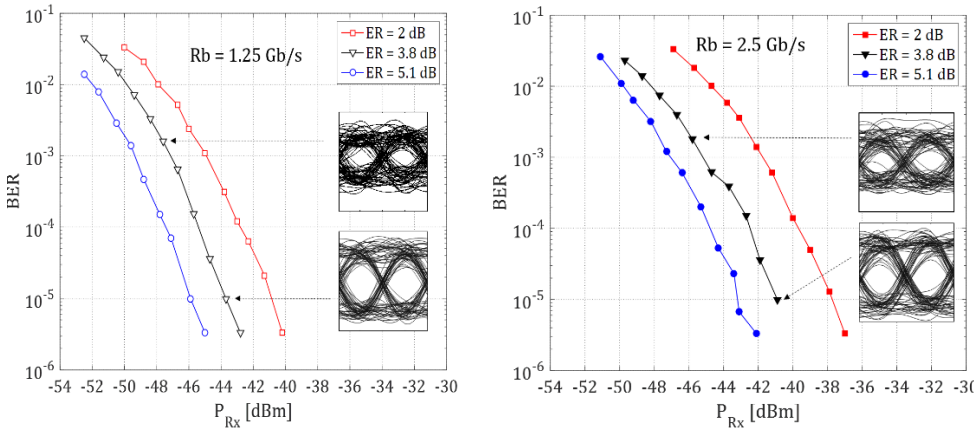

Figure 5.17. BER against Rx power for ASK modulation at: (a) 1.25 Gbaud (R_b=1.25 Gb/s) and (b) 2.5 Gbaud (R_b=2.5 Gb/s). The insets show the eye diagram at BER=10^{-5} & BER=10^{-3} for ER=3.8 dB.

Differential 8-APSK performance

Finally, DQPSK and ASK formats were combined for testing the proposed differential 8-APSK modulation. Ideally, for the DEML, it is desired to consider the laser as a pure frequency modulator and the EAM as an amplitude modulator. However, this is not the case and a strict evaluation of the devices chirp is required [19]. Therefore, a small and large signal evaluation of the DFB and EAM chirp characteristics were performed using an optical filter as frequency discriminator [23]. For the DFB laser the optical phase variation is related with the frequency chirp by [29]:

$$2\pi\Delta\upsilon(t) = \frac{d\phi(t)}{dt} = \frac{\alpha_H}{2}\left(\frac{1}{P(t)}\frac{dP(t)}{dt} + \kappa P(t)\right) \quad 5.5$$

where *P(t)* is the signal power, α_H is the linewidth enhancement factor or Henry coefficient, and κ is the adiabatic chirp coefficient. The α_H and κ parameters can be obtained from the relation between the amplitude of the IM and FM responses, both measured using a vector network analyzer, and considering that [30]:

$$\lim_{fm\to\infty} \frac{2\beta}{m} = |\alpha_H| \quad 5.6$$

where β and m are the frequency and intensity modulation indexes respectively. The α_H parameter was measured for different DFB bias currents and when the EAM was unbiased. The sign of α_H is given by the phase of the IM and FM responses ratio [30]. The results plotted in Figure 5.18, show that for the DFB, α_H was approximately equal to 2, a value that is not strongly dependent on the laser bias current. Considering the adiabatic chirp regime, a value of κ = 1.08 x 10^{13} Hz/W was obtained for a DFB bias current of 60 mA. This value is proportional to the photon density and increases with the bias current [23]. For the EAM, the optical phase variation is exclusively dependent on the transient chirp, then only the first term of Eq. 5.5 must be considered. Conversely to the DFB case, the value of α_H parameter for the EAM is strongly dependent on the applied bias voltage, ranging approximately from -1.2 to 2. This behavior is shown in Figure 5.18 for a fixed DFB bias current of 60 mA. To perform the desired PM with the DFB, the chirp inherent to EAM needs to be reduced. Hence the EAM was properly biased around the zero-chirp point observed in Figure 5.18 ($V_{EAM} \approx$ -2.2 V). In addition, the ASK modulation was optimized for an ER = 3.8 dB, because it represented the symmetric Euclidean distance among the constellation points of the 8-APSK signal.

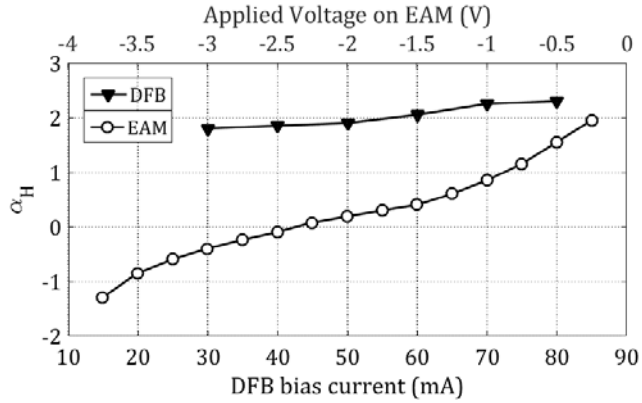

Figure 5.18. Measurements of α_H parameter for the DFB (V_{EAM}= 0 V) and the EAM ($I_{bias\ DFB}$ = 60 mA)

Next, the DFB was directly modulated in phase, and synchronously the amplitude of the optical signal was modulated with the EAM. Figure 5.19 shows the BER against the received optical power. At BER = $4x10^{-3}$ the Rx sensitivities were -45.5 dBm and -43.5 dBm at 3.75 Gb/s and 7.5 Gb/s, respectively. Notably, when transmitting through 25 km of SMF, the measured penalty was only 1 dB, and the achieved Rx sensitivity was -42. 5 dBm at 7.5 Gb/s. Under laser direct-phase modulation, the achieved results improved in approximately 4 dB the performance of similar experimental test with 8-ary modulation formats like 8–DPSK [31]. This is because the Euclidean distance between the constellation points of the 8-APSK Tx is larger than in 8-DPSK for the same mean power. Additionally, an ECL with narrower linewidth than the DFB laser used in [31] was employed in this demonstration.

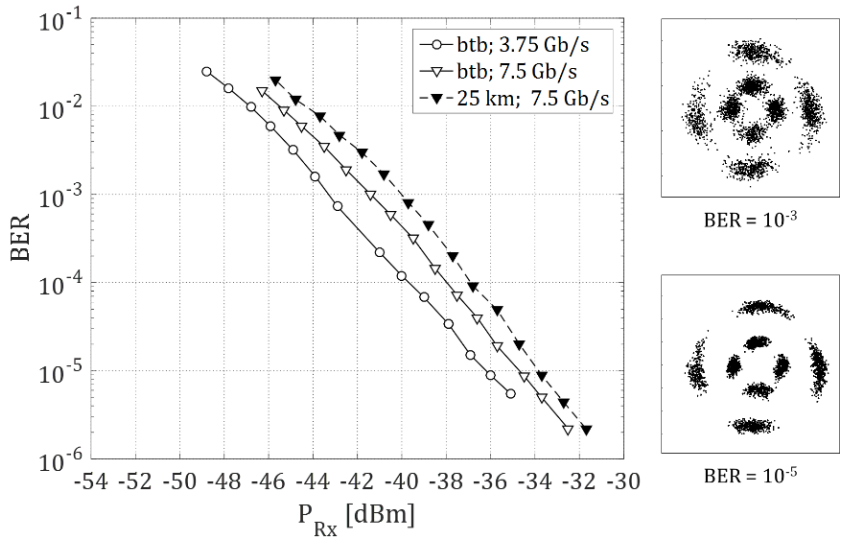

Figure 5.19. BER against Rx power for differential 8-APSK at 1.25 Gbaud/s (R_b = 3.75 Gb/s) and 2.5 Gbaud/s (R_b = 7.5Gb/s). The I-Q diagrams show the recovered symbols at BER=10^{-3} and BER=10^{-5}.

Table 5.4 summarize the obtained results at 2.5 Gbaud (maximum symbol rate) for each format, and considering a penalty of 1 dB after 25 km of SMF.

Table 5.4 Spectral efficiency for ASK, DPSK, and 8-APSK modulation formats in 6.25 GHz channel grid, and Rx sensitivity for BER = $4x10^{-3}$ after 25 km at 2.5 Gbaud.

	Modulation format		
	ASK	DPSK	8-APSK
Sensitivity @ $4x10^{-3}$	-45.5 dBm	-45.5 dBm	-42.5 dBm
Bit rate	2.5 Gb/s	5 Gb/s	7.5 Gb/s
Spectral efficiency	0.4 bit/s/Hz	0.8 bit/s/Hz	1.2 bit/s/Hz

Despite the improved performance, there are two limitations worth mentioning. First, although both devices are usually considered to be independent, they appear not to be totally uncorrelated [19]. When the EAM is modulated, the wavelength slightly fluctuates and shows drifts mainly due to temperature variations in the chip. This is because the fast amplitude transitions in the EAM affect the temperature due to the thermal heating drift in the resistor matching the EAM to 50Ω. As mentioned before, to overcome this problem, a differential m^{th} power algorithm was applied, at the Rx DSP, for frequency estimation and to compensate the frequency drifts caused by the temperature instabilities in the chip [26]. Second, an additional frequency chirp is caused by the optical feedback from the front faced (modulator site) and is dependent on the modulator bias [19], [30]. This contribution can be noted in the slight widening of the recovered symbols as shown in the I-Q diagram of Figure 5.19. To minimize the power penalty, especially at lower SNR, additional optical isolation is needed [32], as well as some degree of equalization at the Rx should be applied.

5.4 Digital pre-emphasis equalization for 10 Gb/s 8-APSK Tx

As previously seen the characterization of DEML-2, while the EAM has not BW limitation up to 10 GHz, with less than 2 dB attenuation (see Figure 5.13(b)), the DFB exhibits non-flat frequency response and severe BW limitation around ~1.7 GHz BW at 3 dB, mostly due to package parasitic effects and constraints of the RF circuitry. To mitigate the non-ideal frequency response $L(f)$ of the DFB, digital pre-emphasis (DPE) was applied as a linear filter at the Tx preceding the laser modulation. The DPE filter was designed in the frequency domain using the minimum mean square error (MMSE) criterion, similar to [33], [34].

5.4.1 Theory approach

Although the zero-forcing equalization $1/L(f)$ could cancel all linear distortions, it presents disadvantages for an effective implementation since it might over-amplify the noise greatly where the frequency response $L(f)$ is more attenuated. It might also present large peaks in the time domain signal that could lead to amplifier saturation and clipping. Instead, the DPE filter $P(f)$ calculated through the MMSE criterion would be:

$$P(f) = \frac{L^*(f)}{|L(f)|^2 + \xi_0} \qquad 5.7$$

The parameter ξ_0 is defined as in [33] and considers the PAPR of the signal and the quantization noise variance of the DAC.

5.4.2 Experimental validation and results

The experimental setup is the same as shown in Figure 5.15. The complete Tx assembled the aforementioned DEML, whose two sections (DFB and EAM) were independently modulated as explained in last section. For the DFB, the differentially encoded symbol sequence passed through the DPE according to Eq. 5.7, implemented as a linear FIR filter with real-valued T/2-spaced taps, being T the symbol time, to compensate for the following non-ideal FM response of the DFB. Next, a RZ pulse-shaping filter with 50% duty-cycle properly adapted the signal for direct phase modulation leveraging the frequency chirp of the DFB [10]. The digital symbol sequence was generated at 2 samples per symbol and converted into the analogue domain by a 6.25 GSa/s DAC with 8-bit nominal resolution, which limited the modulated symbol rate to 3.125 GBd.

Then the BER of the three modulation formats (ASK, DPSK and 8-APSK) generated by the DEML at 3.125 GBd was evaluated separately. The results plotted in Figure 5.20(a)show that for FEC threshold of BER = 10^{-3} the 8-APSK, that provides the highest data rate (9.375 Gb/s), achieves a sensitivity of -36 dBm, improving by 8 dB the required sensitivity of the standardized 10 Gb/s NG-PON2 IM-DD transceivers [5]. The sensitivities of the individual DQPSK and ASK separately were 3 and 6 dB better, respectively, but at lower data rates.

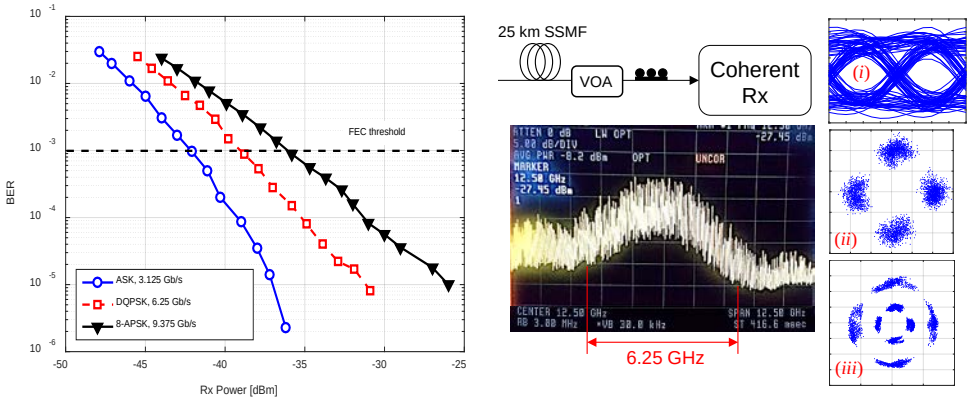

Figure 5.20. (a) BER vs. received power for the DEML at 3.125 GBd symbol rate. (b) RF photodetected spectrum for 8-APSK at 3.125 GBd, centred at 12.5 GHz intermediate frequency. The insets show the three modulation formats generated by the DEML: (i) ASK, (ii) DQPSK, (iii) 8-APSK.

In addition, the received heterodyning RF spectrum for 8-APSK at 3.125 GBd (Figure 5.20(b)) presents a spectral width below 6.25 GHz and suggests a feasible optical grid of 12.5 GHz spacing between 10 Gb/s dedicated wavelength channels. Moreover, Figure 5.20(b) shows the ASK eye diagram for BER = 10^{-5} and the constellation of DQPSK and 8-APSK signals.

The constellations in Figure 5.21(a) illustrate the benefit of DPE for the PM data at 3.125 GBd when the received power was set to -35 dBm and -31 dBm for DQPSK and 8-APSK, respectively. In both cases, the constellations without DPE are highly distorted, whereas after 16-tap DPE they are recovered with BER = 10^{-4}. Finally, Figure 5.21(b) shows the performance of the DPE when varying the number of filter taps. The results, in terms of the power penalty at BER = 10^{-4}, indicate that at 1 dB maximum penalty a DPE with only 12 taps is needed to transmit 10 Gb/s using the DEML. As expected, DQPSK and 8-APSK require the same number of DPE taps since the AM response of the EAM does not have any BW limitation at the tested symbol rate and makes no substantial impact on the DQPSK at the selected EAM bias. However, it is worth noting the phase-widening of the constellation points for 8-APSK compared to that of DQPSK where the EAM is off, due to the increment of the spectral linewidth along with the residual chirp of the EAM.

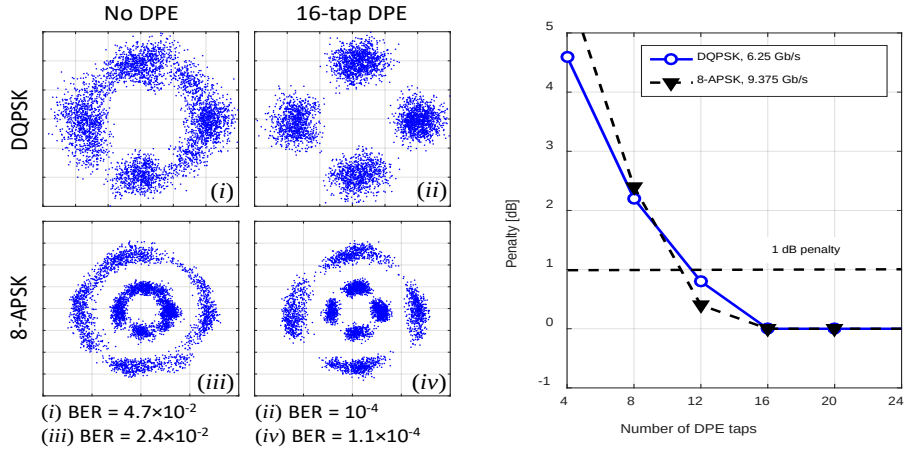

Figure 5.21. With 3.125 Gbaud symbol rate: (a) constellation diagrams with/without DPE for DQPSK and 8-APSK, (b) power penalty at BER = 10^{-4} vs. number of DPE filter taps.

Therefore, the band-limited electro-optical response of the commercial low-cost devices can be effectively mitigated by linear DPE filtering, enabling high-data rate coherent optical

access. It can be dimensioned and compared with the WDM solution for NG-PON2, as summarized in Table 5.5.

Table 5.5 10G PON dimensioning and comparison

	Sensitivity [dBm]	**Channel spacing [GHz]**	**Number channels**	**Aggregated PON capacity [Gb/s]**
-APSK (Coherent)	-36	12.5	32	320
NG-PON2 (IM-DD)	-28	50	8	80

The NG-PON2 allocates up to 8 channels separated by a minimum of 50 GHz, achieving an aggregated PON capacity of 80 Gb/s in an optical band of 400 GHz. In contrast, the proposed 8-APSK coherent ultra-dense WDM solution can allocate up to 32 channels separated by 12.5 GHz, within the same optical spectrum; this implies an aggregated PON capacity of 320 Gb/s, i.e., four-times the capacity of NG-PON2 without increasing the optical and the electrical BW requirements. Besides, the 8 dB enhanced Rx sensitivity also improves the available power budget allowing for either, additional splitting ratio or extended fiber reach.

5.5 Chapter summary

In this chapter three novel proposals of low-cost transceivers for coherent WDM-PONs were introduced and experimentally demonstrated. The main idea was to combine different modulation formats to increase the bit rate, the SE, and the Rx sensitivity.

First, two different modulation formats like ASK and DPSK were interleaved in time (TDHF) to modulate a low-cost commercial DFB laser. The first portion of the bit period was used to produce the phase shifts of 0 or π, and then the unoccupied part could transmit additional information, in this case using ASK modulation. Hence an alternate DPSK/ASK optical signal was transmitted. The sequence was detected with an heterodyne balanced coherent receiver. With this scheme and after 25 km of SMF, an Rx sensitivity of -44 dBm at BER = $4x10^{-3}$ for R_b of 2.5 Gb/s was obtained. Compared to pure ASK, the performance was 2 dB better for the same R_b. This simple technique can add flexibility to the Tx and gives the possibility for operators to offer differentiated services in a future optical access network.

Second, a novel application for a small-footprint integrated DEML with low energy consumption, was proposed and experimentally demonstrated by modulating both sections with independent electrical signals. The DFB section was directly modulated in phase producing a DPSK signal and the EAM was modulated in amplitude generating an ASK signal, both at 2.5 Gb/s. As a result, an optical signal at R_b of 5 Gb/s was transmitted achieving an Rx sensitivity of -40 dBm at BER=10^{-3}, in a 25 km SMF link with a heterodyne reception. This system is able to tolerate LO frequency drifts of ±50 MHz with <1 dB of penalty. These results show that the proposed DEML can be employed as Tx in low-cost coherent ONU employing simultaneous phase and amplitude modulated signals.

Finally, and for the first time, a simple external-modulator-free differential 8-APSK Tx using the aforementioned DEML was experimentally demonstrated. The transmitted optical signal uses both the amplitude and phase of the optical signal to improve the spectral efficiency compared to the 4-ary case (2-DPSK/2-ASK), and was detected with an intradyne coherent Rx. Compared with the conventional ASK or DQPSK modulation, the spectral efficiency increases by 3-times and 2-times, respectively, achieving a Rx sensitivity of -42.5 dBm at 7.5 Gb/s and channel spacing of 6.25 GHz.

Despite these outstanding results, and due to setup constraints with the RF circuitry, the modulation BW of the DFB was limited to 1.7 GHz. To mitigate this problem, a linear DPE filtering was applied at the Tx, enabling 10 Gb/s data rate coherent optical access. These results show the feasibility for a simple, small footprint and low-cost Tx, able to support flexible transmission capacity, and to compete with NG-PON2 standard.

Bibliography Chapter 5

[1] M. Nekovee, Y. Wang, M. Tesanovic, S. Wu, Y. Qi, and M. Al-Imari, "Overview of 5G modulation and waveforms candidates," *J. Commun. Inf. Netw.*, vol. 1, no. 1, pp. 44–60, Mar. 2016.

[2] Y. Cai, Z. Qin, F. Cui, G. Y. Li, and J. A. McCann, "Modulation and Multiple Access for 5G Networks," *IEEE Commun. Surv. Tutor.*, vol. 20, no. 1, pp. 629–646, 2018.

[3] W. Shieh and I. Djordjevic, *Orthogonal Frequency Division Multiplexing for Optical Communications*. USA: Elsevier Inc, 2010.

[4] J. Armstrong, "OFDM for Optical Communications," *J. Light. Technol.*, vol. 27, no. 3, pp. 189–204, Feb. 2009.

[5] A. Barbieri, G. Colavolpe, T. Foggi, E. Forestieri, and G. Prati, "OFDM versus Single-Carrier Transmission for 100 Gbps Optical Communication," *J. Light. Technol.*, vol. 28, no. 17, pp. 2537–2551, Sep. 2010.

[6] G. Bosco, "Advanced Modulation Techniques for Flexible Optical Transceivers: The Rate/Reach Tradeoff," *J. Light. Technol.*, vol. 37, no. 1, pp. 36–49, Jan. 2019.

[7] W. Peng, I. Morita, and H. Tanaka, "Hybrid QAM transmission techniques for single-carrier ultra-dense WDM systems," in *16th Opto-Electronics and Communications Conference*, Kaohsiung, Taiwan, 2011.

[8] Q. Zhuge, M. Morsy-Osman, X. Xu, M. Chagnon, and D. V. Plant, "Spectral Efficiency-Adaptive Optical Transmission Using Time Domain Hybrid QAM for Agile Optical Networks," *J. Light. Technol.*, vol. 31, no. 15, pp. 2621–2628, Aug. 2013.

[9] J. C. Velásquez, M. Domingo, V. Polo, and J. Prat, "Time Interleaved DPSK/ASK Transmitter with Directly Beat Modulated DFB for Coherent WDM-PON," in *Proc. 44th Eur. Conf. on Opt. Commu. (ECOC)*, Rome, Italy, 2018.

[10] J. C. Velásquez, M. Domingo, V. Polo, and J. Prat, "Simultaneous DPSK-ASK Modulated Dual-EML Transmitter for Coherent UDWDM-PON," in *Proc. Opt. Fiber Commun. Conf. (OFC)*, San Diego, CA, USA, 2018.

[11] J. Camilo Velásquez, Jeison Tabares, and Josep Prat, "Differential 8-APSK monolithically integrated dual-EML transmitter for flexible coherent PONs," *Opt. Lett.*, Posted on April 30, in press.

[12] Jeison Tabares, J. Camilo Velásquez, Antonio Napoli, and Josep Prat, "direct amplitude-phase modulated dual-eml 10 gb/s optical transmitter," in *Proc. 45th Eur. Conf. on Opt. Commu. (ECOC)*, Dublin, Ireland., Submitted.

[13] J. C. Velasquez, I. N. Cano, V. Polo, M. Domingo, and J. Prat, "15-dB Differential Link-Loss UDWDM-PON With Direct Beat Phase Modulated DFBs," *IEEE Photonics Technol. Lett.*, vol. 30, no. 2, pp. 137–140, Jan. 2018.

[14] I. N. Cano, A. Lerín, V. Polo, and J. Prat, "Simplified Polarization Diversity Heterodyne Receiver for 1.25Gb/s Cost-Effective udWDM-PON," in *Proc. Opt. Fiber Commun. Conf. (OFC)*, San Francisco, CA, USA, 2014.

[15] T. Mizuochi *et al.*, "Next generation FEC for optical transmission systems," in *Proc. Opt. Fiber Commun. Conf. (OFC)*, Atlanta, GA, USA, 2003.

[16] International Telecommunication Union, "ITU-T G.1010 Recommendation, End-user multimedia QoS categories." Nov-2001.

[17] C. Kazmierski, D. Carrara, K. Ławniczuk, G. Aubin, J. Provost, and R. Guillamet, "12.5GB operation of a novel monolithic 1.55µm BPSK source based on prefixed optical phase switching," in *Proc. Opt. Fiber Commun. Conf. (OFC)*, Anaheim, CA, USA, 2013.

[18] C. Kazmierski, "Electro-Absorption-Based Fast Photonic Integrated Circuit Sources for Next Network Capacity Scaling [Invited]," *J. Opt. Commun. Netw.*, vol. 4, no. 9, pp. A8–A16, Sep. 2012.
[19] D. Erasme *et al.*, "The Dual-Electroabsorption Modulated Laser, a Flexible Solution for Amplified and Dispersion Uncompensated Networks Over Standard Fiber," *J. Light. Technol.*, vol. 32, no. 21, pp. 4068–4078, Nov. 2014.
[20] G. Y. Chu, I. Cano, V. Polo, and J. Prat, "Application on Minimizing Residual AM in DPSK UDWDM-PON ONU by Integrated Dual-EML," *IEEE Photonics J.*, vol. 8, no. 3, pp. 1–7, Jun. 2016.
[21] G. Y. Chu, I. N. Cano, V. Polo, C. Kazmierski, R. Brenot, and J. Prat, "Monolithically Integrated Dual-Output DEML for Full Duplex DPSK-ASK and DPSK-SSB ONU in Ultra-Dense Channel Spaced Access Network," *J. Light. Technol.*, vol. 34, no. 8, pp. 2042–2048, Apr. 2016.
[22] "COst-effective COhereNt Ultra-dense-WDM-PON for lamda-To-the-user access." [Online]. Available: http://www.ict-coconut.eu.
[23] K. Sato, S. Kuwahara, and Y. Miyamoto, "Chirp characteristics of 40-gb/s directly Modulated distributed-feedback laser diodes," *J. Light. Technol.*, vol. 23, no. 11, pp. 3790–3797, Nov. 2005.
[24] I. N. Cano, A. Lerin, V. Polo, and J. Prat, "Direct Phase Modulation DFBs for Cost-Effective ONU Transmitter in udWDM PONs," *IEEE Photonics Technol. Lett.*, vol. 26, no. 10, pp. 973–975, May 2014.
[25] J. C. Velásquez, I. N. Cano, V. Polo, and J. Prat, "Direct beat phase modulated DFB for flexible 1.25–5 Gb/s coherent UDWDM-PONs," in *Proc. Opt. Fiber Commun. Conf. (OFC)*, Los Angeles, CA, USA, 2017.
[26] J. Tabares, S. Ghasemi, V. Polo, and J. Prat, "Simplified Carrier Recovery for Intradyne Optical PSK Receivers in udWDM-PON," *J. Light. Technol.*, vol. 36, no. 14, pp. 2941–2947, Jul. 2018.
[27] J. Tabares, V. Polo, I. Cano, and J. Prat, "Automatic $\lambda $ -Control With Offset Compensation in DFB Intradyne Receiver for udWDM-PON," *IEEE Photonics Technol. Lett.*, vol. 27, no. 4, pp. 443–446, Feb. 2015.
[28] S. Tsukamoto, K. Katoh, and K. Kikuchi, "Coherent demodulation of optical multilevel phase-shift-keying signals using homodyne detection and digital signal processing," *IEEE Photonics Technol. Lett.*, vol. 18, no. 10, pp. 1131–1133, May 2006.
[29] D. Che, Q. Hu, F. Yuan, Q. Yang, and W. Shieh, "Enabling Complex Modulation of Directly Modulated Signals Using Laser Frequency Chirp," *IEEE Photonics Technol. Lett.*, vol. 27, no. 22, pp. 2407–2410, Nov. 2015.
[30] P. Brosson and H. Bissessur, "Analytical expressions for the FM and AM responses of an integrated laser-modulator," *IEEE J. Sel. Top. Quantum Electron.*, vol. 2, no. 2, pp. 336–340, Jun. 1996.
[31] I. N. Cano, J. C. Velásquez, and J. Prat, "7.5 Gb/s direct DFB phase modulation with 8-DPSK for 6.25 GHz spaced coherent UDWDM-PONs," in *Proc. Opt. Fiber Commun. Conf. (OFC)*, Anaheim, CA, USA, 2016.
[32] Ning Hua Zhu *et al.*, "Electrical and Optical Coupling in an Electroabsorption Modulator Integrated With a DFB Laser," *IEEE J. Quantum Electron.*, vol. 43, no. 7, pp. 535–544, Jul. 2007.
[33] A. Napoli *et al.*, "Digital Compensation of Bandwidth Limitations for High-Speed DACs and ADCs," *J. Light. Technol.*, vol. 34, no. 13, pp. 3053–3064, Jul. 2016.
[34] J. Tabares *et al.*, "Digital Pre-emphasis for 10Gb/s with Low-cost Directly Phase-Modulated Lasers for PONs," in *Advanced Photonics 2018 (BGPP, IPR, NP, NOMA, Sensors, Networks, SPPCom, SOF)*, Zurich, 2018, p. SpTh3G.2.

Chapter 6 . Simplified ONU/OLT architectures for coherent UDWDM-PONs

Conventional coherent receivers offer an improved sensitivity compared with legacy PONs based on IM/DD systems[1], allowing to support long-haul links with higher losses, by increasing the power budget [2]. Typically, these links provide high-speed (>100 Gb/s/λ) connections through long distances (>100 km), including transoceanic communications by using submarine optical fiber cables [3], [4]. However, in residential scenarios, where such high-speeds per user seems not to be necessary, and short distances (< 30 km) are installed [5], [6], the most important challenge seems to be the scalability to dense urban areas with huge number of users, and in consequence the associate cost constrain [7], [8]. This has motivated the research for alternatives to conventional coherent Rx and modulation techniques that enable the deployment of splitter-based UDWM-PONs as an alternative to provide high aggregated capacities, dedicated WTTU, and compatibility with legacy systems. In this context, several solutions have already been demonstrated to support 1 Gb/s per subscriber in a 6.25 GHz grid [9], [10]. However, as a future step, and in order to provide data rates for future radio solutions, the user bit rate should be extended at least to 10 Gb/s [11] while keeping an affordable cost.

Following these ideas and understanding that the ONU is a cost sensitive component for making coherent UDWDM-PONs commercially attractive, in this chapter, two different proposals are presented to simplify the ONU and then to reduce its cost. First, a direct modulated DFB laser is proposed to be used as Tx and at the same time as LO. This proposal is demonstrated in a bidirectional PON and the results were published in [12]. On the other hand, and to be compatible with NG-PON2[13], a 10 Gb/s TRx is proposed, performing a phase-time diversity scheme through a directly phase modulated laser as Tx, and

implementing a novel polarization insensitive intradyne coherent Rx involving only 2 photodiodes (PD). The results of this proposal were published in [14].

6.1 Conventional coherent TRx

In a conventional coherent TRx, a light source (typically a laser diode) is accompanied by complex and high cost external modulators composing the Tx [15], [16]. On the other side, the Rx employs both phase and polarization diversity schemes to process separately each polarization component, and to be able to tolerate wider laser linewidth and large polarization fluctuations [17], [18]. As well, they require a second light source in CW mode, acting only as LO to be beaten with the incoming optical data signal. To provide phase and full polarization diversity the traditional optical coherent front-end is built with a pair of 90º hybrid and 4 pair of balanced PD per each polarization component. Additionally, a PBS is used before optical mixing for split the polarization states in two orthogonal components, horizontal (H) and vertical (V). This architecture implies duplicate the photodetection branches, one for the I and the other for the Q components, and then up to 8 PD are needed. A scheme of a typical coherent Tx based on two I-Q modulators, and the optical front-end of the conventional coherent Rx are depicted in Figure 6.1(a) and Figure 6.1(b) respectively.

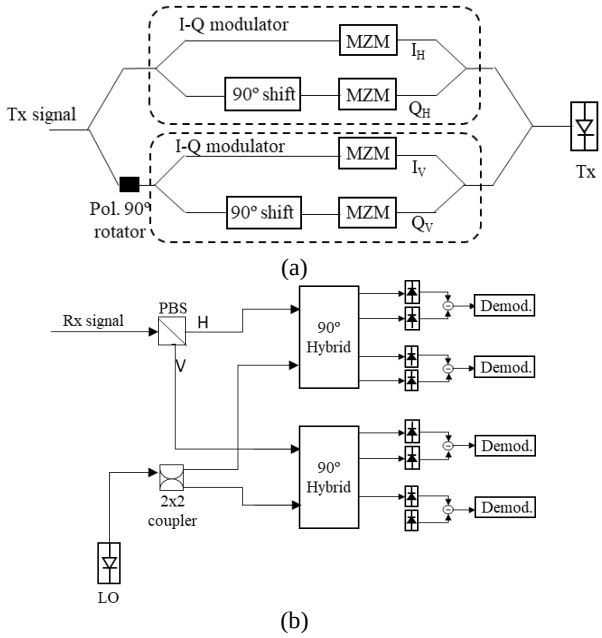

Figure 6.1. Conventional coherent TRx: (a) Tx, (b) Rx.

6.2 Bidirectional coherent PON with ONU based reused direct modulated LO

As mentioned, one of the elements that adds cost to the coherent TRx is the second light source acting as LO which must be added for beating with the incoming signal. Hence, reusing the transmitted signal from the direct modulated DFB laser could simplify the coherent ONU. An idea based on this principle was proposed in [7] where continuous phase frequency shift keying (CPFSK) direct modulated-DFB has been used. As an alternative, the feasibility of using a DPSK direct-modulated DFB laser as LO at ONU was experimentally investigated in [12], and the results will be discussed below.

6.2.1 Experimental setup

The proposed bidirectional architecture was based on ASK/DPSK transmitters. Two identical DFB lasers (nominal λ = 1550 nm) were used at OLT (DFB-1) and at ONU (DFB-2 with an IF of 5 GHz, set by thermal tuning. The DS signal was generated by externally modulating DFB-1 through a LiNbO3 MZM, driven by a PRBS (2^{15}-1 bits long). The MZM was biased at the quadrature point producing an intensity modulated optical signal. For US a DPSK signal was generated by directly modulating a DFB as described in [19]. The US data was differentially coded and modulated a pre-equalized DFB laser (DFB-2). Both DS/US transmitters were operated at 1.25 Gb/s. The ODN consisted of a 50 km of SMF followed by a VOA to emulate a power splitting stage.

The OLT and ONU receivers were based on heterodyne detection (IF = 5 GHz); such detuning leaded to a Rayleigh back-scattering contribution out of the received signal bandwidth and then its effect was minimized. A 3dB coupler mixed the received signal with the LO. Direct-modulated DFB-2 was split and used as LO in the ONU whereas DFB-1 was divided before the MZM and employed as LO in the OLT. A polarization controller was used to compensate the SOP fluctuations of the signal in the fiber. A scheme with a single PD per polarization can be used to avoid the polarization controller [20]. Two 10 GHz p-i-n PDs detected the signal and their electrical photo-currents were amplified, sampled and processed with a 50 GSa/s RTO. The samples were first filtered with a 5 GHz BW band-pass filter centered at 5 GHz. In the ONU the samples were processed with an envelope detection block whereas at the OLT a differential demodulation scheme (delay-and-multiply operation) was implemented. Before

bit decision, signals were low-pass filtered at cutoff frequency of 1 GHz. Lastly, BER was computed over 2^{18} bits. The proposed PON architecture is depicted in Figure 6.2.

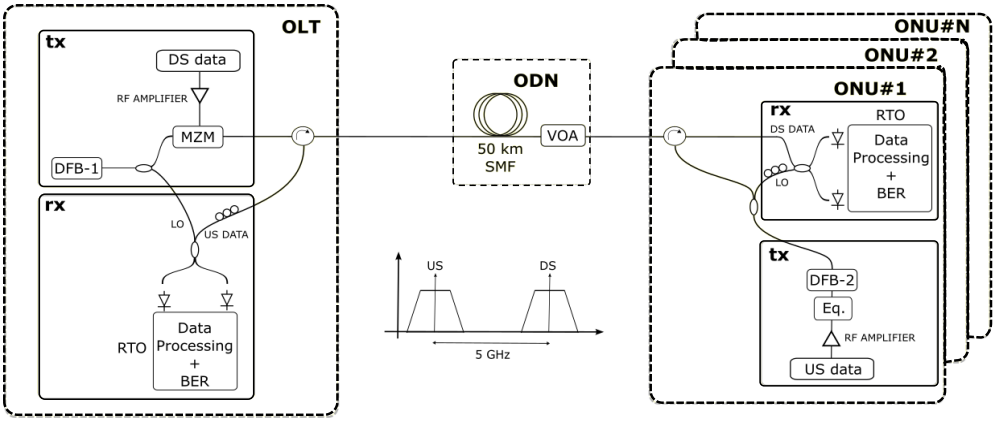

Figure 6.2. Experimental setup. The inset show the spectral separation between US and DS signals.

6.2.2 Results and discussion

First, the optical btb DS operation was tested. The performance with CW-LO and then with the DFB-2 used as LO were measured for comparison. The results are plotted in Figure 6.3(a) as well as the CW-LO (Figure 6.3(b)) and DPSK direct modulated (DM) LO (Figure 6.3(c)) electrical spectra. When using the LO as CW a sensitivity of approximately -48 dBm was obtained; with DM-LO a penalty of almost 5 dB can be observed. This high penalty was caused by the intermodulation products between the received signal and residual IM term produced when directly modulating DFB-2.

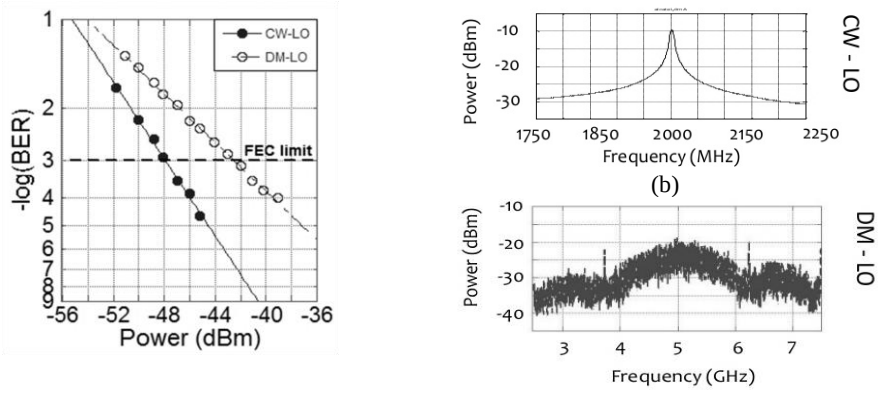

Figure 6.3. (a) DS performance CM-LO vs DM-LO, electrical spectra (b) CW-LO, (c) DPSK DM-LO

In this context, the effect of changing the signal voltage amplitude on the DPSK spectrum was studied. A direct consequence was that the residual IM noise was reduced. As well, reducing the amplitude of the driving voltage leads to a residual carrier in the DPSK spectrum. To measure the effect in the performance, the parameter residual carrier to signal ratio (RCSR) was defined as the difference, in dB, between the power of the residual optical carrier and the average power of the DPSK spectrum. Increasing the RCSR value improves the DS performance (Figure 6.4(a)); namely the penalty, with respect to CW-LO, was reduced from 5 dB (RCSR = 0 dB) to around 2 dB (RCSR = 5 dB). However, the US performance (Figure 6.4(b)) is degraded since the power taken by the residual carrier does not carry any information and might be detected as noise in the OLT coherent Rx. The electrical spectra for RCSR = 0 dB and RCSR = 5 dB are shown in Figure 6.4(d) and Figure 6.4(e) respectively. Therefore, the optimum RCSR value to find an acceptable trade-off between DS/US performance was investigated. Results indicate that RCSR = 5 dB is a good compromise to achieve -46/-48 dBm as DS/US sensitivity at BER = 10^{-3}. Results are shown in Figure 6.4(c), for DS and US transmission over 50 km SMF. The penalty with respect to optical btb was <1 dB. When the IF was reduced to 3.75 GHz; the penalty increased in 1.5 dB with respect to IF = 5 GHz. In order to improve the SE, a pulse shaping technique can be potentially used, similar to Nyquist shaping proposed in chapter 3. A summary of the results is show in Table 6.1.

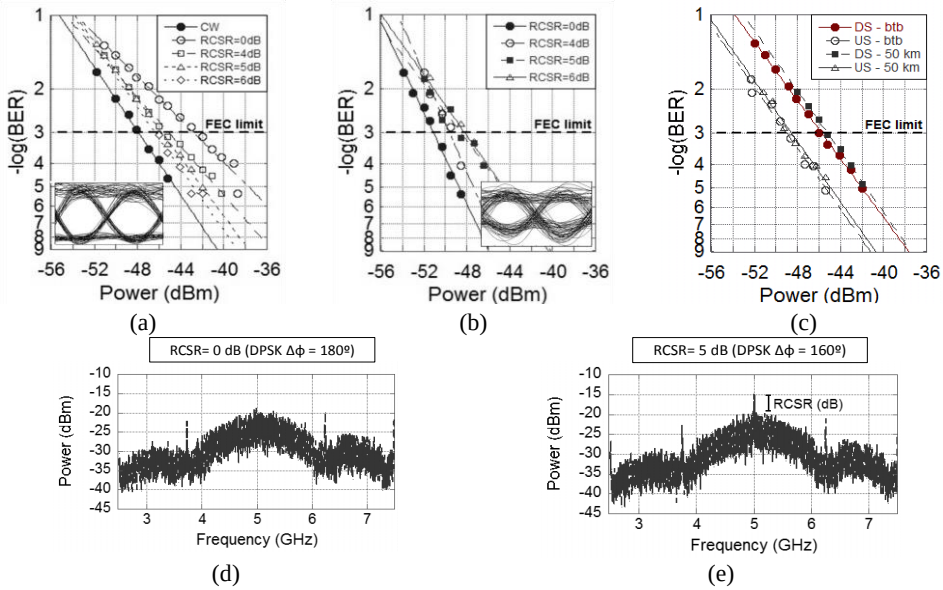

Figure 6.4. System performance in (a) btb DS, in the inset eye-diagram for RCSR = 5 dB at -42 dBm, (b) btb US, in the inset eye-diagram for RCSR = 5 dB at -46 dBm, (c) 50 km transmission performance at optimized RCSR, i.e. 5 dB, (d) and (e) electrical spectra DPSK DM-LO with RCSR = 0 dB and RCSR = 5 dB, respectively.

Table 6.1. Rx sensitivity at BER=10^{-3} after 50 km at 1.25 Gb/s with reused LO and IF=5 GHz

Link	RCSR = 0 dB	RCSR = 5 dB
DS	-43 dBm	-46 dBm
US	-51 dBm	-48 dBm

The proposed architecture can be advantageous for high-power budget next-generation access networks based on WTTU approach, where many WDM 1.25 Gb/s channels are employed. Considering for example 64x1.25 Gb/s channels (+0 dBm/ch), first combined by a power combiner (insertion loss around 18 dB for 64 channels) and then mapped to single AWG ports (insertion loss around 5 dB) and assuming on the receiver side a sensitivity at BER=10^{-3} around -46 dBm (DS), there would be about 23 dB left of loss budget, without the need of optical amplification at the OLT or along the ODN.

6.3 Phase Time Diversity Directly Modulated DFB with Single-PD Intradyne Receiver

Recently, I. Cano et.al [21] demonstrated a novel intradyne Rx with centralized phase time diversity and low-cost direct phase modulation (PM) Tx operating at 2.5 Gb/s. In that work the idea was to produce a PM with alternated orthogonal phases in consecutive bits, i.e alternating I and Q components at the OLT. In the ONU, the coherent Rx was reduced to a 3dB coupler and two photodiodes (PD), with each one detecting separate polarization component as in [20]. With this scheme, the number of photodetection branches are reduced by half in a single polarization Rx scheme, compared with the conventional coherent Rx explained in section 6.1, maintaining polarization independence, and reducing its complexity and cost. As extension of that work, a 10 Gb/s phase scrambled directly modulated laser detected with a polarization insensitive intradyne coherent Rx is proposed to keep compatibility with NG-PON2 systems, and even more without the need for optical filters.

6.3.1 Phase-time diversity Tx and signal generation

To generate a DPSK signal with phase-time diversity, two independent RZ sequences consisting of 2^{18} bits each must be independently generated and differentially encoded. One of them is a unipolar RZ stream (lower branch of Figure 6.5(a)), delayed by half the bit period,

and amplified to twice its amplitude. Both data streams are added producing an interleaved sequence with four levels. Two values corresponded to the odd bits (±A) whereas the other two (0, 2A) corresponds to even bits, as is shown in Figure 6.5(b). The data waveform was then electrically amplified and equalized to directly modulate the phase of a DFB laser by deriving the frequency variations produced by the adiabatic chirp with a simple RC network [19]. As a result, a DPSK signal was generated with odd bits corresponding to 0º and 180º phases, whereas even bits corresponded to another DPSK signal corresponding to 90º and 270º phases, i.e., the constellation is shifted by 90º at each half symbol, and the optical signal had phase diversity in time, alternating the I and Q components in consecutive bits. The complete scheme of the Tx and the evolution of the electrical signal at each stage are depicted in Figure 6.5(a) and Figure 6.5(b) respectively.

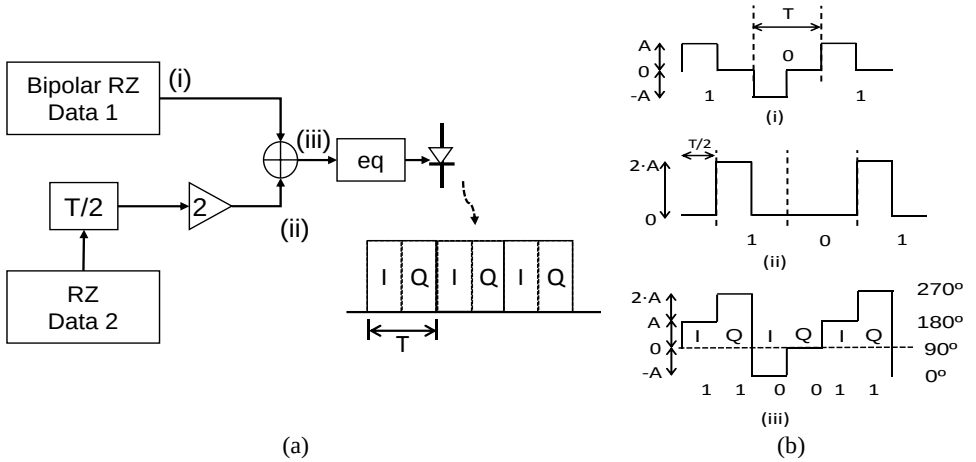

Figure 6.5. (a) Phase-time diversity Tx, (b) electrical sequences: i) bipolar RZ (I), ii) unipolar RZ (Q), and iii) phase-scrambled sequence (I-Q).

6.3.2 Experimental setup and simplified intradyne Rx

Two 5 Gb/s RZ sequences consisting of 2^{18} bits each were independently generated, encoded and equalized as explained before, to produce an optical signal with phase diversity in time, alternating the I and Q components in consecutive bits, and doubling the transmission speed to 10 Gb/s. A DFB laser emitted at λ_1=1545.4 nm and had 10 GHz modulation BW and 4 MHz linewidth. A second Tx (Tx_2) based on External Modulation (EM) was added to emulate an UDWDM-PON. For Tx_2, an independent electrical signal was generated, amplified and used to modulate another DFB laser by means of a 10 GHz BW phase modulator. The Tx_2 wavelength was tuned to λ_2 = 1545.8 nm. The two optical signals were joined through a 3-dB

optical coupler. The total launched optical signal had 0 dBm of power and was sent through 25 km of SMF. A VOA was used to reproduce splitting losses and limit the power into the Rx.

The Rx consisted of an 80:20 optical coupler which mixed the optical data signal with a LO. The latter was a 1 MHz linewidth DFB whose wavelength was tuned in temperature to emit very close to λ_1 (~±100 MHz difference). The LO power was 3 dBm. A PBS divided the mixed optical signal in two orthogonal polarization components, both detected with a 10 GHz p-i-n- PDs followed by low-noise electrical amplifiers. The electrical signals were sampled with a 50 GSa/s RTO and processed in pseudo-real-time. After synchronization, the polarization samples were added, and low-pass filtered. A bit-delay and multiply operation demodulated the signal which then passed through a 4th order low-pass electrical filter with cut-off frequency of 8 GHz. The samples were divided in half bit periods to separate the I and Q components. Finally, the BER considering both I and Q data was computed by deciding on the middle sample. A scheme of the tested PON is shown in Figure 6.6.

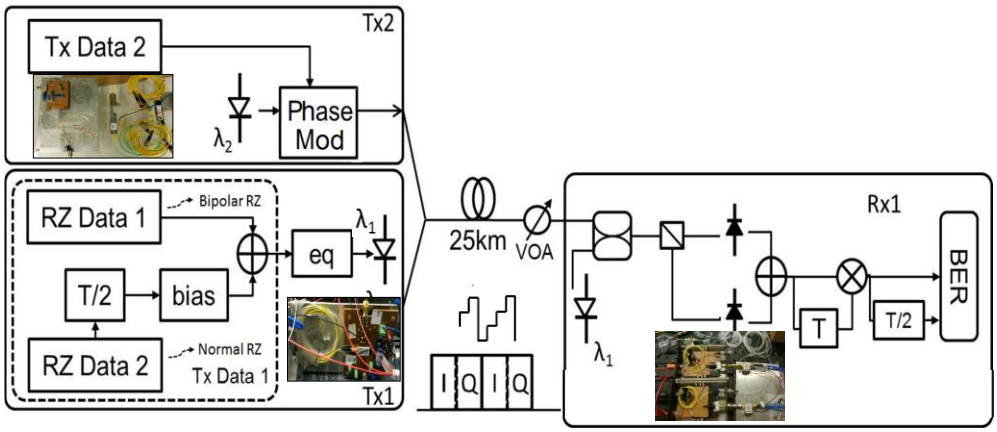

Figure 6.6. Experimental setup schematics; the inset shows photos of the Tx_1, Tx_2 and the PD.

6.3.3 Results and discussion

After properly equalizing the electrical signals, the system was tested firstly at 5 Gb/s. The results are plotted in Figure 6.7(a). The Rx sensitivity measured at a pre-FEC BER of 10^{-3} was around -42 dBm. When scaling to 6 Gb/s and 7 Gb/s the penalty was around 2 dB and 3 dB respectively. Then, at a R_b of 8 Gb/s the Rx sensitivity was -37 dBm. However, a BER floor appeared close to 10^{-5}. The 5 dB penalty appearing at 8 Gb/s compared with the 5 Gb/s performance was because of the higher amplitude required for modulating the DFB when

increasing R_b. As a consequence, the residual IM produced when directly modulating the DFB was also enlarged. This residual IM adds noise in baseband in the Rx signal. Remarkable that for this technique, a four level driving data signal is required to achieve phase changes up to 270º. This condition was needed to ensure having I and Q parts.

At 10 Gb/s, the electrical driving data required to be further amplified. The penalty was of almost 9 dB with an Rx sensitivity of -34 dBm. Even if the performance was below the threshold, a BER floor appeared at $5x10^{-4}$. This is explained due to the residual IM, and because of some jitter that appeared in the Rx signal.

For comparison, Tx_2 was added to the network and tested at 10 Gb/s with the same technique. For detecting Tx_2, the LO in the Rx was tuned close to λ_2. Figure 6.7(b) plots the results for both Tx_1 with direct modulation (DM) and Tx_2 with EM. The Rx sensitivity at BER=10^{-3} with EM improved to -38 dBm. This enhancement was expected because the EM avoids the residual IM. The penalty between EM and DM was around 4 dB. The performance can be improved by making a flatter frequency response of the DFB which can be done with a higher order equalizer. Another alternative for improving the performance would be replacing the Rx for one based on a 120º optical hybrid. However, this Rx would be polarization dependent. Further studies with this Rx need to be done in order to guarantee polarization independence.

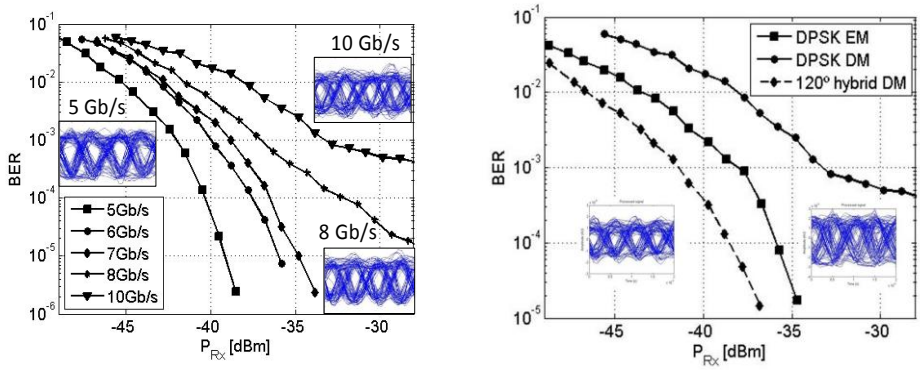

(a) (b)

Figure 6.7. (a) BER against Rx optical power Tx_1 at several bit rates and eye diagrams at BER=10^{-5} for 5Gb/s and 8 Gb/s, and BER=10^{-3} at 10 Gb/s. (b) Sensitivity comparison at 10 Gb/ for Tx_1 (DM), and Tx_2 (EM) with the proposed 2-PD Rx and with a 120º hybrid.

Finally, the spectral separation between users was evaluated. Tx_1 laser wavelength was left constant and the LO in the Rx was tuned to λ_1. The channel frequency separation was adjusted from 0 GHz to 60 GHz by varying λ_2 in Tx_2. The optical power in the Rx was set just below Tx_1 BER threshold to a power of -33 dBm (see Figure 6.7(a)) when only Tx_1 was transmitting.

The effect on the BER was measured when changing λ_2. Figure 6.8 plots the BER against the channel spacing. A 1 dB penalty would correspond to a point above BER = 10^{-3}. Thus the spectral separation between users should be around 40 GHz.

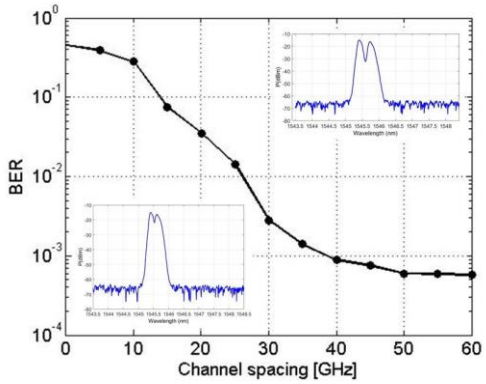

Figure 6.8. BER against channel spacing for λ_1. The insets show the optical spectra for a frequency separation of 20 GHz and 50 GHz.

The Rx sensitivity of the proposed system complies with the NG-PON2 TWDM 10 Gb/s requirement (-28 dBm at BER=10^{-3}) [13]. Furthermore, the channel spacing to keep the penalty in the performance <1 dB was just 40 GHz which is less than half the required in NG-PON2 (100 GHz as typical value). In addition, the transceiver is very simple compared to conventional coherent implementations [16], [22].. Although two lasers would be needed, one for Tx and one for LO, integrated devices can be proposed for having a single laser in the TRx [23].

6.4 Chapter summary

In this chapter, two proposals for simplifying the coherent ONU and reduce its cost were presented and experimentally demonstrated in an UDWDM-PON.

First, the feasibility of using only one direct-modulated DFB laser as DPSK Tx and LO at ONU was tested. By optimizing the power of the LO residual carrier, a symmetrical 1.25 Gb/s ASK/DPSK bidirectional PON with 50 km SMF link was demonstrated reaching a DS/US sensitivity of -46/-48 dBm. By reducing the ONU complexity, associated to the use of a second light source as LO, the proposed architecture can be suitable for future λ-to-the-user access networks.

Second, a direct phase modulated DFB at 10 Gb/s with an alternate phase transmission in a 25 km WDM-PON scenario was proposed and experimentally tested. The Rx was based on simplified intradyne detection with only 1 PD per polarization demonstrating polarization independence. Due to the high residual IM as compared to an ideal PM, a BER floor was observed; however, the performance was still below BER = 10^{-3} with an Rx sensitivity of -34 dBm. The performance improves by 4 dB the Rx sensitivity specified for the 10 Gb/s NG-PON2 downstream (DS) [13]. In addition, the minimum channel spacing to keep the performance penalty < 1dB was as low as 40 GHz without optical filters. Hence, the total spectrum could be reduced by less than half compared to NG-PON2 DS requirement (100 GHz in the most popular studied case). The performance and low complexity of the technique makes it another attractive option for a future coherent TRx in optical access networks.

Bibliography Chapter 6

[1] L. Kazovsky, A. E. Willner, and S. Benedetto, *Optical Fiber Communication Systems*. Boston: Artech House Publishers, 1996.

[2] D. Lavery, R. Maher, D. S. Millar, B. C. Thomsen, P. Bayvel, and S. J. Savory, "Digital Coherent Receivers for Long-Reach Optical Access Networks," *J. Light. Technol.*, vol. 31, no. 4, pp. 609–620, Feb. 2013.

[3] S. Ryu, S. Yamamoto, H. Taga, N. Edagawa, Y. Yoshida, and H. Wakabayashi, "Long-haul coherent optical fiber communication systems using optical amplifiers," *J. Light. Technol.*, vol. 9, no. 2, pp. 251–260, Feb. 1991.

[4] Lei Xu, I. B. Djordjevic, and Ting Wang, "Digital coherent communication and advanced coding technologies for ultra-long-haul optical transmissions," in *9th International Conference on Optical Communications and Networks (ICOCN 2010)*, Nanjing, China, 2010, pp. 227–229.

[5] International Telecommunication Union, "ITU-T G.984.1 Recommendation: Gigabit-capable passive optical networks (GPON): General characteristics." Mar-2008.

[6] The Institute of Electrical and Electronics Engineers, Inc, "IEEE 802.3ah Standard for Local and metropolitan area networks. Ethernet in the First Mile (EFM): 1G-EPON." 2004.

[7] A. Teixeira, A. Shahpari, R. Ferreira, F. P. Guiomar, and J. D. Reis, "Coherent access," in *Proc. Opt. Fiber Commu. Conf. (OFC)*, Anaheim, CA, USA, 2016.

[8] J. Prat *et al.*, "Technologies for Cost-Effective udWDM-PONs," *J. Light. Technol.*, vol. 34, no. 2, pp. 783–791, Jan. 2016.

[9] M. Presi *et al.*, "Field-Trial of a High-Budget, Filterless, λ -to-the-User, UDWDM-PON Enabled by an Innovative Class of Low-Cost Coherent Transceivers," *J. Light. Technol.*, vol. 35, no. 23, pp. 5250–5259, Dec. 2017.

[10] H. Rohde *et al.*, "Field trials of a coherent UDWDM PON: Real-time LTE backhauling, legacy and 100G coexistence," in *Proc. 40th Eur. Conf. on Opt. Commu. (ECOC)*, Cannes, France, 2014.

[11] G. Vall-llosera *et al.*, "COCONUT cost, power consumption and migration analysis: A route towards NG-PON3," in *Proc. 17th Int. Conf. on Transp. Opt. Netw. (ICTON)*, Budapest, Hungary, 2015.

[12] I. Cano, F. Bottoni, J. C. Velasquez, E. Ciaramella, and J. Prat, "Bidirectional coherent PON with ONU based on reused direct-modulated LO," in *Proc. Opt. Fiber Commu. Conf. (OFC)*, Anaheim, CA, USA, 2016.

[13] International Telecommunication Union, "ITU-T G.989.2 Recommendation, 40-Gigabit-capable passive optical networks (NG-PON2): Physical Media Dependent Layer Specification." May-2014.

[14] I. N. Cano, J. C. Velasquez, V. Polo, and J. Prat, "10 Gbit/s Phase Time Diversity Directly Modulated DFB with Single-PD Intradyne Receiver for Coherent WDM-PON," in *Proc. 42nd Eur. Conf. on Opt. Commu. (ECOC)*, Düsseldorf, Germany, 2016.

[15] A. Shahpari *et al.*, "Coherent ultra dense wavelength division multiplexing passive optical networks," *Opt. Fiber Technol.*, vol. 26, pp. 100–107, Dec. 2015.

[16] D. Lavery, M. Paskov, and S. J. Savory, "Spectral Shaping for Mitigating Backreflections in a Bidirectional 10 Gbit/s Coherent WDM-PON," in *Proc. Opt. Fiber Commun. Conf. (OFC)*, Anaheim, CA, 2013.

[17] L. G. Kazovsky, "Phase- and polarization-diversity coherent optical techniques," *J. Light. Technol.*, vol. 7, no. 2, pp. 279–292, Feb. 1989.

[18] S. J. Savory, "Digital Coherent Optical Receivers: Algorithms and Subsystems," *IEEE J. Sel. Top. Quantum Electron.*, vol. 16, no. 5, pp. 1164–1179, Sep. 2010.
[19] I. N. Cano, A. Lerin, V. Polo, and J. Prat, "Direct Phase Modulation DFBs for Cost-Effective ONU Transmitter in udWDM PONs," *IEEE Photonics Technol. Lett.*, vol. 26, no. 10, pp. 973–975, May 2014.
[20] I. N. Cano, A. Lerín, V. Polo, and J. Prat, "Simplified Polarization Diversity Heterodyne Receiver for 1.25Gb/s Cost-Effective udWDM-PON," in *Proc. Opt. Fiber Commun. Conf. (OFC)*, San Francisco, CA, USA, 2014.
[21] I. N. Cano, A. Lerin, V. Polo, and J. Prat, "Polarization independent single-PD coherent ONU receiver with centralized scrambling in udWDM-PONs," in *Proc. 40th Eur. Conf. on Opt. Commu. (ECOC)*, Cannes, France, 2014.
[22] R. M. Ferreira *et al.*, "Field-trial of a real-time bidirectional UDWDM-PON coexisting with GPON, RF video overlay and NG-PON2 systems," in *Proc. 43rd Eur. Conf. on Opt. Commu. (ECOC)*, Valencia, Spain, 2015.
[23] G. Y. Chu, I. N. Cano, V. Polo, C. Kazmierski, R. Brenot, and J. Prat, "Monolithically Integrated Dual-Output DEML for Full Duplex DPSK-ASK and DPSK-SSB ONU in Ultra-Dense Channel Spaced Access Network," *J. Light. Technol.*, vol. 34, no. 8, pp. 2042–2048, Apr. 2016.

Chapter 7 . Conclusions and open research lines

This chapter discusses the conclusions of the research activity developed across five years of PhD studies. A summary of the main achievements is presented, highlighting the author contributions to each topic, especially to the coexistence of NG-PON and legacy systems, low-cost coherent transceivers for access networks and hybrid modulation formats using integrated photonic devices such as DEML. Finally, some guidelines for future research are suggested.

7.1 General conclusions

GPON and/or EPON have been successful technologies deployed around the world that reach millions of installations per year providing FTTH services for either residential or business users. Nevertheless, the emerging technologies and new multimedia applications have generated an exponential growth for high-speeds and large bandwidth demands.

The overall goals of this thesis were focused in the study of next-generation PON technologies and standards such as NG-PON2 which open a new-paradigm with the acceptance of DWDM as the evolution path for a balanced cost and performance. However, NG-PON2 already propose IM/DD as the enabling technology, restringing the reach and number of users due to the limited sensitivity and power budget. As well, the added complexity to the Rx DSP should be considered when the system needs to be scaled to higher modulation levels (PAM-4, PAM-8, etc). In addition, NG-PON2 introduces challenges such as ONUs operated in burst mode, and the necessity for keeping a complex MAC layer control due to the use of TDM.

To face those limitations and knowing that the spectrum scarcity is a reality which needs attention by standardization groups like IEEE 802.3 and ITU-T, the concept of "Wavelength to the User" is exploited in this thesis. The implementation of UDWDM architectures, reducing the channel spacing between users from 50 or 100 GHz to only 6.25 GHz or 12.5 GHz, was demonstrated for delivering large bandwidth services to a very large number of users. The main conclusion and achievement of this thesis is the development of a new class of low-cost coherent transceivers that eliminate the need of optical filters, based on low-cost directly modulated lasers and simplified coherent receivers, able to coexist with legacy systems.

The results presented in chapter 2, allows to achieve the first specific objective of this thesis. It was to study the coexistence between the proposed UDWDM-PON and legacy systems like GPON/E-PON. This aspect is very relevant since coexistence is one of the major requirements by network operators, to guarantee a smooth and non-disruptive evolution of the PON roadmap. This topic was studied during the COCONUT project though theoretical studies and real-time experiments. The use of a coexistence element (CE), at the CO and proper wavelength blocking filters (WBF) for legacy systems (G/EPON, XG(S)-PON/10G-EPON) and recently NG-PON2 are indispensable devices for guarantying enough isolation and rejection of interferer wavelengths. To demonstrate full coexistence of the proposed UDWDM-PON approach, real-time experiments were carried out on two laboratory test-beds, one at GCO laboratories, and another during the COCONUT field-trial across dark fibers deployed in the city of Pisa, Italy.

On the other hand, the proposed coherent technologies addressed in this thesis are based in simplified transceivers schemes, showing the feasibility for cost-effective solutions suitable for access networks, and facing the typical concept of complexity of conventional coherent Rx. Among those technologies, the author propose the implementation of a direct phase modulated Tx, fully reconfigurable at different data rates, by using a simple digital pre-equalizer, achieving the second objective stated in this thesis.

To achieve the third objective, and to face the issue of the increase of high-speed demands, the author has proposed several alternatives, in both the Tx and the Rx. Regarding to the Tx, the implementation of low complexity multilevel phase modulation formats, by using limited 2.5 GHz BW low-cost DFB lasers were proposed. Several schemes such as DQPSK, 8-DPSK and optical duobinary coding were compared. Rx sensitivity of -36 dBm at 7.5 Gb/s (with 8-

DPSK) was achieved. As well the spectral efficiency was improved to 1.2 bit/s/Hz, by keeping the channel spacing as low as 6.25 GHz. In addition, a novel time-interleaved DPSK/ASK Tx at data rate of 2.5 Gb/s, with simultaneous amplitude and phase data recovery, was presented and demonstrated achieving a Rx sensitivity of -44 dBm at BER = $4 \cdot 10^{-3}$. These techniques add flexibility to the Tx and give the possibility for operators to offer differentiated services and adaptability to the user needs in future optical access networks.

Other research field that has received an important attention by the telecom community is the photonic integration, a new technological solution for implementing low-cost and energy efficient next-generation PONs. Benefits of photonic integration such as smaller size, lower cost and better manufacturability are being exploited by many companies. In this thesis, the possibility of implementing simultaneously a hybrid amplitude and phase modulation format in an integrated DFB-EAM device, best known as DEML, was demonstrated for the first time to the best of the author knowledge. Each section of the DEML was modulated with different data streams and through independent RF inputs. Thanks to the use of the integrated DEML a small footprint and energy efficient low-cost Tx performing a multilevel 8-APSK modulation, operating at 10Gb/s/λ, was presented as a feasible solution to fulfill many of the requirements of upcoming 5G access networks. These solution allowed to achieve the fourth objective of this thesis.

Finally, and understanding that the Rx is a cost sensitive component for making coherent ONUs commercially attractive, two different proposals were presented to simplify the Rx and to reduce its cost. First, a direct modulated DFB laser used as DPSK Tx and at the same time as LO was demonstrated in a bidirectional heterodyne UDWDM-PON. Second, to be compatible with the second next-generation of PON (NG-PON2), a 10 Gb/s phase scrambled directly modulated laser, detected with a novel polarization insensitive intradyne coherent Rx involving only 2 photodiodes, was presented. The latter was tested in a coherent PON without optical filters and with enhanced sensitivity and spectral efficiency than 100GHz basic NG-PON2. This achievements fulfill with the fifth objective stated in this PhD thesis.

7.2 Open research lines

This PhD thesis addressed some of the most important challenges for deployment of next generation optical access networks, such as bandwidth efficiency, spectral flexibility, simplicity and low-cost implementation of the transceivers. In addition, a first inside to

photonic integration was addressed, as well as the issue of coexistence between the next generation and legacy PON systems was wide studied.

Nevertheless, there are some key topics that requires further investigation and would signify a step forward. Some of them are listed below:

1. Techno-economic and energy consumption studies of the proposed coherent transceivers and UDWDM-PON architectures for a feasible third generation passive optical network (NG-PON3) standardization.
2. Real-time implementations of hybrid modulation formats using photonic integrated devices and simple pre and post equalization techniques.
3. Versatile metro-access network convergence integrating FTTH, IoT and 5G services.

7.2.1 Techno-economic and energy consumption studies of coherent transceivers and UDWDM architectures

In addition to the addressed coexistence requirements, other network operator conditions are the cost and power consumption of the technological solutions, in order to demonstrate their feasibility for a future NG-PON3 standard.

A study of techno-economic aspects of the proposed technologies should be addressed, considering the impact of user profiles (modeled by data rate demands) and the scalability of the network for adding capacity according to operator needs (pay-as-you-grow). Although the cost of coherent TRx seems to be higher than in legacy systems based on IM/DD, these costs analysis should be derived in terms of cost/Gbit for a fair comparison, considering transparent ODN topologies. Regarding to power consumption, both contributions from OLT and ONU should be considered, due to in Wavelength-to-the-User approach this consumption is equally split between both subsystems. Finally, it is important to remark that special attention must be paid to energy consumption of signal processing units and the cost of DACs and ADCs.

7.2.2 Real-time implementation of hybrid modulation formats using photonic integrated devices

During 2019 Optical Fiber Communication Conference and Exhibition (OFC-19), CTO founder of Acacia Communications gave a comprehensible plenary talk about the advances

of photonic integration for coherent transceivers. As well, the 6th Workshop on photonic integrated circuits (PIC) was organized by 7Pennies consulting firm with the objective of bringing together the PIC Ecosystem and give a perspective of market maturity. Several foundries such as Fraunhofer, PICAdvanced or Smart Photonics, as well as design software companies such as VPIphotonics or Synopsys, are strongly investing in a growing market, with successful introductions of telecom corporations such as Infinera or Acacia Communications.

For this reason, the benefit of monolithically integrated devices such as DEML is a hot research topic that is worth exploiting, in order to design versatile and flexible transceivers, able to produce more complex multilevel modulation formats. Nevertheless, and based on the gained experience, both a strict temperature control of InP devices, and an optimization of their electro-optic responses are necessary. This could be achieved by using simple DSP techniques, in order to solve issues such as wavelength instabilities and bandwidth limitations, especially in real-time implementations.

7.2.3 Metro-access network convergence integrating FTTH, IoT and 5G services

Because NG-PON2 was recently standardized, it may be considered that FTTH will probably not be the main driver for a new PON generation, and instead, new PON technology will be driven by cloud-computing, business services, Internet of Things (IoT) and emerging next generation 5G mobile networks with a high dynamic bandwidth behavior.

Then, a deep investigation must aim at supporting variable patterns, allowing dynamic traffic conditions and reconfigurable capabilities. Furthermore, to achieve a high sensitivity and bandwidth efficiency, versatile capabilities are mandatory, by using flexible WDM grids with minimum channel bandwidths and higher Gb/s capacities. Finally, the upcoming solutions must be focused on increasing the maturing of coherent transceivers and UDWDM access in metro-access networks, guaranteeing as much as possible the coexistence with legacy systems, while keeping the cost as low as possible.

Appendixes

A. NG-PON2 upstream inter-channel crosstalk analysis

As explained in chapter 2, the power penalty (P_c) allowed by a specific target channel, depends of the crosstalk induced by the interferer channels, which follows Eq. (2.3).

Next, the inter-channel crosstalk (XT) analysis is done for NG-PON2, the first standard that considers several WDM channels. There are two conditions that are worth mentioning:

1. The eye closure described by the ER should be considered, taking into account that NG-PON2 is a typical IM based system.
2. The inter-channel crosstalk analysis is done for US operation since this represents the worst case. This is due to the power difference between the target and the total interferer channels could be larger than in DS operation, where the different ONUs can be located at different distances respect the power splitter placed in the ODN.

In ITU-T G.Sup 39 [1] and ITU-T [2] G.989.2 Recommendations, there are some guidelines to calculate XT and P_c, as function of the typical isolation values of multiplexing/demultiplexing elements, and the ER of the IM signal.

Consider the asymmetric architecture depicted in Figure A.1. In [2], the maximum defined differential optical path loss (d_{max}) at S/R-CG point is 15dB. In addition, the maximum power difference among upstream signals (ΔP_{ONU}) is 5dB, resulting in a total power difference of 20 dB, between the target and the interferer channels. Considering these specifications, the maximum allowed upstream XT for optical WDMs, such as AWGs, cascaded filters, etc, can be obtained as function of the adjacent channel isolation (I_A), and the non-adjacent channel isolation (I_{NA}). The former is the isolation value considering only the neighborhood channels. The latter (I_{NA}), is the isolation of the non-adjacent disturbing channels. In [3], these isolation values are defined as the measured optical powers at each wavelength exiting from the port at wavelengths different from the nominal wavelength relative to the power at the nominal wavelength. In real optical WDMs, $I_A < I_{NA}$.

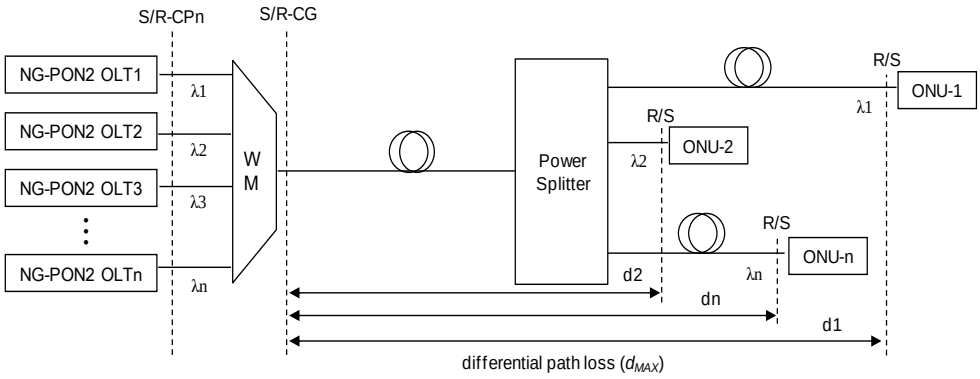

Figure A.1. Reference architecture for inter-channel crosstalk calculation in NG-PON2. Source: [2]

Considering the worst case approach, XT can be calculated using the equation defined in [2]:

$$XT = \Delta P_{ONU} + d_{MAX} + 10\,log_{10}\left(2 \times 10^{\frac{-I_A}{10}} + (N-3) \times 10^{\frac{-I_{NA}}{10}}\right) \quad dB \qquad A.1$$

In Eq A.1, the first term refers to the adjacent isolation for the two (2) neighborhood channels, and the second term is related with the non-adjacent isolation (N-3) channels, i.e., the total number of channels (N) subtracting the two adjacent channels and the target channel.

Where the crosstalk (*N-1)* channels increase, a Gaussian noise statistics approximation can be considered, and *Pc* can be calculated by [2]:

$$Pc = -5\,log_{10}\left(1 - \frac{10^{\frac{2XT}{10}}}{N-1} Q^2 \left(\frac{ER+1}{ER-1}\right)^2\right) \qquad A.2$$

with $Q = \sqrt{2} erfc^{-1}(2 * BER)$.

Considering NG-PON2 US operation at 2.5Gbit/s, the minimum ER that should be guaranteed is 8.2dB [2]. In Eq. A.2, the factor (N-1) represents the total number of disturbing channels (adjacent and non-adjacent) subtracting the target channel. Then, it can also be concluded that different values of I_A and I_{NA} can be used to design systems with different P_c values, but where XT is the same. Figure A.2 represents the power penalty at BER = 10^{-4} as function of XT for different N values. Table A.1 summarizes some *XT* values inferred from Figure A.2, in order to guarantee maximum power penalties of 0.5 or 1dB at BER = 10^{-4}.

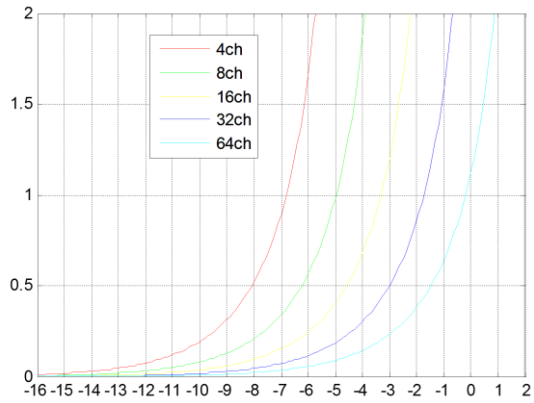

Figure A.2. Power penalty at BER = 10^{-4} vs upstream inter-channel crosstalk for NG-PON2.

Table A.1. Maximum tolerable upstream XT in NG-PON2 for different power penalties at BER = 10^{-4}

N	P_c = 0.5 dB	P_c = 1 dB
4	-8.2	-6.8
8	-6.2	-5
16	-4.6	-3.3
32	-3	-1.8
64	-1.5	-0.2

Figure A.3(a), Figure A.3(b) and Figure A.3(c) show the possible combinations of I_A and I_{NA} values, in order to guarantee a maximum upstream *XT* for scenarios of 4, 8 and 16 channels, respectively. As well Figure A.3(d), Figure A.3(e) and Figure A.3(f) show the power penalties according to the calculated XT values for each case. For example, the isolation values I_A = 32 dB and I_{NA} = 36 dB guarantee XT = -8.2 dB and P_c = 0.47dB at BER = 10^{-4}, for N = 4. One important conclusion that can be deduced is that for lower number of channels (N = 4) the I_A is more relevant than I_{NA}. However, for large number of channels (N = 16) the most relevant parameter is I_{NA}. In addition, Table A.2 presents some values of I_A and I_{NA} for typical AWGs and cascade filters [2]. For typical AWGs with I_A = 23 dB and I_{NA} = 30 dB, the penalty due to XT goes to infinite, mostly due to the high difference of received power from ONUs that must be tolerated. For other technologies such as cascaded filters with I_A = 32 dB and I_{NA} = 36 dB a tolerable penalty around 0.47dB can be obtained for scenarios with 4 channels, and 0.57 dB with 8 channels. In a system with 16 channels this penalty increases until 0.93dB. Here, the great selectivity of COCONUT may offer an interesting advantage.

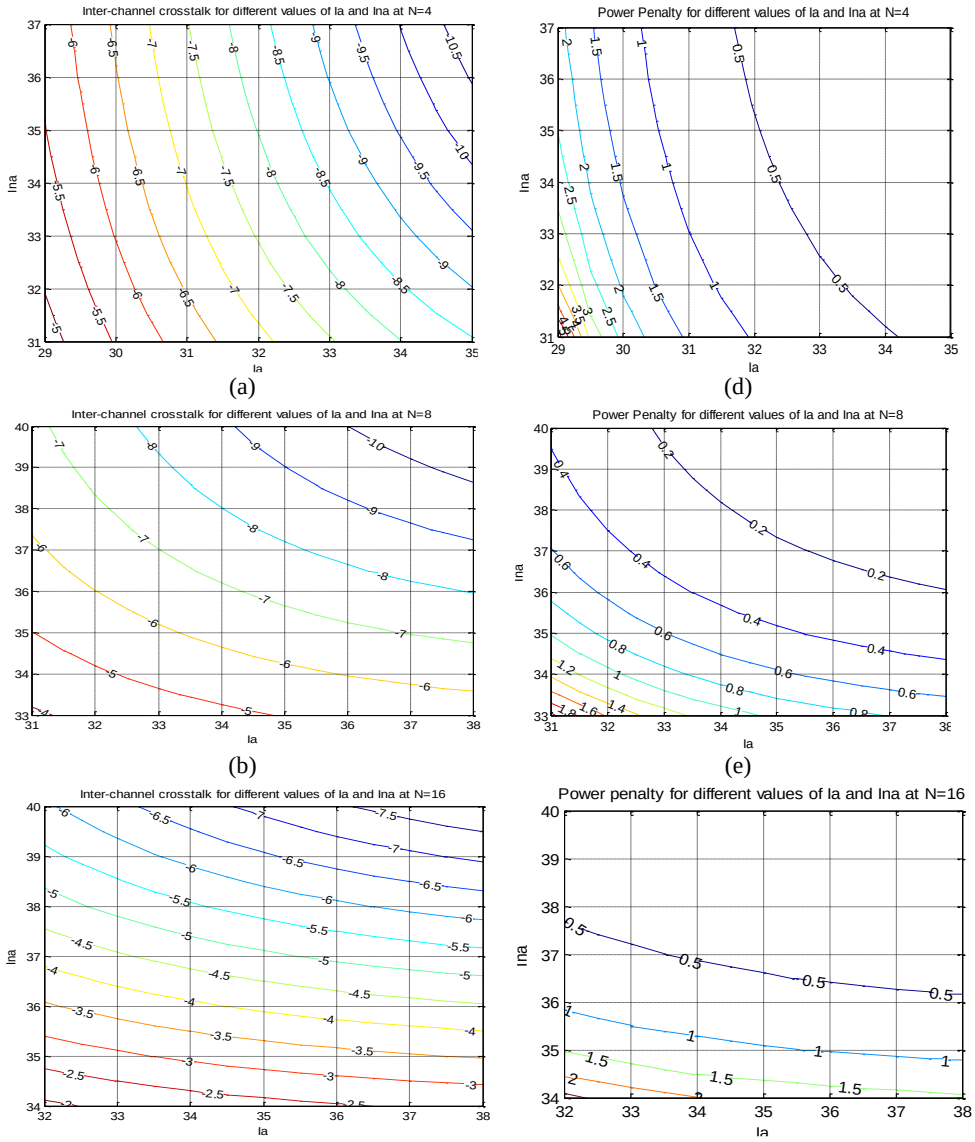

Figure A.3. Left: XT due to different combinations of I_A and I_{NA} for (a) N = 4, (b) N = 8, (c) N = 16; right: P_c at BER = 10^{-4} due to different combinations of I_A and I_{NA} for (d) N = 4, (e) N = 8, (f) N = 16.

Table A.2. Typical values of I_A and I_{NA}, and corresponding XT and Pc at BER = 10^{-4}

Device	ΔP_{ONU} + dmax	I_A	N	XT (dB)	P_c (dB)
Typical AWG	20	23	4	0.42	∞
			8	1.76	∞
			16	3.62	∞
Cascade Filter	20	32	4	-8.2	0.47
			8	-5.99	0.57
			16	-3.44	0.93

B. Example of nominal central frequencies of ITU-T DWDM grid plus the COCONUT proposed 6.25 GHz grid

Nominal Central frequencies (THz) for spacing of:					Nominal central wavelength (nm)
6.25 GHz	**12.5 GHz**	**25 GHz**	**50 GHz**	**100 GHz**	
184.80000	184.8000	184.800	184.80	184.8	1622.2536
184.79375	-	-	-	-	1622.3084
184.78750	184.7875	-	-	-	1622.3633
184.78125	-	-	-	-	1622.4182
184.77500	184.7750	184.775	-	-	1622.4731
184.76875	-	-	-	-	1622.5279
184.76250	184.7625	-	-	-	1622.5828
184.75625	-	-	-	-	1622.6377
184.75000	184.7500	184.750	184.75	-	1622.6926
184.74375	-	-	-	-	1622.7475
184.73750	184.7375	-	-	-	1622.8024
184.73125	-	-	-	-	1622.8573
184.72500	184.7250	184.725	-	-	1622.9122
184.71875	-	-	-	-	1622.9671
184.71250	184.7125	-	-	-	1623.0220
184.70625	-	-	-	-	1623.0770
184.70000	184.7000	184.700	184.70	184.7	1623.1319
184.69375	-	-	-	-	1623.1868
184.68750	184.6875	-	-	-	1623.2417
184.68125	-	-	-	-	1623.2967
184.67500	184.6750	184.675	-	-	1623.3516
184.66875	-	-	-	-	1623.4065
184.66250	184.6625	-	-	-	1623.4615
184.65625	-	-	-	-	1623.5164
184.65000	184.6500	184.650	184.65	-	1623.5714
184.64375	-	-	-	-	1623.6264
184.63750	184.6375	-	-	-	1623.6813
184.63125	-	-	-	-	1623.7363
184.62500	184.6250	184.625	-	-	1623.7912
184.61875	-	-	-	-	1623.8462
184.61250	184.6125	-	-	-	1623.9012
184.60625	-	-	-	-	1623.9562
184.60000	184.6000	184.600	184.60	184.6	1624.0111
184.59375	-	-	-	-	1624.0111
184.58750	184.5875	-	-	-	1624.0661
184.58125	-	-	-	-	1624.1211
184.57500	184.5750	184.575	-	-	1624.1761
184.56875	-	-	-	-	1624.2311
184.56250	184.5625	-	-	-	1624.2861
184.55625	-	-	-	-	1624.3411
184.55000	184.5500	184.550	184.55	-	1624.3961
184.54375	-	-	-	-	1624.4511
184.53750	184.5375	-	-	-	1624.5062
184.53125	-	-	-	-	1624.5612
184.52500	184.5250	184.525	-	-	1624.6162
184.51875	-	-	-	-	1624.6712
184.51250	184.5125	-	-	-	1624.7263
184.50625	-	-	-	-	1624.7813
184.50000	184.5000	184.500	184.50	184.5	1624.8363

C. COCONUT coherent heterodyne ONU transceiver datasheet for NG-PON3

General Description

The coherent heterodyne ONU has a single optical port for connecting to the PON, and two electrical interfaces: one for data transmission input and one for output of the recovered data. It is polarization insensitive and presents high sensitivity values in a defined temperature range.

The transmitter (Tx) module uses the same DFB laser acting as LO, which is externally modulated by an RSOA. The ONU-Tx is tunable in its wavelength (± 1nm) and the US and DS signals are spectrally separated by 2.5GHz to limit the effect of Rayleigh backscattering (RB).

The receiver (Rx) is based on heterodyne detection. The DS signal is mixed with the LO with a 3 dB coupler. A polarization beam splitter (PBS) divides the signal into two orthogonal polarizations. Each of them is detected independently by a single photodiode, then filtered and differentially decoded. Afterwards, the two polarization contributions are added.

Functional scheme, I/Os Block diagram :

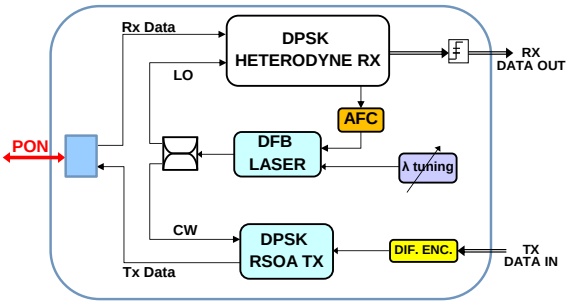

Features

- Polarization insensitive
- Dedicated 1.25Gb/s bit rate
- Automatic Frequency Control (AFC) internal loop for data wavelength tracking.
- Continuous mode operation (US & DS)
- Wavelength tuning (±1nm/ºC) by temperature control of the butterfly package DFB laser.
- ±15V symmetrical power supply
- Operating temperature range from 10ºC to 50ºC
- Compatible with legacy PON standards
- 4k video transmission

Applications

- UDWDM – PON
- Multiple service agnostic transmission
- Wireless Front-haul

Performance (Tx, E-O specifications)

Name	Min.	Typ.	Max.	Units	Comments
Optical					
Center wavelength	1549	1550	1551	nm	Full C & L-band available
Optical Output Power	-3	0	2	dBm	
Electrical					
Tx Data in	-	400	-	mVpp	Typ. 1 Vpp at LD input
Current Supply[1]	-	370	650	mA	

[1]Tx by DFB laser, Peltier cell, encoder, driver amplifier

Performance (Rx, O-E specifications)

Name	Min.	Typ.	Max.	Units	Comments
Optical					
Center wavelength	1549	1550	1551	nm	Full C & L-band available
λ tuning LO @1V monitor	-	25	-	ºC	±1ºC/nm tuning
Rx Sensitivity (FEC level)	-49	-44	-40	dBm	btb & LO = 0dBm (Typical)
Sensitivity (BER = 10e-9)	-43	-38	-34	dBm	btb & LO = 0dBm (Typical)
Electrical					
Rx Data out	-	400	-	mVpp	
Current Supply[2]	-	1250	1700	mA	

[2]Rx by LOL DFB, Peltier cell, Rx Front-end (3x2), (I&Q) Analog demodulator, CAF Homodyne, LA amplifier

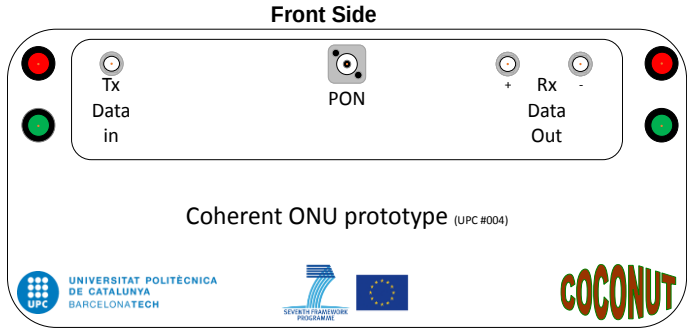

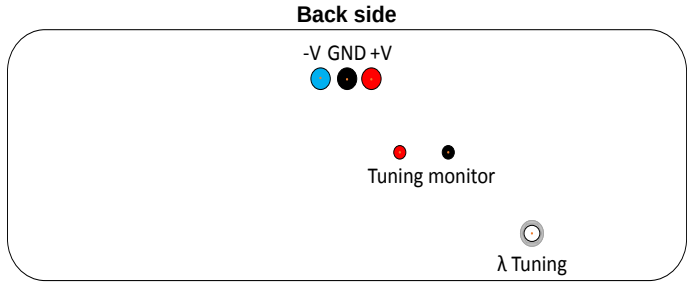

Bibliography Appendixes

[1] International Telecommunication Union, "Supplement 39 Optical system design and engineering considerations." 2012.
[2] International Telecommunication Union, "ITU-T G.989.2 Recommendation, 40-Gigabit-capable passive optical networks (NG-PON2): Physical Media Dependent Layer Specification." May-2014.
[3] International Telecommunication Union, "ITU-T G.671 Recommendation: Transmission characteristics of optical components and subsystems." Feb-2012.

Biography

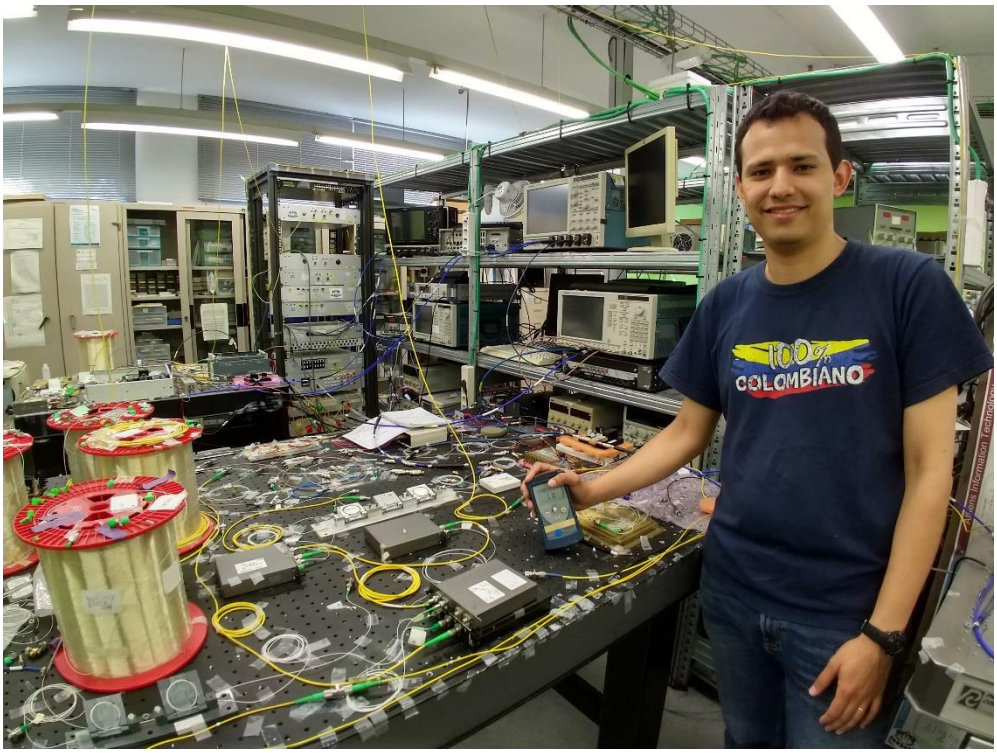

Juan Camilo Velásquez Micolta was born in Manizales, Colombia, in 1986. He received his B.Sc in Electronic Engineering from Universidad Nacional de Colombia in 2009 and M. Sc. degree in Telecommunications Engineering and Management from Universitat Politècnica de Catalunya (UPC) in 2014. During the same year, he joined the Optical Communications Group (GCO) of the Department of Signal Theory and Communications (TSC) at UPC, where he developed his PhD research from 2014 to 2019 under supervision of Prof. Josep Prat and Dr. Iván N. Cano. He also received a degree in Advanced Project Management from Fundación Universitat Politècnica de Catalunya in 2019.

His work focuses on next generation optical access networks, including technologies for directly modulated lasers, advanced modulation formats, coherent detection, integrated photonic devices, WDM networks, PON standardization and coexistence between NG-PON and Legacy PON systems.